FlowDike-D

Freibordbemessung von Ästuar- und Seedeichen unter Berücksichtigung von Wind und Strömung

Stand der Arbeiten - März 2011

Dipl.-Ing. Stefanie Lorke[1]
Dr.-Ing. Antje Bornschein[2]
Univ.-Prof. Dr.-Ing. Holger Schüttrumpf[1]
Prof. Dr.-Ing. habil. Reinhard Pohl[2]

Aachen und Dresden, März 2011

[1] Institut für Wasserbau und Wasserwirtschaft (IWW), RWTH Aachen
[2] Institut für Wasserbau und Technische Hydromechanik (IWD), TU Dresden

Zuwendungsempfänger:		Förderkennzeichen:
	Lehrstuhl und Institut für Wasserbau und Wasserwirtschaft (IWW) Rheinisch-Westfälische Technische Hochschule (RWTH) Aachen Univ.-Prof. Dr.-Ing. Holger Schüttrumpf	03KIS075
	Institut für Wasserbau und Technische Hydromechanik (IWD) Technische Universität (TU) Dresden Lehrgebiet Hydromechanik im Wasserbau Prof. Dr.-Ing. habil. Reinhard Pohl	03KIS076
	Unterstützt durch EU - Hydralb III	
Vorhabenbezeichnung: Verbundprojekt: FlowDike-D Vorhaben: Freibordbemessung von Ästuar- und Seedeichen unter Berücksichtigung von Wind und Strömung		
Laufzeit des Vorhabens: 01/2009 bis 10/2011		
Berichtszeitraum: 04/2010 bis 03/2011		

Anschriften der Projektpartner:

Institut für Wasserbau und Wasserwirtschaft (IWW), RWTH Aachen

Univ.-Prof. Dr.-Ing. Holger Schüttrumpf

Mies-van-der-Rohe-Straße 1, 52056 Aachen

Institut für Wasserbau und Technische Hydromechanik (IWD), TU Dresden

Prof. Dr.-Ing. habil. Reinhard Pohl

George-Bähr-Str. 1, Beyer-Bau Zimmer 82/84, 01069 Dresden

Inhaltsverzeichnis

Vorwort

Eine Analyse von Deichschäden z.B. nach dem Hurrikan Katrina in den USA oder der großen Sturmflut in Hamburg im Jahr 1962 hat gezeigt, dass viele Deichschäden und Deichbrüche auf Wellenüberlauf zurückzuführen sind. Daher ist der Wellenüberlauf aber auch die Wellenauflaufhöhe für die Ermittlung der Kronenhöhe von Fluss-, Ästuar- und Seedeichen eine maßgebende Bemessungsgröße. Heutige Bemessungsformeln für Wellenauflauf und Wellenüberlauf (z.B. EUROTOP-Manual, 2008) berücksichtigen neben der Deichgeometrie insbesondere die Wellenhöhe, die Wellenperiode sowie die Wellenangriffsrichtung. Die deichparallele Strömung sowie der lokale Wind werden bislang in diesen Formeln nicht berücksichtigt. Im Rahmen eines Hydralab III - Projektes wurden daher zu diesem Aspekt experimentelle Untersuchungen im Wellenbecken von DHI in Kopenhagen im Jahr 2009 an einem 1:3 geböschten Deich durchgeführt. Die experimentellen Daten stehen für das vorliegende Projekt vollständig zur Verfügung und wurden durch eine zweite Versuchsreihe mit einem 1:6 geböschten Deich im Rahmen dieses BMBF Projektes erweitert.

Ziel des Projektes ist es, den Einfluss von Strömung und Wind auf die mittlere Wellenauflaufhöhe und Wellenüberlaufrate auf der Grundlage verfügbarer experimenteller Untersuchungen aus dem Projekt zu ermitteln und bestehende Wellenauflauf- und -überlaufformeln (siehe Eurotop-Manual) entsprechend zu adaptieren bzw. zu erweitern.

Dieser Zwischenbericht 2010 stellt in Stichworten die bisher vorliegenden wesentlichen Erkenntnisse und Ergebnisse aus dem Projekt FlowDike-D vor und gibt einen Überblick über die bereits durchgeführten und noch zu bearbeitenden Teilaufgaben des Projektes. Als Anhang liegt die aktuelle Version des Berichtes „FlowDike-D: Freibordbemessung von Ästuar- und Seedeichen unter Berücksichtigung von Wind und Strömung“ in englischer Sprache bei.

1 Kurzgefasste Angaben zum Projekt

1.1 wichtige wissenschaftlich-technische Ergebnisse und wesentliche Ereignisse

Die experimentellen Untersuchungen wurden am DHI in Kopenhagen erfolgreich durchgeführt. Die Ergebnisse der Referenztests zeigen eine gute Übereinstimmung mit früheren Untersuchungen. Im Folgenden werden die ersten Ergebnisse stichpunktartig zusammengestellt.

Wellenfeld

- Jonswap-Spektrum liefert gute Übereinstimmungen mit früheren Untersuchungen
- Für die Analyse des Wellenauflaufs und –überlaufs werden spektrale Wellenparameter wie Tm-1,0 bestimmt, um unter anderem die Vergleichbarkeit mit anderen Spektren (z.B. TMA) sicherzustellen
- Zur Bestimmung des Einflusses der Strömung wird der Energiewinkel der Welle eingeführt

Wellenauflauf

- Wellenauflaufergebnisse im brandenden und Übergangsbereich zeigen gute Übereinstimmung mit früheren Versuchen
- Schräge Anlaufrichtung der Wellen ergibt leichte Abminderung der Auflaufhöhe
- Erweiterung der Analyse des Wellenauflaufs durch Auswertung der Videoaufzeichnungen über 10 vertikale Streifen, Auslesen von 10 Ganglinien der Wellenauflaufhöhe über der Zeit, Randstreifen sind in weiterer Auswertung zu vernachlässigen
- Streifen liefern vergleichbare Ergebnisse für den Wellenauflauf, ermöglichen die Angabe einer Verteilung der Auflaufhöhe $R_{2\%}$
- Abminderungsfaktor für schrägen Wellenauflauf und Einfluss der Querströmung auf den Wellenauflauf: je schräger der Wellenangriff desto geringer ist der Wellenauflauf; durch Einführung des Energiewinkels Berücksichtigung der Querströmung und des Angriffswinkels in einer Einflussfunktion möglich (bisher Ergebnisse 1:3 Deich)

Wellenüberlauf

- Schräger Wellenangriff hat einen reduzierenden Einfluss auf den Wellenüberlauf; gute Übereinstimmung mit bestehenden Untersuchungen (BMBF-Projekt Schräger Wellenauflauf)
- Eine küstenparallele Strömung hat einen erhöhenden Einfluss auf den Wellenüberlauf bei zur Wellenangriffsrichtung entgegengesetzter Strömung
- Wind hat einen Einfluss auf kleine Wellenüberlaufraten, bei hohen Wellenüberlaufraten ist der Windeinfluss jedoch vernachlässigbar
- Eine Kombination der verschiedenen Einflussfaktoren ist noch nicht ausreichend untersucht worden

Strömungsprozesse auf der Deichkrone

- Stochastische Auswertung aller Tests liefern für die Schichtdicke $h_{2\%}$ und die Fließgeschwindigkeit v2% gute Übereinstimmungen mit früheren Untersuchungen von Schüttrumpf (2001) und van Gent (2002)
- Analyse der Einzelereignisse. Produkt aus Fließgeschwindigkeit und Fließtiefe überschätzt (wie zu erwarten war) die gemessene Wellenüberlaufrate auf der Deichkrone

1.2 Arbeits-, Zeit- und Aufgabenplanung

Die folgende Tabelle gibt einen Überblick über die einzelnen Arbeitsschritte und deren Fortschritt in dem Projekt.

Tabelle 1 Arbeitsschritte und deren geplanter Bearbeitungszeitpunkt sowie Stand der Arbeiten (— heute; fertig gestellt; in Bearbeitung; noch nicht bearbeitet), Teil 1

	Teilaufgabe/Spezifikation	Meilensteine	2009	2010												2011									
				J	F	M	A	M	J	J	A	S	O	N	D	J	F	M	A	M	J	J	A	S	O
1.	Theorie zu Wellenausbreitung unter Strömung und Wind																								
2.	Datenerfassung und Zusammenstellung typischer bemessungsrelevanter Szenarien	1:3 Deich																							
		1:6 Deich																							
3.	Detaillierte Versuchsplanung (Versuchsaufbau, Versuchsprogramm, Messtechnik)	1:3 Deich																							
		1:6 Deich																							
4.	Aufbau Versuchsstand	1:3 Deich																							
		1:6 Deich																							
5.	Modellversuche	1:3 Deich																							
		1:6 Deich																							
6.	Detaillierte Versuchsauswertung und -analyse	1:3 Deich																							
		1:6 Deich																							
7.	Diskussion von Modell- und Maßstabseffekten	1:3 Deich																							
		1:6 Deich																							
8a.	Entwicklung neuer Berechnungsansätze unter Einbeziehung der experimentellen Ergebnisse – Einfluss Strömung	Deich 1:3																							
		Deich 1:6																							

Tabelle 2 Arbeitsschritte und deren geplanter Bearbeitungszeitpunkt sowie Stand der Arbeiten (— heute; fertig gestellt; in Bearbeitung; noch nicht bearbeitet), Teil 2

	Teilaufgabe/Spezifikation	Meilensteine	2009	2010												2011									
				J	F	M	A	M	J	J	A	S	O	N	D	J	F	M	A	M	J	J	A	S	O
8b.	Entwicklung neuer Berechnungsansätze unter Einbeziehung der experimentellen Ergebnisse – Einfluss Wind	Deich 1:3																							
		Deich 1:6																							
9.	Erstellung einer benutzerfreundlichen Anwendersoftware zur Freibordbemessung	Beta-Version																							
		Fertigstellung																							
10.	Testrechnungen- Auswahl Testfälle für Bemessungssoftware																								
	Testrechnungen - Beendigung Testrechnung																								
11.	Handbuch/Empfehlungen/ Zwischenberichte/ Abschlussbericht	Zwischenbericht 2009																							
		Zwischenbericht 2010																							
		Fertigstellung Handbuch/Empfehlungen																							
		Abschlussbericht																							

zu 1.) Siehe Bericht im Anhang

zu 2.) Bemessungsrelevante Szenarien wie Wasserstände, Strömungsgrößen, Windgeschwindigkeiten wurden festgelegt. Eine detaillierte Zusammenstellung von Beispielprojekten ist im Bericht noch nicht enthalten.

zu 3.) Siehe Bericht im Anhang

zu 4.) Siehe Bericht im Anhang

zu 5.) Modellversuche haben erfolgreich stattgefunden

zu 6.) Die Standardauswertungen zu Wellenauflauf und Wellenüberlauf sind fertig gestellt (siehe Bericht im Anhang). Eine detaillierte ist in Bearbeitung und zum Teil bereits im Bericht zusammengestellt.

zu 7.) Siehe Bericht im Anhang

zu 8a.) Vorläufige Ergebnisse sind im Bericht enthalten

zu 8a.) noch in Bearbeitung

zu 9. bis 11.) geplant für 2011

1.3 Aussichten für die Erreichung der Ziele des Vorhabens

- Arbeiten sind gut im Zeitplan (vgl. Tabelle 1 und Tabelle 2)
- Erste Ergebnisse der Referenztests stimmen gut mit bestehenden Untersuchungen überein (siehe Bericht)
- Erste Analysen der Untersuchungen zeigen plausible Ergebnisse
- Es sind keine Änderungen in dem weiteren Vorgehen des Projektes geplant

1.4 Ergebnisse von dritter Seite, die für die Durchführung des Vorhabens relevant sind

Es sind keine Ergebnisse von dritter Seite bekannt geworden, die für die Durchführung der vorliegenden Arbeit relevant sind.

1.5 Änderungen in der Zielsetzung

Zurzeit sind keine Änderungen der Zielsetzungen vorgesehen.

1.6 Fortschreibung des Verwertungsplans

Weitreichende Ziele des Projektes:

- Ermittlung neuer Bemessungsansätze für die Bestimmung der Freibordhöhe von Ästuar- und Seedeichen unter Berücksichtigung von Wind und Strömung
- Höhere Sicherheit von Deichen, ggf. Einsparungen von Sanierungs- und / oder Baukosten
- Es ist geplant, die Ergebnisse in die Erarbeitung des International Levee Manual einfließen zu lassen

Anhang

- Preliminary report 2010 of FlowDike-D

  "Influence of wind and current on wave run-up and wave overtopping"

- Veröffentlichungen:

Brüning, A.; Gilli, S.; Lorke, S.; Pohl, R.; Schlüter, F.; Spano, M.; van der Meer, J.; Werk, S.; Schüttrumpf, H. (2009); FlowDike - Investigating the effect of wind and current on wave run-up and wave overtopping; 4th SCACR - International Short conference on APPLIED COASTAL RESEARCH, Barcelona

Brüning, A.; Gilli, S.; Lorke, S.; Pohl, R.; Schlüter, F.; Spano, M.; van der Meer, J.; Werk, S.; Schüttrumpf, H. (2010); FlowDike - Investigating the effect of wind and current on wave run-up and wave overtopping; Hydralab III Joint User Meeting, Hannover

Lorke, S., Brüning, A.; Bornschein, A.; Gilli, S.; Pohl, R.; Spano, M.; van der Meer, J.; Werk, S.; Schüttrumpf, H. (2010); On the effect of wind and current on wave run-up and wave overtopping; 32nd International Conference on Coastal Engineering ICCE. Shanghai

Lorke, S.; Schüttrumpf, H.; Bornschein, A.; Pohl, R.; van der Meer, J. W. (2010): FlowDike-D: Freibord-bemessung von Ästuar- und Seedeichen unter Berücksichtigung von Wind und Strömung. KFKI aktuell, Ausgabe 02/2010

Pohl, R. (2010); Neue Aspekte der Freibordbemessung an Fluss- und Ästuardeichen; Wasserbauliche Mitteilungen des Institutes für Wasserbau und Technische Hydromechanik der Technischen Universität Dresden, Heft 40, S. 467 - 478 (nicht im Anhang)

Rahlf, H.; Schüttrumpf, H. (2010); Critical overtopping rates for Brunsbüttel lock; 32nd International Conference on Coastal Engineering ICCE. Shanghai

Schüttrumpf, H. (2009) Wellenüberlauf an Deichen - Stand der Wissenschaft und aktuelle Untersuchungen. 3. Siegener Symposium "Sicherung von Dämmen, Deichen und Stauanlagen". Tagungsband

Van der Meer, J.; Hardeman, B.; Steendam, G.J.; Schüttrumpf, H.; Verheij, H. (2010) Flow depths and velocities at crest and inner slope of a dike, in theory and with the wave overtopping simulator. 32nd International Conference on Coastal Engineering ICCE. Shanghai

FlowDike-D

Influence of wind and current on wave run-up and wave overtopping

Preliminary report 2010

Dipl.-Ing. Stefanie Lorke[1]
Dr.-Ing. Antje Bornschein[2]
Univ.-Prof. Dr.-Ing. Holger Schüttrumpf[1]
Prof. Dr.-Ing. habil. Reinhard Pohl[2]

Aachen and Dresden, March 2011

[1] Institute of Hydraulic Engineering and Water Resources Management, RWTH Aachen University, Germany
[2] Institute of Hydraulic Engineering and Technical Hydromechanics, TU Dresden, Germany

Following partners and authors are responsible for the chapters:

Chapter 1	IWW (RWTH Aachen):	Lorke, Schüttrumpf
	IWD (TU Dresden):	Bornschein, Pohl
Chapter 2	IWW (RWTH Aachen):	Lorke, Schüttrumpf
	IWD (TU Dresden):	Bornschein, Pohl
Chapter 3	IWW (RWTH Aachen):	Lorke, Schüttrumpf
	IWD (TU Dresden):	Bornschein, Pohl
Chapter 4	IWW (RWTH Aachen):	Lorke, Schüttrumpf
Chapter 5	IWW (RWTH Aachen):	Lorke, Schüttrumpf
Chapter 6	IWW (RWTH Aachen):	Lorke, Schüttrumpf
	IWD (TU Dresden):	Bornschein, Pohl
Chapter 7	IWW (RWTH Aachen):	Lorke, Schüttrumpf
Chapter 8	IWW (RWTH Aachen):	Lorke, Schüttrumpf
	IWD (TU Dresden):	Bornschein, Pohl
Chapter 9	IWW (RWTH Aachen):	Lorke, Schüttrumpf
	IWD (TU Dresden):	Bornschein, Pohl

The following researchers have contributed to the project and report:

Anja Brüning, Stefan Carstensen, Ladislav Dvorak, Stefano Gilli, Torsten Heyer, Jens Kirkegard, Nadine Krüger, Flemming Schlütter, Miroslav Spano, Jaromir Riha, Jentsje W. van der Meer, Stefan Werk

Table of contents

List of figures

Annex

List of tables

Annex

List of symbols

Letters

a	[-]	correction factor single overtopping events
b	[-]	best-fit coefficients
b	[-]	inclination of the slope
c	[m/s]	wave velocity
C	[-]	coefficient
c_1	[-]	empirical parameters to determine the run-up height
c_2	[-]	empirical parameters to determine the run-up height
c_3	[-]	empirical parameters to determine the run-up height
c_2*	[-]	parameter for describing the layer thickness
$c_{g,rel}$	[m/s]	relative group velocity of waves
c_h	[-]	empirical coefficient determined by model tests concerning flow depth on crest
C_r	[-]	average reflection coefficient
c_v	[-]	empirical coefficient determined by model tests
C_ξ	[-]	parameter considering infl. of shallow foreshore, roughness, obliqueness
d	[m]	flow depth, water depth
d_b	[m]	flow depth at breaker point without wind
$d_{b(wind)}$	[m]	flow depth at breaker point with wind
f	[Hz]	frequency
f_p	[Hz]	spectral peak frequency
Fr_{crest}	[-]	Froude number at the crest
Fr_{wave}	[-]	Froude number of the wave
g	[m/s²]	acceleration due to gravity (= 9.81 m/s²)
h	[m]	flow depth on the dike crest

H	[m]	wave height
$h_{2\%}$	[m]	flow depth on dike crest exceeded by 2% of the incoming waves
h_c	[m]	layer thickness (flow depth) on dike crest
h_{crest}	[m]	layer thickness (flow depth) on dike crest
H_{m0}	[m]	significant wave height from spectral analysis
$H_{m0,dike\ toe}$	[m]	significant wave height from spectral analysis at toe of the dike
$H_{m0,wave\ generator}$	[m]	significant wave height from spectral analysis in front of wave generator
H_{max}	[m]	measured maximum wave height
H_s	[m]	significant wave height (defined as highest one-third of wave heights)
H_{WM}	[m]	wave height, adjusted at the wave machine
k	[rad/m]	wave number
K_R	[-]	reflection coefficient
L	[m]	wave length measured in direction of wave propagation
$L_{0m-1,0}$	[m]	deep water wave length based on $T_{m-1,0}$
L_{0p}	[m]	wave length corresponding to T_p and deep water conditions
L_m	[m]	wave length corresponding to T_m
$L_{m-1,0}$	[m]	deep water wave length based on $T_{m-1,0}$
L_p	[m]	wavelength corresponding to T_p
L_s	[m]	airy wave length corresponding to T_s
m_0	[m²/s]	zero order moment of spectral density
$m_{0,inc}$	[m²/s]	energy density of the incident wave spectrum
$m_{0,refl}$	[m²/s]	energy density of the reflected wave spectrum
m_{-1}	[m²]	minus first moment of spectral density
m_n	[m^2/s^n]	nth moment of spectral density
N	[-]	number of incoming waves
p	[-]	percentage

p_{br}	[-]	coefficient for deterministic and probabilistic design, breaking waves
p_{nbr}	[-]	coefficient for deterministic and probabilistic design, breaking waves
P_{OW}	[-]	probability of overtopping per wave
q	[m³/(sm)]	mean overtopping rate per meter structure width
q^*	[-]	dimensionless overtopping discharge
Q_0	[-]	interception with the y-axis
$q_{\beta=0°}$	[m³/(sm)]	overtopping rate with angle of wave attack $\beta = 0°$
$q_{\beta>0°}$	[m³/(sm)]	overtopping rate with angle of wave attack $\beta > 0°$
R_*	[-]	dimensionless freeboard height
R^2	[-]	coefficient of determination
R_c	[m]	freeboard height of the structure
R_u	[m]	run-up level, vertical measured with respect to the SWL
$R_{u2\%}$	[m]	run-up height exceeded by 2% of the incoming waves
$R_{u2\%;\beta=0°}$	[m]	run-up height exceeded by 2% of the incoming waves with $\beta = 0°$
$R_{u2\%;\beta>0°}$	[m]	run-up height exceeded by 2% of the incoming waves with $\beta > 0°$
$R_{ux\%}$	[m]	run-up level exceeded by x% of incoming waves
Re_{wave}	[-]	Reynold number of the wave
Re_{crest}	[-]	Reynold number at the crest
s	[-]	wave steepness s = H/L
SJ(f)	[m²/Hz]	Jonswap-energy-density-spectrum
$s_{m-1,0}$	[-]	wave steepness based on H_{m0} and $L_{m-1,0}$
SP(f)	[m²/Hz]	Phillips-spectrum describing the decreasing part of the graph
SPM(f)	[m²/Hz]	energy density spectrum of Pierson-Moskowitz
T	[s]	wave period
T_m	[s]	mean wave period (here: from time-domain analysis)
$T_{m0,1}$	[s]	average wave period defined by m_0/m_1

$T_{m0,2}$	[s]	average wave period defined by $\sqrt{m_0/m_2}$
$T_{m-1,0}$	[s]	spectral wave period defined by m_{-1}/m_0
T_p	[s]	spectral peak wave period
u	[m/s]	wind velocity
u_{10}	[m/s]	wind velocity 10 m above still water level
v	[m/s]	current velocity
V	[m³]	overtopping volume per wave
V'	[m³/s]	overtopping volume per meter wave
$v_{2\%}$	[m/s]	flow velocity on dike crest exceeded by 2% of the incoming waves
v_c	[m/s]	overtopping velocity (flow velocity) on the dike crest
v_{crest}	[m/s]	overtopping velocity (flow velocity) on the dike crest
$v_{crest,no\ wind}$	[m/s]	flow velocity on the dike crest, wind $u_{10} = 0$ m/s
$v_{crest,wind}$	[m/s]	flow velocity on the dike crest, wind $u_{10} \neq 0$ m/s
v_n	[m/s]	current velocity in the direction of wave propagation
v_x	[m/s]	current velocity parallel to the dike crest
We_{crest}	[-]	Weber number at the crest
x	[m]	horizontal coordinate parallel to the dike crest
y	[m]	horizontal coordinate perpendicular to the dike crest
z	[m]	vertical coordinate

Greek letters

α	[°]	slope of the front face of the structure
α	[-]	Phillips-constant $\alpha = 8.1 \cdot 10\text{-}3$
β	[°]	angle of wave attack relative to normal on structure
β'	[°]	ratio of angle of wave attack and dike parallel wave attack
β_e	[°]	angle of wave energy relative to normal on structure

γ	[-]	peak raising factor [-] $\gamma = 3.3$ for mean Jonswap-spectrum
γ	[-]	correction factor considering run-up and overtopping design
γ_b	[-]	correction factor for a berm considering run-up and overtopping design
γ_f	[-]	correction factor for surface roughness considering run-up and ov. design
γ_β	[-]	correction factor for oblique wave attack considering run-up and ov. design
$\gamma_{\beta,cu}$	[-]	correction factor to take the influence of current v_x into account
γ_υ	[-]	correction factor for a vertical wall on the slope
Δt	[s]	duration of a wave overtopping event
ξ_{eq}	[-]	surf similarity parameter considering influence of a berm
$\xi_{m-1,0}$	[-]	surf similarity parameter based on $s_{m-1,0}$
ξ_p	[-]	surf similarity parameter based on H_s and L_{0p}
ξ_{tr}	[-]	surf similarity parameter describing transition between br. and non-br. waves
ν	[m²/s]	dynamic viscosity
ν_{crest}	[m/s]	velocity at the crest
σ_0	[N/m]	surface tension
ω_{abs}	[rad/s]	absolute angular frequency
ω_{rel}	[rad/s]	relative angular frequency

Index

*	dimensionless parameter
0	deep water conditions
abs	absolute value
average	considering average / measured wave spectra
incident	considering incident wave spectra
lc	load cell measurements
m-1,0	spectral parameter

orth	perpendicular wave attack
reflected	considering reflected wave spectra
rel	relative parameter
vh	considering product of flow depth h and flow velocities v on crest
x%	value exceeded by x% of the incoming waves
β	considering the angle of wave attack
β=0	perpendicular wave attack
β>0	oblique wave attack

List of abbreviations

br	breaking wave conditions
fd 1	FlowDike 1 – 1:3 sloped dike
fd 2	FlowDike 2 – 1:6 sloped dike
nbr	non-breaking wave conditions
w1	wave condition number 1
w2	wave condition number 2
w3	wave condition number 3
w4	wave condition number 4
w5	wave condition number 5
w6	wave condition number 6
wc II	wave characteristics II
wcI	wave characteristics I
WS	water level

1 Introduction

A variety of structures has been built in the past to protect the adjacent areas during high water levels and storm surges from coastal or river flooding. Common use in practice is the application of smooth sloped dikes as well as steep or vertical walls. The knowledge of the design water level, wind surge, wave run-up and/or wave overtopping is used to determine the crest height of these structures. Due to the return interval considered of the design water level, the uncertainties in applied formula for wave run-up respectively wave overtopping and the incoming wave parameters, wave overtopping cannot be avoided at all times.

Relevant for the freeboard design in wide rivers, estuaries and at the coast, are the incoming wave parameters at the toe of the structure. At rivers these are probably influenced by local wind fields and sometimes by strong currents - occurring at high water levels mostly parallel to the structure (cross flow). In the past no investigations were made on the combined effects of wind and current on wave run-up and wave overtopping. Only few papers, dealing either with wind effects or current influence, are publicized. To achieve an improved design of structures these effects should not be neglected, otherwise the lack of knowledge may result in too high and expensive structures or in an under design of the flood protection structure which increases the risk of flooding.

Today systematically investigations about the influence of dike-parallel flow on the wave run-up and overtopping are not yet known. Furthermore detailed studies about the interaction of wind and current in their impact on wave run-up and overtopping are not available in national or international publications. Nevertheless data from previous KFKI projects “Oblique wave attack at sea dikes” and “Loading of the inner slope of sea dikes by wave overtopping” and from the CLASH-database are at hand for comparison purposes. They represent a set-up without wind and dike parallel flow. The aim of the research project presented is to close the knowledge by experimental investigations in an offshore wave basin together with currents and wind.

The subject of investigation is a dike with an outer slope of 1:3 and 1:6 which is typical for rivers, estuaries and coastal lagoons. The research deals with the wave run-up and overtopping rate originated by short-crested waves considering different current and wind velocities, dike crest levels and wave directions. The obtained data form the basis to determine the dependencies between the wave run-up respectively the overtopping rate and the swell, coastal parallel flow and wind under consideration of former approaches and theoretically analysis. Furthermore the results ought to be incorporated into freeboard design of estuary and sea dikes.

Model tests at the DHI in Hørsholm (Denmark)

The experimental investigations on run-up and overtopping for smooth sloped dikes were performed twice at the DHI in Hørsholm. The first part of the model tests for a 1:3 slope took place in January 2009 (titled FlowDike 1 in the following). In November 2009 the second phase of investigations (FlowDike 2) were performed for a 1:6 sloped dike.

During both model tests, the dike was divided into two separate parts to perform wave run-up and wave overtopping experiments simultaneously. This was done due to the fact that the measuring area within the basin and the testing time was limited. Overtopping was measured for two different crest heights (70 cm and 60 cm) in order to include the influence of the freeboard and acquire more data for the analysis. A first overall view of the model set-up and a more detailed description of the model tests are given in chapter 2.3.

The test program covered model tests on wave run-up and wave overtopping with 3 set-ups. Combinations with and without currents and with and without wind for different wave conditions were scheduled. Wave conditions included long crested waves and perpendicular, respectively oblique wave attack.

Acquired raw data are processed to determine the degree of dependence of wave run-up and wave overtopping on wind, current and oblique wave attack. Therefore the incoming wave parameters at the toe of the structure are measured for different variations of the influencing variables. Existent approaches and theoretical investigations will be used to verify and compare the data. Finally design formulae for freeboards of dikes are supposed to be developed or modified.

Status quo of the project work

This work is a preliminary report. It includes both test programs, model construction, instrumentation and short literature view, data processing for the reference test and first results of the analysis of the wave field, wave run-up and wave overtopping.

The analysis of the wave run-up is done for the three parameters of interest wave direction, wind and current for FlowDike 1 while the analysis for FlowDike 2 is in progress. The combined effect of wave direction and current is presented within this report but considering preliminary test results.

The wave overtopping is analyzed for both FlowDike 1 and FlowDike 2 for the three parameters of interest wave direction, wind and current. The combined effects are only done for the combination of wind and current.

It has to be mentioned that a more detailed analysis concerning the wave field, run-up heights and overtopping rates is obligatory in the next steps. The presented results in this report are preliminary.

2 Experimental procedure

2.1 Overview of test program

The test program covered model tests with and without current and with and without wind for normal and oblique wave attack. Three different angles of wave attack 0°, ±15°, ±30° and ±45° should be determined under conditions with and without current of 0.15 m/s and 0.3m/s and with and without wind of 5 m/s and 10 m/s. Six different long-crested waves using a Jonswap spectrum were applied. Table 2.1 presents a summary of the test program. Normal wave attack is defined with an angle of β = 0°. Positive angles of wave attack are in the direction of the current, while negative angles of wave attack are directed against the current. In whole 119 tests were performed on the 1:3 sloped dike and 152 tests were performed on the 1:6 sloped dike.

Table 2.1. Summary of the test program and test configurations

freeboard height R_C [m]	1:3 dike:0.10 and 0.20 1:6 dike:0.05 and 0.15						
wave spectrum	longcrested waves using a Jonswap spectrum						
wave height H_s [m] and wave period T_p [s]	1:3 dike:H_s	0.07	0.07	0.10	0.10	0.15	0.15
	T_P	1.474	1.045	1.76	1.243	2.156	1.529
	1:6 dike:H_s	0.09	0.09	0.12	0.12	0.15	0.15
	T_P	1.67	1.181	1.929	1.364	2.156	1.525
angle of wave attack β [°]	-45	-30	-15	0	+15	+30	
current v_x [m/s]	0.00	0.15	0.30	0.40 (only 1:6 dike)			
wind u (at the dike crest) [m/s]	0	5 (only 1:3 dike)		10			

2.2 Wave parameter

Generation and control of the wave maker was done by using the wave synthesizer. The wave spectra are defined by significant wave heights H_s and peak periods T_p. Each test series, defined by a constant water depth, wave direction, current velocity and wind velocity, contains a set of six tests using the Jonswap wave spectrum. These tests differ in three different wave heights and wave steepness´. These tests are covering the field of small (or no) overtopping to high overtopping rates.

Tests with the 1:3 sloped dike were conducted with a water depth of 0.50 m and waves characterized Table 2.2. In order to get a significant overtopping rate the water depth for the tests on the 1:6 sloped dike was changed during the test program between 0.50 m and 0.55 m applying both wave characteristics I (c.f. Table 2.2) and II (c.f. Table 2.3). The corresponding parameters like spectral wave length $L_{m-1,0}$, wave steepness $s_{m-1,0}$ and test duration for 1000 waves are given in Table 2.2 and Table 2.3 for both flow depths.

It is worth to mention that all tests are still comparable, because all analyzed data will be described in relation to incoming wave parameters and freeboard heights.

Table 2.2 Wave parameters of **wave characteristics I (wc I)**

wave no.	Hs [m]	Tp [s]	$T_{m-1,0} \approx \frac{T_p}{1.1}$ [s]	$L_{m-1,0} = \frac{g \cdot T_{m-1,0}}{2\pi} \cdot \tanh\left(\frac{2\pi}{L_{m-1,0}} \cdot d\right)$ [m]	$s_{m-1,0} = \frac{H_s}{L_{m-1,0}}$ [-]	duration for 1000 waves [min]

flow depth			-	0.50 m	0.55 m	0.50 m	0.55 m	-
w1	0.07	1.474	1.340	2.416	2.478	0.029	0.028	25
w2	0.07	1.045	0.950	1.379	1.390	0.051	0.050	18
w3	0.10	1.76	1.600	3.078	3.180	0.032	0.031	30
w4	0.10	1.243	1.130	1.862	1.893	0.054	0.053	21
w5	0.15	2.156	1.960	3.960	4.113	0.038	0.036	36
w6	0.15	1.529	1.390	2.545	2.614	0.059	0.057	26

Table 2.3 Wave parameters of **wave characteristics II (wc II)**

wave no.	Hs [m]	Tp [s]	$T_{m-1,0} \approx \frac{T_p}{1.1}$ [s]	$L_{m-1,0} = \frac{g \cdot T_{m-1,0}}{2\pi} \cdot \tanh\left(\frac{2\pi}{L_{m-1,0}} \cdot d\right)$ [m]		$s_{m-1,0} = \frac{H_s}{L_{m-1,0}}$ [-]		duration for 1000 waves [min]
flow depth			-	0.50 m	0.55 m	0.50 m	0.55 m	-
w1	0.09	1.670	1.518	2.873	2.962	0.031	0.030	28
w2	0.09	1.181	1.074	1.710	1.734	0.053	0.052	20
w3	0.12	1.929	1.754	3.459	3.581	0.035	0.033	33
w4	0.12	1.364	1.240	2.154	2.201	0.056	0.055	23
w5	0.15	2.156	1.960	3.960	4.113	0.038	0.036	36
w6	0.15	1.525	1.386	2.535	2.605	0.059	0.058	26

For efficient use of the test facility during testing time the dike was divided in two separate parts to measure wave run-up and wave overtopping simultaneously. The domain where the fully developed sea state reached the dike was limited by the length of the wave machine. In addition the influence of current and angle of wave attack restricted the section which was reliable for measurement of run-up and overtopping on the dike too. Therefore three different set-up configurations for each dike slope have been installed to cover the intended range of all angles of wave attack within the test program. Table 2.4 gives an overview of all six test set-ups. Detailed information for every test set-up is given in the Annex (Figure-annex 1 to Figure-annex 6).

Table 2.4 Definition of set-up numbers

angle of wave attack [°]	1:3 dike	**1:6 dike**
-15, 0, +15	set-up1	set-up4
+30	set-up2	set-up5
-30, -45	set-up3	set-up6

In case of more inclined wave direction ($\theta = -45°$) the wave run-up board was situated a little bit outside the part of the dike where the fully developed sea arrived. Moreover the almost diagonal up rushing waves could not develop their full run-up height because of the limited run-up board width. This will have to be considered during post processing and data analysis.

The recorded video films were serially numbered (see Annex J). The tables contain in addition the record date, set-up number and test series, the name of the file respectively the folder with the raw data as well as comments and remarks.

Some changes in test program took place between the FlowDike 1 (1:3 sloped dike) and FlowDike 2 (1:6 sloped dike) tests. On the one hand an additional current of 0.4 m/s was adapted in the second test phases, because they give another important item for the analysis. On the other hand, wind tests were done mainly for or wind velocity of 10 m/s (49 Hz) and barely for wind velocities of 5 m/s (25 Hz).

The following tables give a matrix of all performed tests on the 1:3 and 1:6 sloped dike respectively. Detailed tables with all tests listed with the test numbers are given in Annex E (1:3 sloped dike) and Annex F (1:6 sloped dike).

Table 2.5. Matrix of test configurations, 1:3 sloped dike

windtest is marked by a velocity [m/s] in the cell

carried out with wc I, flow depth 0.50 m

Current [m/s]	-45	-30	-15	0	+15	+30
0.40						
0.30				5 10		5 10
0.15						
0.00		5 10		5 10		5 10

Wave direction [°]

Table 2.6. Matrix of test configurations, 1:6 sloped dike

windtest is marked by a velocity [m/s] in the cell

carried out with wcI, flow depth 0.50 m

carried out with wcI, flow depth 0.55 m

Current [m/s]	-45	-30	-15	0	+15	+30
0.40						
0.30				5		
0.15						
0.00				5 10		

Wave direction [°]

windtest is marked by a velocity [m/s] in the cell

carried out with wcII, flow depth 0.55 m

Current [m/s]	-45	-30	-15	0	+15	+30
0.40				10		10
0.30				10		10
0.15				10		
0.00		10		10		10

Wave direction [°]

2.3 Short overview of the data storage management

For each test of a test series a process file (*.xls) is generated. One process file includes i.e. the graphics for the spectral energy density, wave height distribution, as well as some exceedance curves for flow velocities and layer thickness. In chapter 6 the preliminary results of the processed data will be explained by means of test s1_01_00_w1_00_00 (reference test on the 1:3 sloped dike).

The filename includes the main information, such as set-up number, test series, current, wave spectra, wind speed and angle of wave attack. A template for all test series would be: set-up no_Test series no_current [cm/s]_wave spectra [i=1…6]_wind Hz]_ angle of wave attack.
For example the first test series from FlowDike 1 is named: s1_01_00_wi_00_00. The term for angle of wave attack was changed from "-" to "m" and from "+" to "p" within the system due to the fact that problems occurred during the data processing.

3 Model construction and instrumentation

3.1 Configuration

3.1.1 General remarks

This chapter describes the details of the facility that remained the same for both model configurations. It also includes a detailed specification of the dimensions and main constructive parts of each set-up configuration. Therefore it starts with the description of the 1:3 sloped dike, which is followed by the details for the 1:6 sloped configuration. A plan view of the different set-ups is given in the Annex.

3.1.2 Details of facility - Basin, Wave generator, Weir, Wind generator, Data acquisition

Basin, Wave generator

The facility provided by the DHI in Hørsholm (Denmark) is a shallow water wave basin. It has a length of 35 m, a width of 25 m and can be flooded to a maximum water depth of 0.9 m. Along the east side (35 m in length) the basin is equipped with a 18 m long multidirectional wave maker composed of 36-segments (paddles) (see Figure 3.1). The 0.5 m wide and 1.2 m high segments can be programd to generate multidirectional, long or short crested waves. Dynamic wave absorption is integrated in the DHI wave generation software by an automatic control system called AWACS (Active Wave Absorption Control System). This system uses the signal of separate wave gauges per paddle, to receive the actual wave height to identify and absorb the reflected waves. For further absorption of reflection and diffraction effects gravel and metallic wave absorbers were placed on the upstream and downstream edges of the dike (see Figure 3.2).

During FlowDike 1 problems with the AWACS occurred for some test with wave spectra w5 and w6. In FlowDike 2 the absorption was turned off all along, otherwise the wave generation was impossible, since the wave generator would have stopped during testing. The reason for this is not known yet.

Figure 3.1 Completed dike slope (view from downstream), wave generator (paddles) and wind generator (fans) on the left side.

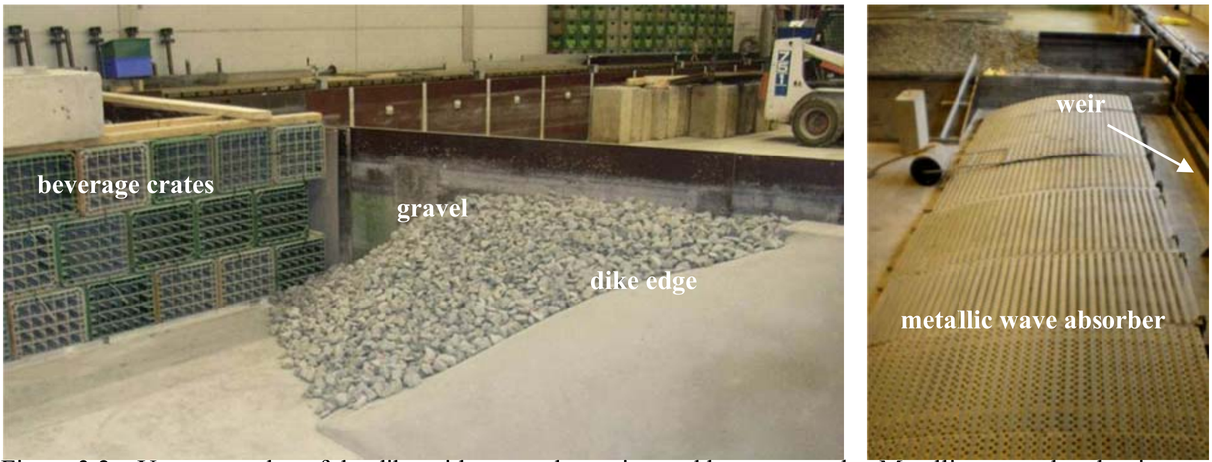

Figure 3.2 Upstream edge of the dike with wave absorption and beverage racks; Metallic wave absorber in front of the weir

Weir and flow calming

For FlowDike 1 parallel current and constant water depth of 0.5 m were controlled by the flow capacity of the basin pump and an adjustable weir at the downstream edge of the basin. This weir had a length of 7.9 m and was adjusted by means of a long metal plate that could be adjusted in height.

Changes in weir adjustment were made, so for FlowDike 2 it was divided by metal stands into six subdivisions of 1.1 m. In the sections, between the stands, wooden parts for the exact height could be inserted. They were placed beneath the parts with a shorter, but still movable, metal plate. These changes facilitated the weir readjustment. All currents were set for the correspondng water depth and controlled again with the flow capacity.

To provide aligned streamlines within the channel three rows of beverage crates were used as shown in Figure 3.2 to straighten the inflow.

Wind generator

The wind field could be generated by six wind machines placed on metal stands (80 cm above the basin floor) in front of the wave generator. Therefore two different frequencies were set to produce a homogenous wind field with an assumed mean velocity of 10 m/s (49 Hz) and a lower one of 5 m/s (25 Hz).

Data acquisition

Only a constant water temperature which is important for the calibration of all wave gauges and especially for the absorption system of the wave generator could be accepted for the accuracy of the tests. Therefore changes of water temperature during the beginning of a tests series with flow induced current was measured.

Data storage was simplified by using the DHI Wave Synthesizer. A sampling frequency of 25 Hz was used during the first investigation phase of FlowDike 1 to include all instrument-signals. This frequency was changed to 40 Hz for the test performed in FlowDike 2, due to the resolution of the pressure sensors which only work with 40 Hz. All acquired data were stored in .dfs0- and *.daf-files. A .dfs0-file stores the frequency of the data storage and all desired signals in a readable format for the Wave Synthesizer from MikeZero, while a *.daf-file (Digital Anchor File) stores the same information in a table format. The calibration could easily be made for all instruments connected to an amplifier, such as wave gauges, load cells, micro propeller and pressure sensors. After installation of all measurement devices the whole basin was flooded. Therefore the data acquisition, amplifier, computer and spotlights, which were situated behind the dike, needed to be placed on platforms. An overall view of the data acquisition for the second investigation period is illustrated by Figure 3.3.

Figure 3.3 Platform with data acquisition; Stand with amplifier and A/D converter

3.1.3 Construction of 1:3 dike – FlowDike 1

The toe of the 1:3 sloped dike was situated at a distance of 6.5 m and the SWL at a distance of 8.0 m from the initial position of the wave maker. The structure had a length over all of 26.5 m. This length depended on the allowable measuring sections for all wave directions of interest (see Annex Figure-annex 1 to Figure-annex 3); thus for the investigations on current and wind influence a homogeneous wave field in front of the dike was necessary. The backside and crest of the dike are brick-built with a width of 0.28 m and its core was out of compacted gravel covered with a 50 mm concreted layer.

In order to acquire wave overtopping data for freeboard heights of 0.1 m and 0.2 m the dike is divided in two sections. The first 15 m upstream from the weir have a crest height of 60 cm and 11.5 m further up the crest level is 70 cm from the basin floor. In Figure 3.4 a variable crest is visualized that extend the 70 cm crest 7 m downstream. This additional part out of plywood is used to change the set-up configuration during the test program. To prevent different roughness coefficients on the variable crest, the run-up plate and in the gap between the concrete and plywood parts a polish with sand was used.

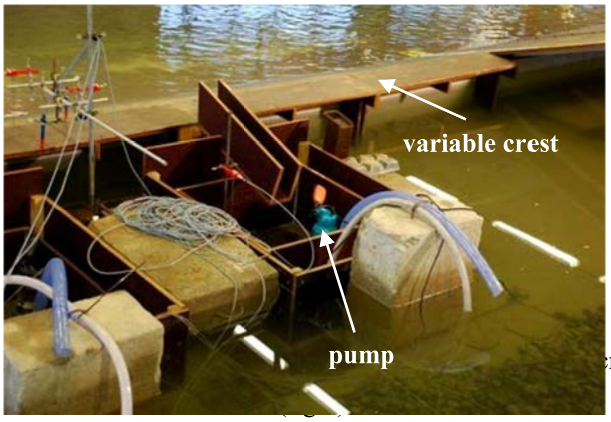

A cross-section for the wave overtopping unit is given in Figure 3.5. For sampling the overtopping water a plywood channel was mounted at the landward edge of the crest to lead the incoming water directly into one of the four overtopping tanks. There were two tanks per section (60 cm and 70 cm crest) and the amount of water was measured by the load cells and wave gauges of each tank. Standard garden pumps were used to empty the tanks during testing, see also the description in chapter 3.2.8. Dry boxes (also named outer boxes) were constructed to contain the overtopping tanks, load cells and wave gauges and prevent these devices from uplift. The outer boxes had to be charged with concrete blocks to prevent themselves from uplift when the basin is flooded.

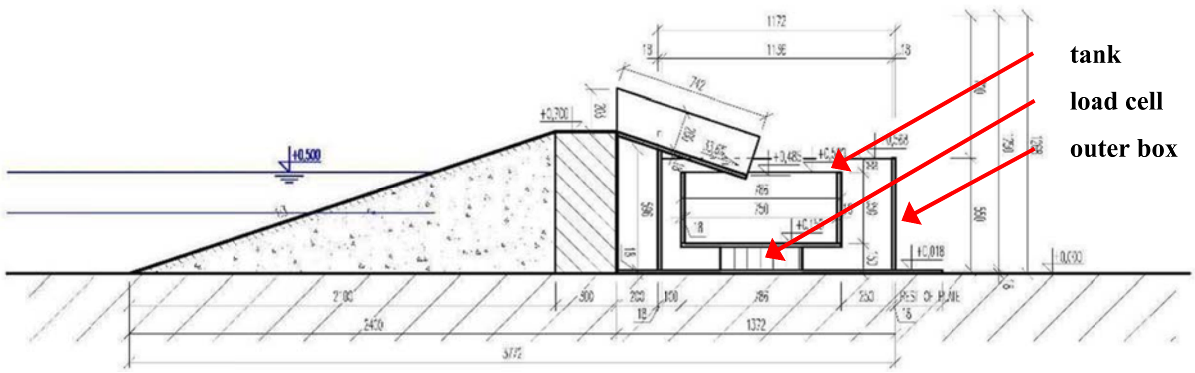

Figure 3.5 Cross section of overtopping unit for the 70 cm crest

For the wave run-up a “run-up board” out of plywood (2 m x 2.5 m) was mounted on the concrete crest to facilitate the up rush measurement by a capacity gauge and video analysis. This plate could be moved easily in its position during the changes of set-ups. The gap between run-up board and crest edge was filled either with a wooden piece and silicone or with a cement cover.

To get films with a better contrast the wave run-up board was enlightened by a 2000-W-spotlight which was positioned such as the light met the run-up plate within an angle of 120° to the optical axis of the digital cameras. On the left side of the run-up plate a digital radio controlled clock with a 0.4 m x 0.4 m display was positioned due to the purpose of synchronizing the measurements (Figure 3.6).

Figure 3.6 Wave run-up plate and rack with both digital cameras (left); Capacitive gauge, clock and scale (right)

In addition step gauges were inserted in the 70 cm crest part with a distance of 2.2 m between each other. Regarding their short length only an up rush and not the full run-up can be measured and was not analyzed yet. The different devices are illustrated in Figure 3.7. The digital signals which came out of the A/D-converter of the capacitive gauge and the step gauges was transmitted to the data collection unit and stored together with the signals of the other measurement equipment.

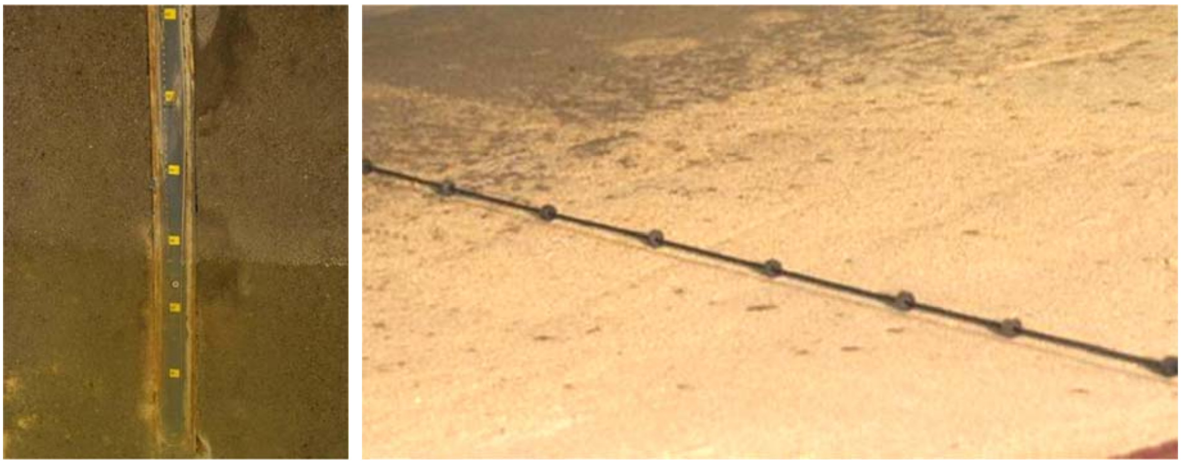

Figure 3.7 Digital step gauge within the 70 cm slope (left); Capacitive wave run-up gauge on the dike slope (right)

3.1.4 Construction of 1:6 dike – FlowDike 2

Compared to the set-up of the first investigations of FlowDike 1 (1:3 sloped dike) the dimensions and some details changed for FlowDike 2. Overtopping units, run-up board and variable crest remained mostly in the same shape or could even be reused. The former inserted step gauges have not been installed during the second investigation period. As a new device, pressure sensors were added to the list of instruments and their positioning had to be taken into consideration during the model configuration.

In order to keep the Still Water Level (SWL) at the same position at 8.0 m from the wave maker, such as during the FlowDike 1 tests, the toe of the 1:6 dike should have been situated at a distance of 5.0 m from the wave maker. Due to the flatter slope of 1:6, the bottom width of the dike from the crest to the toe of the structure increased from 2.10 m to 4.20 m for the 70 cm crest section and from 1.80 m to 3.60 m for the 60 cm section.

With regard to construction failures while positioning the structures the channel width or distance between the toe of the structure and the wave maker decreased. The brick built crest was build 0.6 m closer to the wave maker, so the channel width became 4.40 m instead of 5.0 m and the SWL was situated at 7.40 m from the initial wave maker position. The length of the dike remained 26.5 m depending on the allowable measuring areas for the different wave directions.

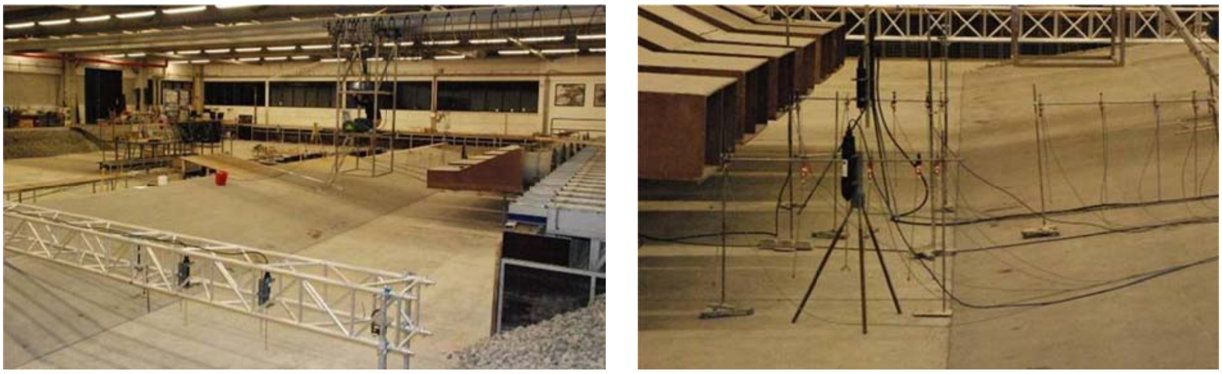

Figure 3.8 View from the upstream inlet of the 1:6 dike set-up, wind machines and wave gauges in front of the dike

The core of the dike was kept out of compacted gravel covered with 50 mm concrete and the backside and crest of the dike remained with a width of 0.28 m. Only for the newly inserted pressure sensors three gaps were left out in the wall in between the positions for both overtopping channels per crest. In these gaps small plywood boxes with a sand covered top of circa 30 cm x 20 cm have been fitted. For mounting the pressure sensors two holes were drilled within a distance of 24 cm in their lid as Figure 3.9 demonstrates.

Figure 3.9 Plywood boxes and drilled holes for pressure cells

As the essentials of the set-up and test program have not changed, i.e. two different freeboard heights (0.1 m and 0.2 m) and positions for run-up board and overtopping units, both investigations should be quite comparable. At this point it has to be mentioned, that the increase of the water level to 0.55 m after the firsts test, affected the set-up configuration only for the position of the SWL. After the increase the SWL was at 7.70 m instead of 7.40 m from the wave maker and additionally the freeboard height decreased to 0.05 m and 0.15 m, which has to be taken into account for the analysis.

3.2 Instrumentation

3.2.1 Remarks

This chapter explains the application of the measurement devices in the previously described model configurations. It is structured in seven subsections each of them dealing with one main topic concerning the data acquisition for the following analysis.

During the second phase of investigations (1:6 dike) additional devices were used or former instruments have been left out, compared to the set-up of FlowDike 1. Every subdivision starts with the general instrumentation for the 1:3 sloped dike followed by the changes made for FlowDike 2.

3.2.2 Measurement devices

For analysis of wind and current influence on wave run-up and wave overtopping in long crested sea state, the alphabetic listed measurement devices below were installed in the basin and on the dike. Better overall views of the placement of measurement devices for both model configurations are given in Figure 3.10 for FlowDike 1 and Figure 3.11 for FlowDike 2.

The drawings give a plan view of the basin with a flow direction of the current (blue arrows) from left to right. The light yellow bars indicate the acceptable measuring area for the set parameters of perpendicular or angled wave attack with and without currents.

At the lower side of the drawing the wind and wave generator are situated. Approximately 2 m further upstream, the beam with two current meters and two micro propellers is indicated. Within the channel two or three wave arrays (FlowDike 2) are displayed in the figure. Each wave gauge array consists of five wave gauges and one velocity meter. For the run up measurements a run up board with the mounted capacitive gauge is situated within the allowable measuring range for perpendicular wave attack with and without currents. The two step gauges are showed in their position in the slope of the 70 cm crest, but only for the FlowDike 1 set-up. On each crest two overtopping units are placed as depicted in the sketch. Between the inlet channels of these units, the instruments for flow velocity and flow depth measurement are marked.

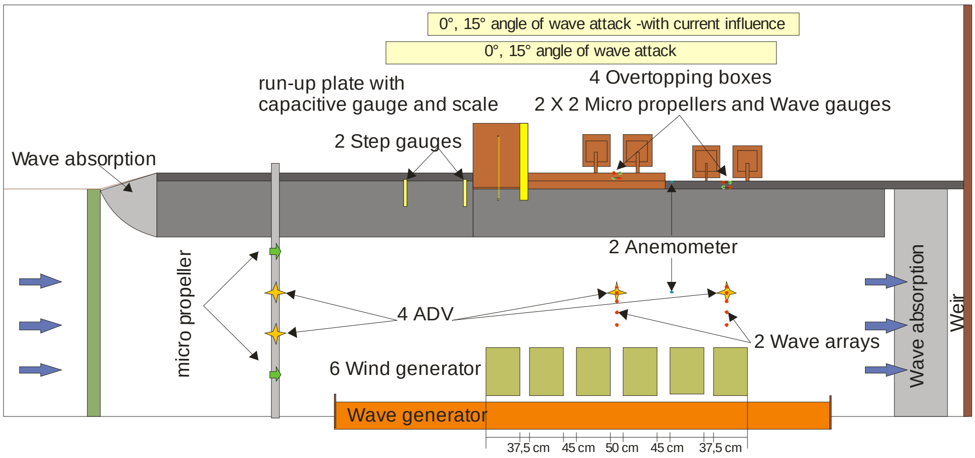

Figure 3.10 Model set-up 1 (FlowDike 1) with instruments and flow direction (1:3 sloped dike)

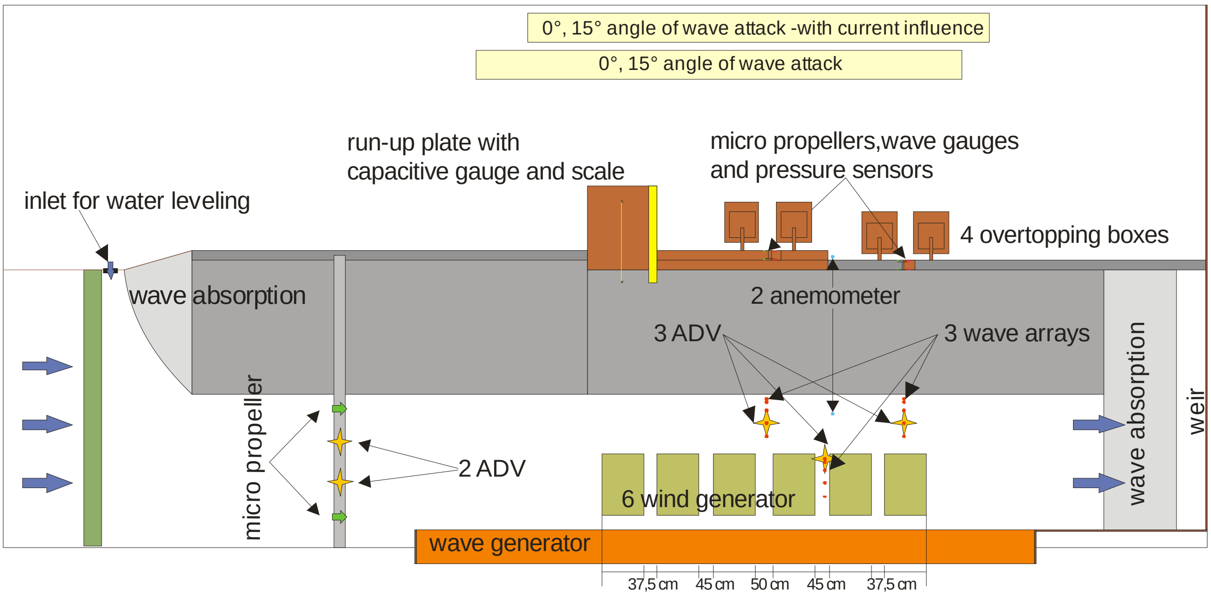

Figure 3.11 Model set-up 4 (FlowDike 2) with instruments and flow direction (1:6 sloped dike)

Instruments:

- Anemometer (TSI):

Two anemometers for wind measurement provided by DHI were installed in the set up. These thin transducers with a small window for the sensor are able to record a range of 0 V – 10 V (0 m/s – 20 m/s) with a frequency of 5 Hz.

- Capacitive gauge:

As schematically shown in Figure 3.22 the required equipment contained a submerged capacitor, a transducer and an A/D-converter. The two electrodes of the capacitor were formed by one isolated and one non isolated wire each 3.5 m long. They were mounted on the run-up plate orthogonally to the dike base. The lower end was fixed about 0.25 m above the bed which is equal to 0.25 below still-water-level (SWL). The upper end was fitted to the highest point of the run-up plate. Thus it is possible to measure both the wave run-up and the run-down. To avoid a water film between the two electrodes after a wave runs down several rubber band spacers assure a minimum distance of about 5 mm between the two wires.

Air or water between the two wires forms the dielectric fluid. Water has a permittivity which is 80 times greater than the permittivity of the air. The variation of the water level produces a measurable variation of the electrical value of the capacitor. The transducer allows loading and unloading the capacitor 25 times per second which is equal to a measurement frequency of 25 Hz. Each value of the time constant τ of the capacitor would be transmitted to the A/D-converter as a voltage value. The scale of the voltage value ranged from 0 V to 5 V.

The capacitive gauge was non-sensitive to environmental conditions like changes in water temperature. The calibration was conducted only one time before the test start. Therefore three tests with regularly waves with a mean wave height of of $\overline{H}$ = 0.1 m, 0.15 m and 0.2 m were run. The calibrated equation depends on the model set-up especially on the wire length and the mounting height. That is why the calibration has to be repeated for each model set-up.

- Cameras:

For FlowDike 1 one digital camera was a compact, professional USB 2.0 camera from VRmagic GmbH which is suitable for industrial purposes. The used model VRmC-3 + PRO contained a 1/3 inch-CMOS-sensor which could record up to 69 frames per second. The picture resolution of 754 x 482 pixels was adequate for measurement purposes in the model tests presented herein. The other digital camera was a SONY Camcorder (Model: DCR-TRV900E PAL), with a 3CCD (Charge Coupled Device, ¼ inch). The objective had a focal distance between 4.3 and 51.6 mm and a 12 x optical zoom.

In FlowDike 2 both cameras were replaced with two others, which have a better resolution. Since the image-processing algorithm works with grey-level images, one color camera was replaced with a more powerful monochrome camera (1/2“ Progressive-scan-CCD sensor JAI CM-140 GE of Stemmer Imaging). Its resolution of 1392 x 1040 pixels allows to produce pictures with a precision of 0.5 mm for the wave run-up. The second camera (a color area scan camera) was used for documentation purpose only. It had the same features like the monochrome one but the output-files are tree times greater (about 2.6 GB/min). The same objectives as in FlowDike 1 were reused.

- Current meter (Acoustic Doppler Velocity meter (ADV), Minilab SD-12, Vectrino):

Both, ADV's and Vectrino, are a single point, Doppler current meters. Each of them has one ultrasound transmitter and three or even four receivers (ADV/ Vectrino). The current velocity is measured using the Doppler Effect, that is, the shift of the frequency received with respect to the frequency transmitted when the source is moving relative to the receiver. The transmitter generates a short pulse of sound at a known frequency. The energy of the pulse passes through the so-called sampling volume (a small volume of water in which measurements are taken). Part of this energy is reflected by suspended matter along the axis of the receiver, where it is sampled by the velocity meter, whose electronics detect the shift in frequency. According to this, to obtain measurements with a velocity meter based on the Doppler Effect, the presence of suspended matter is necessary for an accurate reflection of the pulse. The sampling volume was set to 25 Hz and a nominal velocity range of ±100 cm/s.

The Minilab SD-12 is an ultrasonic current meter. It contains a transducer, a reflector and four receivers that measure the velocity from time difference between the send and received signal. The resolution of this current meter is 1 mm/s.

- Load cell:

The cubic shaped weighing scale has a height of 10 cm and can be mounted to beneath the overtopping tank. They were used to measure the amounts of overtopping water. It is measuring in all 3 directions, but only the z-component with a maximum capacity of 2150 N (≈ 220 kg), was used. Due to its accuracy, it was used for single event detection and oscillations in x and y directions were assumed to be negligible. Therefore it had to be calibrated every day with an occurrence of 20 kg per 1 Volt.

- Micro propeller (Schiltknecht):

Schildknecht micro propellers are based on the concept of an impeller. The rotations of the fan wheel will be measured and transformed to an output signal in Volt.

MiniWater 20 - FlowDike 1:

The measuring range of MiniWater20 Micro lies within 0.04 m/s - 5 m/s and their accuracy is 2% of the full scale. The calibration of the micro propeller was done by the partner from Braunschweig (LWI) before using them in the Hydralab project. They evaluated for each of them its specified calibration curve containing the measured voltage for defined velocities within their flume (see Figure annex 7 in the Annex).

MiniWater 6 - FlowDike 2:

The MiniWater 6 Micro has a measuring range of 0.04 m/s – 5 m/s with a full scale accuracy of 2%. For the 1:6 sloped dike these new type of micro propeller were bought and calibrated at the DHI. Due to its low voltage output for the signal, it had to be gained up first through an amplifier. Then the calibration was done in the set-up by recording the Voltage for certain defined flow velocities in a circular flow (see calibration curves in the Annex Figure-annex 8).

- Pressure sensors:

The water resistant pressure sensors have a threaded "head" that was inserted flush to the top of the lid. A small air filled pipe secured that the pressure module stayed water tight within their welded body. Therefore it had to be assured, that the end of this pipe never submerged. The measuring range of the pressure sensors is 25 mV for 0.75 m water column. The voltage outputs for a constant calibration of 10 cm per 1 Volt worked within a full scale accuracy of +/- 0.1%.

- Step gauges:

The step gauges have a total length of 1 m and include 4 successive parts with 24 electrodes and a continuous wire. Wave run-up is measured by a signal when a short cut is caused between electrode and wire. A constant distance between the pins of 1 cm gives for a slope of 1:3 a vertical precision of 0.32 cm. This device was only applied during FlowDike 1 and has not been evaluated yet.

- Wave gauges:

The water surface elevation and the flow depth on the crest were determined by wave gauges as a change of conductivity between two thin, parallel stainless steel electrodes. The conductivity changes proportionally to changes in the surface elevation of the water between the electrodes. An analogue output is taken from the Wave Meter conditioning module, where the wave gauge is connected to, and compiled in the data acquisition system.

Calibration should be done for a constant water temperature and has to be repeated if it deviates more than 0.5°C. Hereby a calibration factor of 10 cm per 1 Volt was used. The calibration factor for the small wave gauges on the crest was 10 cm per 0.5 Volt during FlowDike 1 and 10 cm per 1 Volt for FlowDike 2.

3.2.3 Wave Field (Wave gauges, ADV)

FlowDike 1

The data readings for wave field analysis on incident and reflected waves and the directional spreading contained both surface elevation and velocity. These signals were determined by two wave arrays of 5 wave gauges (with a length of 60 cm each) and a current meter. An overall view given in Figure 3.12 demonstrates that each of them is orthogonal aligned between the wave machine and the overtopping unity per dike crest. Each array was assigned to one crest height and placed at the toe of the structure positioned between the overtopping channels.

Figure 3.12 Overview of the basin: Wind machines; Wave array, Anemometer; Dike and overtopping unities

For the following reflection analysis a defined alignment of 0.00 m– 0.40 m– 0.75 m– 1.00 m– 1.10 m was kept for the single wave gauges. Both, ADV and Minilab SD-12 are positioned close to one wave gauge of the array (see

Figure 3.13). The simultaneously measured surface elevation and velocity in this point will be used for the directional spreading analysis. Reflection, crossing and directional analysis will be evaluated from each array and its defined velocity meter.

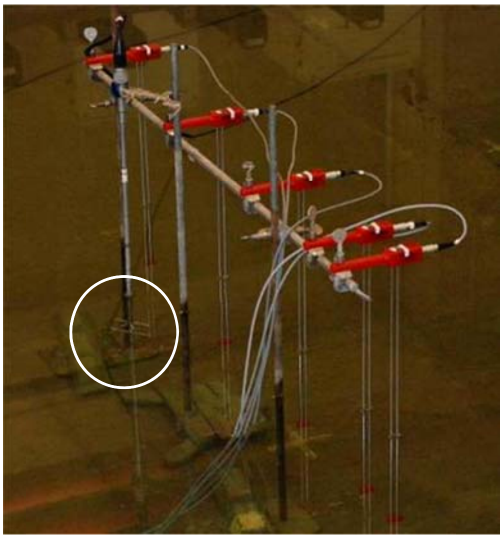

Figure 3.13 Wave gauge array with minilab SD-12 (encircled)

FlowDike 2

An additional interest during FlowDike 2 was to determine the development of the wave field due to current affection. This was taken into account by adding a third wave array, which was placed in front of the wave maker. Both other arrays were situated as close as possible to the toe of the structure. Each of them was assigned to one of the crests and aligned between the channels of the overtopping units. In order to distinguish the effect of the current on the directional change of the wave field a distance of 1.12 m was kept between the two wave arrays at the toe of the structure and the one near the wave maker. For the directional analysis of this third wave gauge array an additional current meter was needed; this is why the Vectrino was used in FlowDike 2.

3.2.4 Wind Field (Wind machine, Anemometer)

FlowDike 1

The wind field, focused onto the dike, was generated by six wind machines using a wind turbine. Each of them was controlled by the frequency adjustment of revolutions for the rotator and performs a conus as wind field. In order to create a homogeneous wind field the distances between the six wind machines are different (37.5 cm - 45 cm - 50 cm - 45 cm - 37.5 cm) and were determined in some preliminary tests (see annex Figure-annex 1 to Figure-annex 3).

Two anemometers for velocity measurements provided by DHI were installed in the set up (see in the annex Figure-annex 1 to Figure-annex 3). One was situated 2m in front of the dike toe and the second was placed above the crest. Both measured within a height of 1m above the basin ground, just in the middle between the overtopping unities for each crest as shown in Figure 3.14.

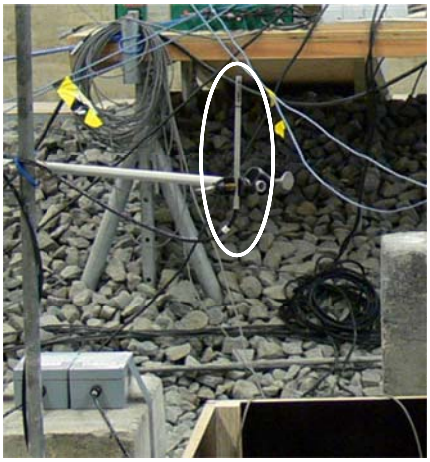

Figure 3.14 Anemometer (left) and fan wheel for air velocity measurement (right)

To prove the homogeneous distributed wind field along the dike, the wind velocity for two different frequencies was measured with a fan wheel (see Figure 3.14) in defined distances on the dike crest before testing. Reflection effects induced by the water surface and parallel flow from adjacent generators were observed by an increase of the velocity range. In Figure 3.15 and Figure 3.16 the results for a frequency of 49 Hz and 25 Hz are plotted along the crest of the 1:3 dike.

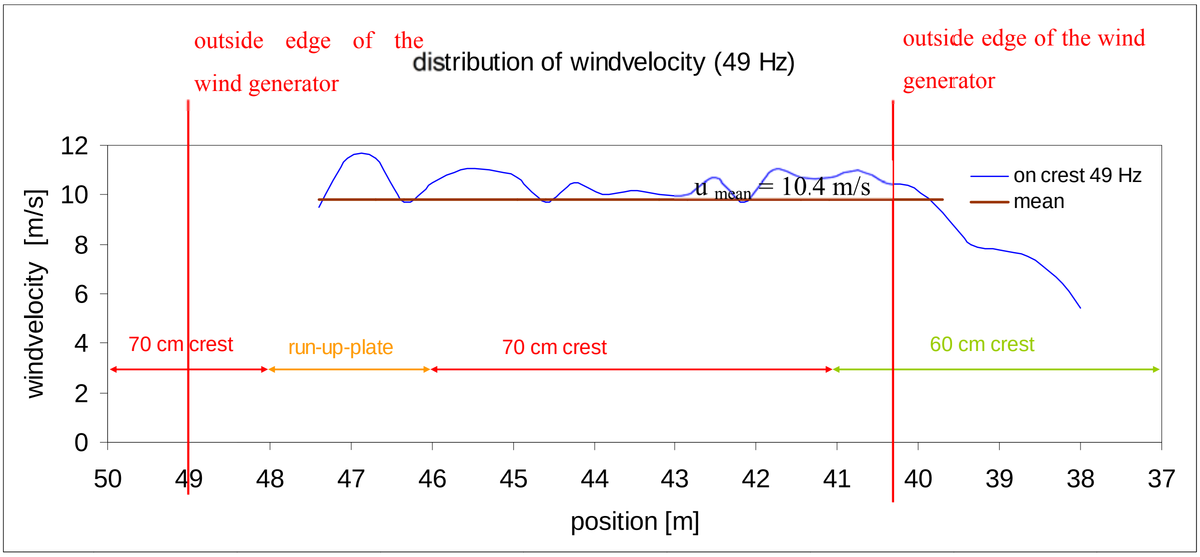

Figure 3.15 Wind velocity distribution for a frequency of 49 Hz (FlowDike 1)

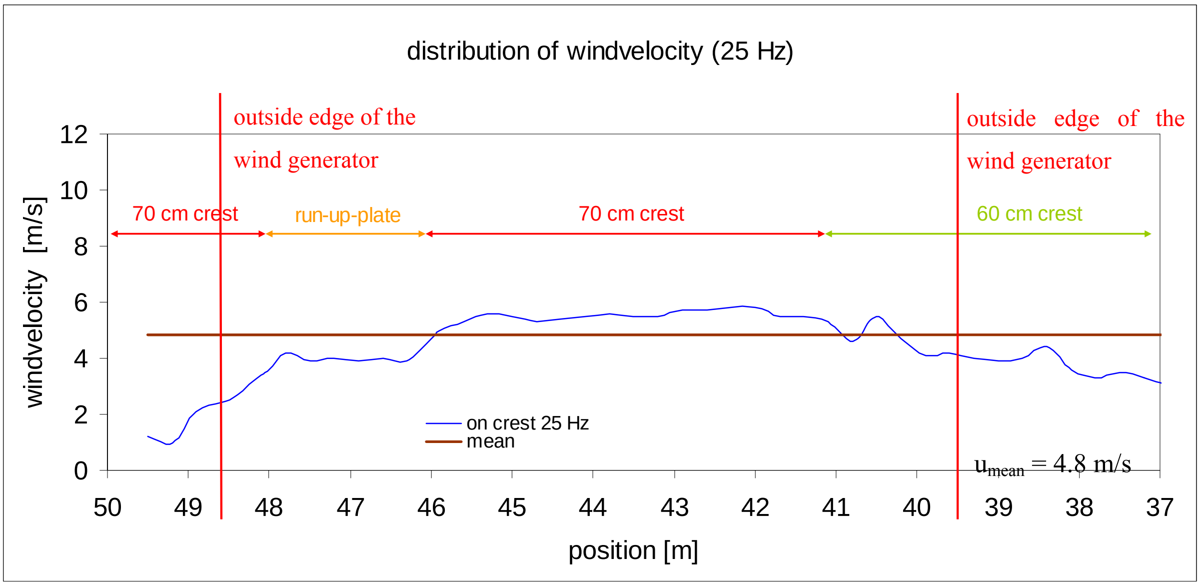

Figure 3.16 Wind velocity distribution for a frequency of 25 Hz (FlowDike 1)

FlowDike 2

The alignment of the wind machines did not change compared to the set-up of the 1:3 dike. Here the average wind velocity was slightly lower than for the 1:3 dike, but still homogeneously distributed. Only the larger distance between the wind generator and the dike crest lead to a wind velocity of 8 m/s and 4m/s on the crest. Furthermore, the anemometer in the channel had to be moved closer to the blower, due to the narrow spacing between dike toe and wind machine. The results for the measurements on the crest of the 1:6 dike are illustrated in Figure 3.17 and Figure 3.18. For both models, wind velocity is assumed to be 10 m/s respectively 5 m/s in the following analysis.

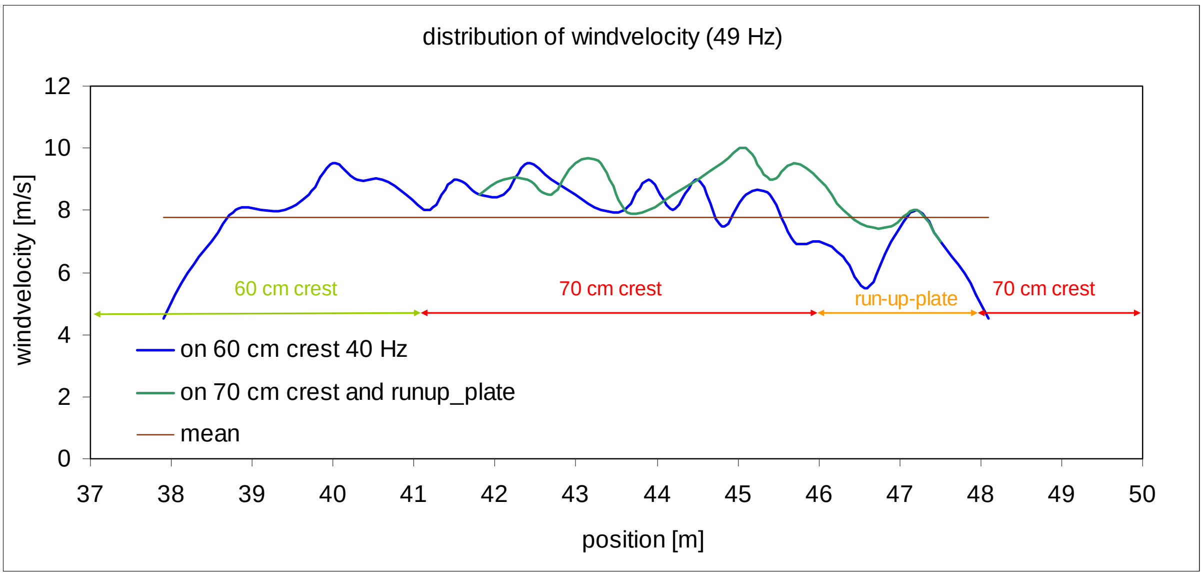

Figure 3.17 Wind velocity distribution for a frequency of 49 Hz (FlowDike 2)

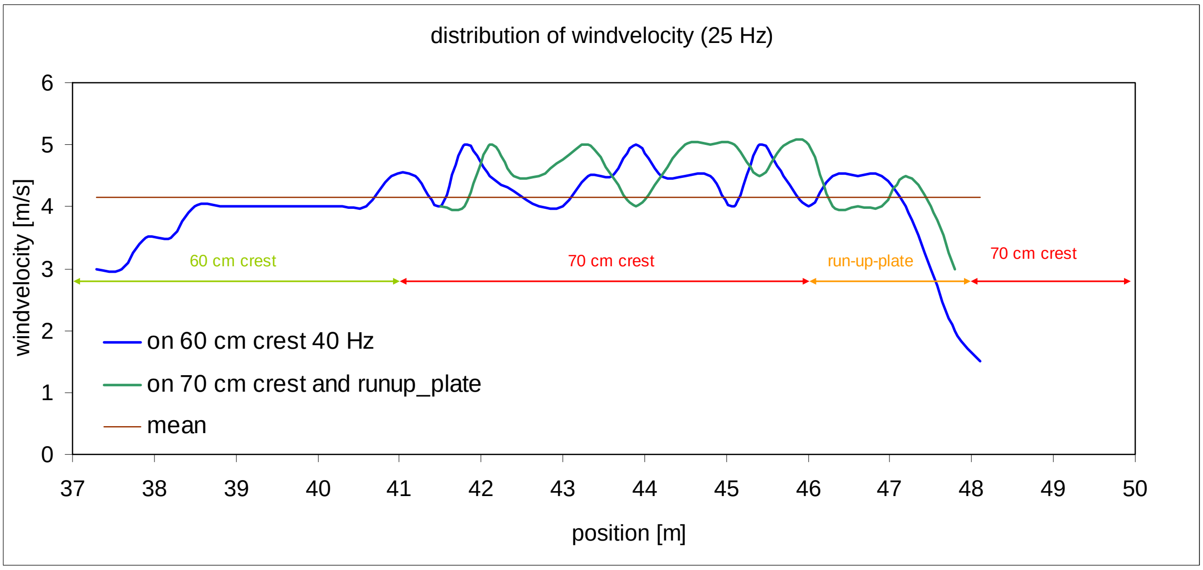

Figure 3.18 Wind velocity distribution for a frequency of 25 Hz (FlowDike 2)

3.2.5 Current (Weir, ADV, Micro propeller)

FlowDike 1

For constant water depth of 0.5 m within the channel a stabilized current of approximately 0.3 m/s was achievable with the maximum pump capacity of 1.12 m^3/s. This limited the range for applicable currents and only a second one was chosen for the data set. This current was taken to be 0.15 m/s. Here, the pump capacity needed to be reduced to 0.6 m^3/s and the weir changed in its height from 32.16 cm to 38.66 cm above the ground.

Current velocities were controlled with two ADV's and two big micro propellers. All these devices were fixed on a beam, which was situated 2 m before the upstream edge of the wave machine (Figure 3.19). The velocity was measured at 1/3 below the water surface (circa 33 cm from the bottom) where an average velocity within the depth profile is assumed. Both ADV's were placed in a distance of 2 m and 3.5 m from the dike toe. For a better knowledge of the velocity distribution in the cross section two micro propellers were installed additionally, within a distance of 1.5 m, besides the ADV's.

Figure 3.19 Beam upstream the wave machine; ADV; Micro propeller (FlowDike 1)

FlowDike 2

The current control did not change a lot from the latest investigations in FlowDike 1. The beam sustaining all mounted current devices was installed at the same position of 55 m in the basin (2 m further upstream than the wave maker). However, the distances between the instruments and from the dike toe were reduced because of the restriction in channel width. Their positions are listed below in Figure 3.20

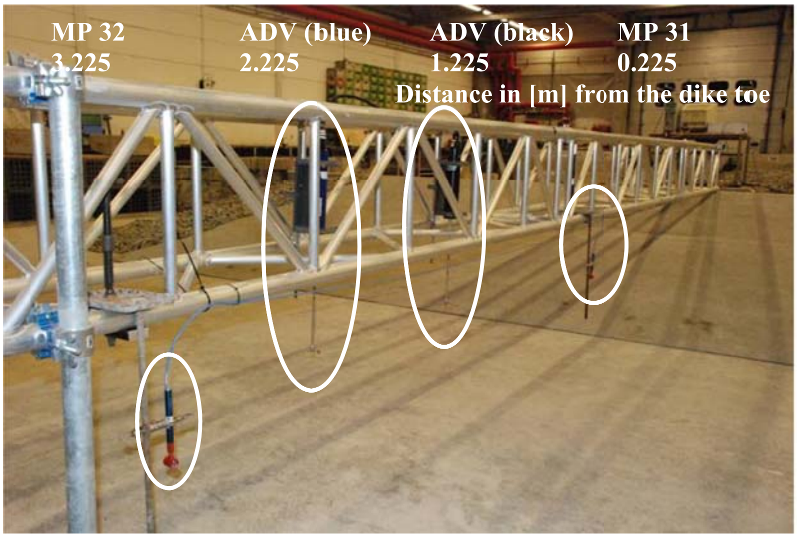

Figure 3.20 Beam upstream the wave machine with current devices (FlowDike 2)

The measuring point within the velocity profile did not change. For a better comparability and with regards to the above stated assumptions, the sampling volumes were kept at a position of approximately 33 cm from the bottom of the channel (like in FlowDike 1).

Due to the narrower channel a new maximum current of 0.40 m/s could be adjusted for the constant water level of 0.55 m. Therefore a weir height of 33.7 cm and a pump capacity of 1.1 m³/s were used. The mean velocity of 0.3 m/s was controlled with a discharge of 0.83 m³/s and a weir height of

38.2 cm. A current of 0.15 m/s was still induced for the comparison of some test series, although the influence was assumed to be negligible from the elder analysis. Here fore the weir was positioned at 44.2 cm from the bottom for a capacity of 0.43 m³/s.

At the beginning of each test day, the velocity measurements of all probes were recorded when the current was stabilised. If the average of the mean values did not deviate more than 5 cm/s from each other, the current was assumed to be correct.

3.2.6 Run-up (Capacitive gauge, Camera, Step gauge)

3.2.6.1 Wave run-up plate

FlowDike 1

The dike height of 0.6 m and 0.7 m was chosen to measure wave overtopping. For wave run-up measurements the dike was to low.

Therefore a 2 m wide and 2.5 m long ply wood plate was installed as an extension of the dike slope (Figure 3.21). Its surface was covered with sand which was fixed by means of shellac to provide a similar surface roughness as of concrete slope.

The capacitive gauge was mounted in the middle of the run-up-plate. At the right side an adhesive tape with a black and yellow pattern was put on as the gauge board. The gauge board had two different scales. The original scale with its 1 cm long sections showed the oblique wave run-up height. The distances at the second scale were multiplied with $10^{0.5}$ and represented the vertical run-up height.

Figure 3.21 Wave run-up plate and rack with both digital cameras

To get films with a better contrast the wave run-up board was enlightened by a 2000 W-spotlight which was positioned such as the light met the run-up plate within an angle of 120 ° to the optical axis of the digital cameras.

For the purpose of synchronizing all measurements a digital radio controlled clock with a 0.4 x 0.4 m display was positioned on the left side of the run-up plate (Figure 3.21).

FlowDike 2

The run-up board was reused after cutting the legs to achieve the slope inclination of 1:6, thus a new scale had to be pasted onto it.

3.2.6.2 Wave run-up gauge

FlowDike 1 and FlowDike 2

The wave run-up height was measured using a capacitive gauge. As schematically shown in Figure 3.22 the required equipment contained a submerged capacitor, a transducer and an A/D-converter.

The two electrodes of the capacitor (Figure 3.23) were formed by one isolated and one non isolated wires each 3.5 m long. They were mounted on the run-up plate orthogonally to the dike base. One end was installed about 0.25 m above the bed which is equal to 0.25 m below still-water-level (SWL). The other end was fitted at the highest point of the run-up plate. Thus it is possible to measure both the wave run-up and the run-down. To avoid a water film between the two electrodes after a wave runs down several rubber bands assure a constant distance of about 5 mm between the two wires.

The air or the water between the two wires is the dielectric fluid. Because the permittivity of water is 80 times greater than that of air, the variation of the water level produces a measurable variation of the electrical value of the capacitor.

The transducer allows loading and unloading the capacitor 25 times per second which is equal to a measurement frequency of 25 Hz. Each value of the time constant of the capacitor τ would be transmitted to the A/D-converter as a voltage value. The scale of the voltage value ranged from 0 V to 5 V. The digital signal which came out of the A/D-converter would be transmitted to the data collection unit and put in storage together with the signals of the other measurement equipment.

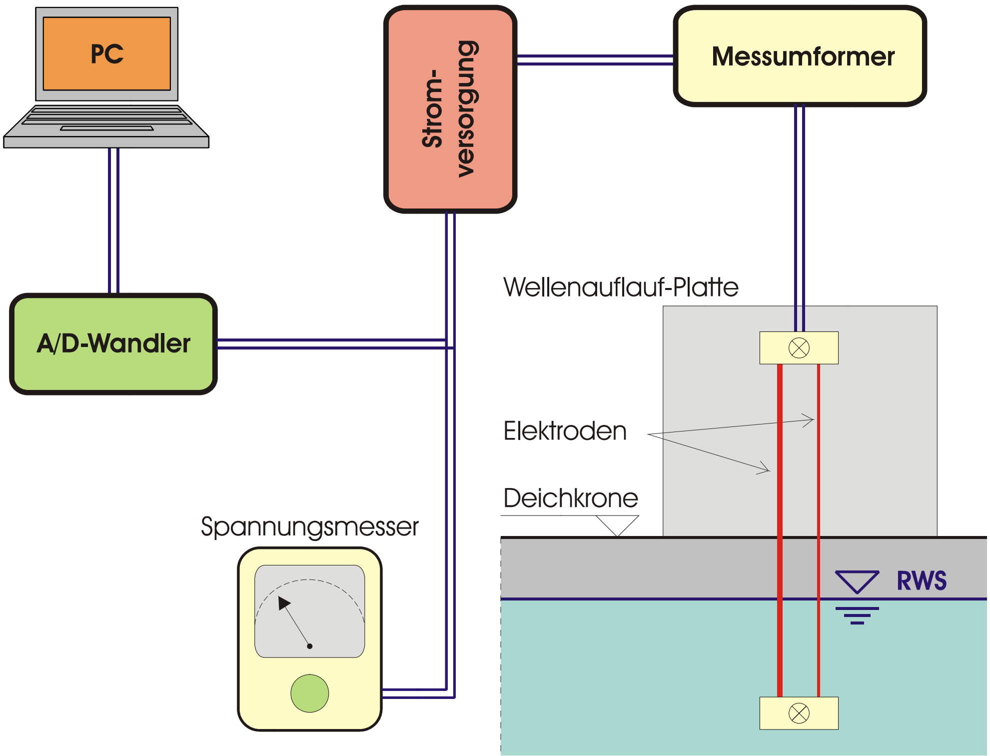

Figure 3.22: Schema of data collecting using the capacitive wave run-up gauge

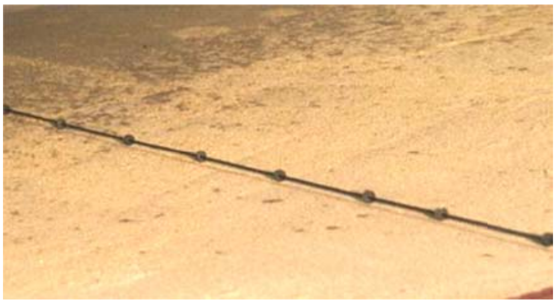

Figure 3.23: Capacitive wave run-up gauge on the dike slope– detailed view with the two electrodes and distance pieces.

In addition to the capacitive gauge the wave run-up height was measured by two digital gauges (*step-gauges)* each 1.5 m long. They were mounted at the 0.7 m high dike slope within a distance of 2.2 m. With these gauges it is only possible to measure the wave run-up till the dike crest.

3.2.6.3 Digital video cameras

FlowDike 1

In addition to the capacitive wave run-up gauge two digital video cameras were used to record the wave run-up (Figure 3.24). Both were mounted on a rack about 4 m above the ground (Figure 3.21). The rack was fixed at a laboratory crane to make the positioning of the two cameras very easy.

One digital camera was a compact, professional USB 2.0 camera from VRmagic GmbH which is suitable for industrial purposes. The used model VRmC-3 + PRO contained a 1/3 inch-CMOS-sensor which could record 69 frames per second. The picture resolution of 754 x 482 pixels was adequate for measurement purposes in the model tests presented herein.

The camera was suitable for recording very fast motions like wave run-up on slopes. One benefit of this camera was the possibility to transmit the data to the computer directly by the high speed USB 2.0 interface and without any additional frame grabber hardware. The recorded films were AVI-files. These files should be automatically analyzed after the end of the model tests.

Figure 3.24: Left: USB-camera, Right: Both cameras mounted on a rack in the model set-up

The other digital camera was a SONY Camcorder (Model: *DCR-TRV900E PAL*), with a 3CCD (*Charge Coupled Device*, ¼ inch). The objective had a focal distance between 4.3 mm and 51.6 mm and a 12 times optical zoom.

The camcorder was employed as a redundant system in the event of a USB-camera malfunction. The camcorder used mini cassettes to store its films. Choosing the LP-modus record time of the mini cassettes could be extended to 90 minutes. Because of test durations between 17 and 34 minutes the cassettes were able to storage films between 2 and 4 test films.

For analysis purposes we have to transform the films on mini cassettes into AVI-files. This is very time expensive and that is why USB camera was chosen as the main system though the SONY camcorder has a better resolution.

FlowDike 2

In FlowDike 2 both cameras were replaced with two others, which have a better resolution. Since the image-processing algorithm works with grey-level images, one color camera was replaced with a more powerful monochrome camera (1/2“ Progressive-scan-CCD sensor (*Charge Coupled Device*, 1/2 inch) JAI CM-140 GE of Stemmer Imaging). Its resolution of 1392 x 1040 pixels with 4.65 µm pixel size allows producing pictures of the run-up plate with a precision of 0.5 mm.

The second camera (a color area scan camera) was used for documentation purpose only. It had the same features like the monochrome one but the output-files are tree times greater (about 2.6 GB/min). The same objectives as in FlowDike 1 were reused.

A benefit of these cameras was their Gigabit Ethernet (C3 series) interface, which allowed placing the laptop in the office room outside the very humid air of the laboratory hall. Laptop and camera were connected with a 30 m cable. In addition the interface allowed a three times higher transfer rate. The MATLAB algorithm has to be upgraded considering the new output-file format.

3.2.6.4 Step gauge

During FlowDike 2 the step gauges, which were not analyzed for FlowDike 1, have been left out. There is no analysis available concerning the step gauges yet.

3.2.7 Overflow velocity and layer thickness (Micro propeller, Wave gauge, Pressure sensor)

FlowDike 1

From the interest in flow velocities and flow depths on the crest during an overtopping event *Schiltknecht* micro propellers and small wave gauges (with a length of 20 cm) were used. As indicated in Figure 3.25 two small micro propellers combined with two wave gauges were situated in every testing section (60 cm and 70 cm crest) between both overtopping boxes. They measured the velocities and water depths on the front and the backward edge of the dike crest. The signals given in Figure 3.26 demonstrate the measurements of wave gauges and micro propeller during single overtopping events – wave by wave.

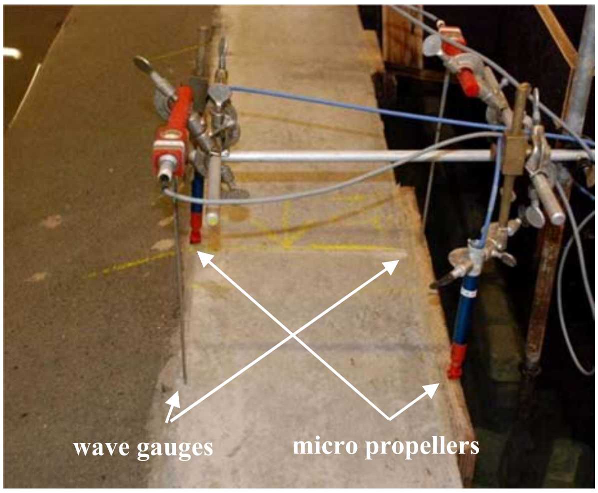

Figure 3.25 Measurement of velocity and depth of flow on the crest

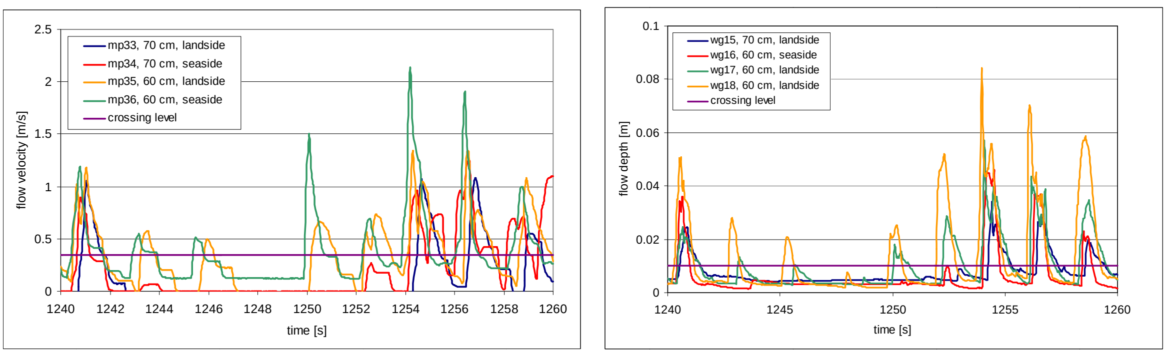

Figure 3.26 Micro propeller (left) and wave gauge (right) measurement for a sequence (s1_03_30_w5_00_00)

FlowDike 2

In FlowDike 1 only wave gauges were used to measure the layer thickness. For FlowDike 2 pressure sensors were used additionally. This new device and the purpose to avoid the influence of the crest edges (drop of water level) induced a change in order for all instruments on the dike. Instead of installing them at the edges all devices were situated 3 cm from each side of the crest, so a distance of 24 cm was kept between the aligned seaward and landward devices. To investigate the influence of the front edge (between the slope and crest), another wave gauge was placed perpendicular onto the slope. Measurements on the wave or the flow depth of the up rushing wave were taken in a horizontal distance of circa 12 cm before the edge (Figure 3.27).

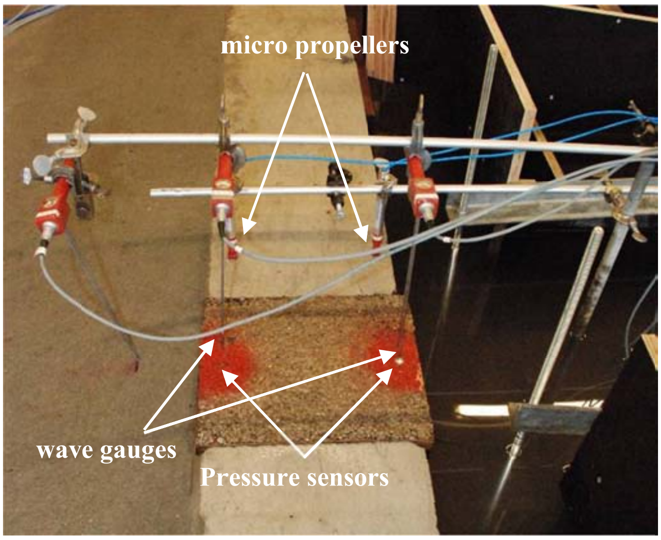

Figure 3.27 Measurement of pressure, velocity and depth of flow on the crest

3.2.8 Overtopping (Load cell, Pump)

FlowDike 1

Wave overtopping was measured by four similar overtopping boxes - two per crest section. One unit constituted an overtopping tank (35 cm x 75 cm x 75 cm) mounted on a load cell of 10 cm height. This load cell was placed on the bottom of a separate dry box (55 cm x 102 cm x 118 cm), which was built to avoid uplift of the overtopping tanks and load cells, when the basin is flooded. A channel of 10 cm inner width leaded a part of the incoming wave into the tank, where the weight of water was constantly recorded by the load cell. The inlet was not really 10 cm in width. Because of the thick plywood parts (1.8 cm) it was not clear whether there were any influences on the overtopping amount. Therefore the edges of the channel were sharpened after the first test series. For data redundancy a wave gauge (60 cm) was placed in every tank to measure the water elevation. Annotation: wave gauges could not be used to detect the single wave events as it records only the water level within the overtopping tank, which is not constant, due to the incoming wave events and the pumping during testing.

For the tests huge amounts of overtopping water were expected, especially for w5 the amount was planned to reach 30 liter at the end of the test. This showed that the dimensions of the tank were not capable to capture them during one test of approximately 30 min. Therefore a pump (standard pump) with a predetermined sufficient flow (i.e. 1.733 l/s) was placed within each tank. All four of them were connected with the data acquisition via a switch, so start and end time of pumping could easily be detected. In special tests each pumping curve was recorded, this allowed to recalculate the lost amount of water during the pumping time. After every test the tanks had to be emptied to ensure that pumping was done not more than necessary. This practice regarded the loss of data for the single event detection during pumping.

Figure 3.28 Overtopping boxes with channel and measurement devices for flow depth and flow velocity measurements

The cross-section of an overtopping unit is sketched in Figure 3.29. On the left hand side the 1:3 sloped dike and the water level in front of the dike is shown. On the right hand side, the overtopping unit has been placed. A 0.1 m wide overflow channel was connected with the dike crest and led the overtopping water to the inner box of the overflow unit. The inner box had a total volume of 0.66 m³ and was weighed by a pressure cell. Because of the completely flooded wave basin, it was necessary to place the inner box in a water-tight external box.

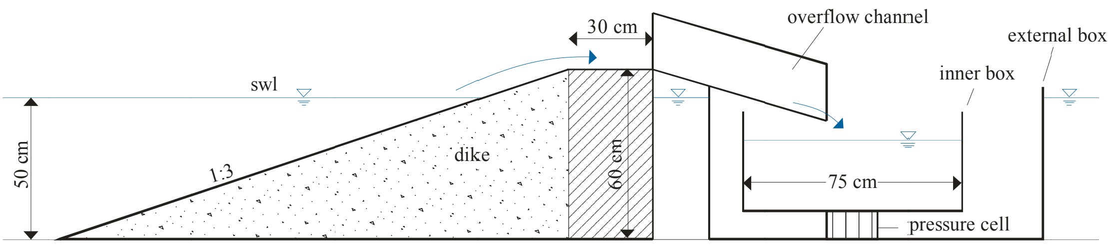

Figure 3.29 Cross-section of the overtopping unit on the 1:3 sloped dike

One of the four overtopping units (two behind each dike height) is shown in Figure 3.30. The photo was taken from the rear of the dike. At the photo the water flows from the back crest via the overflow channel into the inner box. Depending on the incoming wave field in front of the dike, the overtopping tanks were sometimes too small to capture the full amount of water for a single test. Then the tanks had to be emptied several times during the test duration of about 30 minutes. Hence, a pump with a predetermined flow was placed in each tank. All pumps (each of them in one of the inner boxes of the four overtopping units) had been connected with the data acquisition system. From the pumping curve and the start and end time of pumping, the lost amount of water could be recalculated to get the whole overtopping volume. An additional pump is located in each external box.

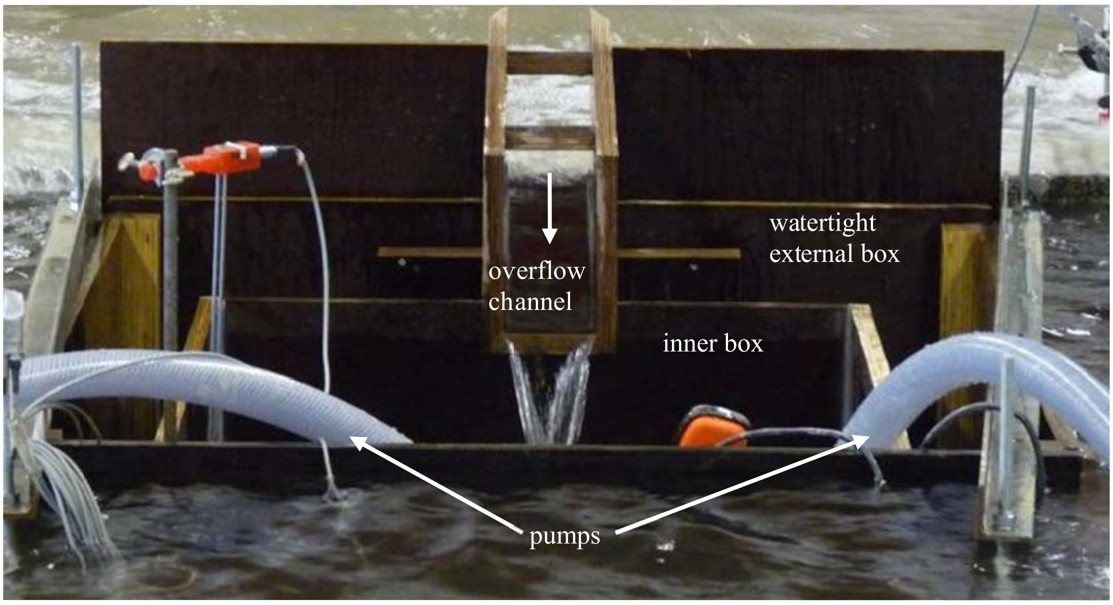

Figure 3.30 Overtopping unit seen from behind the dike

In Figure 3.31 the overtopping amount measured during one test is displayed. Here the descending part indicates the pumping of water. The signals given in Figure 3.32 demonstrate the measurements of the load cells for wave by wave overtopping during 20 seconds.

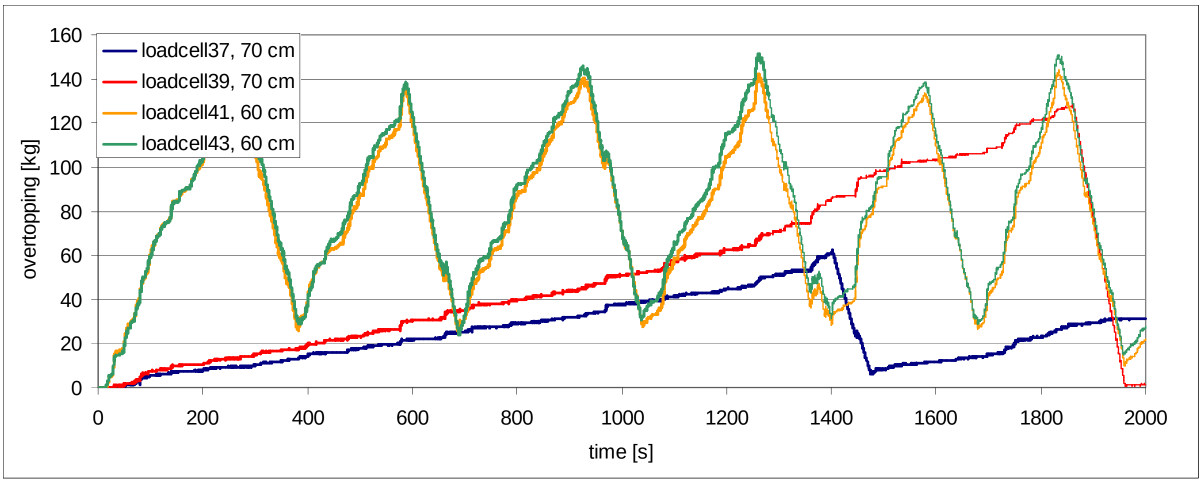

Figure 3.31 Overtopping measurement a whole test (s1_03_30_w5_00_+00)

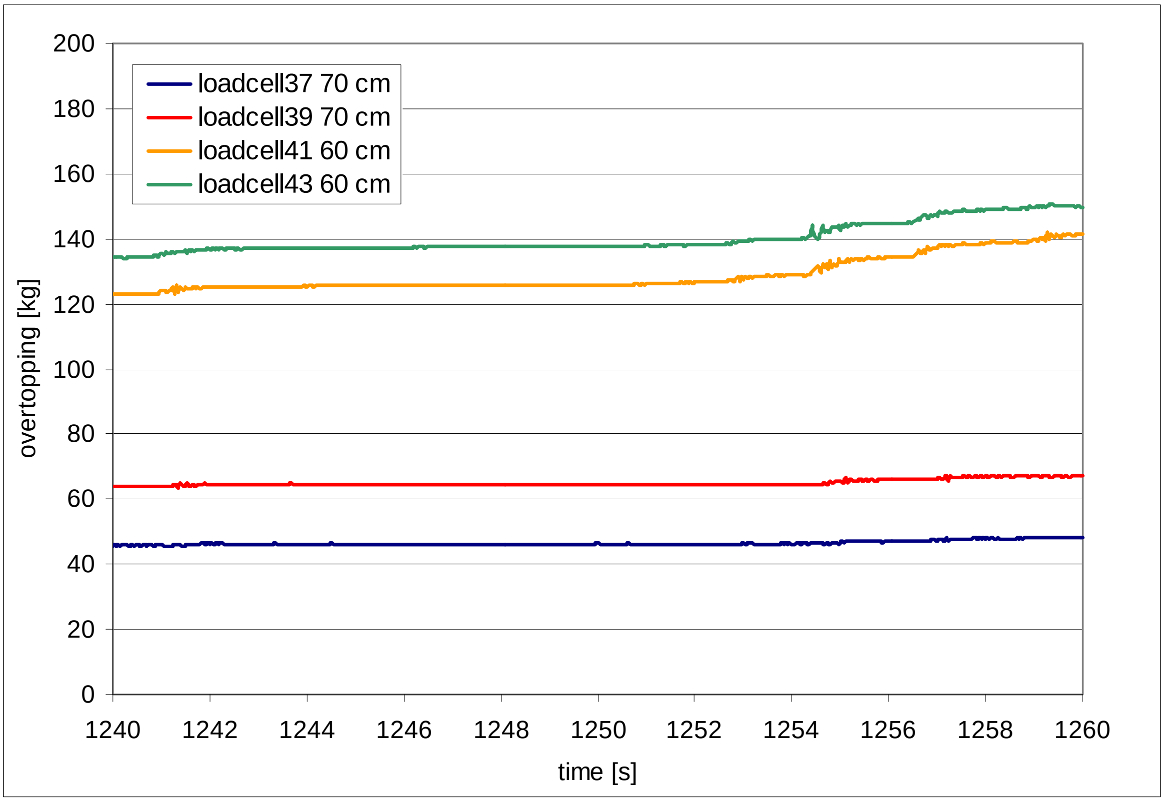

Figure 3.32 Overtopping measurement for a sequence of 20 s (s1_03_30_w5_00_+00)

FlowDike 2

For the second phase of investigations, the remained overtopping units of FlowDike 1 were reused. Only new channels with sharpened edges had to be built. Although the overtopping amount on a 1:6 dike decreases due to the inclination of the slope and breaking wave conditions, the pumps were still needed for the largest waves in period and wave height.

3.3 Calibration

3.3.1 Gauge scale adaptation

After fixing the adhesive gauge tape on the run-up plate the scale was longer because of its elasticity. In order to control possible changes, a post measurement was conducted. As a result the label of 2.9 m was placed in a distance of 2.923 m to the zero-point which is equal to an extensibility of 0.8%. In the end the measured wave run-up is to short and has to be corrected.

Assuming a linear correlation between the original and the extended scale the following formula was obtained to match both:

$$\text{length}_{\text{correct}} = 1{,}0087 \cdot \text{length}_{\text{gauge board}} \tag{3.1}$$

The even little difference has to be considered in the post processing and the data analysis using AVI-files from the camera.

3.3.2 Capacitive run-up gauge calibration

The measurement results of the 18 resistance wave gauges were influenced by water temperature and salinity. That's why one had to calibrate these gauges twice a day.

Otherwise the capacitive gauge was non-sensitive to these environmental conditions. The calibration was conducted only one time before the test start. Therefore three test with regularly waves with a mean wave height of $\overline{H}$ = 0.1; 0.15 and 0.2 were run. Data analysis considered the measured values x in Volt together with the still-water-level and the maximum water level during wave run-up (WS in meters) from video films.

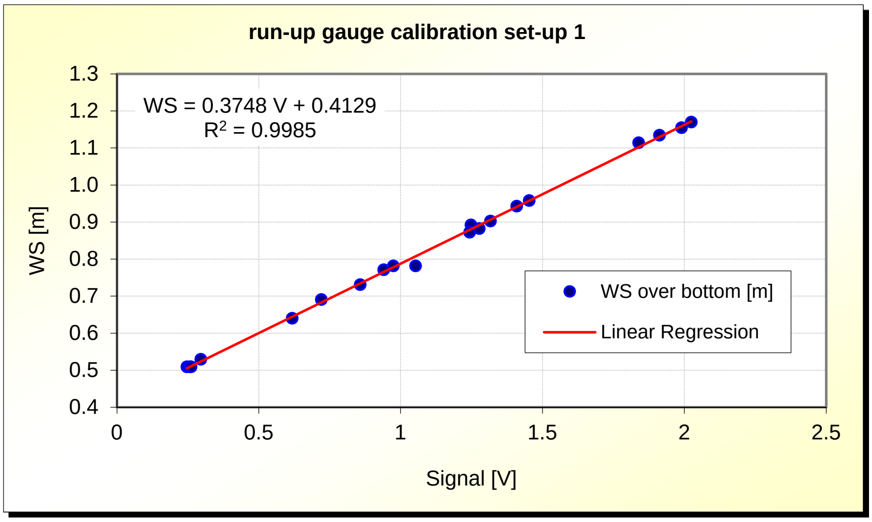

Figure 3.33 Run-up gauge calibration (set-up 1)

The result of data analysis considering equation (3.1) shows Figure 3.33. As the result of a linear regression with 20 values ($R^2 = 0.9985$) the following equation was obtained:

$$WS = 0.3748 \cdot x + 0.4047 \tag{3.2}$$

Than the wave run-up height h_r could be calculated as the difference between WS and the still-water-level h_{sw}:

$$h_r = WS - h_{sw} \tag{3.3}$$

Equation (3.2) depends on the model set-up especially on the wire length and the mounting height. That's why the calibration has to be repeated for each model set-up (see equation (3.4) to (3.7)).

$$WS = 0.3674 \cdot V + 0.2279 \ (R^2 = 0.9977, \text{set-up 2}) \tag{3.4}$$

$$WS = 0.3708 \cdot V + 0.4095 \ (R^2 = 0.9977, \text{set-up 3}) \tag{3.5}$$

$$WS = 0.1179 \cdot V + 0.5092 \ (R^2 = 0.9945, \text{set-up 4 and 5}) \tag{3.6}$$

$$WS = 0.117 \cdot V + 0.5224 \ (R^2 = 0.9788, \text{set-up 6}) \tag{3.7}$$

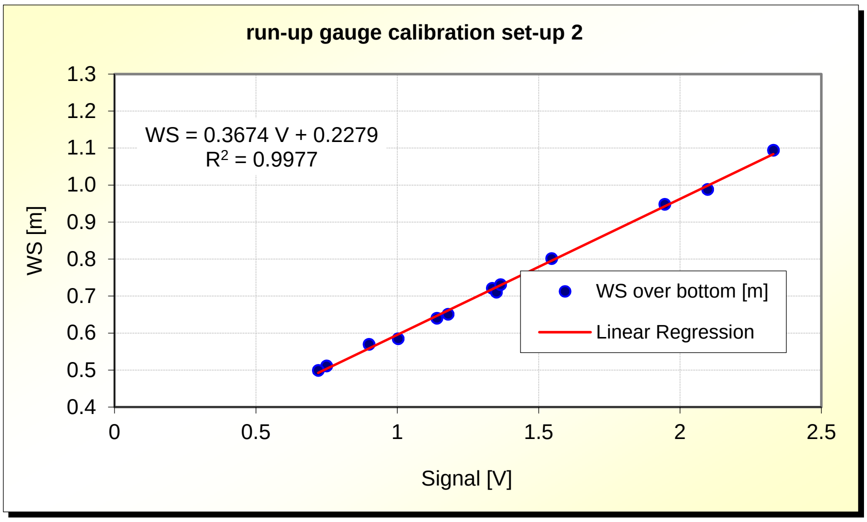

Figure 3.34 Kalibrierung des kapazitiven Auflaufpegels beim Set-up 2

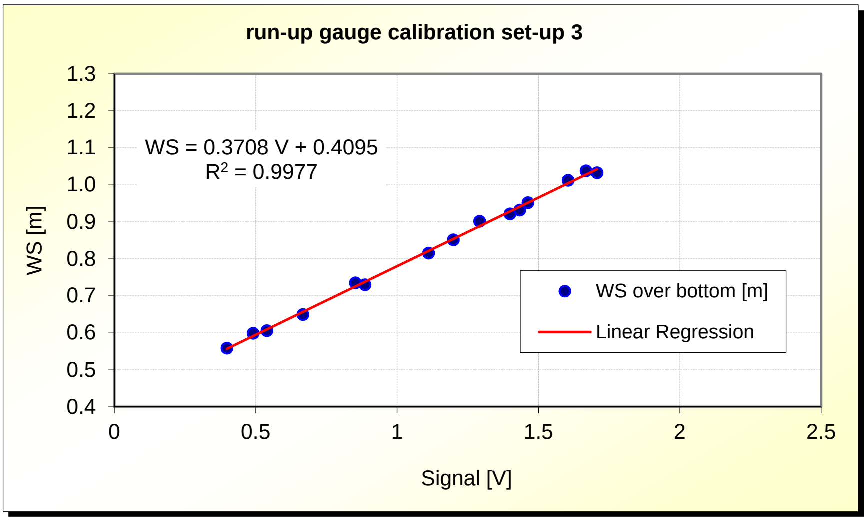

Figure 3.35 Kalibrierung des kapazitiven Auflaufpegels beim Set-up 3

3.4 Model and scale effects

3.4.1 General

The current research project was applied to consider the influence of wind and current on wave run-up and wave overtopping at which small-scale-model-tests using a smooth sloped dike were performed. In these tests no specific natural dike was reproduced. Nevertheless the results can be devolved to natural relations.

During both test phases (FlowDike 1 – 1.3 sloped dike and FlowDike 2 – 1:6 sloped dike) the same laboratory with its equipment was used. Only the measurements of the flow velocity on the crests have been changed to new instrumentations in FlowDike 2.

3.4.2 Model effects

The main model effects of the physical model tests of the FlowDike-D-project are

- width of the channel
- dimension of the overtopping channel
- reflection besides the wave machine

To minimize the mentioned model effects some adaptions have been done during the physical model tests. To ensure low turbulence during the wave overtopping process the edges of the overtopping channel were sharpened after the first test series. Nearby the dikes and the wave generator, wave absorber have been installed to reduce the reflection of the waves.

3.4.3 Scale effects

To ensure the similarity between the model and the prototype, the geometric similarity, the kinematic similarity and the dynamic similarity have to be considered. The geometric similarity assures the scaling of the design and the wave heights end lengths. The kinematic similarity describes the relation of the time scale for example of the wave period. More difficult is to ensure the dynamic similarity which includes the model laws by Froude, Reynolds, Weber, Thoma and Cauchy. The model law by Cauchy includes the equality of the elasticity and the inertia force. Thoma considers the inertia forces and pressure. Both Thoma and Chauchy are negligible for relevance of this approach (free surface).

The main complexity in scaling the wind tests is the different theory which has to be used for wind and water waves. Wind has to scaled according to Reynolds, whereas waves are scaled by the Froude-theory. Both theories cannot be combined, that is why only a few investigations by physical model tests considering the influence of wind on wave overtopping have been done (GONZÁLEZ-ESCRIVA, 2006).

Regarding DE ROUCK ET AL. (2002) the roughness of the dike has only an influence of scaling for porous dikes. Therefore this factor is in this study with a smooth dike negligible.

The model laws by Froude, Reynolds and Weber have been already analyzed in detail by SCHÜTTRUMPF (2001). The same procedure will be used to determine the influence of the surface tension (Weber). The influence of the surface tension on scale effects of the incoming wave field is negligible because of the flow depth and the scale effects of run-up and overtopping-process also.

Based on SCHÜTTRUMPF (2001) the scale effect of the surface tension will be described using the following formula:

$$\frac{1}{2} = \frac{1}{c_2^{\ *} \cdot Fr_{crest}^{\ 2}} + \frac{1}{We_{crest}} \tag{3.8}$$

$$Fr_{crest} = \frac{v_{crest}}{\sqrt{g \cdot h_{crest}}} \tag{3.9}$$

$$\mathrm{We}_{\mathrm{crest}} = \frac{\mathrm{v}_{\mathrm{crest}}^{\ 2} \cdot \mathrm{h}_{\mathrm{crest}} \cdot \rho_{\mathrm{w}}}{\sigma_0} \tag{3.10}$$

with: Fr_{crest} Froude number at the crest [-]

We_{crest} Weber number at the crest [-]

$c_2^{\ *}$ parameter for describing the layer thickness [-]

v_{crest}	velocity at the crest [m/s]
h_{crest}	layer thickness at the crest [m]
σ_0	surface tension, *here:* σ_0 = 0.0732 N/m for a temperature of 16.5°

Figure 3.36 shows the Froude number against the Weber number using formula (3.8). The Weber number describes the influence of surface tension on the flow process. The different graphs are based on different parameters c_2^*. All graphs show a constant Froude number for Weber numbers higher than 10. For the FlowDike data the parameter for describing the layer thickness c2* is set to 0.4 for the 1:3 sloped dike and 0.7 for the 1:6 sloped dike.

The corresponding data of the FlowDike-D experiments are plotted with the red and blue data points, and have Weber numbers higher than 10 (except one value). So the surface tension has no effect on the overtopping events on the dikes.

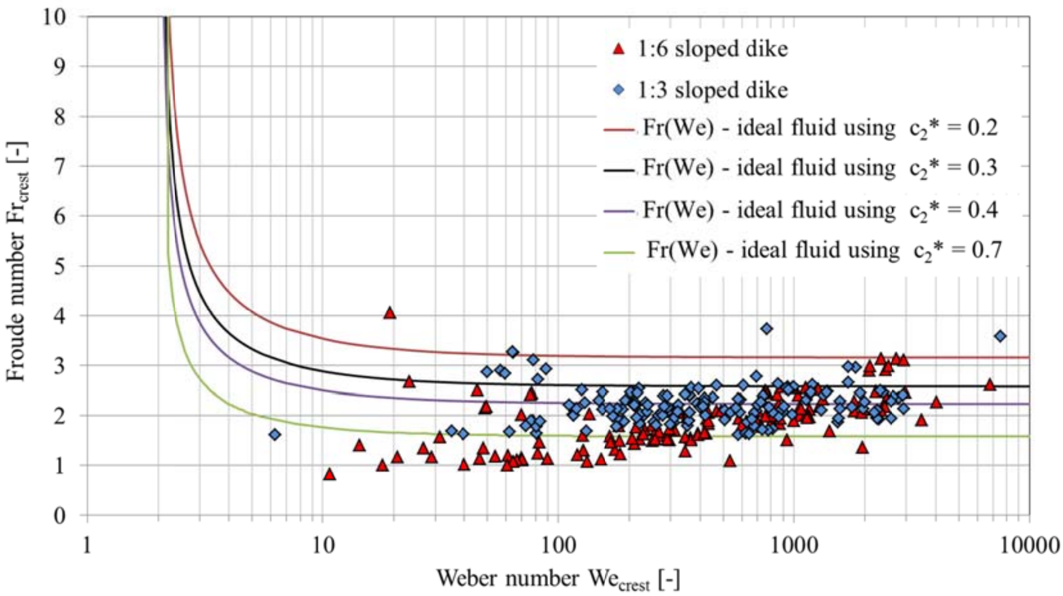

Figure 3.36 Influence of surface tension on the dike crest

The influence of the viscosity has to be analyzed for the wave propagation as well as for the wave overtooping process. For both the Froude and Reynolds-numbers have been determined using the formula by SCHÜTTRUMPF (2001) to identify if the viscosity has to be considered while interpretend the results:

Wave propagation:

$$\mathrm{Fr}_{\mathrm{wave}}^2 = \left[1 - \frac{1}{2 \cdot \sqrt{\mathrm{Re}_{\mathrm{wave}} \cdot \mathrm{kd}}}\right]^2 \quad \text{with} \quad \mathrm{kd} = \frac{2\pi \cdot \mathrm{d}}{\mathrm{L}_{\mathrm{m-1,0}}} \tag{3.11}$$

$$\mathrm{Re}_{wave} = \frac{c \cdot d}{\nu} \tag{3.12}$$

$$Fr_{wave} = \frac{c}{\sqrt{g \cdot d}} \tag{3.13}$$

with: Fr_{wave} Froude number of the wave [-]

Re_{wave} Reynold number of the wave [-]

d flow depth, water depth [m]

$L_{m-1,0}$ deep water wave length based on $T_{m-1,0}$ [m]

c wave velocity [m/s]

ν dynamic viscosity [m²/s]

Wave overtopping processe:

$$Fr_{crest} = \sqrt{\frac{1}{\left(1 - \frac{64}{4 \cdot Re_{crest} \cdot c_2}\right)}} \tag{3.14}$$

$$Re_{crest} = \frac{2 \cdot \left(R_{u2\%} - R_C\right)^2}{\left(\nu \cdot T\right)} \tag{3.15}$$

$$Fr_{crest} = \frac{v_{crest}}{\sqrt{g \cdot h_{crest}}} \tag{3.16}$$

$$c_2 = \frac{c_2^*}{n} \text{ with } \begin{array}{l} c_2^* = 0.4 \; and \;\; n = 3 \;\; for \; 1:3 \; sloped \;\; dike \\ c_2^* = 0.7 \; and \;\; n = 6 \;\; for \; 1:6 \; sloped \;\; dike \end{array} \tag{3.17}$$

with: Fr_{crest} Froude number at the crest [-]

Re_{crest} Reynold number at the crest [-]

$R_{u2\%}$ run-up height exceeded by 2% of the incoming waves [m]

R_C freeboard height of the structure [m]

ν dynamic viscosity [m²/s]

T wave period [s]

v_{crest} velocity at the crest [m/s]

h_{crest} layer thickness at the crest [m]

c_2^* parameter for describing the layer thickness [-]

As shown in Figure 3.37 the viscosity has only an influence on the wave evolution for Reynolds-numbers lower than 10 000. No influence on the results of the wave field are expected because of the Reynolds-number for the FlowDike-tests higher than 10^6.

The influence of the viscosity on the wave overtopping process is shown in Figure 3.38. Subsequently the viscosity does not influence the wave overtopping process for Reynolds-numbers higher than 1000, which is observed for nearly all tests.

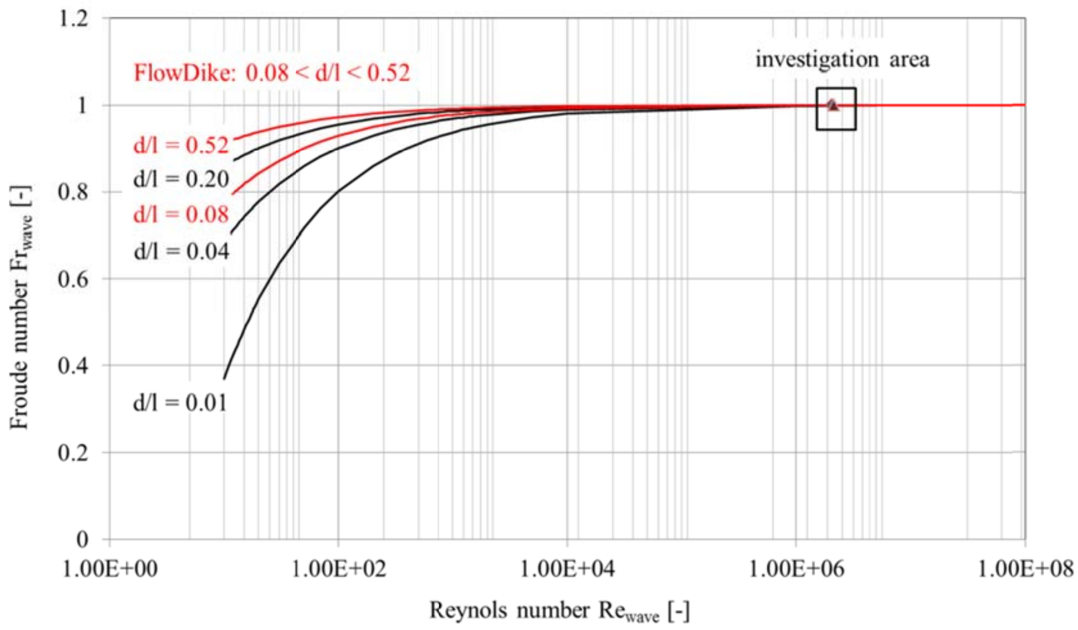

Figure 3.37 Influence of viscosity on wave evolution

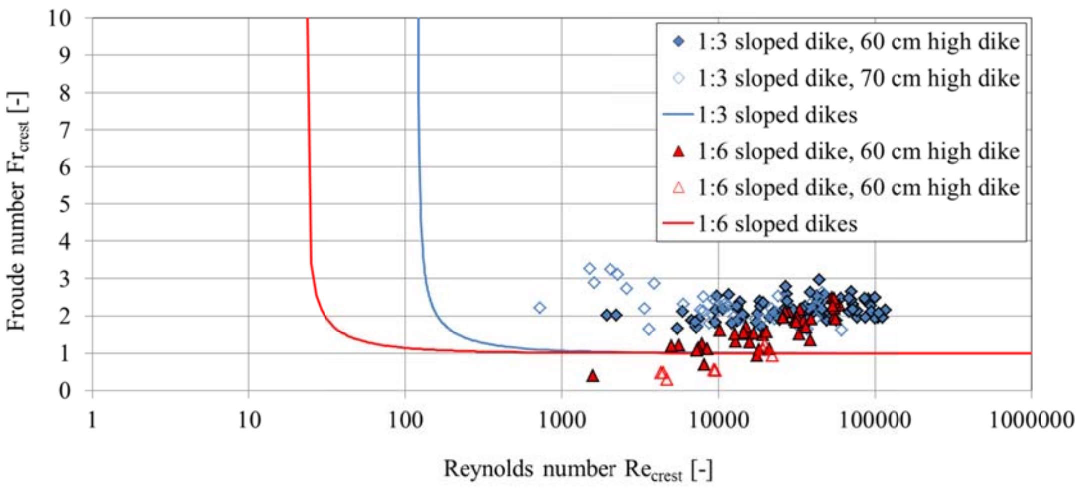

Figure 3.38 Influence of viscosity on wave overtopping processes

4 Literature review and method of analyzing data on wave field

4.1 Wave spectrum

First investigations on wave spectra were done by Phillips (1958) and serve as basis for the investigations of fully developed wind sea by Pearson and Moskowitz (1964), which are still used for off-shore technics. During the Joint-North-Sea-Wave-Project (Jonswap) not fully developed wind seas were analyzed. Main aim of that project was to describe the wave spectrum while increasing of the sea state as well as the behavior of the sea state in shallow water. Hence the so called Jonswap-spectrum was developed. The also often used TMA-spectrum is based on the Jonswap spectrum and applicable for shallow water conditions.

The Jonswap spectrum is the most common used spectrum in current research projects. To guarantee comparability this spectrum is applied in the present tests in the FlowDike-D research project and will be presented in more detail.

The theoretical Jonswap-spectrum can be described with the Jonswap-energy-density S as a function of the frequency f and a Jonswap-portion θ_J, which describes the maximum energy of the spectrum. The Jonswap-spectrum Sj(f) can determined using the formula (4.1) based on the formula of Pearson-Moskowitz (4.3) and of Phillips (4.5) (cf. MALCHEREK, 2010):

$$S_J(f) = S_{PM}(f) \cdot \Theta_J(f, f_P, \gamma, \sigma_a, \sigma_b) \tag{4.1}$$

with $S_J(f)$ Jonswap-energy-density-spectrum [m²/Hz]

$S_{PM}(f)$ energy density spectrum of Pierson-Moskowitz [m²/Hz]

θ_J Jonswap-coefficient describing the maximum of the energy density [-]

$$\Theta_J = \gamma^{\exp\left(\frac{-(f-f_p)^2}{2\sigma^2 \cdot f_p^{\,2}}\right)} \tag{4.2}$$

γ peak raising factor [-] $\gamma = 3.3$ for mean Jonswap-spectrum

σ form parameter describing the forward peak width [-]

$f < fp \rightarrow \sigma = 0{,}07$

$f > fp \rightarrow \sigma = 0{,}09$

$$S_{PM}(f) = S_p(f) \cdot \Theta_{PM} \frac{f}{f_p} \tag{4.3}$$

with $S_{PM}(f)$ energy density spectrum of Pierson-Moskowitz [m²/Hz]

$S_P(f)$ Phillips-spectrum describing the decreasing part of the graph [m²/Hz]

θ_{PM} Pierson-Moskowitz parameter describing the spectrum [-]

$$\Theta_{PM} = \exp\left(-\frac{5}{4} \cdot \left(\frac{f}{f_p}\right)^{-4}\right) \tag{4.4}$$

with f_p peak frequency [Hz]

$$S_p(f) = \frac{\alpha \cdot g^2}{(2\pi)^4 \cdot f^5} \tag{4.5}$$

with α Phillips-constant $\alpha = 8.1 \cdot 10^{-3}$ [-]

f frequency [Hz]

4.2 Wave and current interaction

4.2.1 General

The model tests were performed with and without a current parallel to the dike. Since the wave propagation is different in flowing water and in still water, it is required to interpret the following results with respect to the interaction of waves and current (TRELOAR, 1986). Two main aspects have to be considered while interpreting the results:

- current induced shoaling: absolute and relative wave parameters
- current induced wave refraction: energy propagation

The wave propagation path can be divided into two parts. The first part reaches from the wave generator to the dike toe. The second part extends from the dike toe to the dike crest.

4.2.2 Current induced shoaling

If a wave propagates on a current, a distinction has to be made between relative and absolute wave parameters and can be described by using the wave celerity. The relative wave celerity is the celerity relative to an observer who moves with the current, while the absolute celerity is defined as the velocity compared to a stationary observer and the ground, respectively.

The wave arrays in front of the dike measured the wave field with its absolute parameters. According to HEDGES (1987), TRELOAR (1986) and HOLTHUIJSEN (2007) waves act only with its relative parameters. To determine the relative wave period $T_{rel,m-1,0}$ from the measured absolute wave period $T_{abs,m-1,0}$, the absolute angular frequency ω_{abs} has to be equalized to the sum of the relative angular frequency ω_{rel} and the corresponding constituent of the current $(k \cdot v_n)$ (cf. HOLTHUIJSEN, 2007):

$$\omega_{abs} = \omega_{rel} + k \cdot v_n = \sqrt{gk \cdot \tanh(k \cdot d)} + k \cdot v_n \tag{4.6}$$

with ω_{abs} absolute angular frequency [rad/s]

ω_{rel} relative angular frequency [rad/s]

k wave number [rad/m]

v_n current velocity in the direction of wave propagation [m/s]

d flow depth [m]

The absolute angular frequency is defined as:

$$\omega_{abs} = \frac{2\pi}{T_{abs,m-1,0}} \tag{4.7}$$

with the absolute spectral period $T_{abs,m-1,0}$ (EurOtop 2007)

$$T_{abs,m-1,0} = \frac{T_P}{1.1} \tag{4.8}$$

with

T_P spectral peak period [s]

By using eq. (4.8) and (4.9), the wave number k can be determined iteratively by using the measured absolute wave period $T_{abs,m-1,0}$, the known flow depth d and the current velocity in the direction of wave propagation v_n (cf. Figure 4.2):

$$v_n = v_x \cdot \sin\beta \tag{4.9}$$

with the current velocity parallel to the dike v_x and the angle of wave attack relative to the normal of the dike β.

The relative angular frequency ω_{rel} results in

$$\omega_{rel} = \sqrt{g \cdot k \cdot \tanh(k \cdot d)} \tag{4.10}$$

and leads to the relative wave period $T_{rel,m-1,0}$:

$$T_{rel,m-1,0} = \frac{2\pi}{\omega_{rel}} \tag{4.11}$$

As shown in Figure 4.1 if the wave propagates against the current, the relative wave period $T_{rel,m-1,0}$ decreases and increases by wave propagation with the current (cf. formula (4.6) and (4.11)).

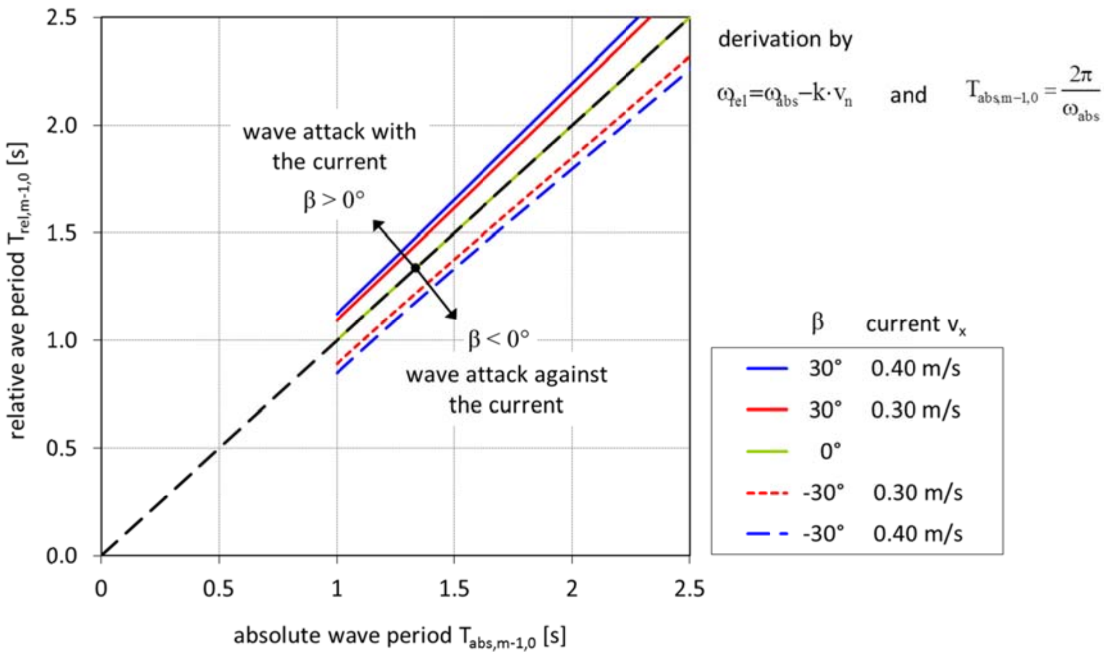

Figure 4.1 Absolute wave period $T_{abs,m-1,0}$ against relative wave period $T_{rel,m-1,0}$, water depth d = 0.5 m

4.2.3 Current induced wave refraction

Figure 4.2 shows schematically the combination of the two vectors for the current and the wave direction for negative (left) and positive (right) angles of wave attack. The dashed arrow describes the relative direction of the wave attack generated by the wave generator and the corresponding angle β. The dotted arrow indicates the direction of the current parallel to the dike. According to HOLTHUIJSEN (2007) the current does not change the angle of wave attack but its energy direction by the combination of the two vectors current velocity v_x and relative group velocity $c_{g,rel}$ marked with the corresponding arrow. As shown in Figure 4.2, negative angles of wave attack lead to a smaller absolute value of the angle of wave energy β_e whereas positive angles of wave attack lead to a higher angle of wave energy β_e than the angle of wave attack β.

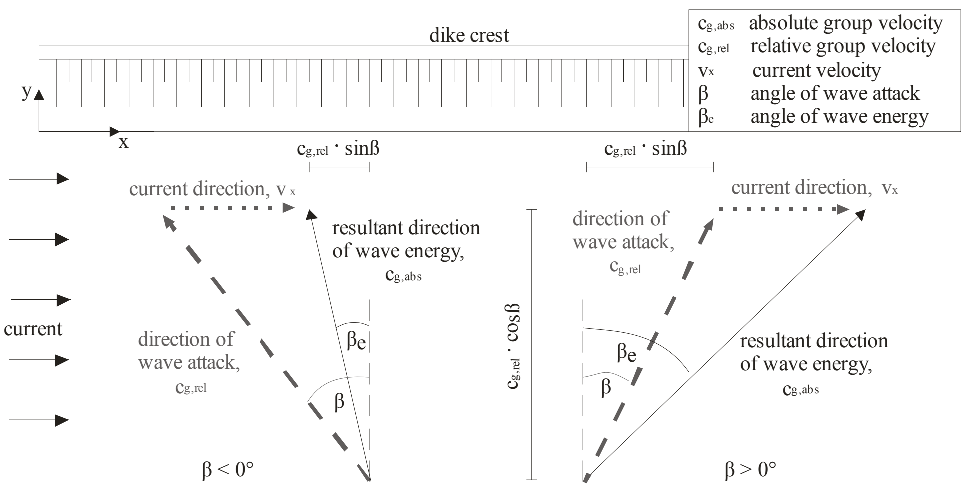

Figure 4.2. Interaction between wave direction and current

With the help of Figure 4.2 the angle of wave energy β_e is determined by the relative group velocity $c_{g,rel}$, the angle of wave attack β and the current velocity v_x by the trigonometrical function:

$$\tan\beta_e = \frac{c_{g,rel} \cdot \sin\beta + v_x}{c_{g,rel} \cdot \cos\beta} \tag{4.12}$$

Herein the relative group velocity $c_{g,rel}$ is determined by the following formula:

$$c_{g,rel} = \frac{\partial\omega}{\partial k} = \frac{\partial\left(\sqrt{g \cdot k \cdot \tanh(k \cdot d)}\right)}{\partial k} \tag{4.13}$$

which leads to:

$$c_{g,rel} = 0.5 \cdot \frac{\omega_{rel}}{k}\left(1 + \frac{2 \cdot k \cdot d}{\sinh(2 \cdot k \cdot d)}\right) \tag{4.14}$$

Figure 4.3 shows the influence of the current on the angle of wave energy. On the abscissa the current is plotted. The ordinate shows the angle of wave attack (dashed line) and the angle of wave energy (continuous line). The graphs show different angles of wave attack with and against the current. For all angles of wave attack the angle of wave energy increases significantly during the currents up to 4 m/s. For currents higher than 4 m/s the changes in the angle of wave attack are lower and converge against 90° which is the direction of the current Fore negative angles of wave attack (against the current, green and blue graph) the angle of wave energy changing of the angle of wave energy is more significant than for the positive angles of wave attack (with the current, orange graph).

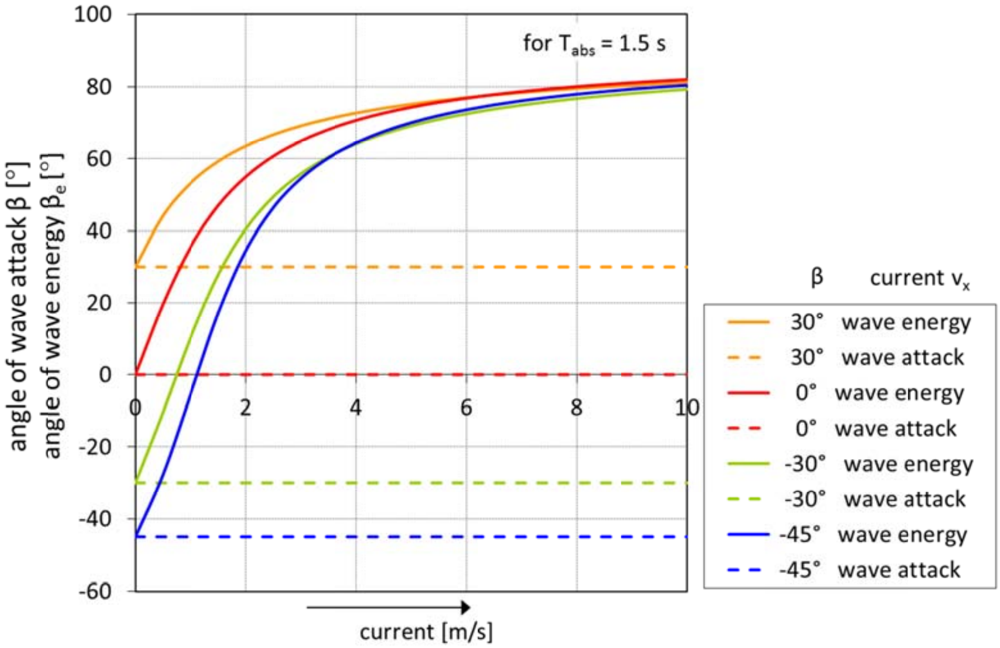

Figure 4.3 Angle of wave energy β_e divided by angle of wave attack β against the current for different angles of wave attack, water depth d = 0.5 m, T_{abs} = 1.5 s

4.3 Influence of wind on waves

In the current research project the waves are induced by a wave generator. Additionally to the wave generator the induced wind influences the wave parameters at the toe of the structure as well as the breaking processes. Galloway (1989) carried out wave observations at coasts to determine the influence of the wind direction of the breaker process of the waves. Wind in the direction of wave propagations leads to previous breaking of the waves which become surging waves. DE WAAL ET AL. (1996) included this knowledge in a formula for wave overtopping by reducing the breaker flow depth d_b. He determines the wind influenced flow depth $d_{b(wind)}$ at the breaker point to:

$$\frac{d_{b(wind)}}{d_b} = \left(1 + p \cdot \frac{u_{10}}{\sqrt{g \cdot d_b}}\right)^2 \tag{4.15}$$

with d_b flow depth at breaker point without wind [m]

u_{10} wind velocity 10 m above still water level [m/s]

$$p = \frac{v_{crest,wind} - v_{crest,no\,wind}}{u_{10}} \approx 0.03 \quad \text{percentage by DE WAAL ET AL. (1996)} \tag{4.16}$$

with $v_{crest,wind}$ flow velocity on the dike crest, wind $u_{10} \neq 0$ m/s [m/s]

$v_{crest,no\,wind}$ flow velocity on the dike crest, wind $u_{10} = 0$ m/s [m/s]

5 Literature review and method of analyzing data on wave run-up and wave overtopping

5.1 Delimitation of literature review

Wave run-up is the rush of water up a structure as a result of wave attack. Wave overtopping is the mean discharge of water in l/(s·m) that passes over a structure due to wave attack and should be limited to a tolerable amount. Analyses for wave run-up and wave overtopping were performed mostly for coastal areas in the past. First investigations have been carried out before 1935 (see WASSING, 1957 and GIBSON, 1930). In the meantime, many experimental, numerical, theoretical and field investigations were performed. Extensive studies on perpendicular wave run-up and overtopping and some investigations on oblique wave run-up are available.

The main aspects which were investigated on wave run-up and wave overtopping can be listed as follows:

- geometry of the dike (inclination, berm)
- long and short crested waves
- regular and spectral wave attack, natural sea spectrum
- normal and oblique wave attack
- dike constitution (roughness, permeability)
- kind of investigation (experimental (laboratory, field), numerical, theoretical)

In the FlowDike-D project long crested waves under a Jonswap spectrum were investigated (cf. chapter 2.2 and 4.1).

A more detailed literature review will be given about the main aspects investigated in FlowDike-D concerning wave run-up and wave overtopping:

- normal wave attack
- influence of spectrum
- influence of oblique wave attack

The complete new aspect - the influence of a dike parallel current and wind on wave run-up and wave overtopping - was not investigated in any project before.

5.2 Wave run-up and wave overtopping under normal wave attack

5.2.1 Wave run-up

The wave run-up height was investigated by several authors. HUNT (1959) gave four basic formulae describing the wave run-up height R

$$R = C \cdot \sqrt{H \cdot L_0} \cdot \tan\alpha \qquad \text{with} \quad C = 1.0 \tag{5.1}$$

$$R = C \cdot \sqrt{H \cdot g} \cdot T \cdot \tan\alpha \qquad \text{with} \quad C = 1/(2\cdot\pi)^{0.5} \approx 0.4 \tag{5.2}$$

$$R = C \cdot \sqrt{H} \cdot T \cdot \tan\alpha \qquad \text{with} \qquad C = 1.25 \tag{5.3}$$

$$\frac{R}{H} = C \cdot \frac{\tan\alpha}{\sqrt{H \cdot L_0}} = C \cdot \xi \qquad \text{with} \qquad C = 1.0 \tag{5.4}$$

with C coefficient [-]

H wave height [m]

L_o wave length [m]

T wave period [s]

α inclination of the structure [°]

In these formulae only regular wave parameters are considered, but the main investigations consider the run-up height depending of wave spectra. According to GRÜNE & WANG (2000) formula (5.4) by HUNT (1959) for R_{98} is the most common formula used by several authors like VAN DER MEER AND JANSSEN (1994):

$$\frac{R_{98}}{H_{1/3}} = C_\xi \cdot \xi_{eq} \quad \text{with} \quad C_\xi = 1.6 \cdot \gamma_h \cdot \gamma_f \cdot \gamma_\beta \quad \text{and} \quad \xi_{eq} = \gamma_b \cdot \frac{\tan\alpha}{\sqrt{\dfrac{2\pi \cdot H_{1/3}}{g \cdot T_p^2}}} \tag{5.5}$$

with C_ξ parameter considering influencing of shallow foreshore, roughness, oblique wave attack

ξ_{eq} parameter considering influence of a berm, surf similarity parameter

Usually the influence of different factors on wave run-up height could be determined using the formula above suggested by HUNT (1959). The upgraded version is given in the EUROTOP- MANUAL (2007) with different correction parameters and is the main common used formula for wave run-up, for short crested waves:

$$\frac{R_{u,2\%}}{H_{m0}} = c_1 \cdot \gamma_b \cdot \gamma_f \cdot \gamma_\beta \cdot \xi_{m-1,0} \tag{5.6}$$

with its maximum value

$$\frac{R_{u,2\%}}{H_{m0}} = \gamma_f \cdot \gamma_\beta \cdot \left(c_2 - \frac{c_3}{\sqrt{\xi_{m-1,0}}} \right) \tag{5.7}$$

with $R_{u,2\%}$ wave run-up height which will be exceeded by 2% of all waves [m]

c_1, c_2, c_3 empirical parameters with $c_2 = c_1 \cdot \xi_{tr} + c_3 / \xi_{tr}$ [-]

for average $R_{u,2\%}$: $c_1 = 1.65$ $c_2 = 4.0$ $c_3 = 1.5$

ξ_{tr} surf parameter describing the transition between breaking and non-breaking waves [-]

γ_b parameter covering influence of a coastal structure with at least two different slopes [-]

γ_f parameter covering influence of surface roughness [-]

γ_β parameter covering influence of wave direction (angle β) [-]

5.2.2 Wave overtopping

The wave overtopping rate is the significant parameter for determine the design flood protection structures. The wave overtopping is a dynamic process with a variable volume of overtopped water during a period of time. The wave overtopping amount depends mainly on the wave parameters and water level at the dike toe as well as the geometry of the flood protection structure. Mostly the wave overtopping rate q is specified in liter per second and meter dike length or the dimensionless overtopping rate including the wave parameters (q_* [-]).

Several formulae are used to determine the mean dimensionless overtopping rate [-]. Most of them are given in one of the two forms:

$$q_* = a \cdot \exp(-b \cdot R_*) \tag{5.8}$$

and

$$q_* = a \cdot (1 - R_*)^{-b} \tag{5.9}$$

with
- a [-] best-fit coefficients; for R = 0 m is a = q_* (dimensionless overtopping rate)
- b [-] best-fit coefficients
- R_* [-] dimensionless freeboard height

Several authors give formula for the dimensionless overtopping rate q_* and the dimensionless freeboard height R_*. In Table 5.1 these formulae are given from investigations on sloped dike and irregular waves. The following parameters are used:

- H_s significant wave height[m]
- T_m mean wave period [s]
- T_p peak wave period [s]
- R_c freeboard height [m]
- $R_{2\%}$ run-up exceeded by 2% of the incoming waves [m]
- L_m wavelength corresponding to T_m [m]
- L_p wavelength corresponding to T_p [m]
- L_s airy wave length corresponding to T_s [m]
- ξ_p surf similarity parameter using H_s and L_{0p}[-]
- L_{0p} wavelength corresponding to T_p and deep water conditions [m]
- α slope of the structure [-]
- γ influence factor of berm, permeability, roughness, oblique wave attack, shallow water [-]

For more formula of vertical walls and regular waves see SCHÜTTRUMPF (2001).

Table 5.1 Recommended dimensionless overtopping rate q* and dimensionless freeboard height R* for sloped structures and irregular waves (modified according to HEDGES & REIS (1998))

Reference		Dimensionless overtopping rate q_*	Dimensionless freeboard height R_*	Overtopping model
OWEN	1982	$\frac{q}{T_m \cdot g \cdot H_s}$	$\frac{R_c}{T_m \cdot \sqrt{g \cdot H_s}}$	$q_* = a \cdot \exp(-b \cdot R_*)$
BRADBURY & ALLSOP	1988	$\frac{q}{T_m \cdot g \cdot H_s}$	$\frac{R_c^2}{T_m \cdot \sqrt{g \cdot H_s^3}}$	$q_* = a \cdot (R_*)^{-b}$
AHRENS & HEIMBAUGH	1988	$\frac{q}{\sqrt{g \cdot H_s^3}}$	$\frac{R_c}{(H_s^2 \cdot L_p)^{1/3}}$	$q_* = a \cdot \exp(-b \cdot R_*)$
SAWARAGI ET AL.	1988	$\frac{q^*}{\sqrt{g \cdot L_s \cdot H_s^2}}$	$\frac{R_c}{H_s}$	-
AMINTI & FRANCO	1988	$\frac{q}{T_m \cdot g \cdot H_s}$	$\frac{R_c}{H_s}$	$q_* = a \cdot (R_*)^{-b}$
PEDERSEN & BURCHARTH	1992	$\frac{q \cdot T_m}{L_m^2}$	$\frac{R_c}{H_s}$	$q_* = a \cdot (R_*)^{-b}$
DE WAAL & VAN DER MEER	1992	$\frac{q}{\sqrt{g \cdot H_s^3}}$	$\frac{R_{2\%} - R_c}{H_s}$	$q_* = a \cdot \exp(-b \cdot R_*)$
VAN DER MEER, SMITH ET AL.; VAN DER MEER & JANSSEN	1993; 1994; 1995	$\frac{q}{\sqrt{g \cdot H_s^3}} \frac{\sqrt{\tan\alpha}}{\xi_p}$ for $\xi_p < 2$ $\frac{q}{\sqrt{g \cdot H_s^3}}$ for $\xi_p > 2$	$\frac{R_c}{H_s} \frac{1}{\xi_p} \frac{1}{\gamma}$ for $\xi_p < 2$ $\frac{R_c}{H_S} \frac{1}{\gamma}$ for $\xi_p > 2$	$q_* = a \cdot \exp(-b \cdot R_*)$
FRANCO ET AL.	1994	$\frac{q}{\sqrt{g \cdot H_S^3}}$	$\frac{R_c}{H_s}$	$q_* = a \cdot \exp(-b \cdot R_*)$
SCHÜTTRUMPF	2001	$\frac{q}{\sqrt{2g \cdot H_S^3}} \cdot \frac{1}{\xi_m}$	$\frac{R_c}{H_s}$	$q_* = a \cdot \exp(-b \cdot R_*)$

The formula first applied by VAN DER MEER (1993) for the dimensionless overtopping rate q_* and the dimensionless freeboard height R_{c*} is the most common form that will also be used in this study (cf. chapter 0 and formula (5.28)).

The mean overtopping rate by the EUROTOP-MANUAL (2007) is determinable using deterministic or probabilistic approaches based on several investigations. The probabilistic design formula is used for comparing measurements. Therefore a 5%-confidence-interval has to be included. The deterministic approach serves for design of dike structures used for safety assessments. Both deterministic and probabilistic designs base on the following formulae (5.26) and (5.27) for breaking and non-breaking wave conditions. The smaller value indicates breaking or non-breaking wave conditions. VAN DER MEER (1993) distinguished between breaking and non-breaking waves by using the surf-similarity-parameter ξ_p.

Breaking wave conditions:

$$q_* = \frac{q}{\sqrt{g \cdot H_{m0}^3}} = \frac{0.067}{\sqrt{\tan\alpha}} \cdot \gamma_b \cdot \xi_{m-1,0} \cdot \exp\left(- p_{br} \cdot \frac{R_c}{\xi_{m-1,0} \cdot H_{m0} \cdot \gamma_b \cdot \gamma_f \cdot \gamma_\beta \cdot \gamma_v} \right) \tag{5.10}$$

probabilistic design: $p_{br} = 4.75$ deterministic design: $p_{br} = 4.3$

Non-breaking wave conditions:

$$q_* = \frac{q}{\sqrt{g \cdot H_{m0}^3}} = 0.2 \cdot \exp\left(- p_{nbr} \cdot \frac{R_c}{H_{m0} \cdot \gamma_f \cdot \gamma_\beta} \right) \tag{5.11}$$

probabilistic design: $p_{nbr} = 2.6$ deterministic design: $p_{nbr} = 2.3$

with	q	mean overtopping discharge per meter structure width [m³/s/m]
	α	slope of the front face of the structure [°]
	R_c	crest freeboard of structure [m]
	γ_b	correction factor for a berm [-]
	γ_f	correction factor for permeability and roughness of the structure [-]
	γ_β	correction factor for oblique wave attack [-]
	γ_υ	correction factor for a vertical wall on the slope [-]
	p_{br}	coefficient for deterministic and probabilistic design, breaking waves [-]
	p_{nbr}	coefficient for deterministic and probabilistic design, breaking waves

5.2.3 Influence of analyzed spectrum

In OUMERACI ET AL. (2000) physical model tests investigating the influence of the wave spectra were presented. Herein regular waves, TMA spectra (single peak), Jonswap spectra (single and double peak) and measured multi peak spectra were investigated. The spectra differ not only in the peak period but also in the energy density of the spectrum. The energy of a spectrum is more significant for the run-up and overtopping measurements than the peak period. So the spectral period is defined as

$$T_{m-1,0} = \frac{m_{-1}}{m_0} \tag{5.12}$$

Concerning the statistical wave parameters GRÜNE & WANG (2000) observed as well a low sensitivity of the wave height and freeboard height compared to the sensitive wave period T. In general it should be used the mean period T_m or the spectral period $T_{m-1,0}$ instead of the peak period (GRÜNE & WANG, 2000).

5.3 Wave run-up and wave overtopping under oblique wave attack

Several investigations were done by analyzing the influence of different angles of wave attack on wave run-up and overtopping. This aspect is described by an influence factor γ_β considering the following ratios for the run-up height and the overtopping rate:

$$\gamma_\beta = \frac{R_{u2\%;\beta>0°}}{R_{u2\%;\beta=0°}} \tag{5.13}$$

$$\gamma_\beta = \frac{q_{\beta>0°}}{q_{\beta=0°}} \tag{5.14}$$

with γ_β influence factor [-]

β angle of wave attack (β = 0° for perpendicular wave attack) [°]

$R_{u2\%;\beta>0°}$ run-up height exceeded by 2% of the incoming waves with $\beta > 0°$

$R_{u2\%;\beta=0°}$ run-up height exceeded by 2% of the incoming waves with $\beta = 0°$

$q_{\beta>0°}$ overtopping rate with angle of wave attack $\beta > 0°$

$q_{\beta=0°}$ overtopping rate with angle of wave attack $\beta = 0°$

First investigations concerning this aspect on smooth sloped dikes were done by WASSING (1957) with regular waves using the following formula for the influence factor:

$$\gamma_\beta = \frac{1+\cos\beta}{2} \tag{5.15}$$

Field measurments have been done by WAGNER & BÜRGER (1973) on different dike slopes (1:2.7; 1:3; 1:3.3; 1:3.6). The following formula for the influence factor was found:

$$\gamma_\beta = 0.35 + 0.65 \cdot \cos\beta \tag{5.16}$$

Further investigations with regular waves were done by TAUTENHAIN ET AL. (1982) on a 1:6 sloped dike for angles of wave attack up to 60°. An increasing wave overtopping rate while increasing the angle of wave attack up to 30° was determined. An increasing of the overtopping rate was also determined by OWEN (1980) for vertical structures and JUHL & SLOTH (1994) for breakwater. The formula for the influence factor for the obliquity by TAUTENHAIN ET AL. (1982) is given by

$$\gamma_\beta = \cos\beta \cdot \sqrt[3]{2-\cos^3(2\beta)} \tag{5.17}$$

DE WAAL & VAN DER MEER (1992) investigated this influence on 1:2.5 and 1:4 sloped dikes with and without berms for angles of wave attack up to 80°. Different formulae were determined for long and short crested waves. For short crested waves different influence factors were determined for wave run-up and wave overtopping (cf. formulae (5.18) and (5.19)). The influence of short crested waves is less than for long crested waves.

$$\left.\begin{array}{lll} \beta < 10° & \Rightarrow & \gamma_\beta = 1 \\ 10° \le \beta \le 50° & \Rightarrow & \gamma_\beta = \cos^2(\beta - 10) \\ \beta > 10° & \Rightarrow & \gamma_\beta = 0.6 \end{array}\right. \quad \text{for long crested waves} \tag{5.18}$$

$$\text{run-up:} \quad \gamma_\beta = 1 - 0.0033 \cdot \beta$$
$$\text{overtopping:} \quad \gamma_\beta = 1 - 0.0022 \cdot \beta \quad \text{for short crested waves} \tag{5.19}$$

OUMERACI ET AL. (2002) do not distinguish between long and short crested waves in the investigations for determine the formulae for the influence factor. Investigations have been done on a 1:3 and 1:6 sloped dike. The formulae, different for the two investigated dike slopes, is based on the formula by WAGNER & BÜRGER (1973):

$$\gamma_\beta = 0.10 + 0.90 \cdot \cos\beta \quad \text{for the 1:3 sloped dike} \tag{5.20}$$

$$\gamma_\beta = 0.35 + 0.65 \cdot \cos\beta \quad \text{for the 1:6 sloped dike} \tag{5.21}$$

The latest formula bases on investigations by KORTENHAUS (2009) also o 1:3 and 1:6 sloped dikes. Only one formula was found:

$$\gamma_\beta = 1.00 + 0.0076 \cdot \beta \tag{5.22}$$

Table 5.2 summarize the main formulae for the influence factor γ_β considering investigations on smooth sloped dikes. The corresponding graphs are given in Figure 5.1. In the literature the increasing influence factor by increasing the angle of wave attack up to 30° by TAUTENHAIN ET AL. (1982) is caused to measurement uncertainties. Up to an angle of wave attack of 40° all listed authors except TAUTENHAIN ET AL. (1982) and KORTENHAUS (2009) give similar characteristics of γ_β. For angles of wave attack higher than 40° the influence on wave run-up and wave overtopping the authors give quite different curves.

Table 5.2 Resume of formula for the influence factor γ_β of former investigations o smooth sloped dikes

author	**year**	**slope of structure (inclination, roughness)**	**kind of waves (long, short, regular, irregular)**	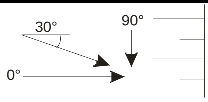 **influence factor γ_β**
Wassing	1957		regular waves	$\frac{1+\cos\beta}{2}$
Tauten-hain et al.	1982	1:6 sloped dike d = 0,35m	regular single waves	$\cos\beta \cdot \sqrt[3]{2-\cos^3(2\beta)}$ $\beta < 60°$
De Waal & Van der Meer; EurOtop-Manual	1992; 2007	1:2.5 and 1:4 sloped dike; with and without berm	long	1; $0 \le \beta < 10$ $\cos^2(\beta-10)$; $10 \le \beta \le 50$ 0.6; $\beta > 50$
			short	$1 - 0.0033 \cdot \beta(\text{ov})$ $1 - 0.0022 \cdot \beta(\text{run-up})$
Oumeraci et al.	2002	1:3 sloped dike	long and short crested waves	$0.1 + 0.90 \cdot \cos\beta$
		1:6 sloped dike		$0.35 + 0.65 - \cos\beta$
Korten-haus et al.	2009	1:3 and 1:6 sloped dike	breaking and non-breaking waves	$1.0 - 0.0076 \cdot \beta$

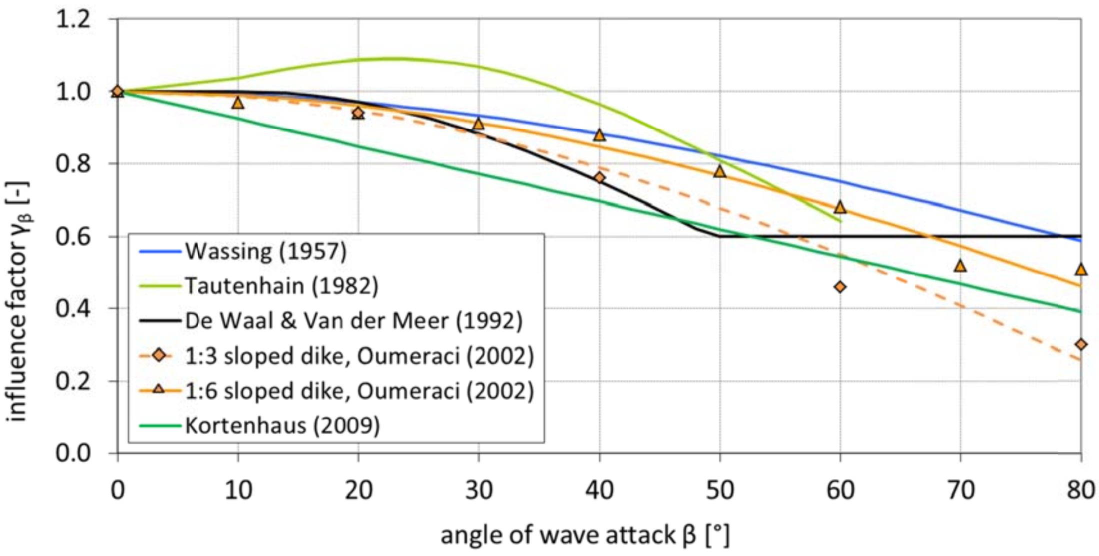

Figure 5.1 Angle of wave attack against influence factor γ_β of former investigations

5.4 Method of analyzing data on wave run-up and wave overtopping

5.4.1 General

The EUROTOP-MANUAL (2007) has been used to analyze the data and to derive influencing factors including current. The EUROTOP-MANUAL (2007) distinguishes between formulae for wave run-up and wave overtopping, for breaking and non-breaking wave conditions. It should be mentioned, that the adapted formulae in this work are stated for short crested waves, but within the model tests only long crested waves were generated. This has to be considered for comparison of the analysis.

5.4.2 Wave run-up

Usually the influence of different factors on wave run-up height could be determined using a formula which was originally suggested by HUNT (1959) and then upgraded in EUROTOP-MANUAL (2007) with different correction parameters:

$$\frac{R_{u2\%}}{H_{m0}} = c_1 \cdot \gamma_b \cdot \gamma_f \cdot \gamma_\beta \cdot \xi_{m-1,0} \tag{5.23}$$

with its maximum:

$$\frac{R_{u2\%}}{H_{m0}} = \gamma_f \cdot \gamma_\beta \cdot \left(c_2 - \frac{c_3}{\sqrt{\xi_{m-1,0}}} \right) \tag{5.24}$$

with	$R_{u2\%}$	[m]	wave run-up height which will be exceeded by 2% of all wave run-ups [m]
	γ_b	[-]	parameter which covers the influence of a berm [-]
	γ_f	[-]	parameter which covers the influence of surface roughness [-]
	γ_β	[-]	parameter which covers the influence of wave direction (angle β) [-]
	$\xi_{m-1,0}$	[-]	surf similarity parameter based on $s_{m-1,0}$ [-]
	$s_{m-1,0}$	[-]	wave steepness based on H_{m0} and $L_{m-1,0}$ [-]

$L_{m-1,0}$	[m]	deep water wave length based on $T_{m-1,0}$ [m]
$T_{m-1,0}$	[s]	spectral wave period [s]
H_{m0}	[m]	significant wave height from spectral analysis [m]

The empirical parameters c_1, c_2 and c_3 are dimensionless and defined as follow:

$$c_2 = c_1 \cdot \xi_{tr} + c_3 / \xi_{tr} \tag{5.25}$$

with ξ_{tr} [-] surf similarity parameter describing the transition between breaking and non-breaking waves

For a prediction of the average run-up height $R_{u2\%}$ the following values $c_1 = 1.65$, $c_2 = 4.0$ and $c_3 = 1.5$ should be used.

5.4.3 Wave overtopping

The EUROTOP-MANUAL (2007) is the base of the analysis of wave overtopping in the current research project (cf. previous chapter 5.2). Therefrom formulae (5.26) can be used to calculate the average overtopping discharge q in liter per second and per meter dike length for given geometry and wave condition based on the van der Meer & Janssen formulae (cf. Table 5.1). As the non-breaking condition the overtopping discharge limits to a maximum value, see formula (5.27). The smallest value of both equations should be taken as the result.

Breaking wave conditions:

$$\frac{q}{\sqrt{g \cdot H_{m0}^{\ 3}}} = \frac{0.067}{\sqrt{\tan\alpha}} \cdot \gamma_b \cdot \xi_{m-1,0} \cdot \exp\left(-4.75 \frac{R_C}{\xi_{m-1,0} \cdot H_{m0} \cdot \gamma_b \cdot \gamma_f \cdot \gamma_\beta \cdot \gamma_\upsilon} \right) \tag{5.26}$$

With a maximum for non-breaking wave conditions:

$$\frac{q}{\sqrt{g \cdot H_{m0}^{\ 3}}} = 0.2 \cdot \exp\left(-2.6 \frac{R_C}{H_{m0} \cdot \gamma_f \cdot \gamma_\beta} \right) \tag{5.27}$$

with

q	mean overtopping discharge per meter structure width [m³/s/m]	
α	slope of the front face of the structure [°]	
R_c	crest freeboard of structure [m]	
γ_υ	correction factor for a vertical wall on the slope [-]	

With $\frac{R_{u2\%}}{c_1} = \xi_{m-1,0} \cdot H_{m0} \cdot \gamma_b \cdot \gamma_f \cdot \gamma_\beta$ (cf. formula (5.23) and EurOtop 2007) and $c_1 = 1.65$ the dimensionless overtopping rate results in:

$$\underbrace{\frac{q}{\sqrt{g \cdot H_{m0}^3}} \frac{\sqrt{\tan\alpha}}{\gamma_b \cdot \xi_{m-1,0}}}_{q_*} = \underbrace{0.067}_{Q_0} \cdot \exp\left(-\underbrace{4.75}_{b} \cdot \underbrace{\frac{1.65 \cdot R_c}{\gamma_\upsilon \cdot R_{u2\%}}}_{R_*} \right) \tag{5.28}$$

This relation gives the probabilistic curves for overtopping calculation using the following factors (see also the graphs in the EUROTOP-MANUAL (2007) :

- breaking waves: $Q_0 = 0.067$; $b = -4.75$
- non-breaking waves: $Q_0 = 0.2$; $b = -2.6$

Contrary to EUROTOP (2007), no difference is made in formula (5.28) between the influence factor for obliquity γ_β for wave run-up and wave overtopping. In the current report there will be determined one influence factor γ_β valid for both wave run-up and overtopping.

In a first step the influence factor γ_β will be determine separately for wave run-up and wave overtopping. Later on they will be compared and one valid parameter will be determined for both wave run-up and wave overtopping.

Reduction factors for wave overtopping for obliqueness γ_β can be determined by comparing the exponential coefficients b_β for normal wave attack ($\beta = 0$) and oblique wave attack ($\beta \neq 0$):

$$\gamma_\beta = \frac{b_{\beta=0}}{b_\beta} \tag{5.29}$$

A new reduction factor $\gamma_{\beta,cu}$ is introduced in the same way to take the influence of current v_x into account:

$$\gamma_{\beta,cu} = \frac{b_{\beta=0,cu=0}}{b_{\beta,cu}} \tag{5.30}$$

5.5 Flow processes on dike crests

Nowadays, the research on wave run-up and wave overtopping intends to describe also the flow processes on the crest. SCHÜTTRUMPF (2001) and VAN GENT (2002) describe these processes related to wave run-up and wave overtopping by flow parameters such as flow depth $h_{2\%}$ and flow velocity $v_{2\%}$. A formula resulting from a simplified energy equation is given to determine the flow depths on the seaward dike crest $h_{2\%}$ which are exceeded by 2% of the incoming waves with the formula

$$\frac{h_{2\%}}{H_s} = c_h \cdot \frac{R_{u2\%} - R_c}{H_s} \quad [-] \tag{5.31}$$

with H_s significant wave height [m]

$R_{u2\%}$ run-up height exceeded by 2% of the incoming waves [m]

R_c freeboard height [m]

c_h empirical coefficient determined by model tests [-]

Additionally flow velocities on the seaward dike crest $v_{2\%}$ are given by

$$\frac{v_{2\%}}{\sqrt{g \cdot H_s}} = c_v \cdot \sqrt{\frac{R_{u2\%} - R_c}{H_s}} \quad [-] \tag{5.32}$$

c_v empirical coefficient determined by model tests [-]

Experimental investigations on the overtopping flow parameters were performed in small and large wave flumes but the three dimensionality of the process was not investigated so far.

6 Data processing

6.1 Remarks

An evaluation of the measured raw data of the wave field, run-up and overtopping is necessary intending to analyze and present the results in order to develop or modify the existing design formulae. As described previously the raw data are available from a digitalization with $\Delta t = 0.04$ sec ($f_s = 25$ Hz) for FlowDike 1 and $\Delta t = 0.025$ sec ($f_s = 40$Hz) for FlowDike 2. In order to reduce their extent to characteristic parameters, analyses driven by time domain or by frequency domain were used.

As data processing tools the Wave Synthesizer from the DHI software package Mike Zero was used for reflection and crossing analysis. For calculation of the average overtopping volumes a MATLAB script was created, that uses the available ascii files (*.daf).

At this point it has to be mentioned, that the processed data files only exist completely for the set-ups 1 to 3 of FlowDike 1. The data processing of FlowDike 2 has not been finished yet and only the parameters of interest for the basic analysis on overtopping, such as average overtopping rate q and the incoming wave parameters at the toe of the structure were processed.

6.2 Wave field

6.2.1 Evaluated parameters

Wind and current as main influencing variables were controlled separately from the data acquisition before starting the tests. A significant reason is that during testing the current recording would be influenced by the wave distribution, thus the length of the channel is limited. The wind could only be determined in one point; hence the distribution along the dike crest had to be validated before testing.

In frequency domain the wave parameters were analyzed using a reflection analysis. Herein the reflection coefficient C_r is determined at the same time. The time-series of water level elevation is transformed and analyzed by a FOURIER-transformation giving the spectral energy density S(f) for incident and reflected wave and their average. Based on the moments m_n of the spectral densities, the following characteristic wave parameters can be calculated:

- wave height $H_{m0} = 4 \cdot \sqrt{m_0}$ [m]
- spectral wave period $T_{m-1,0} = \dfrac{m_{-1}}{m_0}$ [s]
- peak period Tp [s]

Determining the wave field in time domain, a zero-down crossing was applied, whereby single wave events were defined. From the certain quantity N of the measured surface elevation, related average values for the maximum wave height H_{max} (peak to peak decomposition) and the mean wave period T_m (event duration), can be calculated. These values are the average of all wave gauges contributing to one of the wave arrays. Other averages for characteristic height parameters, such as the significant wave height $H_S = H_{1/3}$, have not been analyzed yet.

Wave run-up events are the maximum elevations of the run-up tongue from the still water level. The wave run-up height is determined with a crossing analysis using a threshold level different from zero. Therefore a different number of events results compared to the number of wave events. The calculation of statistical wave run-up characteristics has to be related to the number of incoming waves. In the following the analysis of the wave field and wave overtopping will be discussed.

The overtopping is calculated by adding the lost pump volumes (recalculation from known capacity and working period) to the collected amount within the tank. By dividing the overtopping amount with the channel width of 0.1 m (0.118 m before sharpening the edges of the inlet) and the testing duration an average overtopping rate q in l/(s·m) is determined for each tank.

Crossing analysis with a defined threshold is done as well for the measurement devices on the crest. Here the micro propellers were measuring the flow velocity on the crest at the seaward $v_{C,s}$ and the landward edge $v_{C,l}$, while the wave gauges gave the signals for the layer thickness $h_{C,s}$ and $h_{C,l}$. As described earlier, statistical characteristics were determined as a relation of detected events and number of waves.

For data analysis the following parameters were distinguished to be analyzed in a first step:

- Evaluation from wave measurements:
- Frequency domain: H_{m0}, T_p, C_r, $T_{m-1,0}$
- Time domain: H_{max}, T_m, N
- Plots: time series, energy density, reflection function
- Analysis on wave run-up and wave overtopping:
- Time domain: $R_{u2\%}$
  percentage of wave overtopping the freeboard heights: P_{OW-60}, P_{OW-70}
  average overtopping rate q
- Plots: time series, exceedance curves
- Analysis on flow velocity and flow depth:
- Time domain: $v_{C0.1\%}$, $v_{C2\%}$, $v_{C5\%}$, $v_{C10\%}$ each for seaward and landward edge
  $h_{C0.1\%}$, $h_{C2\%}$, $h_{C5\%}$, $h_{C10\%}$ each for seaward and landward edge
- Plots: time series, exceedance curves

These signals were determined by two wave arrays of 5 wave gauges (with a length of 60 cm each) and a current meter. An overall view given in Figure 6.1 and Figure 6.2 and demonstrates that each of them is orthogonal aligned between the wave generator and an overtopping unit. Each array was assigned to one crest height and placed at the toe of the structure positioned between the overtopping channels.

For the following reflection analysis a defined alignment of 0.00 m– 0.40 m– 0.75 m– 1.00 m– 1.10 m was kept for the single wave gauges. Both, ADV and Minilab SD-12 are positioned close to one wave gauge of the array (see Figure 6.1 and Figure 6.2). The simultaneously measured surface elevation and velocity in this point will be used for the directional spreading analysis. Reflection, crossing and directional analysis will be evaluated from each array and its defined velocity meter.

During tests on the 1:6 sloped dike the development of the wave field due to current affection was analyzed by adding a third wave array, which was placed in front of the wave generator. Both other arrays were situated as close as possible to the toe of the structure. Each of them was assigned to one of the crests and aligned between the channels of the overtopping units. In order to distinguish the effect of the current on the directional change of the wave field a distance of 1.12 m was kept between the two wave arrays at the toe of the structure and the one near the wave generator. For the directional analysis of this third wave array an additional current meter was needed. Therefore the Vectrino was used.

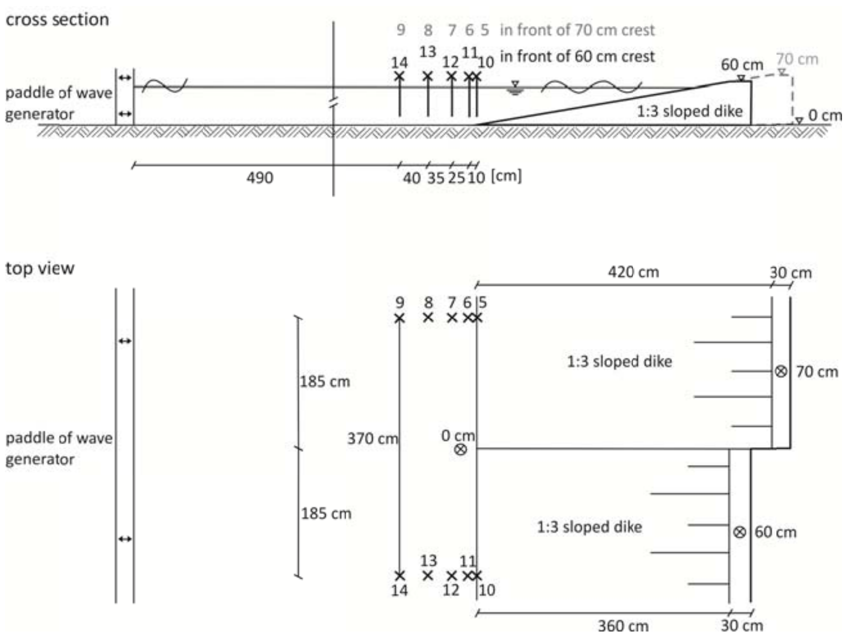

Figure 6.1 Cross section and top view of the configuration of the wave arrays exemplary for the 1:3 sloped dike

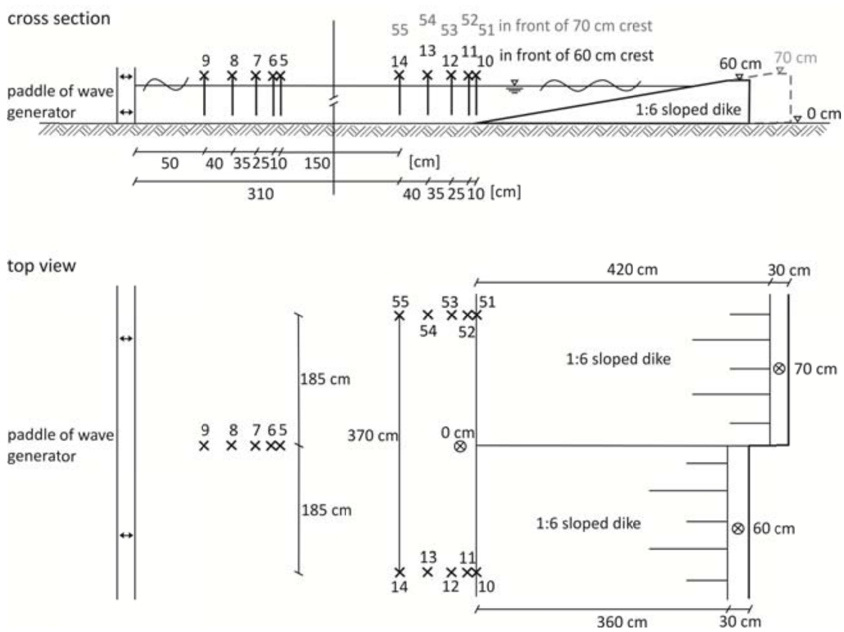

Figure 6.2 Cross section and top view of the configuration of the wave arrays exemplary for the 1:6 sloped dike

6.2.2 Signals wave field

In the previous chapters it was mentioned, that a JONSWAP spectrum was used for the investigations. A typical raw data is illustrated in Figure 6.3. The red line is the fixed crossing level at the SWL when the wave gauges should give no surface elevations. The shift between the peaks of each wave gauge is due to the defined distances within the alignment of 0 - 0.4 - 0.75 - 1.0 - 1.1 in the wave array. These defined distances have to be specified within MikeZero for the reflection analysis. For oblique wave attack the array was not changed in position to a perpendicular attack of the long crested waves, so the distance was recalculated with a factor of the cosine of the angle of wave attack. From the crossing analysis the maximum of detected events of all wave gauges is taken as number of waves N.

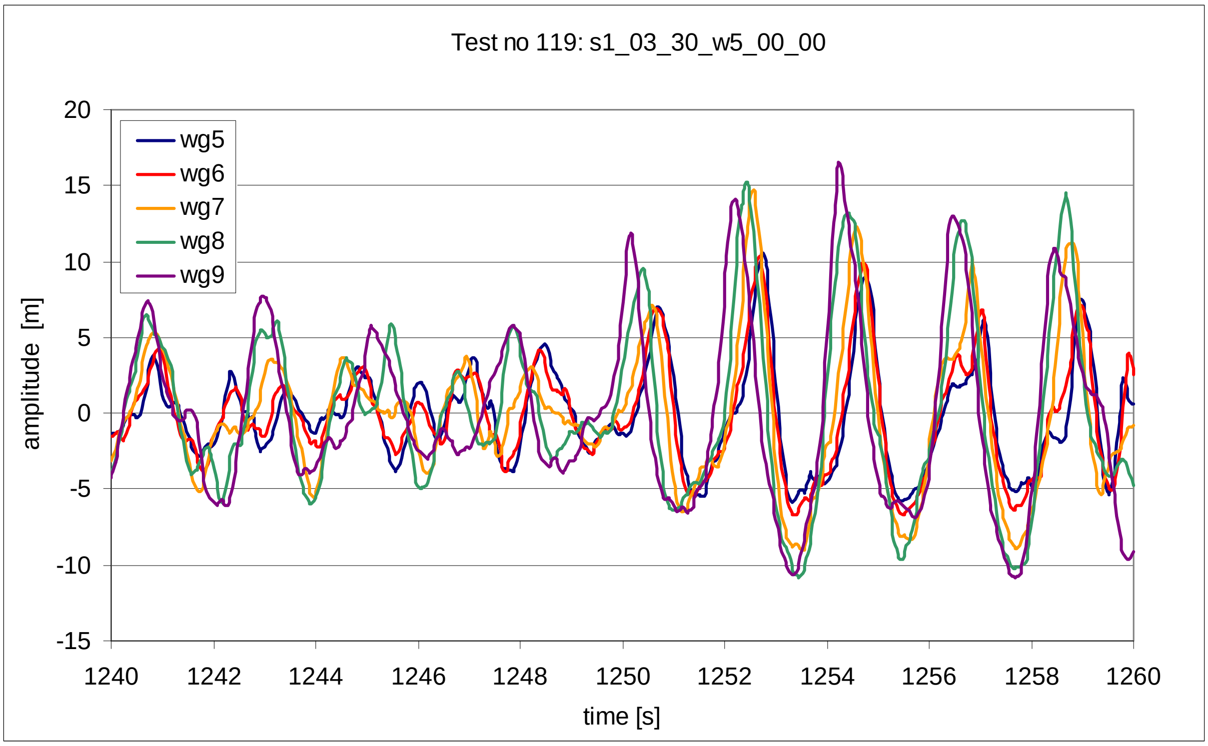

Figure 6.3 Raw data for the wave gauge array of gauges 9-5

6.3 Wave run-up

6.3.1 Video analysis

Stored video data had a compacted AVI-format (*Codec VRMM*) with 10 frames per second. To detect the highest wave run-up height for each frame a MATLAB procedure has been used. In order to get the run-up time series we have to assign the recording time of each frame to the detected run-up in it.

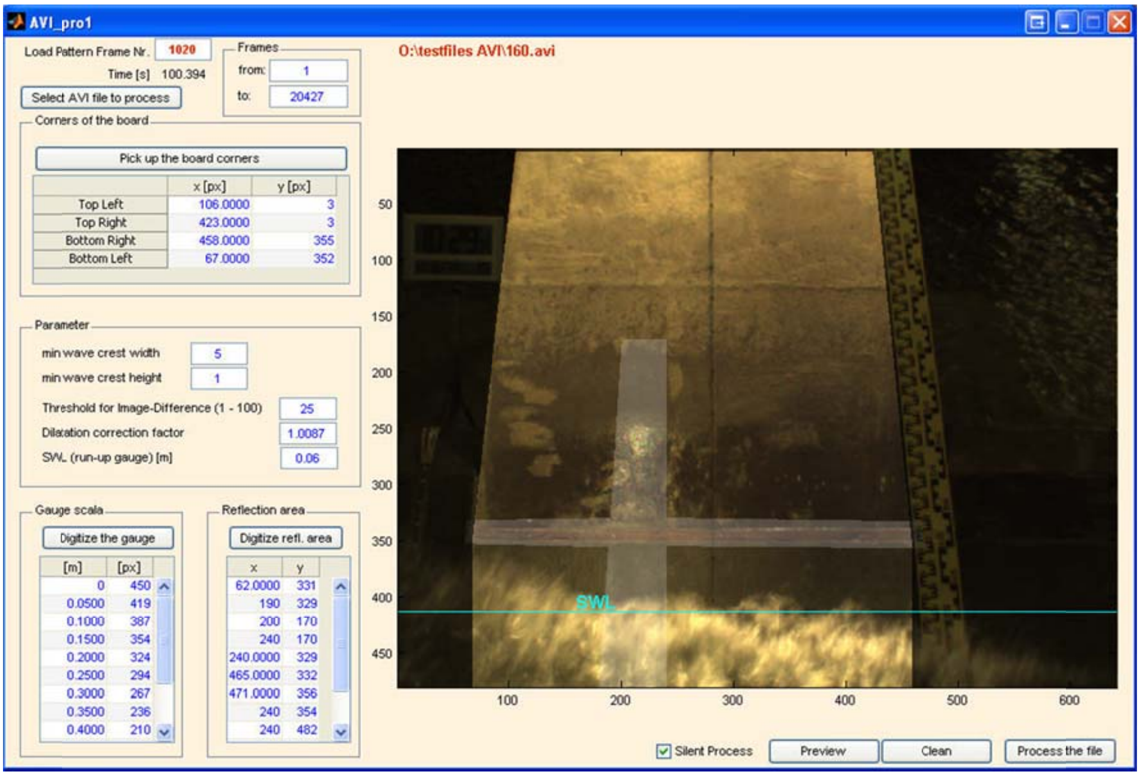

Figure 6.4 MATLAB interface which was used to analyse video films

In the first step of the procedure we have to find in which parts (pixel) of the frame a movement has taken place which is visible by changes in pixel brightness. Therefore the difference between two pictures in sequence was calculated. The difference is equal zero if there was no movement and unequal zero if there was a movement. A variable threshold (threshold for image difference, see “Parameter” in Figure 6.4) has been used to adjust the sensitivity in detection of pixels with significant brightness difference.

In a next step the value “1” (white) was assigned to pixels with significant brightness difference and the value “0” (black) to all others.

After than we have to determine that pixel region of a certain width (min. wave crest width = 5 pixel) and height (min. wave crest height = 1 pixel) which was located at the highest level within one frame. The setting of these two parameters is possible within the left section “Parameter” of the designed MATLAB interface (see Figure 6.4). It was necessary to determine a minimum wave crest width to avoid false detection of reflections on the rough surface of the run-up board or due to water drops as wave tip. A min. wave crest width of 5 pixels was sufficient in most cases.

Now the level value [pixel] of all white regions wider than or equal to min. wave crest width was determined. At the end the region with the global maximum of all level values was identified.

Before one could start the procedure several parts of the pictures has to be excluded from analysis due to several reasons. The size and the location of the excluded picture regions have to be determined for each model test because it could be possible that the location of the camera had be changed between two model tests.

The parts at the left and the right side of the pictures for instance are not necessary within the analysis because they only include things which are located behind the run-up board. These parts were "cut out" by means of a tool which was integrated in the designed MATLAB interface (left below in Figure 6.4). These parts are marked with a darker color in Figure 6.5.

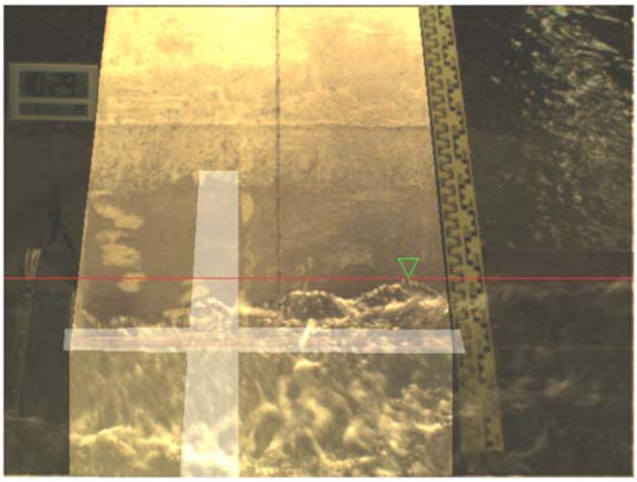

Figure 6.5 Detected position of the highest wave tip on the run-up plate (red line with green triangle)

Another almost perpendicular bar, which is marked with a lighter color in Figure 6.5 was excluded due to frequent reflections causing by the light of a ceiling lamp which occurred still after the waves run down. The third region is shaped like a horizontal bar and is also marked with a lighter color in Figure 6.5. This bar covers the boundary between the dike slope and the run-up board. Water drops remain there due to very small roughness elements and could be detected as wave tips although the wave runs already down.

In order to get a photo documentation of the model tests every single test and every device has been photographed during test program. Due to its smooth surface camera flash lights were reflected by the gauge scale and false detections of wave run-up could be created. That's why the gauge scale at the right side of the run-up plate was excluded from analysis too.

The detected wave run-up height can be visualized within the video in order to verify the detection process. This is marked with a red line and a green triangle in Figure 6.5. During the video analysis every picture was transformed into grey scale and there was no visualization on the screen in order to get a higher detection speed. Therefore the procedure was started in batch modus.

The last step in the procedure was to calculate the run-up height value in meter out of the run-up height in pixel. There was a nonlinear function due to the optical distortion within the camera lens and due to the effects of perspective because the image plane was not parallel to the run-up board.

This nonlinear function has to be determined for each model test before the analysis was conducted. Therefore several data are used. At first one has to click on the gauge scale in the picture displaced within the designed MATLAB interface. The obtained data set [cm; pixel] is visible as a table in the left and below corner in Figure 6.4 (“gauge scale”). Another used value was the still-water-level. One has to determine its height above level zero of the gauge scale in the set “Parameter” as “SWL” (see Figure 6.4, left and middle). Another needed parameter was the dilatations correction factor. Its determination has been described in chapter 3.3. All these data has been used to obtain a polynomial function of degree 3 to calculate R [m] out of R [pixel].

During the data analysis it was considered to get more data with the existing model tests. Therefor an advanced data analysis routine was developed. Within this routine the run-up height for 10 stripes each representing the tenth part of the run-up board width (see Figure 6.6) was determined.

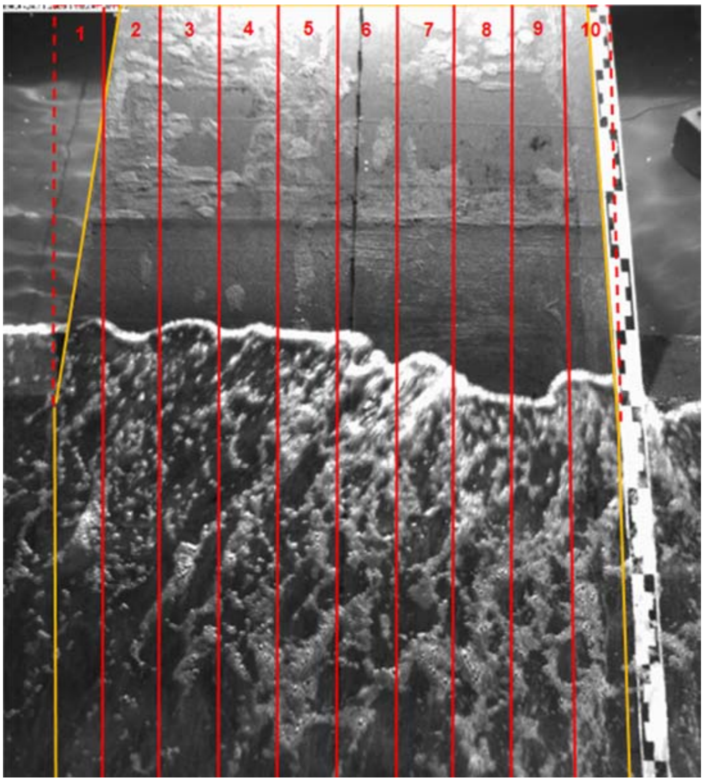

Figure 6.6 Definition of 10 stripes for advanced run-up data analysis within the MATLAB interface.

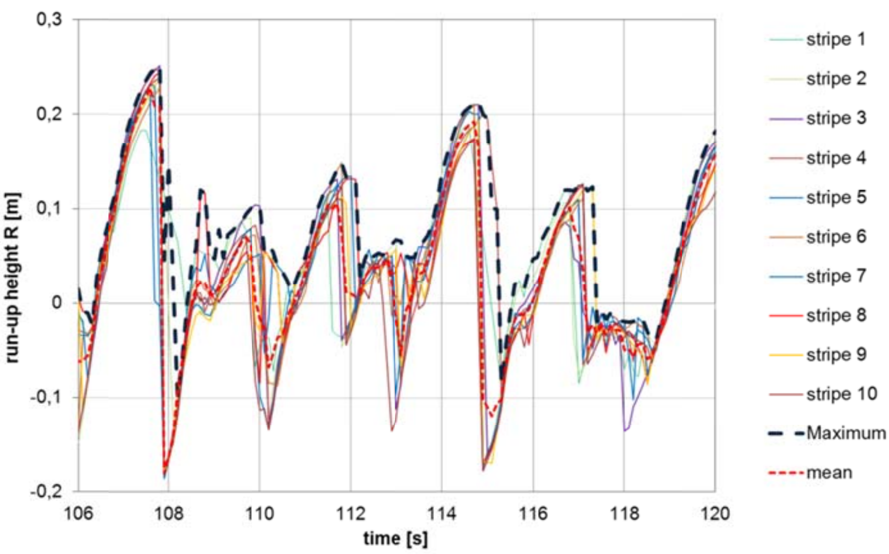

Figure 6.7 Run-up height depending on time for 10 stripes of the run-up plate.

It is possible to get 10 time variation curves of wave run-up R for each test and not only one (see Figure 6.7). The data extraction is still in work and will be finished soon.

6.3.2 Measurement results of the run-up-gauge

The values measured by the capacitive gauge has been stored with all values from other devices as wave gauges, anemometers, micro propellers and ADV in central data storage directly. The unit of these values is Volt and the time series format is *.dsf0. The latter is a binary code developed by DHI.

Functions (3.2) to (3.5) have been used to calculate the run-up height in meter according to the model set-up.

During the analysis it has been found that the still-water-level in some test records was higher at the end of the test ($t = t_{END}$) than at the beginning ($t = t_0$). The difference was about 1 cm. The reason was that after the first waves run up little water remained between the two wires above the ring-shaped distance pieces. This was only visible when the water had enough time to evaporate from the wires for instance overnight and the wires were totally dry before the tests began. This effect was easily identifiable and has been considered within the data analysis.

6.3.3 Determination of $R_{2\%}$

As wave run-up height the value $R_{2\%}$ is often used within literature. This is the run-up height which has been exceeded by 2 % of all arriving waves of a wave spectrum. Another MATLAB procedure has been used to calculate $R_{2\%}$ on basis of run-up time series (see chapter 6.3.1).

Within the procedure a zero-down-crossing has been used to get the maximum height of each wave run-up. These n maximum values were than sorted in descending order.

In a second step the number m of all waves which run up the slope during one model test has been determined. The number of m could differ from n.

The value of $R_{2\%}$ was equal to that wave run-up height which has been exceeded by more than $k = 0.02 \cdot m$ wave run-ups.

6.4 Wave overtopping

For the following analysis the amount of overtopping water was calculated. It occurs that the amounts of both overtopping boxes per crest heights differ a lot from each other. This would be noticeable as scattering in the analysis. Since for analysis an averaged amount of both tanks is used, this information will be lost in the analyzing chapter.

The Figure 6.8 (left) shows the raw signal for the evaluated overtopping. This time no pumping was applied and the single events are visible, as well as the final overtopping amounts (65 kg for load cell 43). A total amount of overtopping is calculated from this raw data at the end of the test series. The load in kg (or l) is divided by the test duration and the width of the inlet channel. So, in this case the calculation for load cell 43 is: $q = 65\ l/(1350\ s \times 0.118\ m) = 0.408\ l/(s \cdot m)$.

The accuracy of the load cell is within a non-linearity of < 0.05%. This means for a maximum measuring range of approximately 220 kg (2150 N) this gives a detectable load of 0.11 kg. For the demonstrated test series, with generated wave spectra w1, the overtopping amount on the 70 cm crest is so small that it would not be taken into account in the analysis. As definition for “detectable” overtopping amounts, a value beneath 0.02 l/(s·m) will be assumed to be negligible.

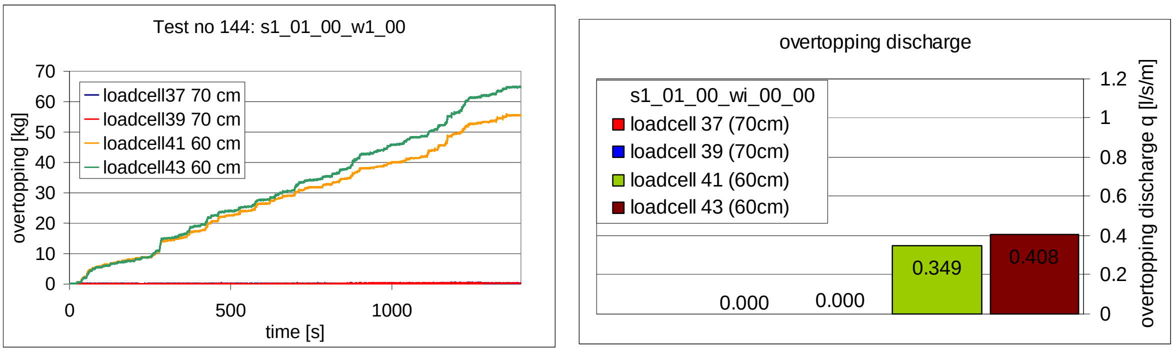

Figure 6.8 Overtopping raw data (left) and calculated overtopping discharge (right)

6.5 Flow processes on crest

6.5.1 Flow velocity on the crest

In future the main interest will focus on the analysis and description of the single overtopping events. Therefore, also the process of the overtopping on the crest will be analyzed in detail. The micro propellers are processed in the same way as the run-up. Threshold levels (0.1 Volt and 1 Volt, see Figure 6.9) were selected to identify the number of events.

Afterwards the measured velocities are displayed within an exceedance curve (see Figure 6.10). Here, values are calculated by adding the threshold and multiplication of the voltage readings with the defined calibration factor (see Annex). The 2%-value for the velocities on the 60 cm are 1.2 m/s (mp 35) and 1.33 m/s (mp 36). For the 70 cm only for the seaward side some items were detected, but do not give any useful results. This fits well with the results from the overtopping.

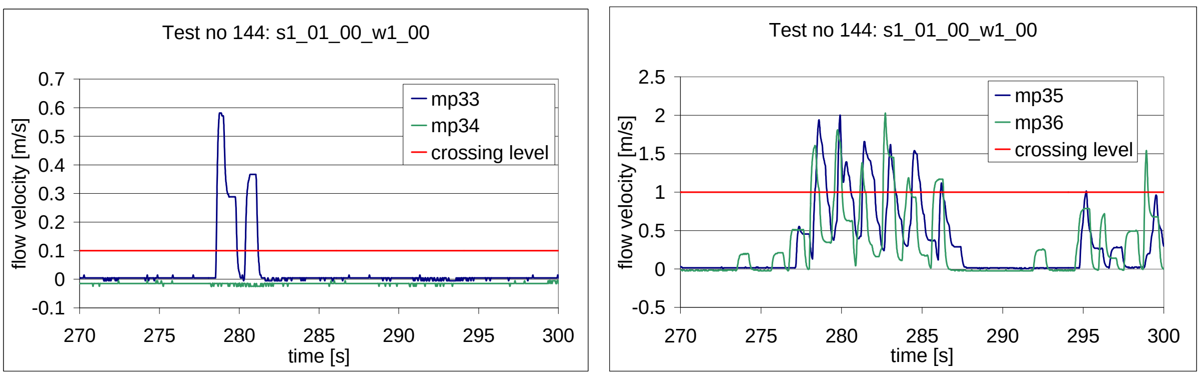

Figure 6.9 Raw data with crossing level - micro propellers on 70 cm crest (left); micro propeller on 60 cm crest (right)

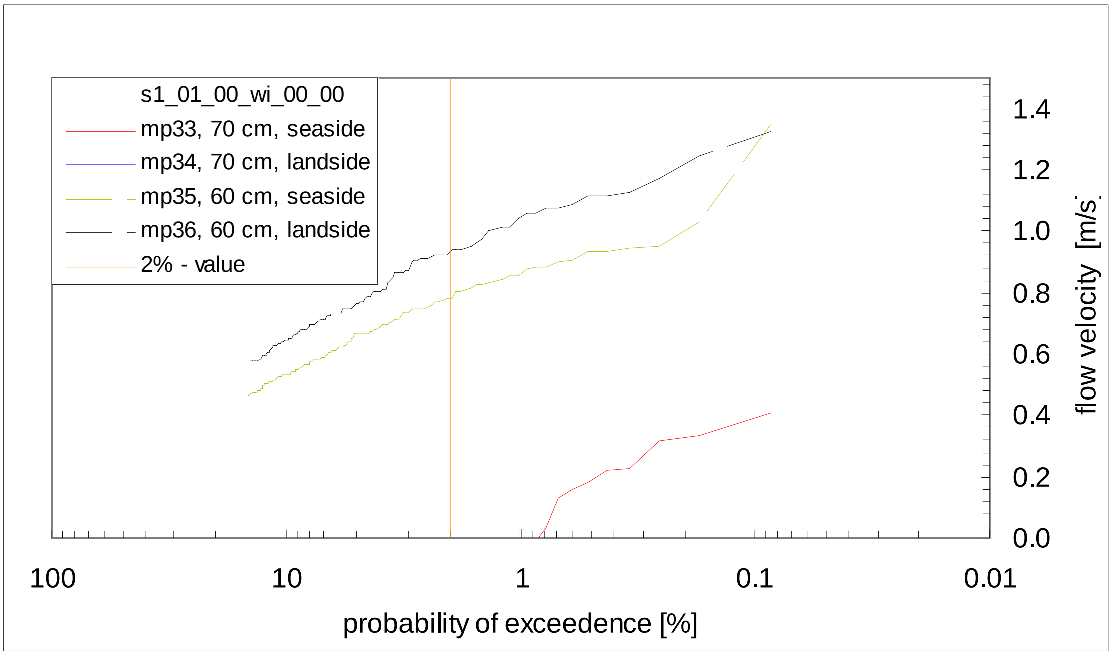

Figure 6.10 Exceedance curves for micro propellers

6.5.2 Flow depth on the crest

The procedure in processing remained the same for the layer thickness, as it was done for run-up and flow velocities. The data from the DHI Wave Synthesizer was already given in m, therefore no calibration hat to be added on it.

As mentioned above for the micro propellers, items for the 70 cm crest are detected (see the raw data in Figure 6.11), but the exceedance curves do not even reach the 2%-value. This illustrates Figure 6.12; the flow depths for both crest heights are given. Due to the different freeboard heights, the layer thickness on the 70 cm crest is lower than on the 60 cm crest. It can be remarked that the flow depth decreases over the width of the crest, since the wave gauges on the landward edge give smaller values than the ones on the seaward side. The 2%-values of the layer thickness on the 60 cm crest are 0.017 m (wg 17) and 0.026 m (wg 16).

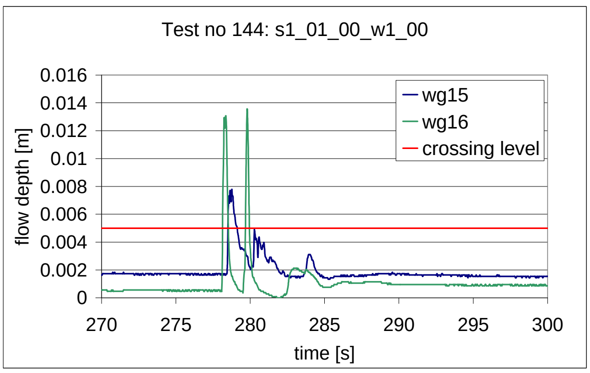

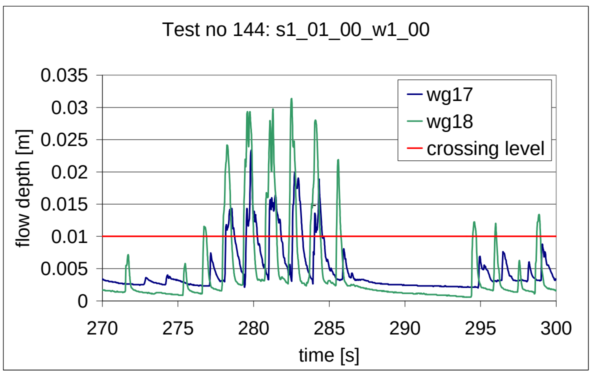

Figure 6.11 Raw data with crossing level – wave gauges on 70 cm crest (left); wave gauges on 60 cm crest (right)

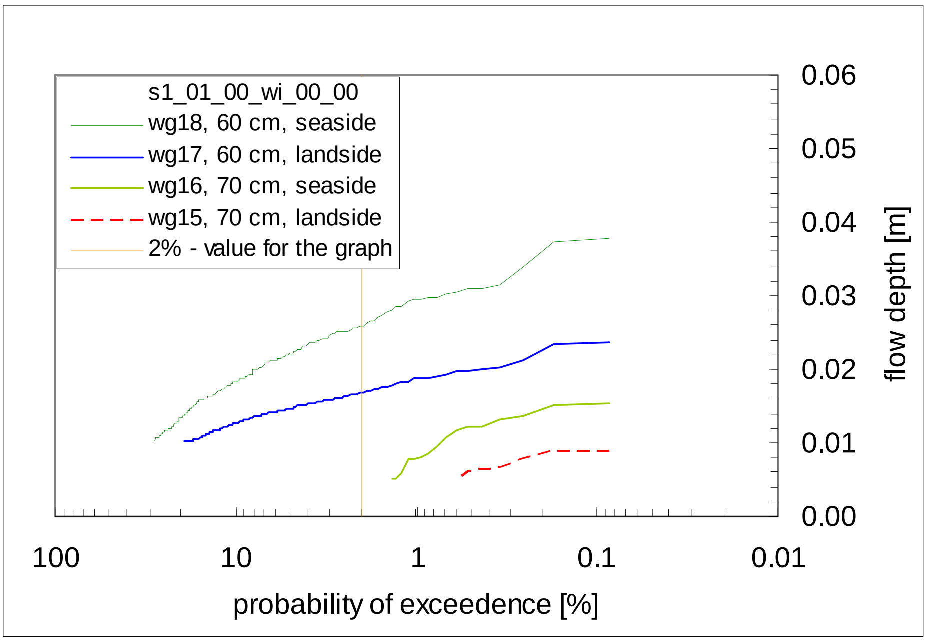

Figure 6.12 Exceedance curves for wave gauges

7 Analysis of wave field and breaking processes

7.1 General

To analyse the wave evolution in front of the dike, the results from reflection and zero-down-crossing analysis were evaluated. The reflection analysis is done in frequency domain, the zero-down-crossing analysis in time domain.

7.2 Homogeneity of wave field

7.2.1 Wave gauge signal

The wave spectrum at the toe of the dike was measured by two wave arrays of 5 wave gauges each (see chapter 3.1 and 3.2.3). The wave array was situated at the toe of the 60 cm high dike and the second wave array was located at the toe of the 70 cm high dike of each dike slope. While testing the 1:6 sloped dike an additional wave array was located in front of the wave generator. In Figure 7.1 and Figure 7.2 the signals during the beginning of the reference tests (no current, no wind, perpendicular wave attack) are given for all wave gauges measuring the wave field exemplary for the wave no. 5:

- 1:3 sloped dike (Figure 7.1):
  - at the toe of the 60 cm high dike
  - at the toe of the 70 cm high dike
- 1:6 sloped dike (Figure 7.2):
  - in front of the wave generator
  - at the toe of the 60 cm high dike
  - at the toe of the 70 cm high dike

During the first waves only the incident wave is measured, because no reflection has occurred at this moment. But the graphs show that some wave gauges give different wave heights for the first incoming waves up to 15% (marked by a red ellipse in Figure 7.1 and Figure 7.2, orange and green graphs). Due to unclear signals of these wave gauges, the incoming waves are analyzed in more detail.

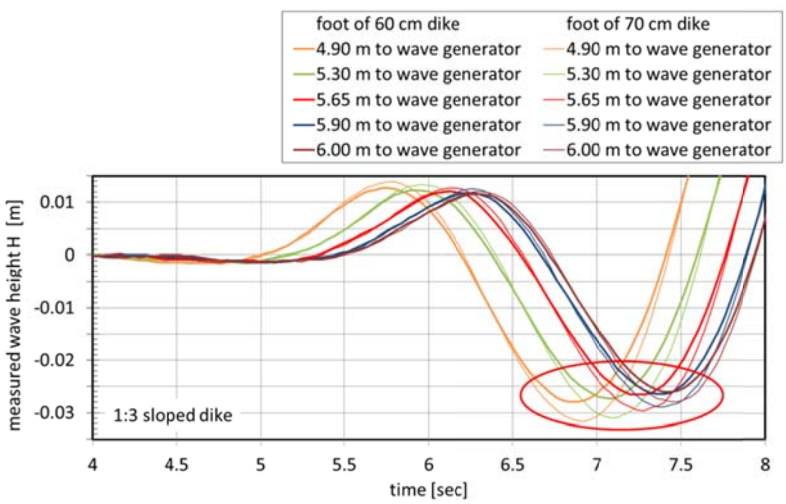

Figure 7.1 Signal of wave gauges exemplary for the reference test, wave spectrum no. 5; 1:3 sloped dike

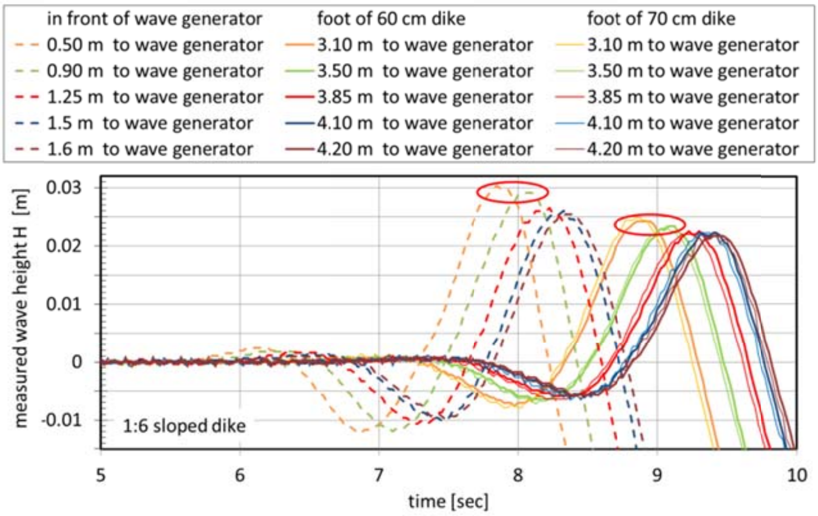

Figure 7.2 Signal of wave gauges exemplary for the reference test, wave spectrum no. 5; 1:6 sloped dike

7.2.2 Zero-down-crossing analysis - time domain

As a result of the zero-down-crossing analysis in time domain of the measured wave heights H_{m0}, Figure 7.3 depicts the Rayleigh distribution of wave heights exemplarily for the wave array at the toe of the 70 cm high and 1:6 sloped dike. The Rayleigh distribution is common for the analysis of Jonswap spectra in deep water. The abscissa is fitted to a Rayleigh scale by means of the relation:

$$x' = (-\ln(1-(100\% - x\%)/100))^{0.5} \tag{7.1}$$

The fit is the reason why a linear trend is found. The similarity of their shape indicates the homogeneous arrangement for both dike heights.

The wave height exceeded by 2% of the waves $H_{2\%}$ in [m] is a dimension for the homogeneity of the wave field as well as the correct measuring of the wave gauges. Figure 7.4 and Figure 7.5 show the standard deviation of the wave heights $H_{2\%}$ of each wave array for the tests without current and wind, but with different angles of wave attack. In contrast Figure 7.6 and Figure 7.7 show also the standard deviation of the wave heights $H_{2\%}$ considering only three wave gauges. The standard deviations of $H_{2\%}$ considering all five wave gauges (Figure 7.4 and Figure 7.5) are higher than the standard deviations of $H_{2\%}$ considering only three wave gauges (Figure 7.6 and Figure 7.7).

The standard deviations of $H_{2\%}$ of the tests on the 1:6 sloped dike are with the exception of one value smaller than 0.01 m. The comparative high standard deviation for the wave spectra 5 of the test with perpendicular wave attack can be traced back to prematurely breaking waves. The standard deviations of $H_{2\%}$ of the tests on the 1:6 sloped dike with a maximum of 6 mm are negligible.

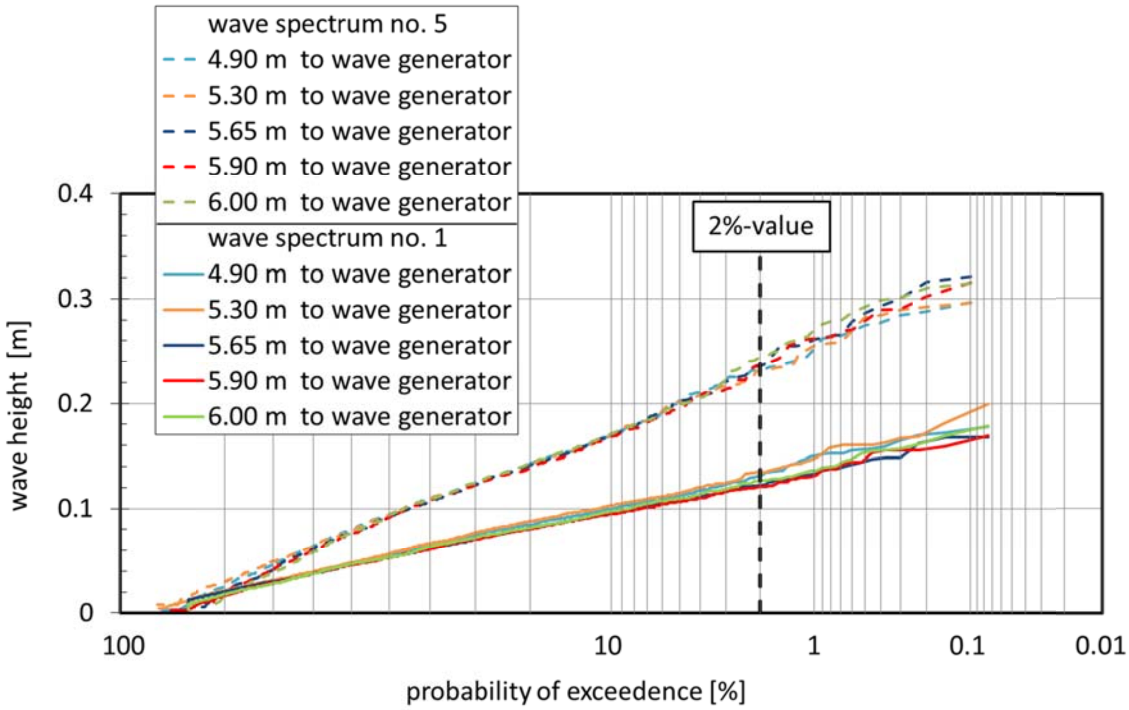

Figure 7.3 Linear distribution of wave height H_{m0} over a Rayleigh scale for a Jonswap spectrum exemplarily for the wave gauges at the toe of the 70 cm dike on the 1:6 sloped dike (wave no. 1 and wave no. 5)

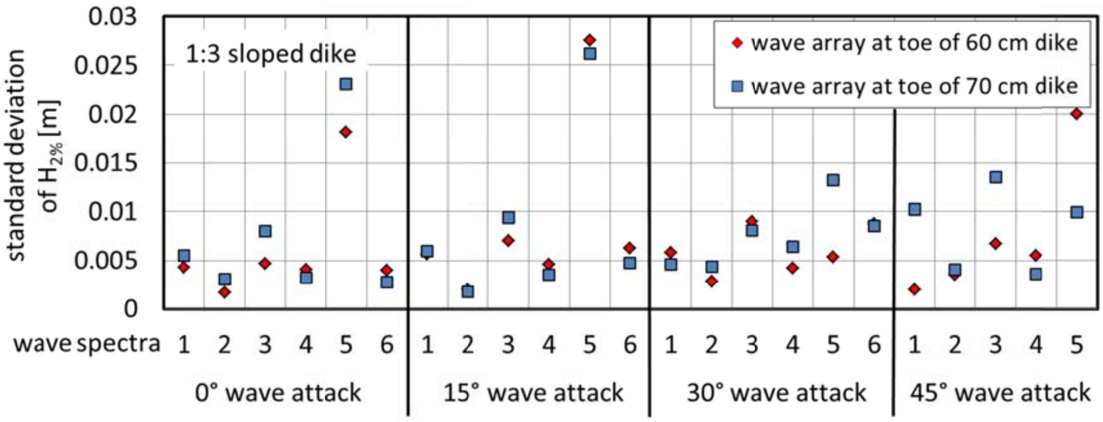

Figure 7.4 Standard deviation of $H_{2\%}$-values; 1:3 sloped dike; zero-down-crossing analysis considering five wave gauges

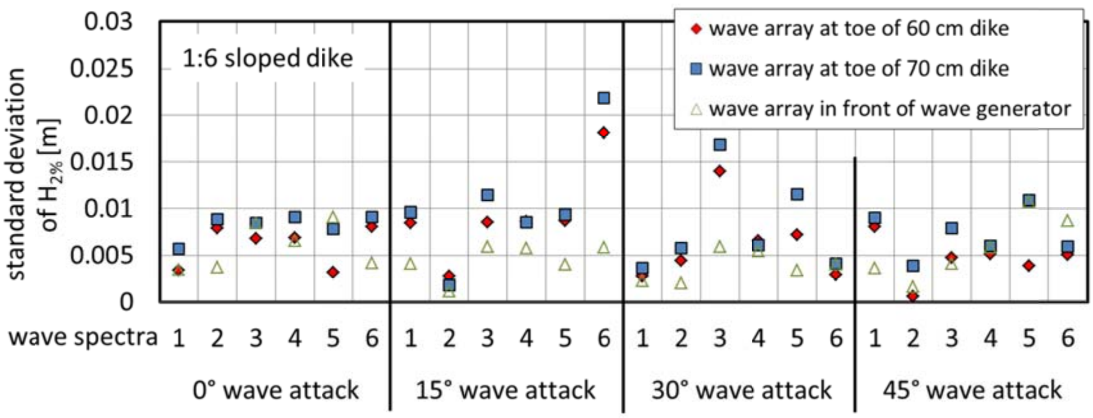

Figure 7.5 Standard deviation of $H_{2\%}$-values; 1:6 sloped dike; zero-down-crossing analysis considering five wave gauges

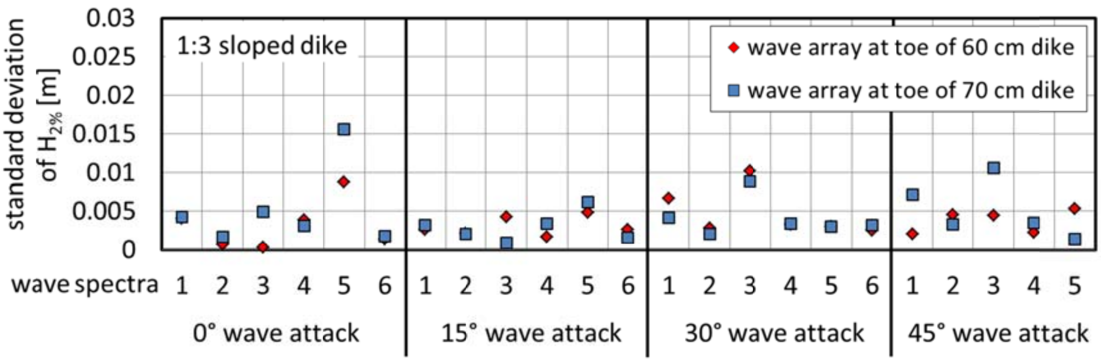

Figure 7.6 Standard deviation of $H_{2\%}$-values; 1:3 sloped dike; zero-down-crossing analysis considering three wave gauges

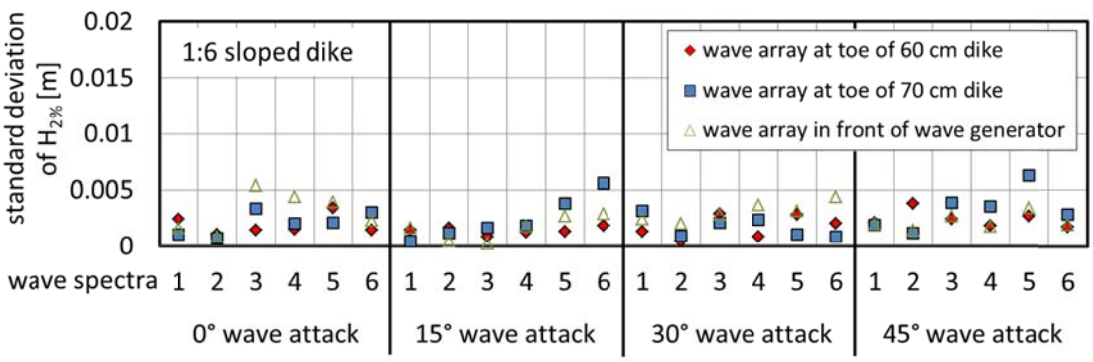

Figure 7.7 Standard deviation of $H_{2\%}$-values; 1:6 sloped dike; zero-down-crossing analysis considering three wave gauges

7.2.3 Reflection analysis - frequency domain

7.2.3.1 General

The wave field was analyzed with the described method in chapter 0. From the reflection analysis, which is performed in frequency domain, the plotted distribution of energy density (reference tests, wave no. 1 and 5, toe of the 60 cm dike) in Figure 7.8 corresponds to the theoretical assumption for a JONSWAP spectrum to be single peaked. The determined reflection coefficients and surf similarity parameters of all tests are described in more detail in chapter 7.2.4.

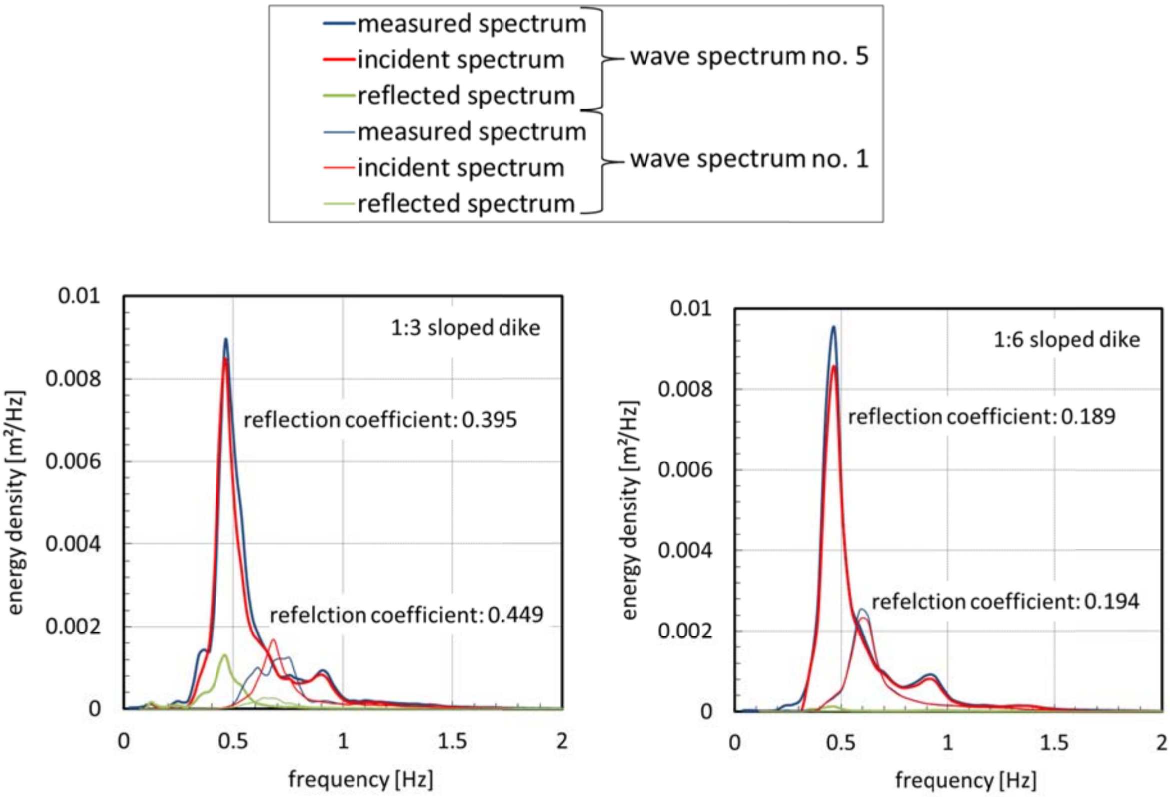

Figure 7.8 Energy density spectrum in front of 60 cm crest of the 1:3 sloped dike (left) and 1:6 sloped dike (right); three wave gauges analyzed

7.2.3.2 Incident wave - significant wave height H_{m0}

The reflection analysis was performed twice. First all five wave gauges were used. Secondly only three wave gauges of each wave array were considered. The wave heights H_{m0} of these wave gauges are plotted for each wave array in Figure 7.9 for the reference test on the 1:3 sloped dike. The left figure shows the wave heights from the analysis of five wave gauges, the left figure from three wave gauges. Figure 7.10 shows the analyzed data for the 1:6 sloped dike.

The wave gauges are listed in direction of wave propagation (from left to right). The different graphs show the wave heights of the six analyzed wave spectra w1 to w6. Uniform wave heights are determinable for each wave gauge, except wave heights of the wave spectra w5 on the 1:3 sloped dike. These wave heights decrease in wave direction. As an explanation two photos of the beginning of the breaking process of some waves during the wave spectra w5 on the 1:3 sloped dike (flow depth 0.5 m) are given in Figure 7.11. The corresponding surf similarity parameter is described in more detail in chapter 7.2.4. A large difference in wave heights is cognizable for wave spectra 5 (1:3 and 1:6 sloped dike). Also the first two wave gauges of the analysis using five wave gauges give different wave heights (left graphs in Figure 7.9 and Figure 7.10).

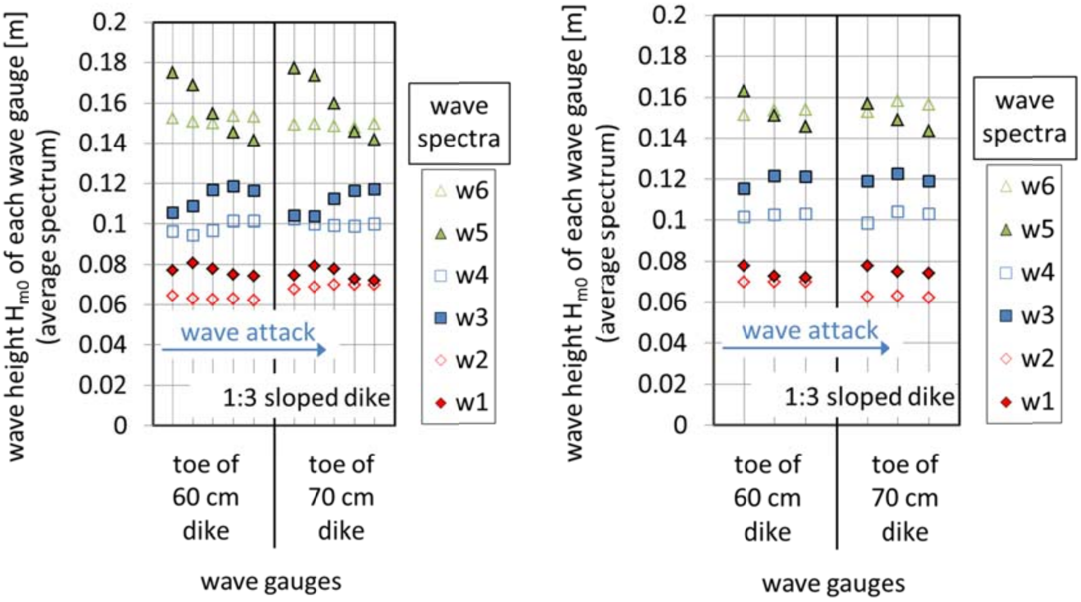

Figure 7.9 Wave height H_{m0} of the analyzed wave gauges - reflection analysis with five wave gauges (left) and reflection analysis with three wave gauges (right); reference test on 1:3 sloped dike

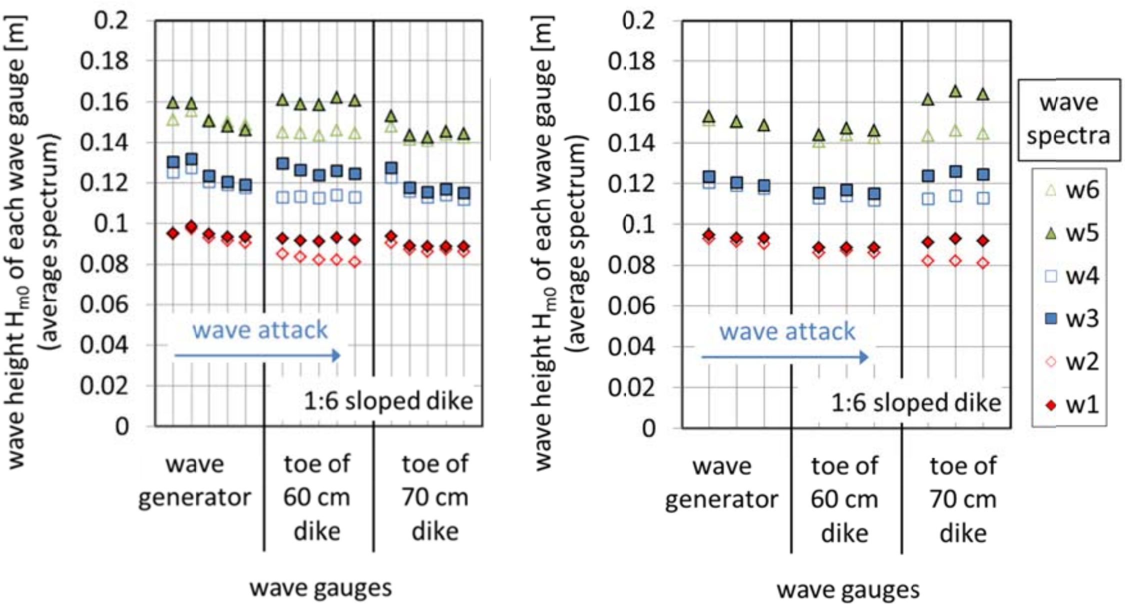

Figure 7.10 Wave height H_{m0} of the analyzed wave gauges - reflection analysis with five wave gauges (left), reflection analysis with three wave gauges (left); reference test on 1:6 sloped dike

Figure 7.11 Beginning of breaker process of waves (wave propagation from right to left)

Under consideration of wave reflection only one value H_{m0} for each wave array was obtained. Figure 7.12 gives the significant wave heights H_{m0} of the incident wave of the reference tests from the reflection analysis with five wave gauges. The wave arrays at the toe of the two dike heights give quite similar significant wave heights H_{m0} for each test phase (1:3 and 1:6 sloped dike). The right graph for the 1:6 sloped dike includes the wave heights in front of the wave generator. For the wave number 6 the wave height in front of the wave generator differs slightly from the wave heights at the toe of the dike. The maximum deviation of 0.01 m appears for wave spectrum number 5 (H_s = 0.15 m).

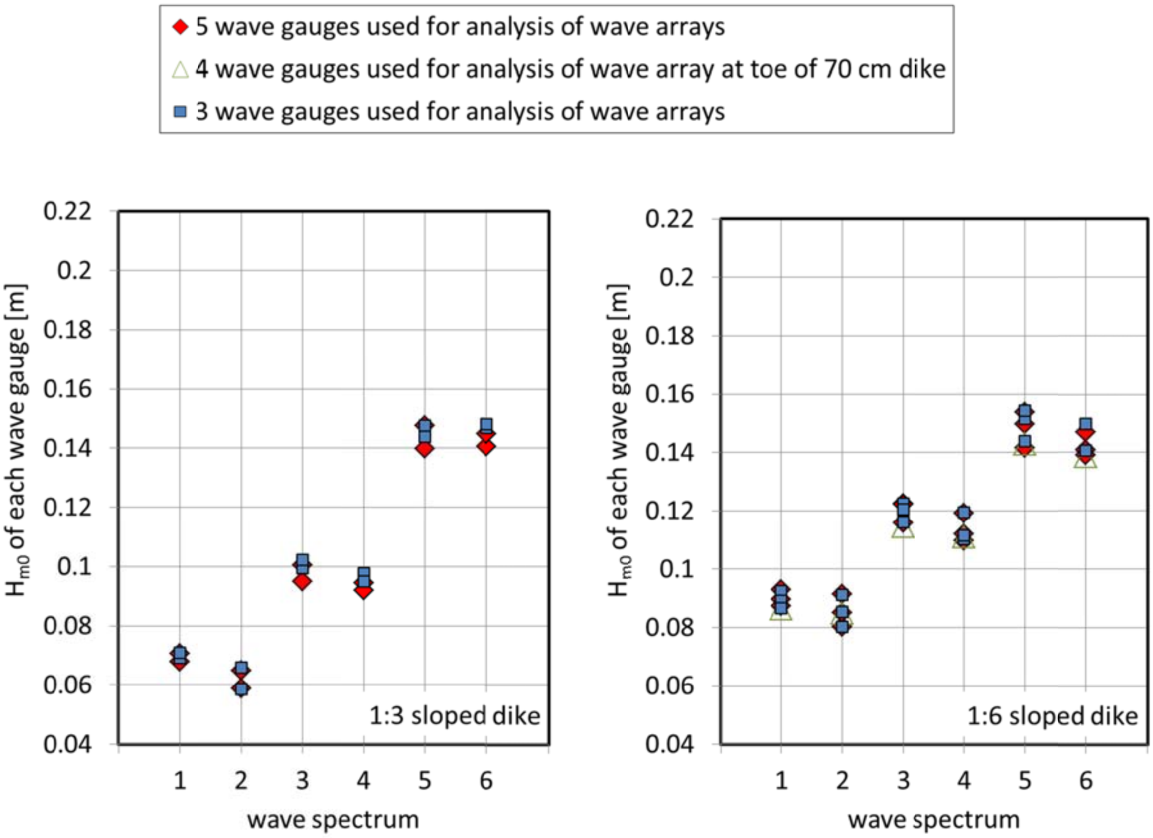

Figure 7.12 Significant incident wave height H_{m0} for the reference model tests calculated for each wave array and the six wave spectra; three wave gauges analyzed

The spectral wave heights H_{m0} are determined for every test at the toe of the 60 cm dike and at the toe of the 70 cm dike. These two wave heights are plotted against each other in Figure 7.13. The black graph demonstrates the equal x-value and y-value. The regression lines of the wave heights on the 1:3 and 1:6 sloped dike correspond well with the so called ideal black graph. For both tests phases (1:3 and 1:6 sloped dike) the data points result in regression coefficients higher than 0.90. Therefore both wave heights can be used for the following analyses on wave run-up and wave overtopping.

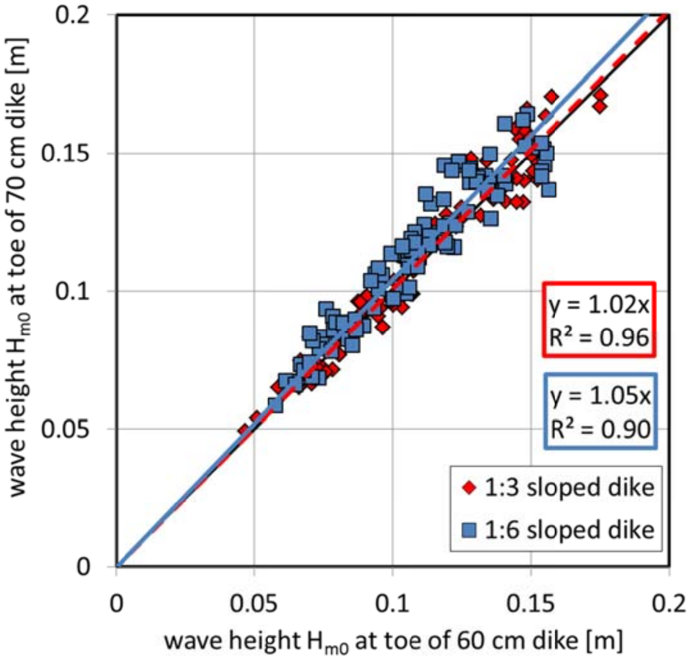

Figure 7.13 Spectral wave heights H_{m0} in front of 60 cm dike against wave heights H_{m0} in front of 70 cm dike; five wave gauges analyzed

7.2.3.3 Spectral moment m_0

The zeroth moment of the average spectrum, which is equal to the measured spectrum, the zeroth moment of the incident spectrum and of the reflected spectrum has been determined for every test. In Figure 7.14 and Figure 7.15 the zeroth moment of the average wave spectrum is plotted against the sum of the incident and reflected spectrum. It should be:

$$m_{0,average} = m_{0,incident} + m_{0,reflected}$$

Figure 7.14 shows the results for the analysis using five wave gauges which scatter less than the results of the analysis using only three wave gauges (cf. Figure 7.15). In the left graphs of these figures the data points of the reference test are filled with a color and correspond well with the ideal black graph. The data points in the right graphs of the two figures show the results for all test without current and wind but with oblique wave attack. Therefore small deviations in comparison to the ideal black graph are noticeable.

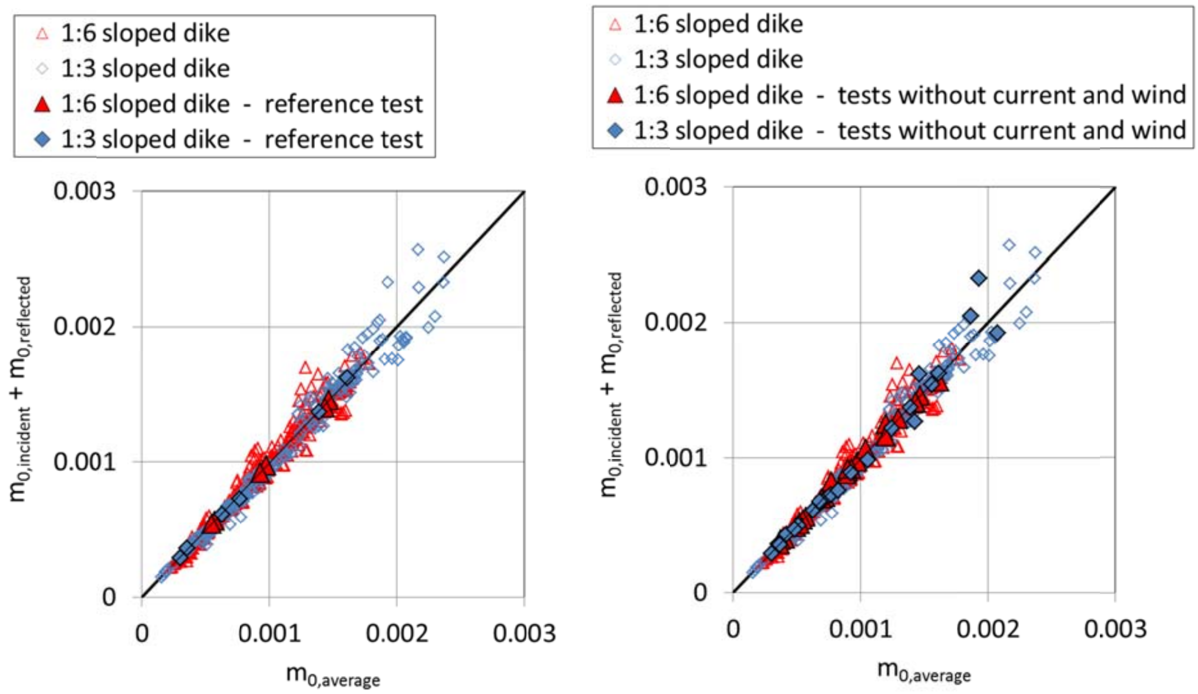

Figure 7.14 $m_{0,average}$ as a function of the sum of $m_{0,incident}$ and $m_{0,reflected}$, analysis with 5 wave gauges

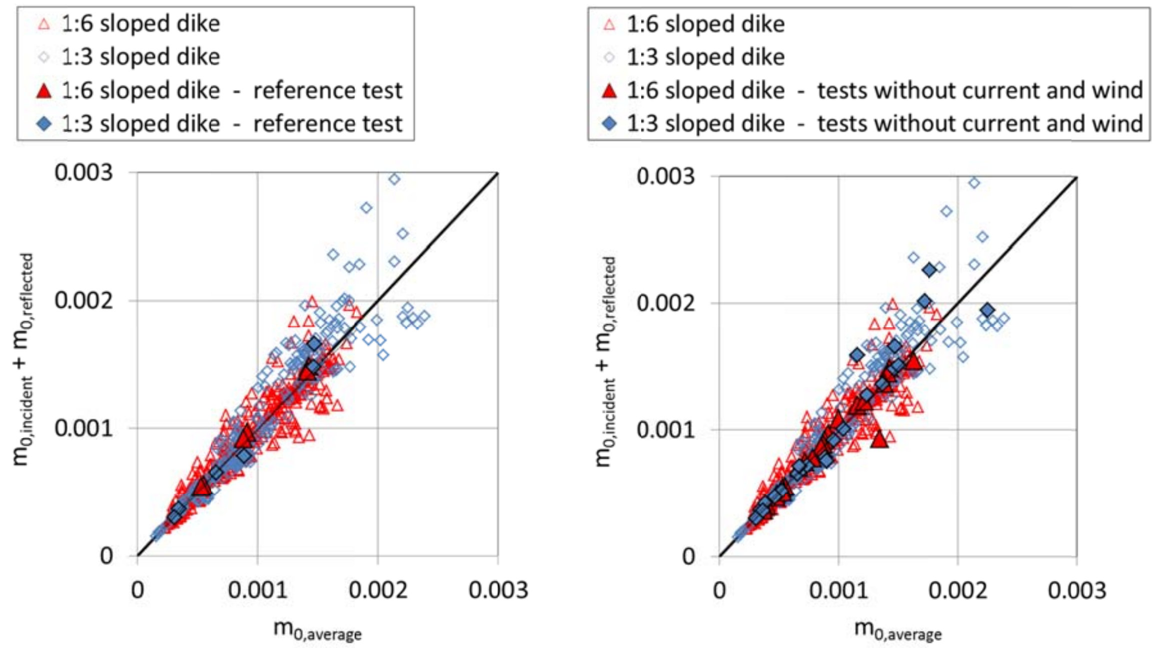

Figure 7.15 $m_{0,average}$ as a function of the sum of $m_{0,incident}$ and $m_{0,reflected}$, analysis with 3 wave gauges

7.2.3.4 Incident wave - spectral wave period $T_{m-1,0}$

Many parameters, like the dimensionless run-up height and the dimensionless overtopping rate, are calculated using the spectral wave period $T_{m-1,0}$ which is defined as

$$T_{m-1,0}=\frac{m_{-1}}{m_0} \quad [s] \tag{7.2}$$

with m_{-1} minus first moment of spectral density [m²]

m_0 zero order moment of spectral density [m²/s]

As shown in the literature review of chapter 4.1 the simplification for the spectral moment $T_{m-1,0}$ is often used:

$$T_{m-1,0}=\frac{T_p}{1.1} \quad [s] \tag{7.3}$$

with T_p peak period [s]

Figure 7.16 shows the calculated spectral wave period $T_{m-1,0} = m_{-1}/m_0$ against the peak period T_p. The green graph shows the approximated function $T_{m-1,0} = T_p/1.1$. For both analyses, using five or three wave gauges for the reflection analysis, the data points agree well with the approximated function. For further analyses the exact value of the calculated spectral period $T_{m-1,0} = m_{-1}/m_0$ will be used.

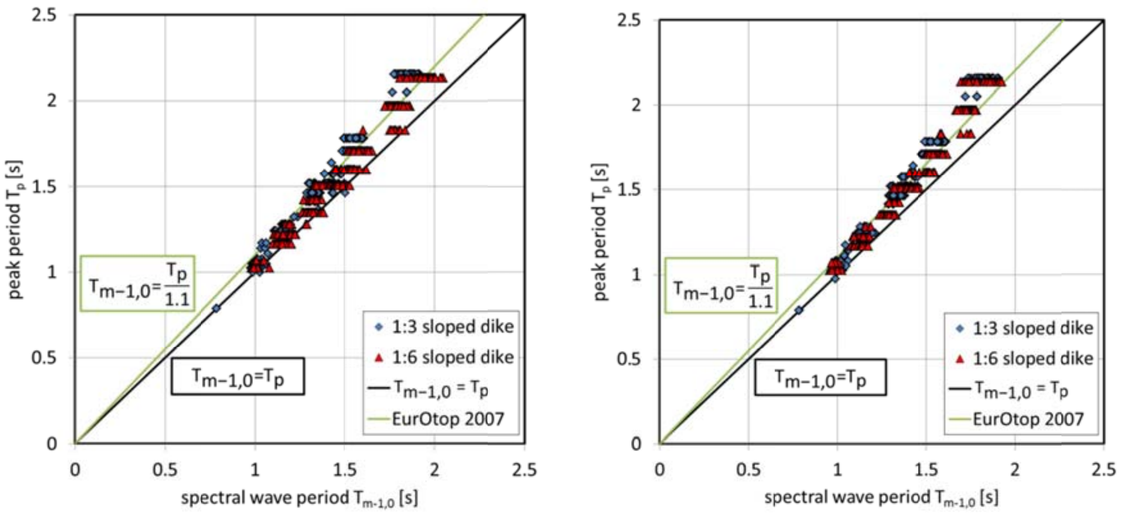

Figure 7.16 Spectral wave period $T_{m-1,0}$ against peak period T_p (left: refl. analysis using five wave gauges. right: refl. analysis using three wave gauges)

7.2.4 Wave breaking

In Figure 7.21 and Figure 7.24 the surf similarity parameter $\xi_{m-1,0}$ is plotted against the reflection coefficients K_R for the reference test on the 1:3 and 1:6 sloped dike. The data points filled in with color are the data points of the investigations on the 1:3 sloped dike. The reflection coefficients for the 1:6 sloped dike are lower because of the less reflection. The reflection coefficients K_R of the FlowDike-tests are slightly higher than given by BATTJES (1974) with:

$$K_R=0.1\cdot\xi^2 \quad [-] \tag{7.4}$$

The surf similarity parameter was determined using the formula (7.5). The reflection coefficient is given by formula (7.6).

$$\xi_{m-1,0}=\frac{tan\alpha}{\sqrt{s_{m-1,0}}}=\frac{tan\alpha}{\sqrt{\frac{H_{m0}}{L_{m-1,0}}}} \quad [-] \tag{7.5}$$

$$K_R=\sqrt{\frac{m_{0,refl}}{m_{0,,inc}}} \quad [-] \tag{7.6}$$

with $m_{0,refl}$ Energy density of the reflected wave spectrum [m²/s]

$m_{0,inc}$ Energy density of the incident wave spectrum [m²/s]

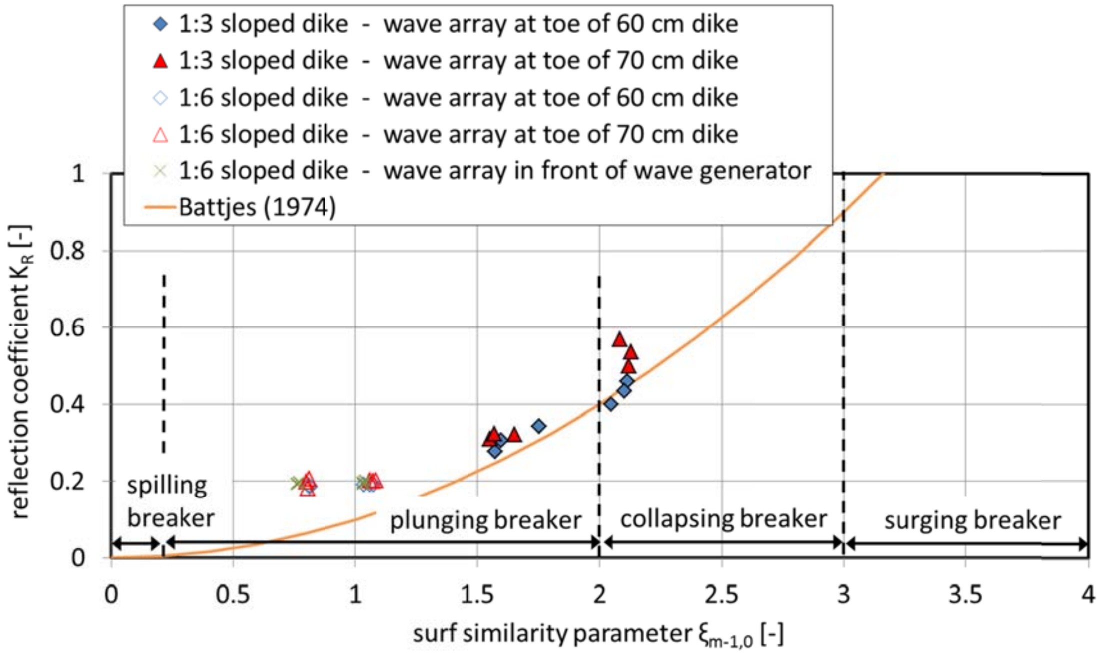

Figure 7.17 Surf similarity parameter $\xi_{m-1,0}$ against reflection coefficient K_R for reference tests; reflection analysis using five wave gauges

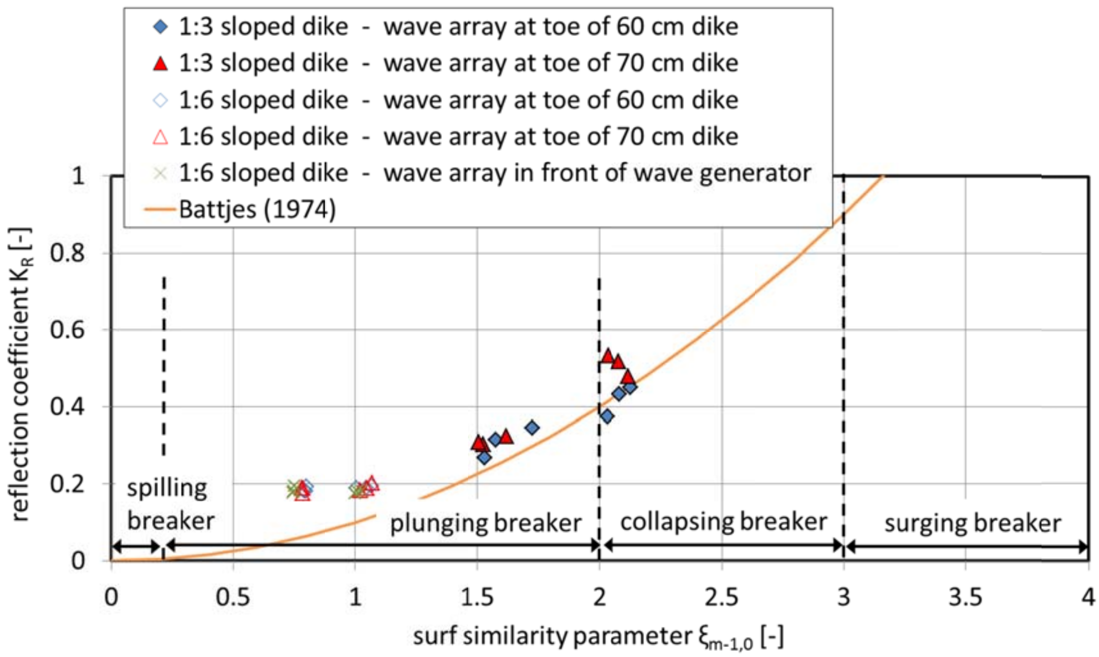

Figure 7.18 Surf similarity parameter $\xi_{m-1,0}$ against reflection coefficient K_R for reference tests; reflection analysis using three wave gauges

Figure 7.19 shows the surf similarity parameter as a function of the reflection coefficient for all tests without current and wind but considering different angles of wave attack. The reflection coefficients K_R on the 1:6 sloped dike ($\xi_{m-1,0} > 1.3$) correspond well with the reflection coefficients of the reference test. The reflection coefficients K_R on the 1:3 sloped dike ($\xi_{m-1,0} > 1.3$) are higher than the values from the reference test.

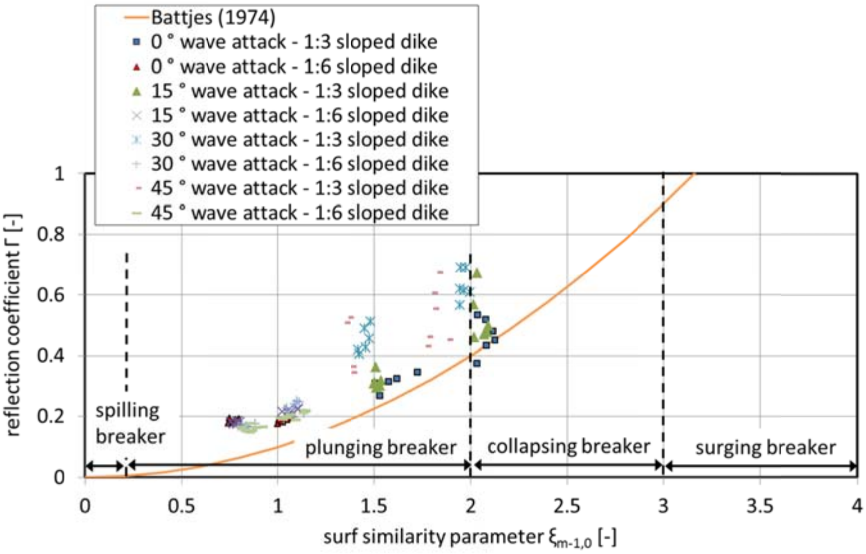

Figure 7.19 Surf similarity parameter $\xi_{m-1,0}$ against reflection coefficient K_R for tests without current and wind, oblique wave attack; reflection analysis using three wave gauges

In Figure 7.20 and Figure 7.21 the surf similarity parameters $\xi_{m-1,0}$ are plotted against the reflection coefficients K_R for all tests using five and three wave gauges for the reflection analysis respectively. The data points filled in with a color are the data points of the investigations on the 1:3 sloped dike. The reflection coefficients differ between 0.26 and 0.71. The reflection coefficients for the 1:6 sloped dike are lower because of less reflection and differ between 0.16 and 0.35.

The waves on the 1:3 sloped dike can mainly be classified as plunging breakers. Some tests have to be related to collapsing breakers. The tests on the 1:6 sloped dike contain only plunging breakers.

For the analysis of the wave overtopping on the 1:3 sloped dike, it has to be distinguished between breaking and non-breaking waves. On the 1:6 sloped dike only breaking waves are considered. The breaker coefficient was determined using formula (7.5). The surf similarity parameter is given below (cf. (7.6)).

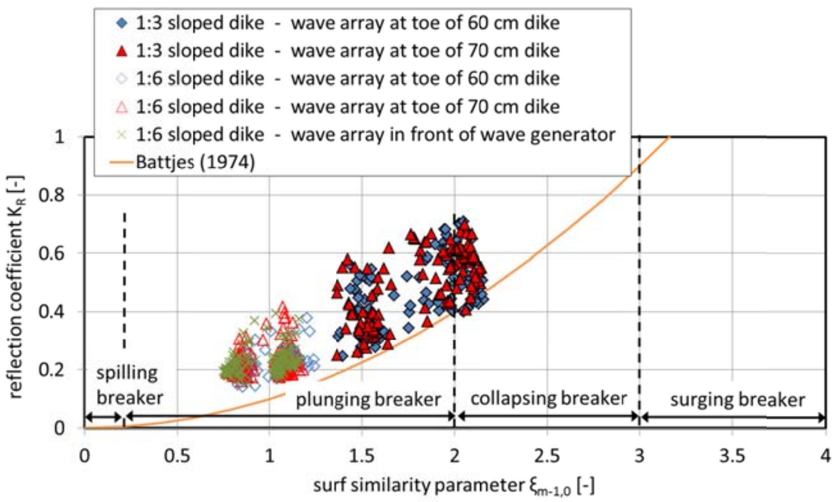

Figure 7.20 Surf similarity parameter $\xi_{m-1,0}$ against reflection coefficient K_R of all tests; reflection analysis using five wave gauges

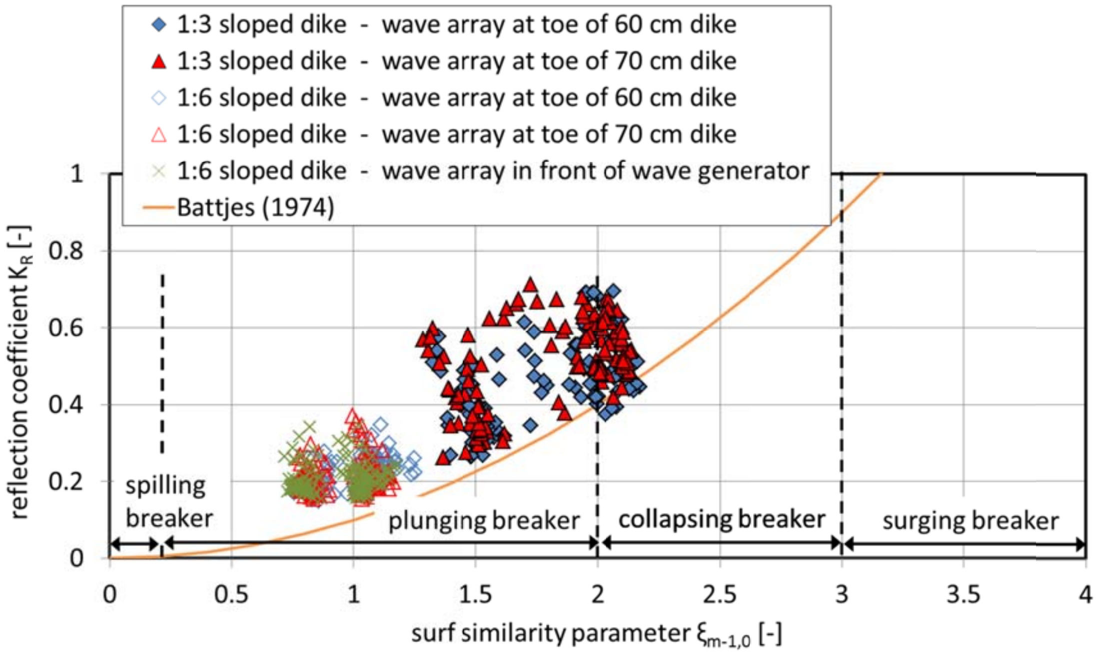

Figure 7.21 Surf similarity parameter $\xi_{m-1,0}$ against reflection coefficient K_R of all tests; reflection analysis using three wave gauges

7.2.5 Detailed analysis of wave array at toe of 70 cm high and 1:6 sloped dike

From the reflection analysis using five wave gauges the wave height H_{m0} of every wave gauge is determined for all tests. Exemplary the wave heights of the test s6_26 (-30° wave attack, 0.15 m/s current, no wind) are given in Figure 7.24. It is observably that for the first wave gauge of the wave array at the toe of the 70 cm dike higher wave heights have been determined (marked by an orange ellipse). Due to that unclear signal, the reflection analysis for the wave array at the toe of the 70 cm dike was repeated using only the rest four wave gauges. The corresponding results for the spectral moments are plotted in Figure 7.23. No big difference is noticeable and the regression coefficient is only slightly higher by using five wave gauges for the reflection analysis (left figure).

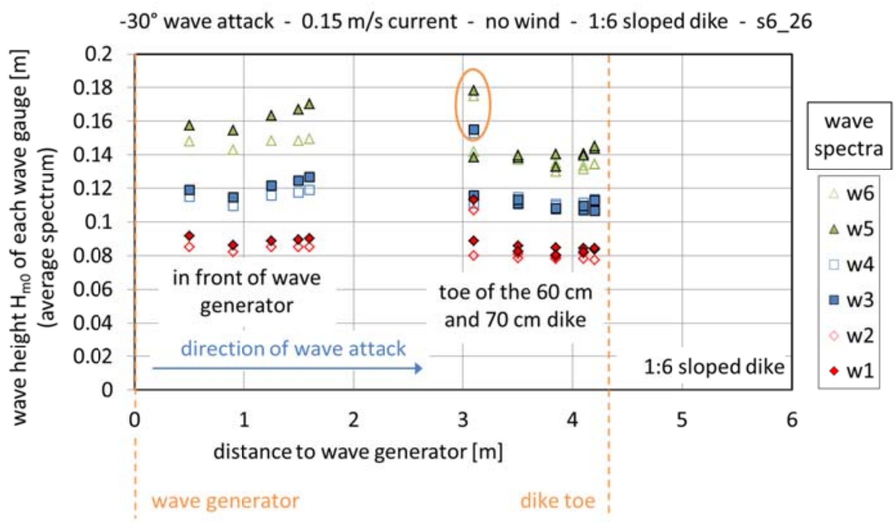

Figure 7.22 Wave heights H_{m0} - s6_26

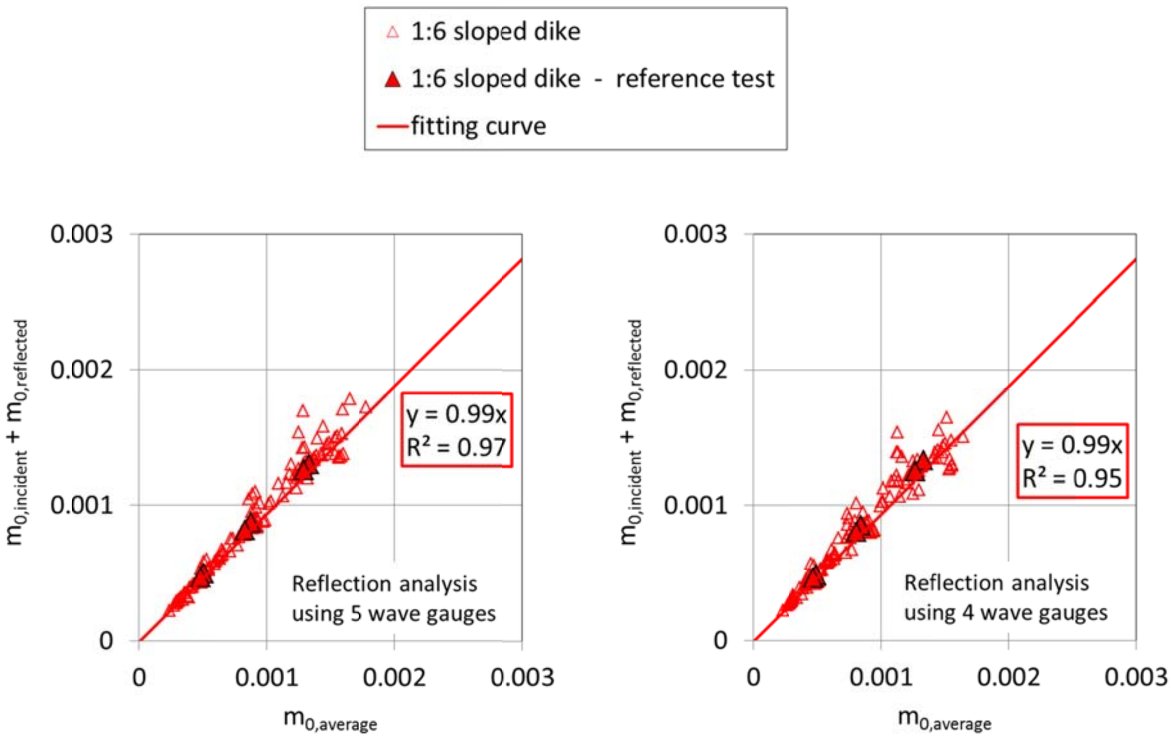

Figure 7.23 $m_{0,average}$ as a function of the sum of $m_{0,incident}$ and $m_{0,reflected}$, analysis with 5 wave gauges

7.2.6 First conclusion on the results of the wave field analysis

The reflection analysis was performed using three and five wave gauges of each wave array. The results are given in this chapter. All wave arrays give similar or better results for the reflection analysis using 5 wave gauges (cf. chapter 7.2.3.3 spectral moment). In spite of the higher standard deviation of the $H_{2\%}$-values from the zero-down-crossing analysis while considering all five wave gauges of each wave array, the results of the reflection analysis using five wave gauges will be used for further analysis. An exception is the analysis of the wave array at the toe of the 70 cm high and 1:6 sloped dike. Due to the unclear signal of the first wave gauge (no. 55) the corresponding wave array will be analyzed without that wave gauge. The wave parameters from the reflection analysis using only four wave gauges will be used for further analysis.

To guarantee the comparability of all tests the same wave gauges are analyzed in each test. Table 7.1 gives an overview of the wave gauges used for the reflection analysis on the 1:3 and 1:6 sloped dike. In Annex H and Annex I all analyzed data concerning the wave field are listed for the analysis on the 1:3 sloped dike and 1:6 sloped dike respectively.

Table 7.1 Wave gauges used in model tests and for analysis

dike slope	**wave array…**														
	…in front of wave generator number of wave gauge distance to wave generator [m]					**…at toe of 60 cm dike** number of wave gauge distance to wave generator [m]					**…at toe of 70 cm dike** number of wave gauge distance to wave generator [m]				
1:3	-	-	-	-	-	14 3.90	13 4.30	12 4.65	11 4.90	10 5.00	9 3.90	8 4.30	7 4.65	6 4.90	5 5.00
1:6	9 0.50	8 0.90	7 1.25	6 1.50	5 1.60	14 3.10	13 3.50	12 3.85	11 4.10	10 4.20	55 not used	54 3.50	53 3.85	52 4.10	51 4.20

7.3 Evolution of wave height influenced by current

To determine the influence of a current on wave height, wave heights in front of the wave generator and wave heights measured at the dike toe of the 60 cm and 70 cm high dikes are compared. The wave heights in front of the wave generator have only been measured during tests with the 1:6 sloped dike.

Figure 7.24 shows the relation between the wave height in front of the wave generator and the wave height at the dike toe $H_{m0,wave\ generator}/H_{m0,diek\ toe}$ against the absolute wave height in front of the wave generator $H_{m0,wave\ generator}$. The relation $H_{m0,dike\ toe}/H_{m0,wave\ generator}$ is 1.0 if the wave height do not change along the channel width. Values higher than 1.0 indicate an increasing wave height along the wave channel width, whereas values smaller than 1.0 present a decreasing wave height along the channel width. To characterize the influence of the current on the wave height Figure 7.21 to Figure 7.29 show the relation $H_{m0,dike\ toe}/H_{m0,wave\ generator}$ against the current for each wave spectrum separated for different angles of wave attack:

- -45° angle of wave attack (Figure 7.26)
- -30° angle of wave attack (Figure 7.27)
- 0° angle of wave attack (Figure 7.28)
- +30° angle of wave attack (Figure 7.29)

The different graphs show the influence of the current parallel to the dike on the relation $H_{m0,dike\ toe}/H_{m0,wave\ generator}$. Figure 7.26 and Figure 7.27 show the relation $H_{m0,dike\ toe}/H_{m0,wave\ generator}$ for the tests with an wave attack against the current. The relation $H_{m0,dike\ toe}/H_{m0,wave\ generator}$ and consequently the wave height $H_{m0,dike\ toe}$ decreases along the channel width ($H_{m0,dike\ toe}/H_{m0,wave\ generator} < 1.0$) and with higher current velocity. For the perpendicular wave attack no significant changes in the relation $H_{m0,dike\ toe}/H_{m0,wave\ generator}$ is obvious (cf. Figure 7.28). Wave attack with the current leads to an increasing wave height along the channel, noticeable by an increasing relation $H_{m0,dike\ toe}/H_{m0,wave\ generator}$ while increasing the current (cf. Figure 7.29). The following conclusions can be done for the evolution of the wave heights along the channel width influenced by current:

- -45° angle of wave attack decreasing wave height along the channel width (Figure 7.26)
- -30° angle of wave attack decreasing wave height along the channel width (Figure 7.27)
- 0° angle of wave attack constant wave height along the channel width (Figure 7.28)
- +30° angle of wave attack increasing wave height along the channel width (Figure 7.29)

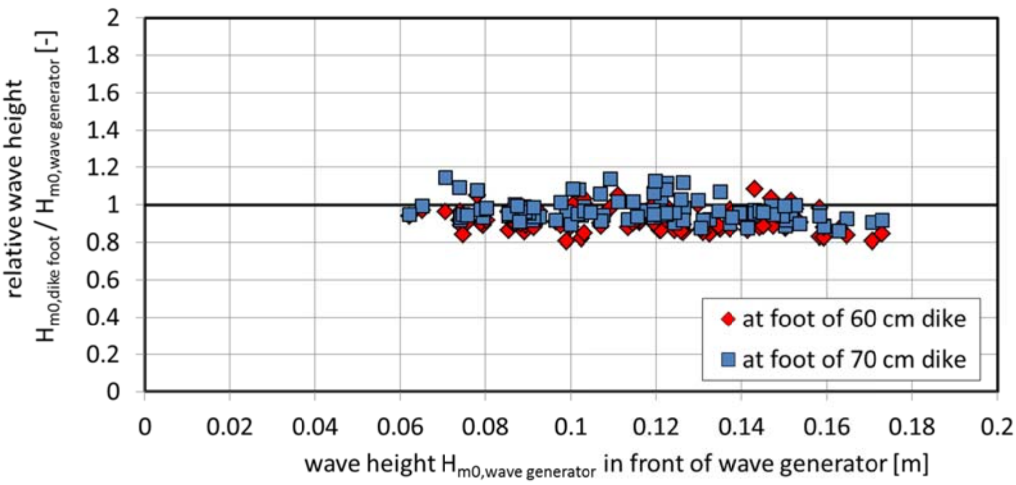

Figure 7.24 Wave height $H_{m0,wave\ generator}$, against relative wave height $H_{m0,dike\ toe}/H_{m0,wave\ generator}$ for all tests on 1:6 sloped dike

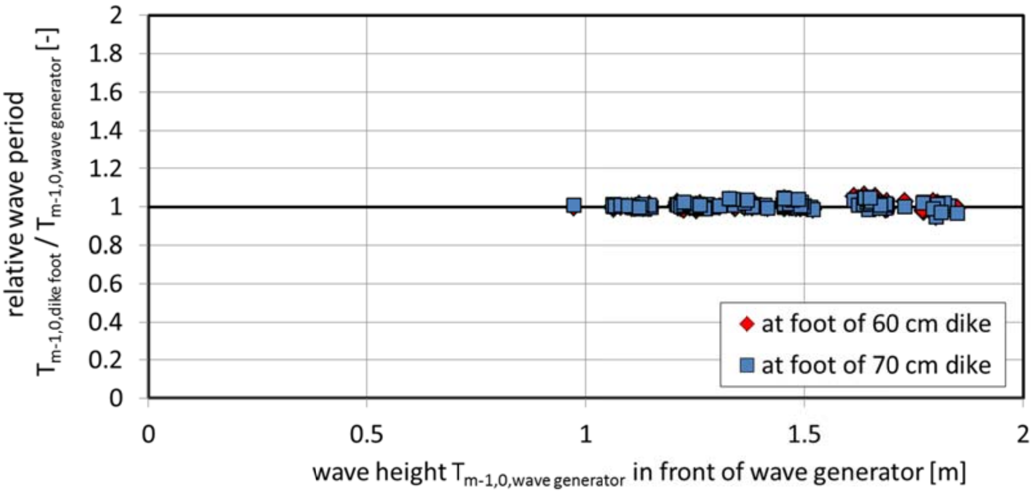

Figure 7.25 Wave period $T_{m-1,0,wave\ generator}$, against relative wave period $T_{m-1,0,dike\ toe}/T_{m-1,0,wave\ generator}$ all test on 1:6 sloped dike

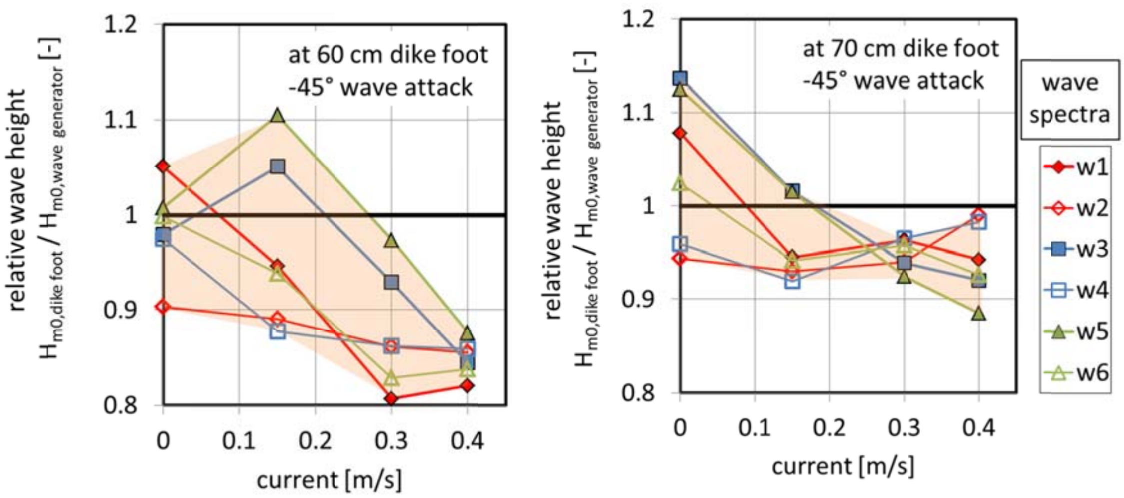

Figure 7.26 Current [m/s] against relative wave height $H_{m0,dike\ toe}/H_{m0,wave\ generator}$ [-]at toe of 60 cm dike (left) and at toe of 70 cm dike (right); -45° wave attack

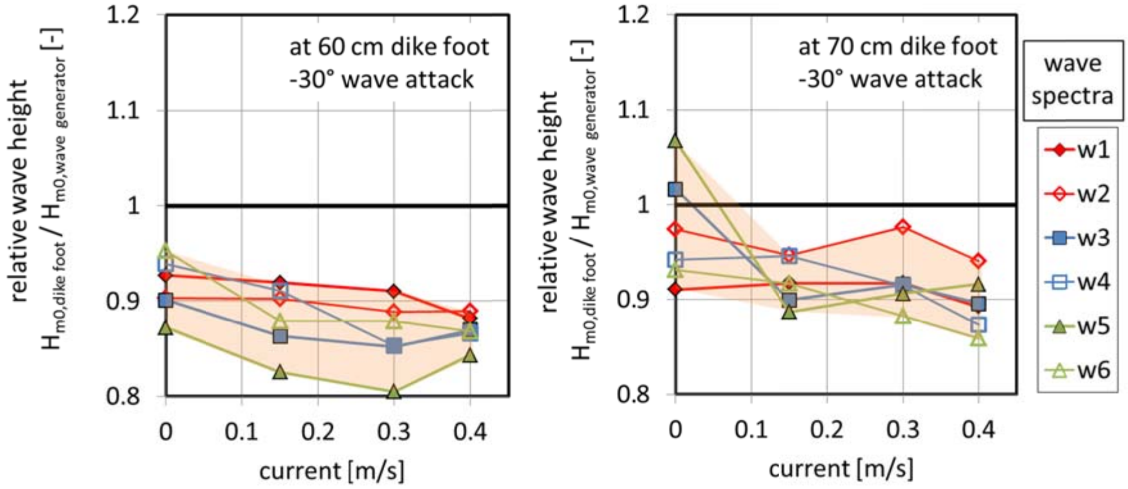

Figure 7.27 Current [m/s] against relative wave height $H_{m0,dike\ toe}/H_{m0,wave\ generator}$ [-]at toe of 60 cm dike (left) and at toe of 70 cm dike (right); -30° wave attack

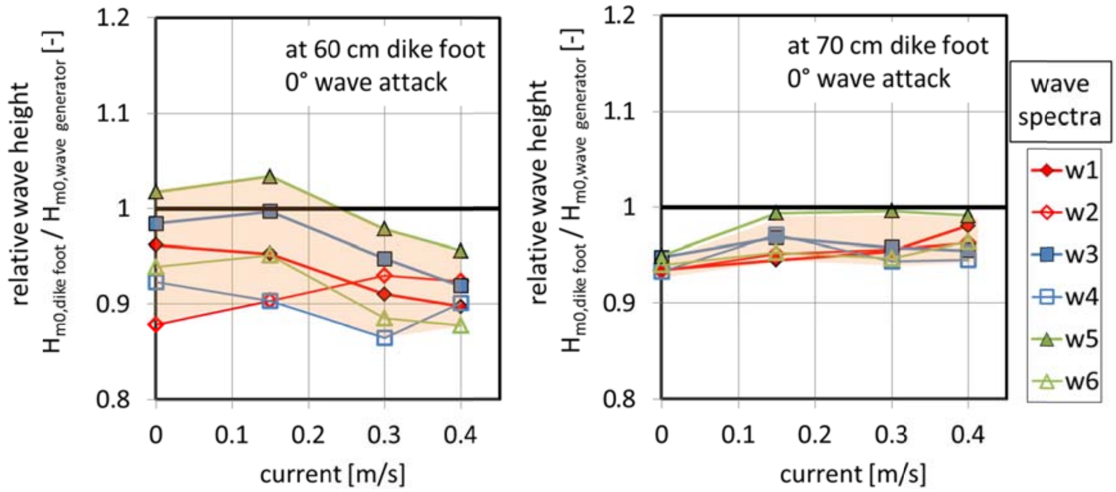

Figure 7.28 Current [m/s] against relative wave height $H_{m0,dike\ toe}/H_{m0,wave\ generator}$ [-]at toe of 60 cm dike (left) and at toe of 70 cm dike (right); 0° wave attack

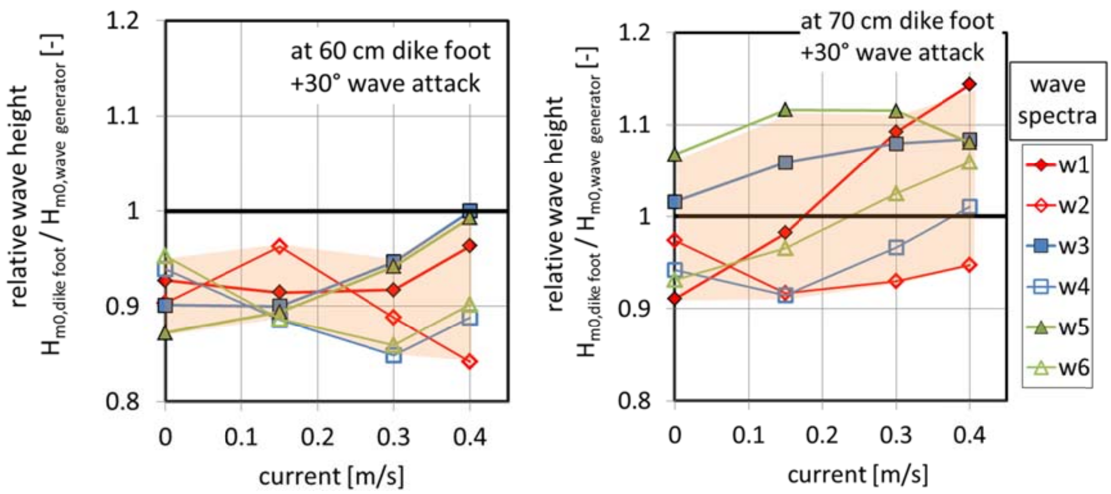

Figure 7.29 Current [m/s] against relative wave height $H_{m0,dike\ toe}/H_{m0,wave\ generator}$ [-]at toe of 60 cm dike (left) and at toe of 70 cm dike (right); +30° wave attack

8 Analysis of wave run-up and wave overtopping

8.1 Remarks

This chapter describes the analysis on the influence of wind, current and oblique wave attack on wave run-up and wave overtopping. The studied data set includes different combinations of all influencing parameters, but can be subdivided in four main sub sets:

- perpendicular wave attack – as reference test
- oblique wave attack
- current influence on wave attack
- wind influence on wave attack

The basic set for perpendicular wave attack and the sub set for oblique wave attack are used for a first comparison of the tests to the currently applied formulae, summarized in the EUROTOP-MANUAL (2007), and former investigations made i.e. by OUMERACI ET AL. (2002). This is done first to validate the applied evaluation method. In addition the newly introduced variables, such as current and wind, are analyzed and compared to the basic tests. As a first step, analysis on current influence is done for perpendicular and oblique wave attack. First analysis of the influence of wind will be presented.

The considered parameters are defined as following:

- wind velocity u: 5 m/s (only 1:3 sloped dike) 10 m/s
- current velocity v: 0.15 m/s 0.3 m/s 0.4 m/s (only 1:6 sloped dike)
- angle of wave attack β: -45° -30° -15° 0° +15° +30°

Positive wave angles are with the current and negative ones against it.

The main objectives of measurement analysis are to estimate the influence of each parameter considered (direction of wave attack, current, wind) on the wave run-up height and to determine correction factors.

The following analysis includes generally these model tests which differ from reference tests (without wind, without current, wave attack orthogonal to the dike crest) only by one parameter (wind, wave direction, current).

8.2 Analysis on wave run-up

8.2.1 Comparison between capacitive gauge and video

Figure 8.1 shows the run-up height depending on time obtained by both measurement facilities – the capacitive gauge and video camera (model test 155). Obviously there is a good agreement and both measurement techniques are suitable to determine wave run-up.

As mentioned before video analysis for FlowDike 1 (1:3 sloped dike) could only determine wave run-up in regions without reflection. So the run-up peaks at time t = 33; 53 and 58 seconds (marked with black ellipses) represent only the lowest boundary of that region which was excluded during video analysis (see chapter 6.3.1). The capacitive gauge gives the right values. But this has no effect on $R_{2\%}$

because the error affects only the smaller run-up heights. For data analysis considering FlowDike 2 (1:6 sloped dike) no such effect was detectable because of no reflections on the run-up board.

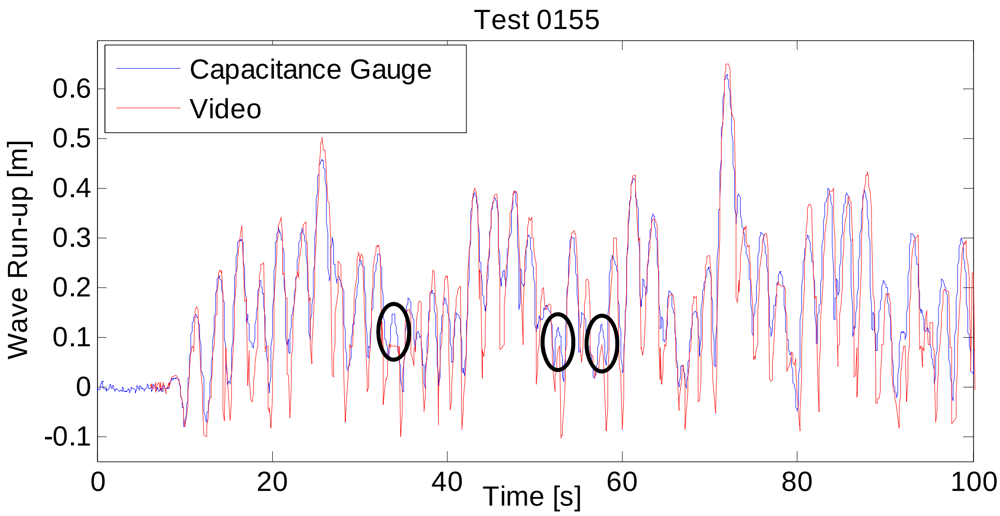

Figure 8.1 Wave run-up depending on time measured by capacitive gauge and video, model test 155

A comparison between calculated values of $R_{2\%}$ for both measurement facilities for all model tests of FlowDike 1 is presented in Figure 8.2. The first number of the data point designation is equal to the set-up number and the second number marks the model test (see Annex J).

The values on basis of capacitive gauge measurement are almost all lower than the values obtained by video analysis. The difference is up to 5 cm and in the case of oblique wave attack up to 7 cm. This is because the capacitive gauge was situated in the middle of the run-up plate and could only measure the wave run-up there although the run-up height differed along the plate width. Result from video analysis captured always the maximum run-up height independent of its location on the run-up plate (see chapter 6.3.1). The wider amplitude of the video measurement results in Figure 8.1 is caused by these characteristics of the used measurement facilities.

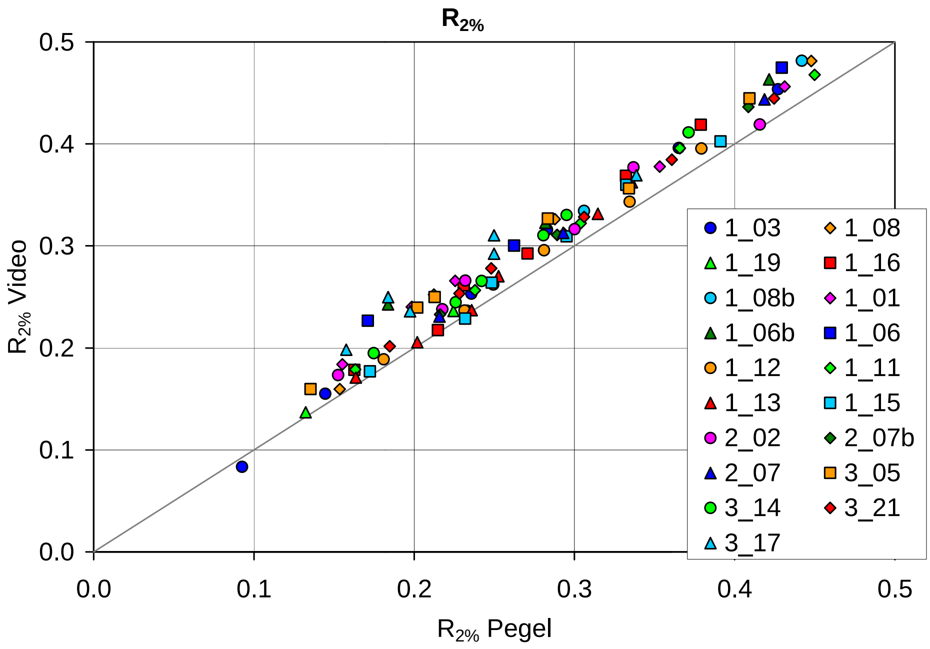

Figure 8.2 Wave run-up height $R_{2\%}$ (percentile 2%) for all model tests: comparison between values on basis of video analysis and capacitive gauge measurement

If the data extraction from video film is limited to a smaller stripe around the capacitive gauge one get the same run-up height from video as from capacitive gauge (see

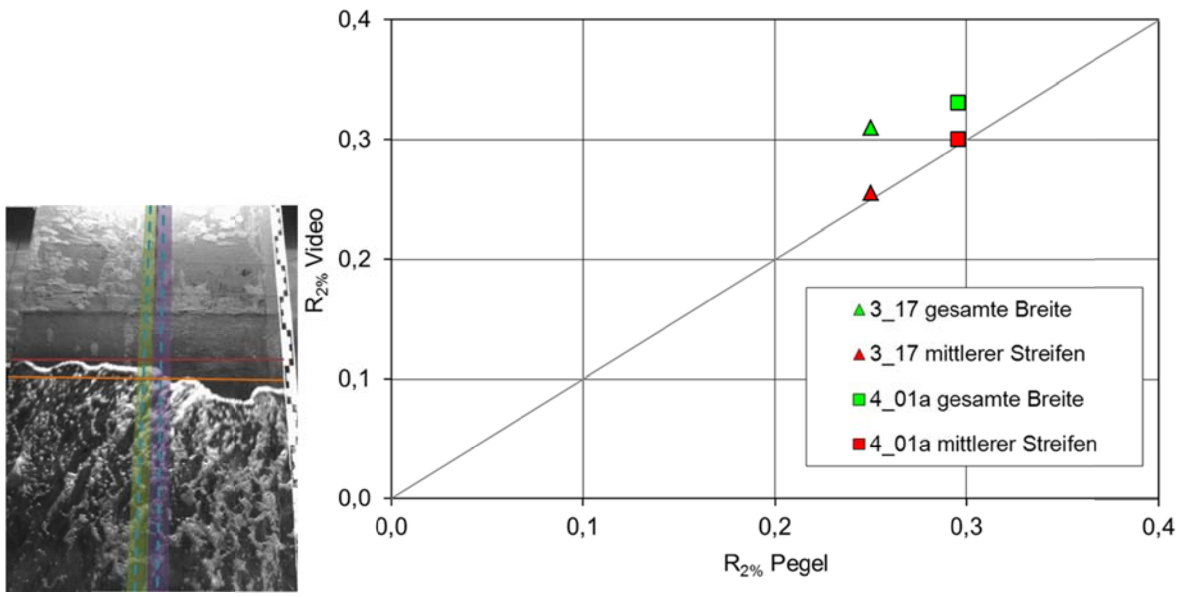

Figure 8.3 Comparison between wave run-up height $R_{2\%}$ (percentile 2%) of two tests measured by capacitive gauge and extracted video film for both the whole run-up board and a smaller stripe around the capacitive gauge (blue scattered lines in the left picture).

The following discussion includes both $R_{2\%}$-values obtained by video analysis and measured by the capacitive gauge.

8.2.2 Reference-test

To validate the overall model set-up, results from reference tests (1:3 dike as well as 1:6 dike) are compared to data of former investigations. Figure 8.4 shows calculated values of relative wave run-up height $R_{u2\%}/H_{m0}$ versus surf similarity parameter $\xi_{m-1,0}$. Several functions of former investigations have been added to the figure including equation (10) and (11) by EurOtop Manual (2007). Values for H_{m0} were obtained analyzing measurement results of the wave array which was situated closer to the run-up plate. Values for wave run-up height were measured by the capacitive gauge.

Relative wave run-up of reference model test is little lower than expected by EurOtop 2007. This is explicable because the function of EurOtop Manual (2007) is only valid for smooth dike slopes. The rougher surface of the dike slope in the model set-up causes slightly lower wave run-up heights. Surf similarity parameter $\xi_{m-1,0}$ is greater than 0.8 for 1:6 dike model tests and greater than 1.5 for the 1:3 dike model tests.

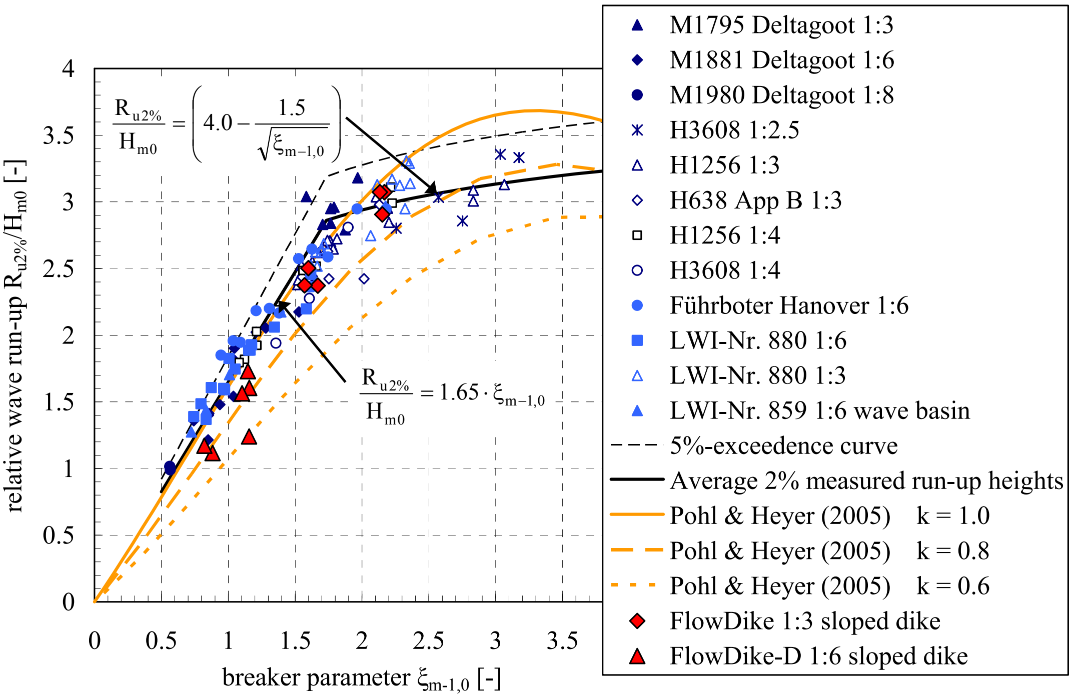

Figure 8.4. Relative wave run-up height $R_{u2\%}/H_{m0}$ versus surf similarity parameter $\xi_{m-1,0}$ – comparison between reference tests and former investigations from the EurOtop-Manual (2007)

8.2.3 Run-up height $R_{2\%}$ and relative run-up height $R_{2\%}/H_{m0}$

Figure 8.5 and Figure 8.6 show calculated values of relative wave run-up height $R_{2\%}/H_{m0}$ versus Surf similarity parameter $\xi_{m-1,0}$ for all model tests. The annotation numbers refer to the tables in Annex J. First number is equal to the model set-up number and second number describes the model test (column “Testserie”). Two functions have been added to the figures, on the one side the function by EURОTOP 2007 (equation (5.23) and (5.24)) and on the other hand function presented by HEYER & POHL 2005. Reference model tests (without current, without wind, wave attack orthogonal to the dike crest) are marked with “+”. Values for H_{m0} were obtained by analysis of wave spectrums measured by the wave gauge set 1 (gauge 5 – 9) because these gauges are situated nearer to the run-up plate.

Relative run-up of reference model tests in Figure 8.5 (values from video analysis) is higher than the function by EUROTOP 2007. This is due to video analysis routine which detects the highest run-up for each time step. EUROTOP 2007 refers to mean values of wave run-up.

Relative run-up of reference model test in Figure 8.6 (values measured by capacitive gauge) is lower than expected by EurOtop 2007. This is explicable because the function of EUROTOP 2007 is only valid for smooth dike slopes. The rougher surface of the dike slope in the model set-up causes lower wave run-up heights.

Surf similarity parameter is $\xi_{m-1,0} > 1.3$ for all model tests and > 2 for the most. That is why breaking waves in the model test could be described as plunging breakers. Still surging breakers are also possible.

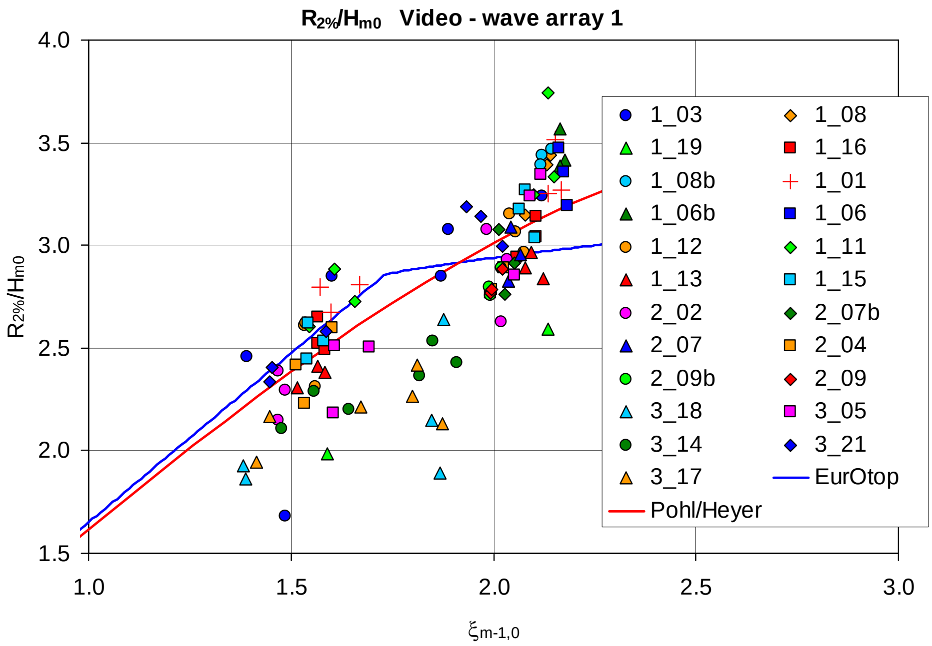

Figure 8.5 Relative run-up height $R_{2\%}/H_{m0}$ versus Surf similarity parameter $\xi_{m-1,0}$ (results from video analysis; H_{m0} measured at wave gauge set 1; the first number of the data point designation is equal to the set-up number and the second number marks the model test (cf. Annex J)

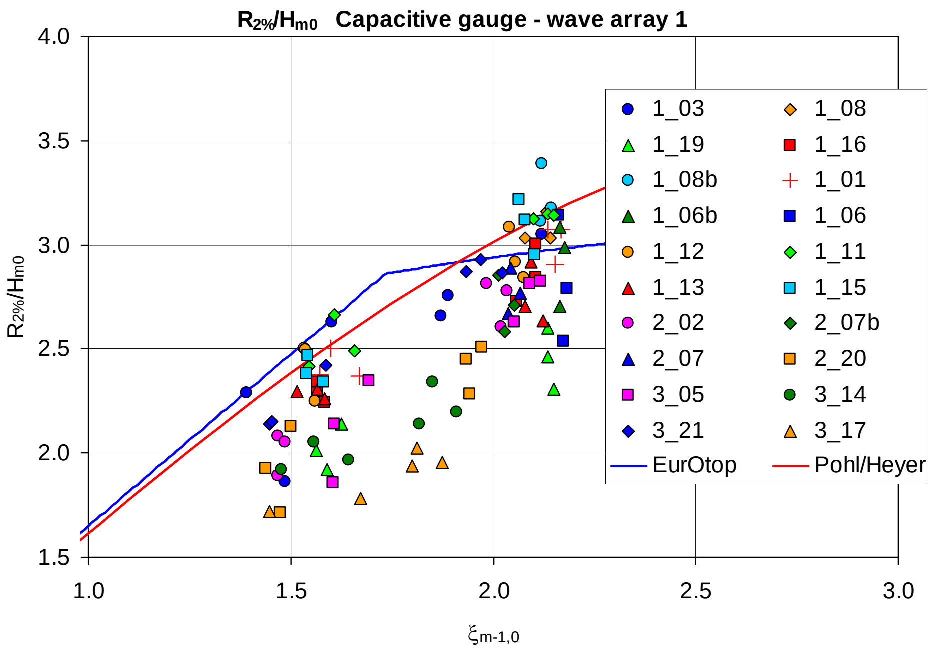

Figure 8.6 Relative run-up height $R_{2\%}/H_{m0}$ versus Surf similarity parameter $\xi_{m-1,0}$ (results from capacitive gauge; H_{m0} at wave gauge set 1; the first number of the data point designation is equal to the set-up number and the second number marks the model test (cf. Annex J)

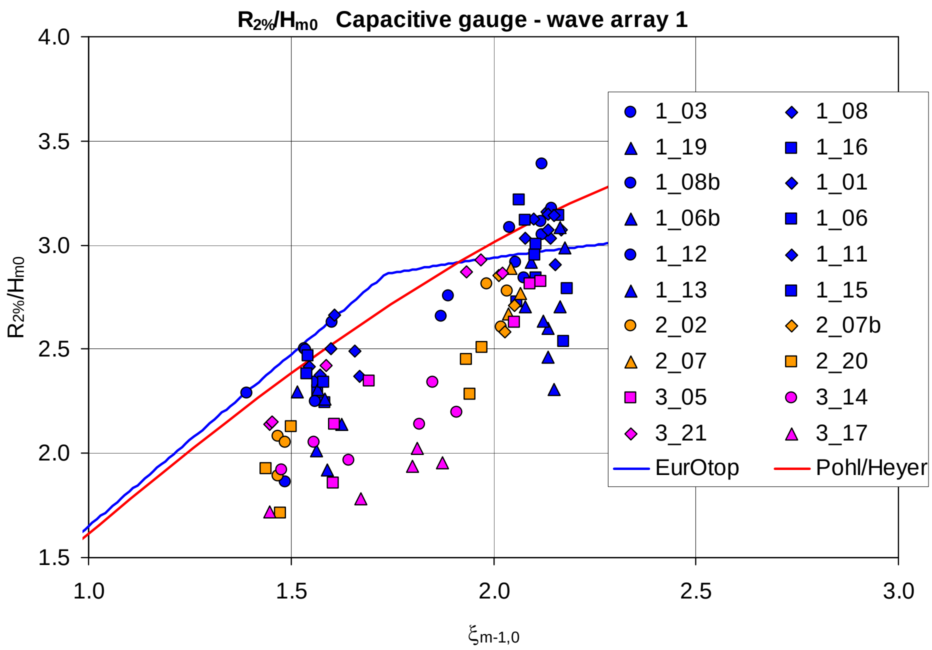

Figure 8.7 Relative run-up height $R_{2\%}/H_{m0}$ versus Surf similarity parameter $\xi_{m-1,0}$ (results from capacitive gauge; H_{m0} at wave gauge set 1; each set-up is marked by different color; the first number of the data point designation is equal to the set-up number and the second number marks the model test (cf. Annex J)

Figure 8.7 shows the same diagram as Figure 8.6 but each set-up is marked by different color. It is visible that the model test with set-up 1 and 2 are characterised by a smaller number of $\xi_{m-1,0}$. Model test with set-up 3 include tests with $\theta = 30°$ and 45° and current. That's why the deformation of each wave spectrum is stronger.

Figure 8.8 presents the calculated values based on measurements by capacitive gauge. The diagram shows the relative wave run-up height $R_{2\%}/H_{m0}$. H_{m0} is the significant wave height of the attacking wave spectrum measured at the dike toe (70 cm high reach) by wave gauge set 1. The diagram is preliminary because the data of H_{m0} were reviewed and were not actualized yet. But the principal data analysis routine should be explained with reference to this picture.

In the diagram relative run-up of reference tests has been compared to model tests with only one different influencing parameter (wind, wave direction, current). Best fit lines obtained by linear regression for each parameter investigated have been added to the diagram. The slope of the best fit lines represents γ which will be considered in the following data analysis.

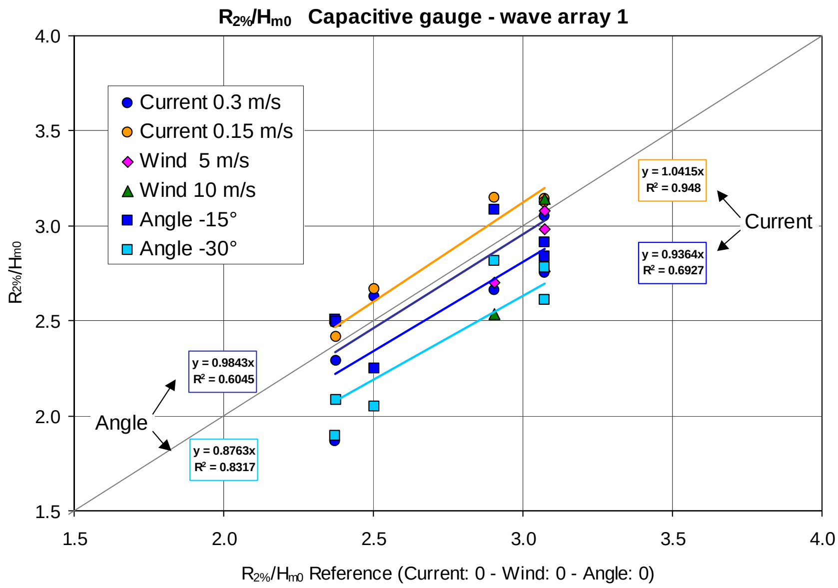

Figure 8.8 Relative run-up measured by capacitive gauge: comparison between reference tests and model tests with only one different influencing parameter (wind, wave direction, current)

8.2.4 Influence of wave direction and current

To analyze the influence of the direction of wave propagation the ratio γ_θ between relative run-up height of oblique waves and waves with a propagation direction orthogonal to the dike crest was considered:

$$\gamma_\beta = \frac{(R_{2\%}/H_{m0})_\beta}{(R_{2\%}/H_{m0})_{orth}} \tag{8.1}$$

Figure 8.9 shows calculated values of γ_β in dependence of the angle of wave attack β. These values are equal to the derivative of γ_β with respect to β or the slope of the linear best fit line in Figure 8.8.

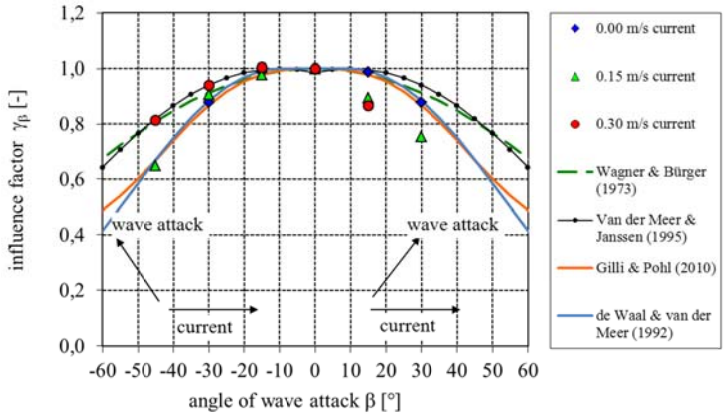

Figure 8.9 Ratio γ_β between relative run-up height of oblique waves and waves with a propagation direction orthogonal to the dike crest (results from model test with and without current) depending on the angle of wave attack.

It is evident that the bigger the absolute value of the angle of wave direction the smaller the ratio γ_θ. Obviously the relation between γ_β and β is nonlinear.

Some function of older investigations (WAGNER & BÜRGER 1973, VAN DER MEER & JANSSEN 1995, DE WAAL & VAN DER MEER 1992) has been added to the calculated values in Figure 8.9.

As a first best fit line for tests without current the following function has been obtained:

$$\gamma_\beta = a + b\left[(1+\beta)e^{-\beta'}\right]^{c\beta'} \tag{8.2}$$

with $\beta' = \dfrac{\beta}{90}$ and β [degree] and the following coefficients:

a = 0.35; b = 0.65 and c = 15.0

Function (8.2) has been added to Figure 8.9 too. The function is only valid for β < 50° considering the model tests. A validation with model test including angle of wave attack β > 45° is desirable.

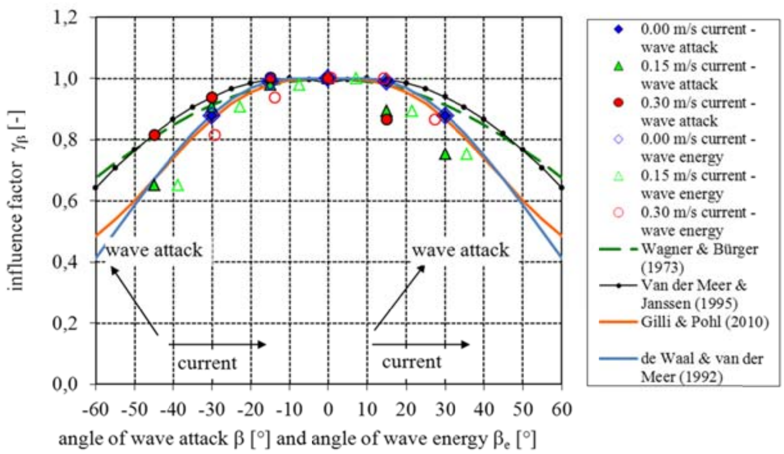

Figure 8.10 Ratio γ_β between relative run-up height of oblique waves and waves with a propagation direction orthogonal to the dike crest (results from model test with and without current) depending on the angle of wave attack (filled markers) and the angle of wave energy (unfilled markers).

As discussed in chapter 4.3.5 the angle of wave attack has to be substituted by the angle of wave energy if the wave propagation is influenced by a current. Figure 8.10 presents the same values of γ_β as in Figure 8.9 in dependence of the angle of wave attack as well as the angle of wave energy. Considering the latter the data points move to the right side in the diagram and became more mirror-inverted on the line $\beta = 0$. Nevertheless the factor γ_β seems to decrease more than described by former formulae. That's why a new function

$$\gamma_\beta = \cos^3(|\beta_e - 10|) \tag{8.3}$$

was fitted which is shown in Figure 8.11.

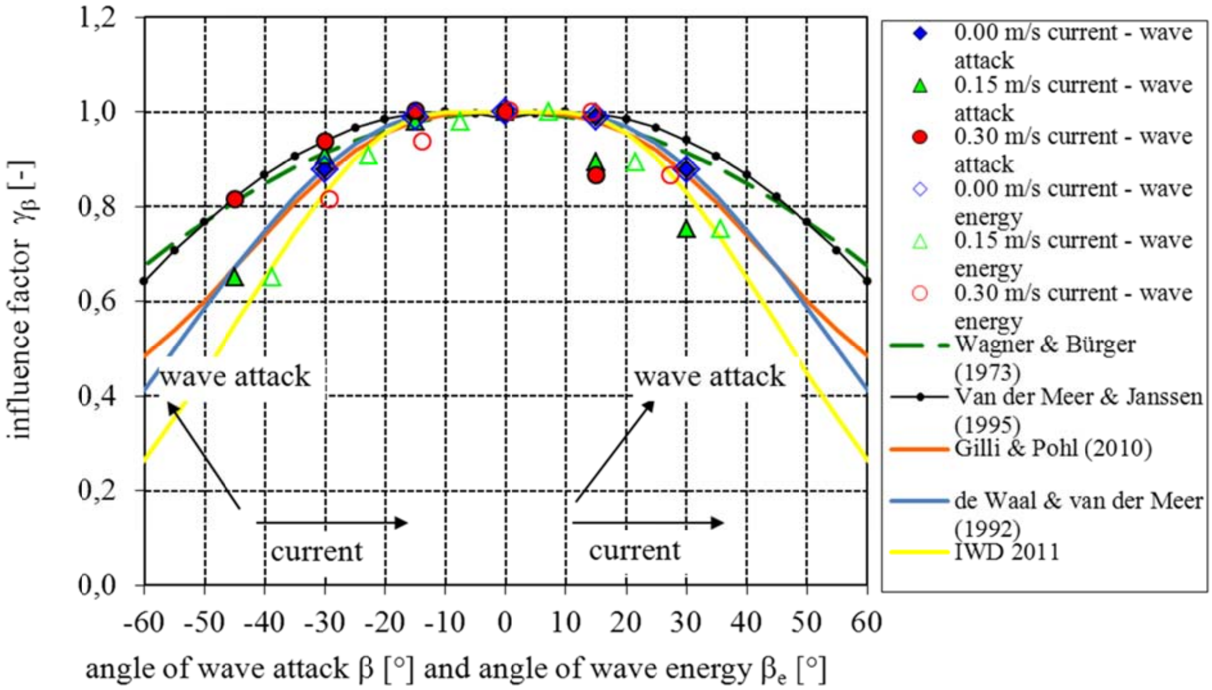

Figure 8.11 Ratio γ_β between relative run-up height of oblique waves and waves with a propagation direction orthogonal to the dike crest (results from model test with and without current) depending on the angle of wave attack (filled markers) and the angle of wave energy (unfilled markers).

The results are preliminary and contain only the FlowDike 1 (1:3 sloped dike) data. They will be updated with the new results from the wave field analysis and the data extracted from the video films considering 10 separate stripes on the run-up board for both FlowDike 1 und FlowDike 2.

The analysis of the wind tests has not been finished yet.

8.3 Analysis on wave overtopping

8.3.1 Reference test

In a first step the results from the basic test without wind and current are compared to the existing formulae from the EUROTOP-MANUAL (2007). The results on the 1:3 sloped dike and 1:6 sloped dike are illustrated below, together with the formulae for breaking and non-breaking waves ((5.26) and (5.27)) and their 90% confidence interval.

First the results for both configurations fit well within the 5% upper and lower confidence limits, which are displayed as dotted lines in the graphics. Most of the points fall below the average probabilistic trend (dashed blue line) from the EUROTOP-MANUAL (2007), but validate altogether the formulae.

An easier comparison for the following analysis is given by adding a “trend line”, in Excel for the results. Here an exponential trend is chosen due to the relation between dimensionless overtopping discharge q_* and freeboard height R_*, given earlier in chapter 5.4.3.

After fitting the trend for the basic reference test, all following analysis will be done by regression analysis. For this purpose the inclinations of the slope b for each test series trend are compared to the inclination b of the basic test. This method is explained more detailed in the summarizing chapter on reduction factors 8.3.7.

Figure 8.12 shows the results of the reference tests for the 1:3 and 1:6 sloped dikes for breaking waves. In Figure 8.13 the regression curve for non-breaking waves for the 1:3 sloped dike is given. All regression lines of the two dike slopes (dotted graph (1:3 dike) and dashed graph (1:6 dike)) are slightly lower than the recommended formula of the EUROTOP-MANUAL (2007), but still lying within the confidence interval of 5%. In the following analysis the inclination of the graph of the corresponding reference test is used to determine the influence factors γ_i for the three different conditions:

- 1:3 dike for breaking wave conditions
- 1:6 dike for breaking wave conditions
- 1:3 dike for non-breaking wave conditions

For better comparison with the formulae from the EUROTOP-MANUAL (2007), a regression with a fixed crossing on the y-axis was applied. The fixed interception Q_0 remains the same as the y-axis crossing from formulae (5.26) and (5.27) for each breaking condition.

The following trend is found for the 1:3 sloped dike (blue line):

- breaking waves: $Q_0 = 0.067$ $b = -4.949$
- non-breaking waves: $Q_0 = 0.2$ $b = -2.677$

The 1:6 sloped dike (red line) gives the following parameter:

- breaking waves: $Q_0 = 0.067$ $b = -4.771$

In each case the results follow an average trend, which is just a bit lower than the stated equation from the EUROTOP-MANUAL (2007). Concluding for the analysis on wind, current and oblique wave attack, the crossing with the y-axis of the basic reference test can remain the same as in the formulae from EUROTOP-MANUAL (2007), but the inclination of the slope b will change. This factor will influence the designated comparison of the results, as it is used to determine the influence of each variable within a parametric study.

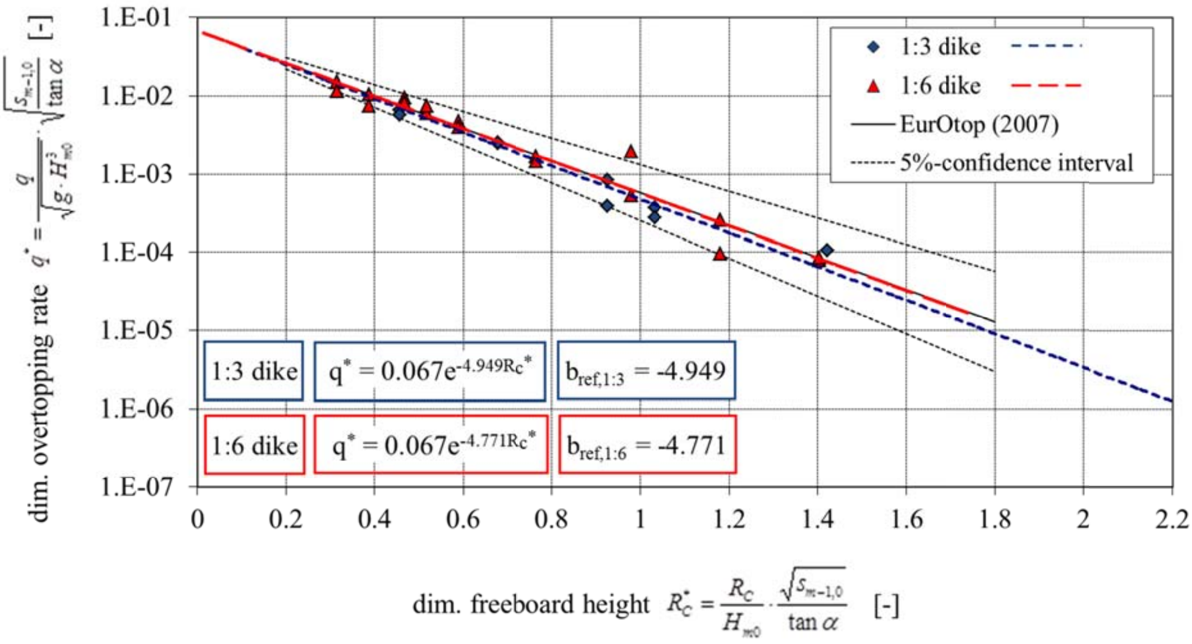

Figure 8.12 Dimensionless overtopping rate - reference tests for breaking wave conditions (1:3 dike, 1:6 dike)

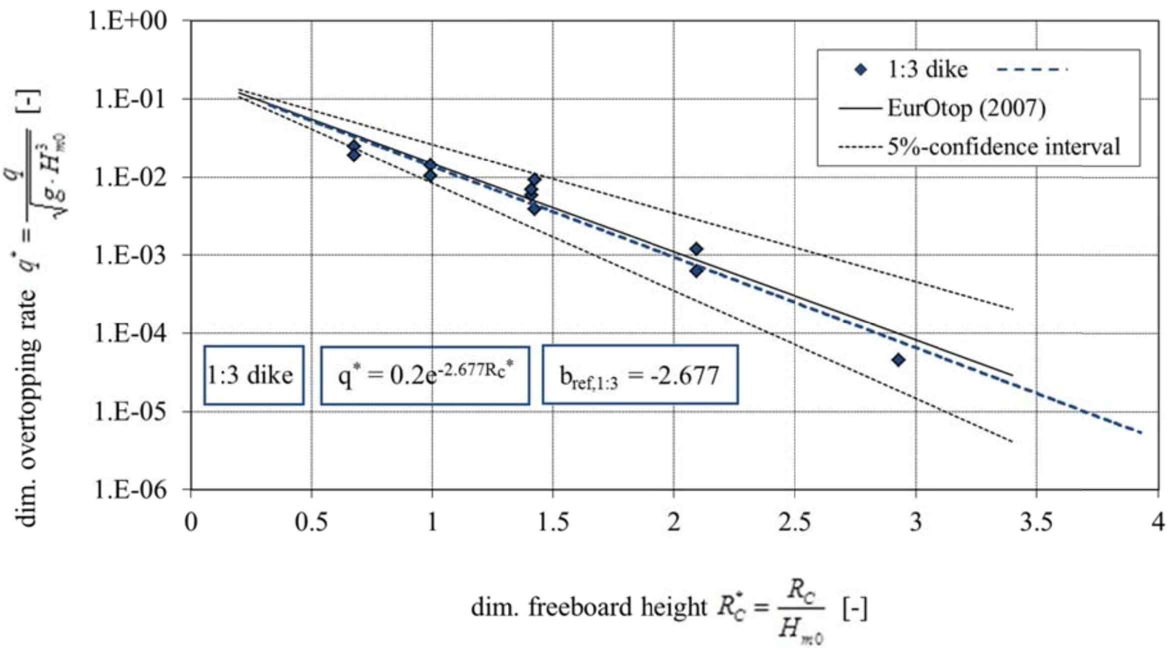

Figure 8.13 Dimensionless overtopping rate - reference test for non-breaking wave conditions (1:3 sloped dike)

Relation of the slopes 1:3 and 1:6

Summarizing the first conclusions drawn in this chapter, it can be stated that:

- The results validate well the theory applied in EUROTOP-MANUAL (2007).
- The overtopping formula underestimate slightly the results found in FlowDike 1, but fits those of FlowDike 2 well.
- The trend lines with fixed interception show an acceptable accuracy.
- The basic trend lines used for regression analysis of the following parametric set can be fixed on the y-axis to the interception values of formulae (5.26) and (5.27).
- Between the results of FlowDike 1 and FlowDike 2 a shift will remain during the analysis. This variance is about 4% conferring the slope inclinations ($b_{1:6}/b_{1:3}$) = (-4.771/-4.949) = 96%.

8.3.2 Influence of wave spectra

Figure 8.14 shows the results of former investigations on mostly 1:6 smooth sloped dikes. Most of the listed tests were performed during the German research project “Loading of the inner slope of sea dikes by wave overtopping” (BMBF KIS 009) where the investigation of different wave spectra was part of it. Also the tests results during the project “Influence of oblique wave attack on wave run-up and wave overtopping – 3D model tests at NRC/Canada with long and short crested Waves –“ are included. In the left graph the data points of all tests are given. The corresponding regression curves are given in the right graph. It can be seen, that the results for the double peak spectra and the TMA spectra is a bit smoother than the regression curve of FlowDike-D (1:3 and 1:6 sloped dike) and the sea state test.

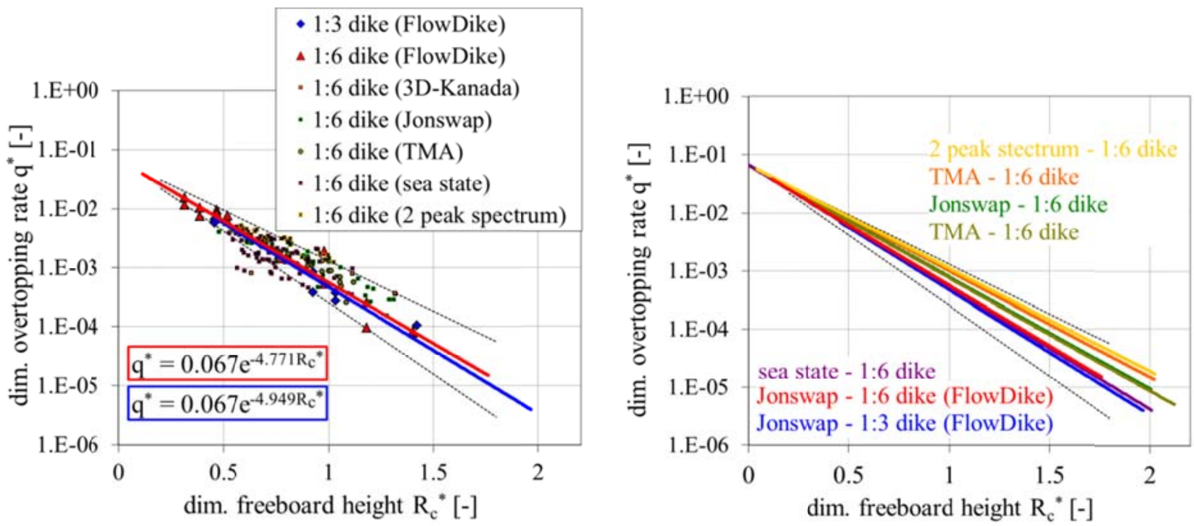

Figure 8.14 Influence of wave spectra on wave overtopping; Comparison of FlowDike results with former investigations by OUMERACI ET AL. (2002)

8.3.3 Comparison of Regression curves by Microsoft Excel and SPSS

By comparing the regression curves of Excel and SPSS Statistics (cf. SPSS USER´S GUIDE, 2007) the reference tests have great deviations while the tests with an angle of wave attack unequal zero degrees have related regression parameters (cf. Figure 8.15 to Figure 8.17). Especially the data of the 1:3 sloped dike with non-breaking waves show the difference between the coefficients.

As a consequence the coefficients b determined by Excel will be used for further analyzes. The results with SPSS have to be analyzed in more detail.

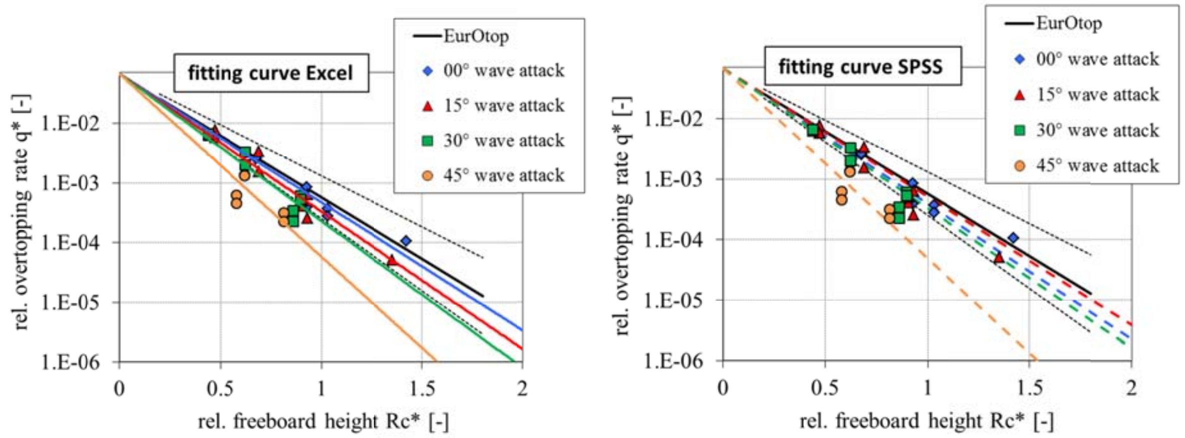

Figure 8.15 Regression curves 1:3 dike breaking waves (Excel left, SPSS right)

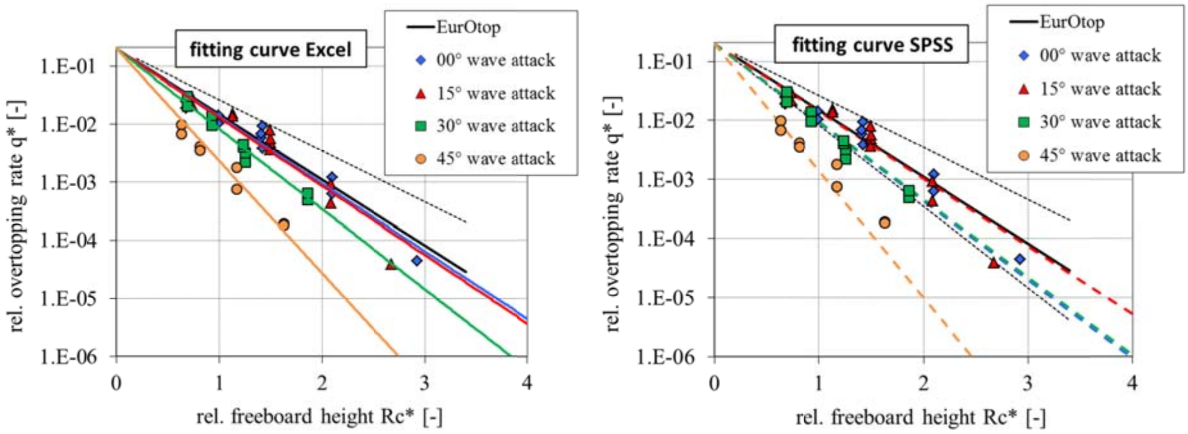

Figure 8.16 Regression curves 1:3 dike non-breaking waves (Excel left, SPSS right)

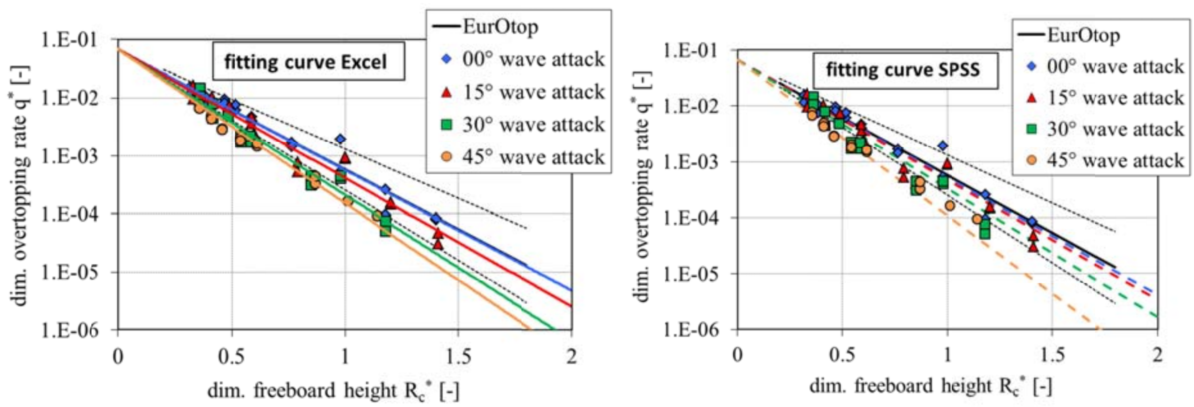

Figure 8.17 Regression curves 1:6 dike breaking waves (Excel left, SPSS right)

8.3.4 Influence of oblique wave attack

Oblique wave attack has been investigated before, so this chapter will only be an adaptation and verification. This is done with regard to the following analyses, which will consider the combined effects of obliqueness, currents and wind.

In the following figures (Figure 8.18 to Figure 8.20) all test results for oblique wave attacks are given. The trend lines have been determined with fixed interception for each angle of wave attack.

Again the data points lay very well around their exponential regression. Only the points for non-breaking waves with -15° oblique waves seam to scatter too much (cf. Figure 8.20). There is an obvious trend in both graphs, where the increase of obliqueness results in a reduction of overtopping. For the larger angles the reduction increases, this means between 0° and 15° the reduction is lower than between 30° and 45°.

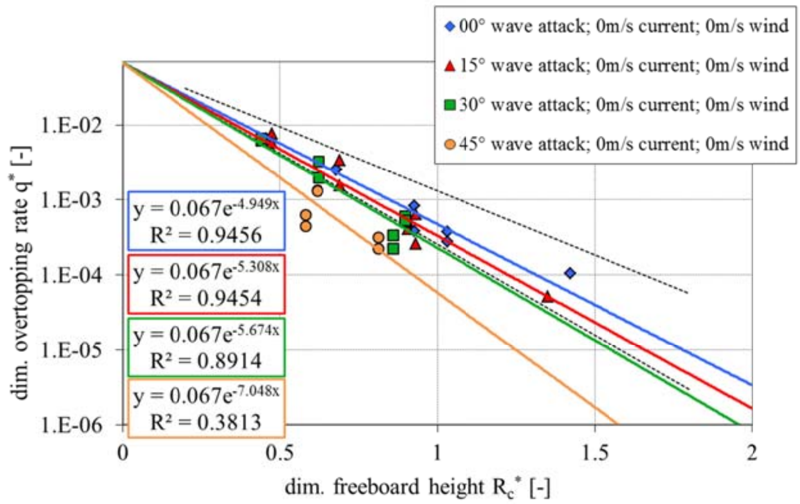

Figure 8.18 Oblique wave attack; 1:3 sloped dike (breaking conditions)

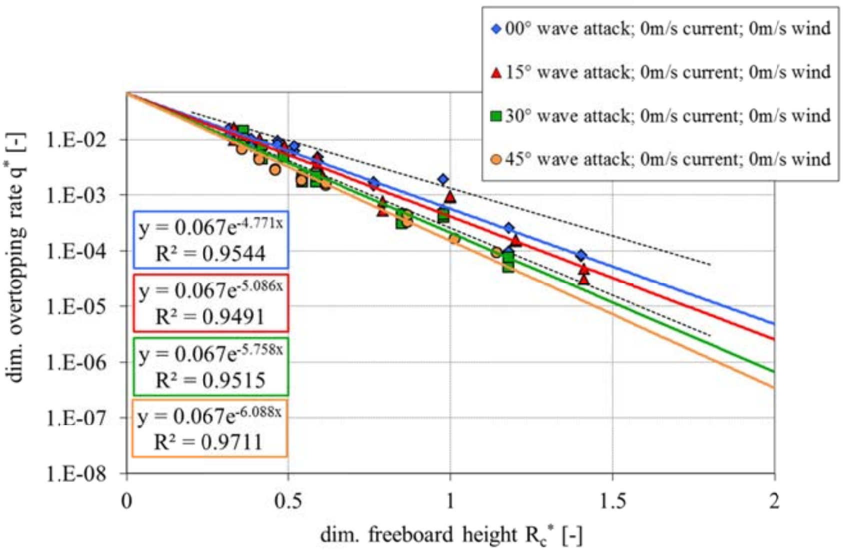

Figure 8.19 Oblique wave attack; 1:6 sloped dike (breaking conditions)

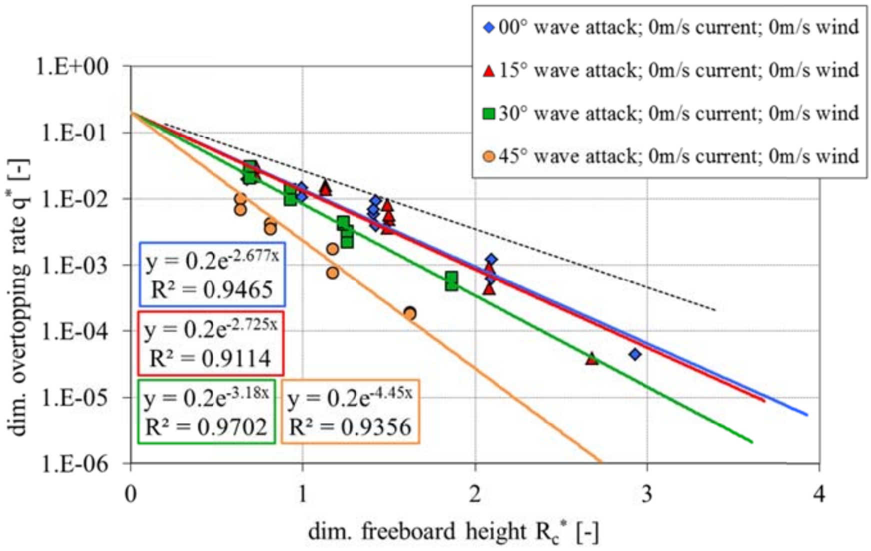

Figure 8.20 Oblique wave attack1:3 sloped dike (non-breaking conditions)

On the 1:6 sloped dike the trend lines and results for oblique wave attack for the breaking conditions are illustrated in Figure 8.19. Still the trend is followed that an increase in obliqueness results in the reduction of overtopping, but this time the reduction, especially between 30° and 45°, is not as large as for the 1:3 sloped dike. It was mentioned before those small overtopping amounts were expected and also recognised during testing due to the slope inclination. An explanation for less difference in the overtopping graphs for FlowDike 2 could be as well the smoother slope of the dike that leads to early breaking on the dike.

Relation of the slopes 1:3 and 1:6

A closer look at the coefficient b shows that for all different angles of wave attack a shift between the 1:3 slope and the 1:6 slope is noticeable. The shift was already perceived for the perpendicular waves (section 8.3.1) and will stay the same through the whole analysis. Table 8.1

Table 8.1 Inclinations of the slopes $b_{1:3}$ and $b_{1:6}$ of tests without current and wind (cf. Figure 8.18 to Figure 8.19)

dike slope	wave conditions	wave attack			
		0°	15°	30°	45°
1:3	breaking waves	-4.949	-5.308	-5.674	-7.048
1:6	breaking waves	-4.771	-5.086	-5.758	-6.088
1:3	non-breaking waves	-2.677	-2.725	-3.180	-4.450

Comparison with former investigations

The results of FlowDike 1 and FlowDike validate well the trend of the former results like DE WAAL & VAN DER MEER (1992) (cf. Figure 8.21). Most data points fall a little bit below the regression. The description of the formulae given by the other authors is given in chapter 5.3 in more detail.

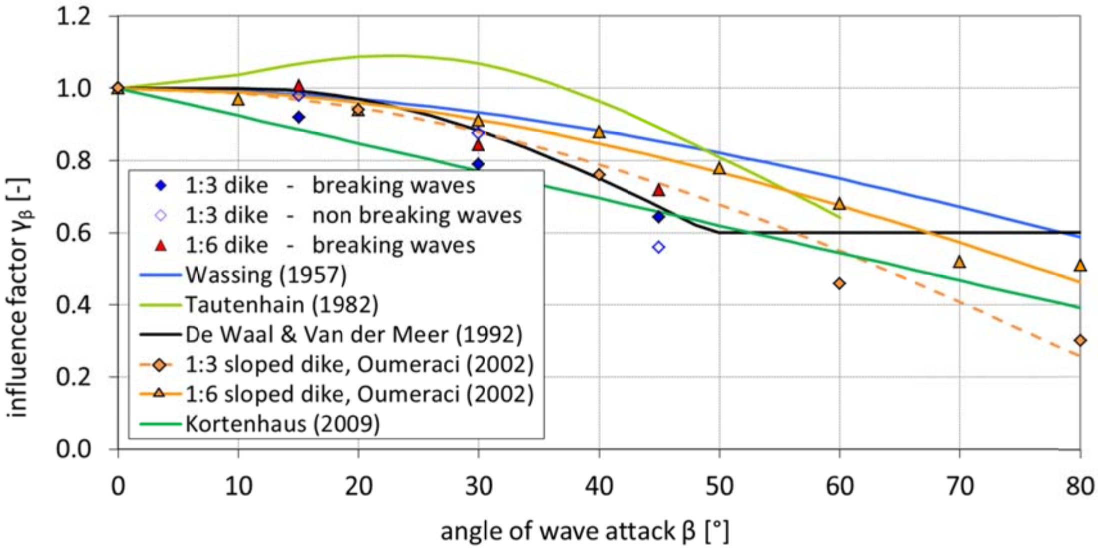

Figure 8.21 Comparison of reduction factors for obliqueness - FlowDike –D (1:3 and 1:6 sloped dike) with former investigations

8.3.5 Influence of wave direction and current

In a first step, a characteristic factor was applied to determine the influence of a combination of oblique waves and current parallel to the dike structure. The absolute wave parameters are used. A distinction was made between the results for the 1:3 sloped dike for breaking and non-breaking waves (cf. Figure 8.22) and the results for the breaking waves on the 1:6 sloped dike (cf. Figure 8.23). The diamonds show the influence factors for tests without current. An increase of the influence factor for increasing current velocity, shown by the triangles (0.15 m/s), circles (0.30 m/s) and squares (0.40 m/s only 1:6 dike), is noticeable for breaking wave conditions. For non-breaking wave conditions (1:3 sloped dike) The influence factor increases for angles of wave attack of -30° and +15° and decreases for angles of wave attack of -15° and +30°. For normal wave attack the 1:3 dike for breaking wave conditions a slightly decrease of the influence factor and consequently an increasing wave overtopping rate is noticeable for increasing current velocities.

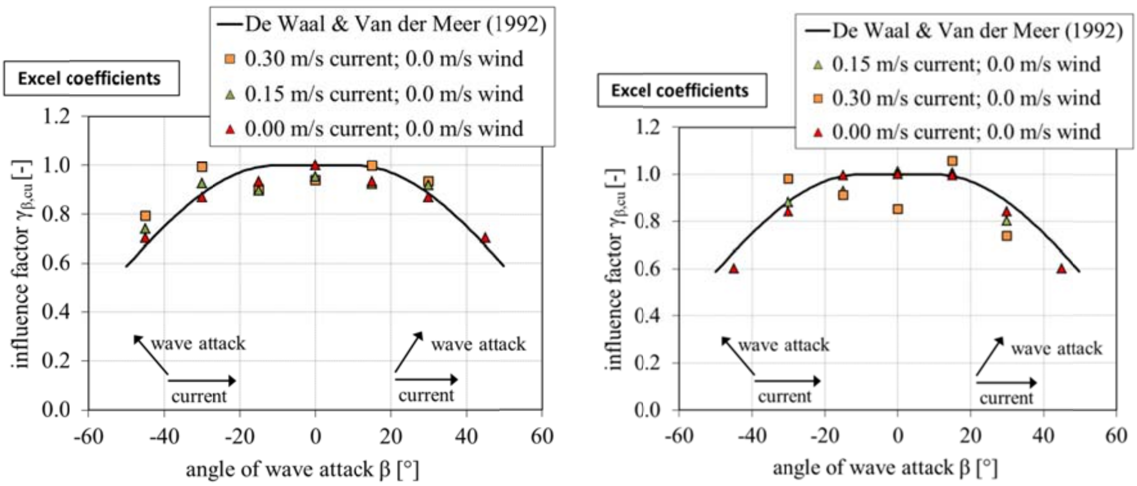

Figure 8.22 Current influence on wave overtopping, 1:3 sloped dike, left: breaking waves; right: non-breaking waves

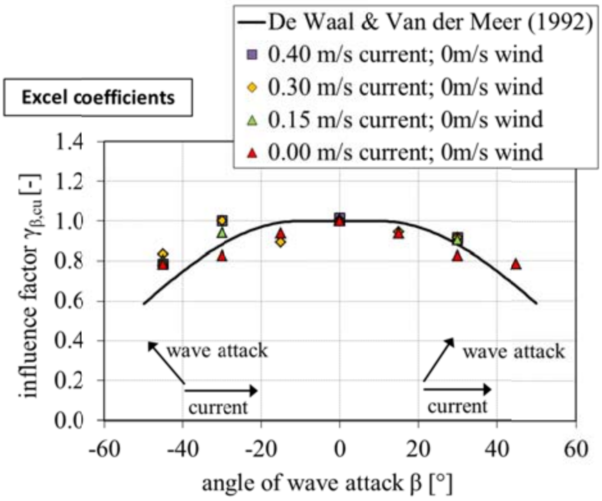

Figure 8.23 Current influence on wave overtopping, 1:6 sloped dike, breaking waves

For non-breaking waves the dimensionless overtopping rate and the dimensionless freeboard height is determined independent of the wave period (cf. Figure 8.12 and Figure 8.13). Hence using the relative wave period only changes the influence factor $\gamma_{\beta,cu}$ for breaking wave conditions and not for non-breaking conditions. The corresponding graphs are given below for the 1:3 and the 1:6 sloped dike (Figure 8.24 and Figure 8.25). The filled data points are results considering the absolute wave period $T_{abs,m-1,0}$. The non-filled data points are determined by using the relative wave period $T_{rel,m-1,0}$. The influence factor decreases for positive angles of wave attack. For negative angles of wave attack the relative wave periods become smaller. Consequently the influence factors increase to high values and cannot be used for describing the influence of current. The here presented data corresponding the relative wave period investigation are preliminary data and do not fit the data of further graphs.

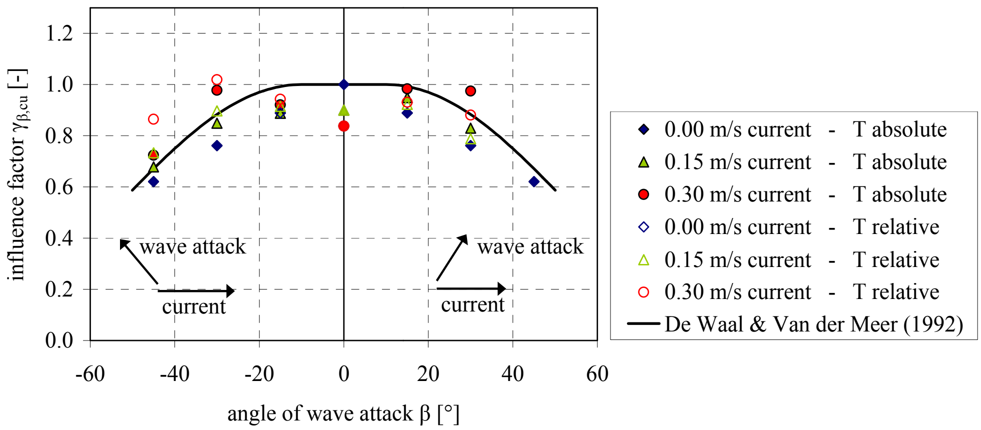

Figure 8.24 Current influence on wave overtopping including the relative wave period, 1:3 sloped dike, br. waves (preliminary results)

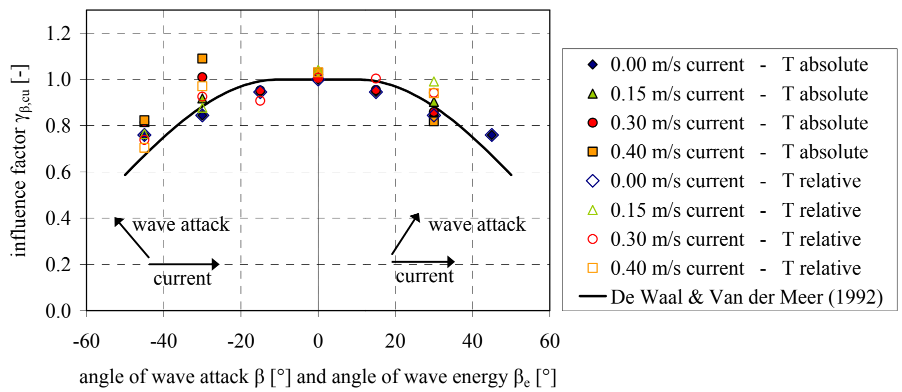

Figure 8.25 Current influence on wave overtopping including the relative wave period, 1:6 sloped dike, br. waves (preliminary results)

In the following, the theory of the wave energy direction is applied to the test results in Figure 8.26 to Figure 8.28 for the 1:3 and 1:6 sloped dike for breaking and non-breaking (only 1:3 sloped dike) waves. The filled data points are plotted against the angle of wave attack β whereas the non-filled data points are plotted against the angle of wave energy β_e. The data using the direction of wave energy are arranged further to the right than the data points that consider only the wave direction and not its energy direction and correspond fairly well to the graph of DE WAAL & VAN DER MEER (1992).

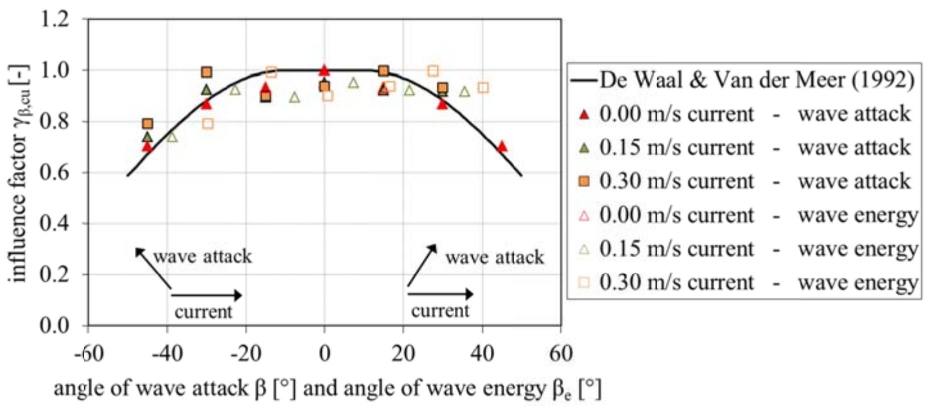

Figure 8.26 Current influence on wave overtopping including the angle of wave energy, 1:3 sloped dike, br. waves

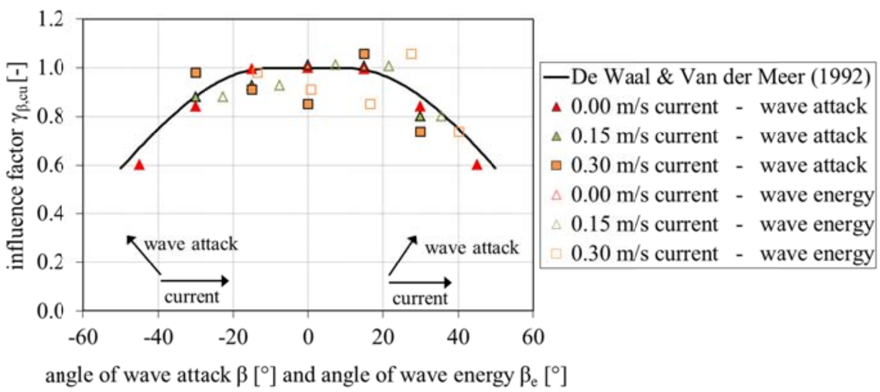

Figure 8.27 Current influence on wave overtopping incl. the angle of wave energy, 1:3 sloped dike, non br. waves

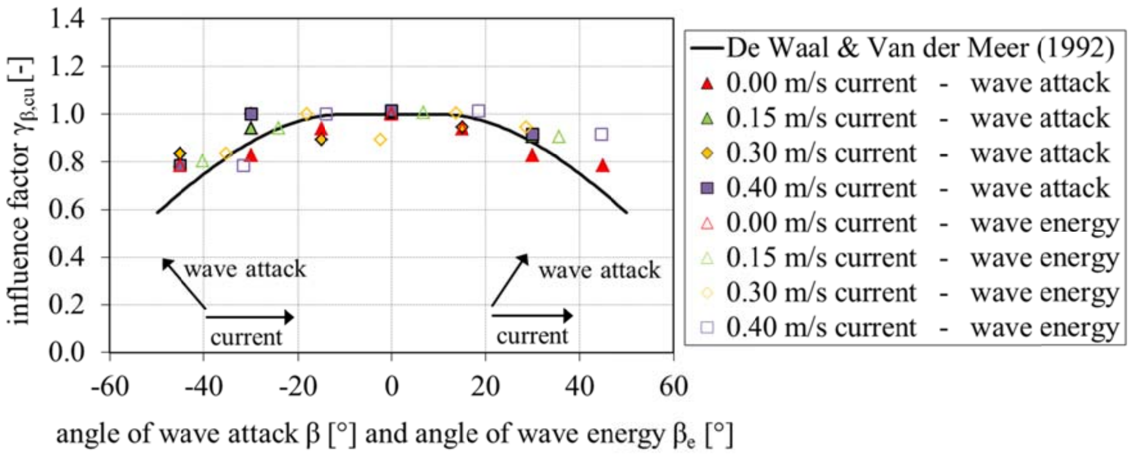

Figure 8.28 Current influence on wave overtopping including the angle of wave energy, 1:6 sloped dike, br. waves

8.3.6 Influence of wind

From the test program it can be seen that the test series on wind contain merely the wave spectra w1, w3 and w5 with a lower steepness than the wave spectra w2, w4 and w6. The steepness is a limiting factor for the surf similarity parameter and affects as well the overtopping formulae. Due to this is the generated waves for wind tests give only results for non-breaking conditions during FlowDike 1. For FlowDike 2 the influence of the slope was governing and still only breaking waves occurred. Another difference between FlowDike 1 and FlowDike 2 is the missing wind tests on u = 5m/s, only two tests on this wind speed exist.

Though the effect in overtopping could be measured, the detected events marked as points in the graphs show almost no influence for high overtopping events (lying nearly on the points of the reference test). For smaller amounts an increasing trend for the average overtopping can be established. This coincides well with the statements from WARD ET AL. (1996) and DE WAAL ET AL. (1996).

It is remarkable in Figure 8.29 that the trend lines stay within the confidence interval. As the trend lines are all above the reference trend from the basic test, it can be concluded that the overtopping increases for wind influence. For both investigated wind velocities the resulting regression is very close, as the inclinations of the slope b do not differ a lot. This effect could be explained with the small difference between the measured velocities. As the scaling of the wind is a very complex issue (GONZÁLEZ-ESCRIVA, 2006) and only two different velocities were applicable, the parametric range is very small.

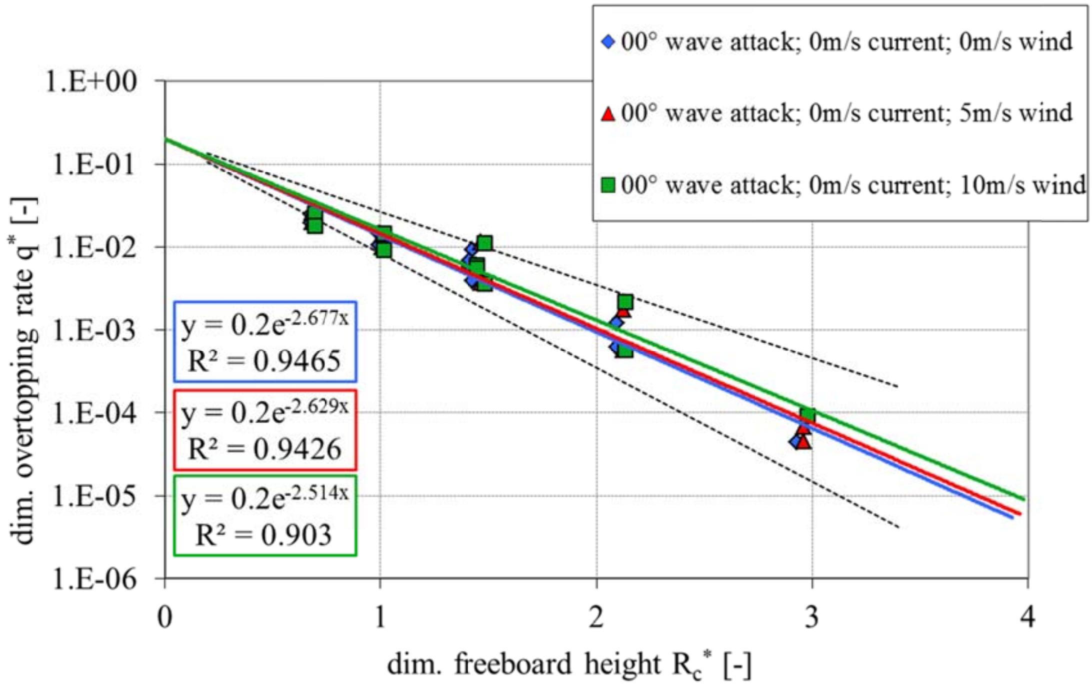

Figure 8.29 Wind influence; 1:3 sloped dike - FlowDike 1 (non-breaking conditions)

For FlowDike 2 the effect of increasing average overtopping amounts for the smaller wave spectra, such as w1 can be stated again. The first data points for high waves in the graph match again the points from the reference test. The regression curves are nearly the same, so that no influence of wind is recognizable.

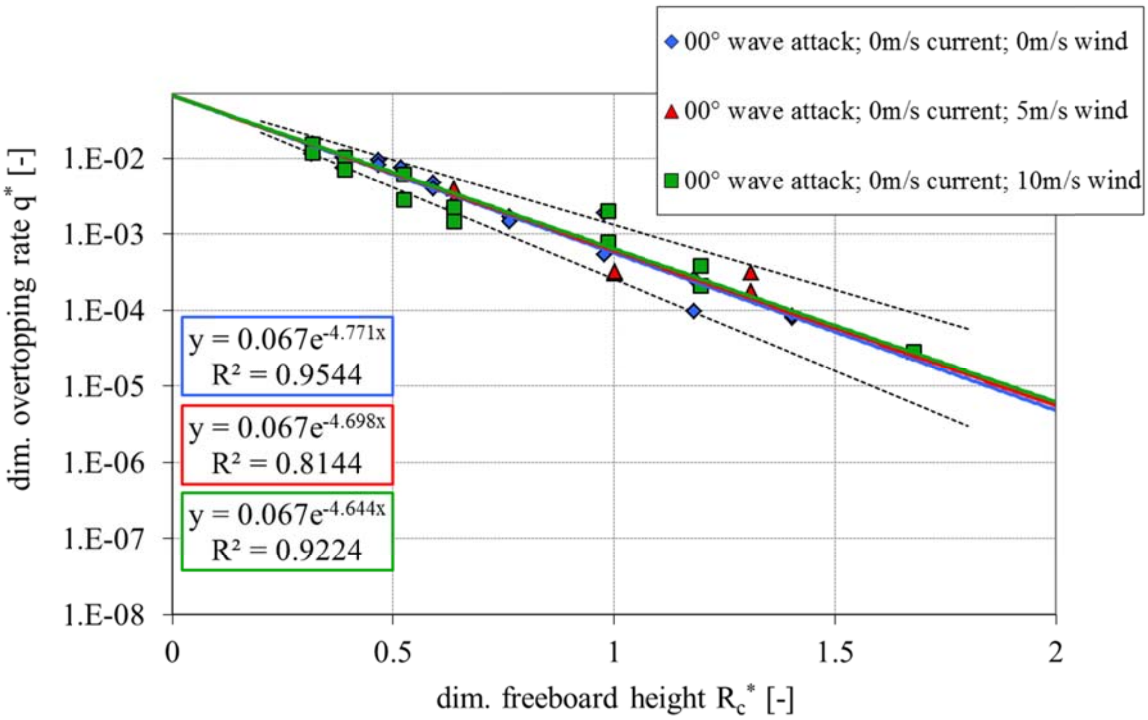

Figure 8.30 Wind influence; 1:6 sloped dike - FlowDike 2 (breaking conditions)

8.3.7 Reduction factors for all combinations

This section summarizes the factors for reduction, or in case of the wind an increase of the overtopping by means of a regression analysis as it is explained in chapter 8.3.1. The tables listed below give the parametric studies on the influences of interest. For every data set the variable of the slope inclination b and the determined influencing factor γ are given.

Table 8.2 Slope inclination b and reduction factors (γ_b) for oblique wave attack

angle of wave attack \ slope of the dike		1:3	1:6
breaking	0°	-4.949 (1.000)	-4.720 (1.000)
	-15°	-5.308 (0.932)	-5.086 (0.938)
	-30°	-5.674 (0.869)	-5.758 (0.829)
	+45°	-7.048 (0.702)	-6.088 (0.784)
non-breaking	0°	-2.677 (1.000)	- (-)
	-15°	-2.725 (0.995)	- (-)
	-30°	-3.180 (0.842)	- (-)
	+45°	-4.450 (0.602)	- (-)

Table 8.3 Slope inclination b and reduction factors (γ) for influencing variables, 1:6 dike (oblique wave attack, current and wind influence (first value: 0 m/s wind test; second value: 5 m/s wind test; third value: 10 m/s wind test)

angle of wave attack \ current		0 m/s	15 m/s	30 m/s	40 m/s
breaking	-45°	-6.088 (0.784) - (-) - (-)	-5.933 (0.804) - (-) - (-)	-5.718 (0.834) - (-) - (-)	-6.074 (0.785) - (-) - (-)
	-30°	-5.758 (0.829) - (-) - (-)	-5.062 (0.942) - (-) - (-)	-4.764 (1.001) - (-) - (-)	-4.760 (1.002) - (-) - (-)
	-15°	-5.086 (0.938) - (-) - (-)	- (-) - (-) - (-)	-5.346 (0.892) - (-) - (-)	- (-) - (-) - (-)
	0°	-4.720 (1.000) -4.698 (1.016) -4.644 (1.027)	-4.730 (1.009) - (-) -4.668 (1.022)	-4.752 (1.004) - (-) - (-)	-4.703 (1.014) - (-) -4.527 (1.054)
	+15°	-5.086 (0.938) - (-) - (-)	- (-) - (-) - (-)	-5.041 (0.946) - (-) - (-)	- (-) - (-) - (-)
	+30°	-5.758 (0.829) - (-) -5.385 (0.886)	-5.269 (0.905) - (-) - (-)	-5.208 (0.916) - (-) -5.269 (0.905)	-5.213 (0.915) - (-) -5.576 (0.856)
	+45°	-6.088 (0.784) - (-) - (-)	- (-) - (-) - (-)	- (-) - (-) - (-)	- (-) - (-) - (-)

Table 8.4 Slope inclination b and reduction factors (γ) for influencing variables, 1:3 sloped dike (oblique wave attack, current and wind influence (first value: 0 m/s wind test; second value: 5 m/s wind test; third value: 10 m/s wind test)

angle of wave attack \ current		0 m/s	15 m/s	30 m/s
breaking	-45°	-7.048 (0.702) - (-) - (-)	-6.679 (0.741) - (-) - (-)	-6.243 (0.741) - (-) - (-)
	-30°	-5.674 (0.869) - (-) - (-)	-5.349 (0.925) - (-) - (-)	-4.984 (0.993) - (-) - (-)
	-15°	-5.308 (0.932) - (-) - (-)	-5.519 (0.897) - (-) - (-)	-5.492 (0.901) - (-) - (-)
	0°	-4.949 (1.000) - (-) - (-)	-5.194 (0.953) - (-) - (-)	-5.271 (0.939) - (-) - (-)
	+15°	-5.308 (0.932) - (-) - (-)	-5.361 (0.923) - (-) - (-)	-4.956 (0.999) - (-) - (-)
	+30°	-5.674 (0.869) - (-) - (-)	-5.395 (0.917) - (-) - (-)	-5.299 (0.934) - (-) - (-)
	+45°	-7.048 (0.702) - (-) - (-)	- (-) - (-) - (-)	- (-) - (-) - (-)
non-breaking	-45°	-4.450 (0.602) - (-) - (-)	- (-) - (-) - (-)	- (-) - (-) - (-)
	-30°	-3.180 (0.842) - (-) - (-)	-3.040 (0.881) - (-) - (-)	-2.733 (0.980) - (-) - (-)
	-15°	-2.725 (0.995) - (-) - (-)	-2.882 (0.929) - (-) - (-)	-2.940 (0.911) - (-) - (-)
	0°	-2.677 (1.000) -2.769 (1.018) -2.514 (1.065)	-2.647 (1.011) - (-) - (-)	-3.140 (0.853) -2.667 (1.004) -2.769 (0.967)
	+15°	-2.725 (0.995) - (-) - (-)	-2.657 (1.008) - (-) - (-)	-2.531 (1.058) - (-) - (-)
	+30°	-3.180 (0.842) -3.117 (0.859) -2.967 (0.902)	-3.336 (0.802) - (-) - (-)	-3.624 (0.739) -3.555 (0.753) -3.366 (0.795)
	+45°	-4.450 (0.602) - (-) - (-)	- (-) - (-) - (-)	- (-) - (-) - (-)

8.4 Analysis of flow processes on dike crests

For each test of the 1:3 and 1:6 sloped dike the coefficients c_h and c_v were determined by using the described formula (5.31) and (5.32) by SCHÜTTRUMPF & VAN GENT (2003). To exclude measuring faults a selection of tests was made: Flow velocities of wind tests and with a corresponding flow depth on the crest lower than 1 cm are not usable because the micro propeller is under these conditions not able to deliver presentable results. These flow velocities are not considered in the following analysis. Figure 8.31 and Figure 8.32 show the coefficients c_h and c_v for all four dike configurations on the seaward side. These coefficients c_h and c_v are determined using the mentioned formula by SCHÜTTRUMPF & VAN GENT (2003):

$$c_h = \frac{R_{u2\%} - R_c}{H_s} \cdot \frac{H_s}{h_{2\%}} \quad [-] \tag{8.4}$$

with H_s significant wave height [m]

$R_{u2\%}$ run-up height exceeded by 2% of the incoming waves [m]

R_c freeboard height [m]

c_h empirical coefficient determined by model tests [-]

Additionally flow velocities on the seaward dike crest $v_{2\%}$ are given by

$$c_v = \sqrt{\frac{R_{u2\%} - R_c}{H_s}} \cdot \frac{\sqrt{g \cdot H_s}}{v_{2\%}} \quad [-] \tag{8.5}$$

c_v empirical coefficient determined by model tests [-]

In Figure 8.31 and Figure 8.32 the standard-deviations ±σ, ±2σ and ±3σ of the coefficients c_h and c_v are plotted respectively.

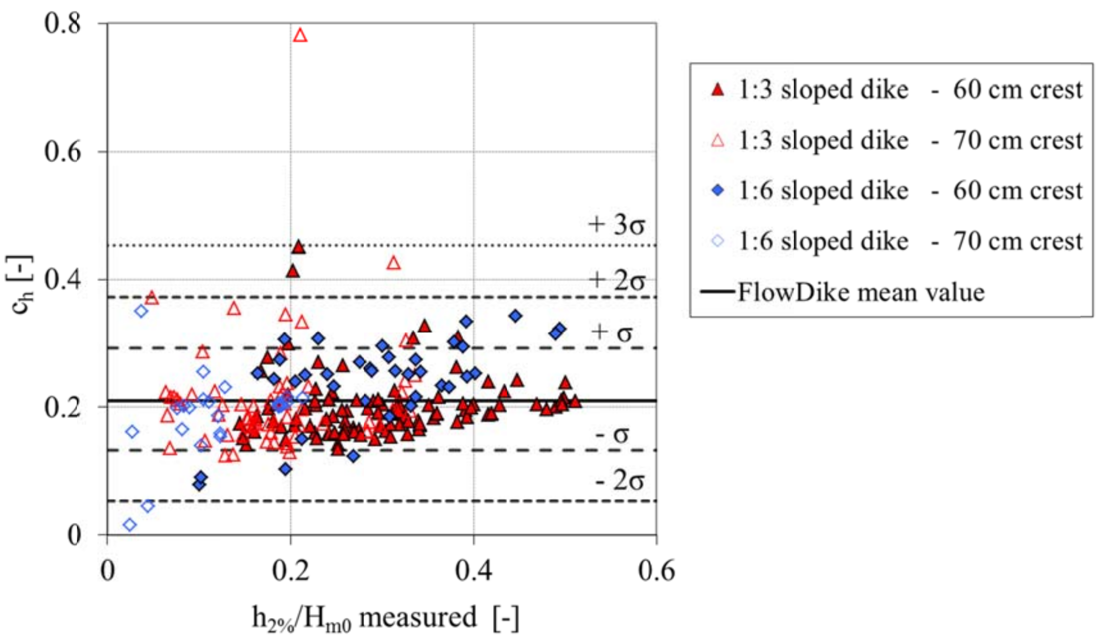

Figure 8.31 Coefficient c_h as a function of $h_{2\%}/H_{m0}$ without tests with wind or flow depth under 1cm

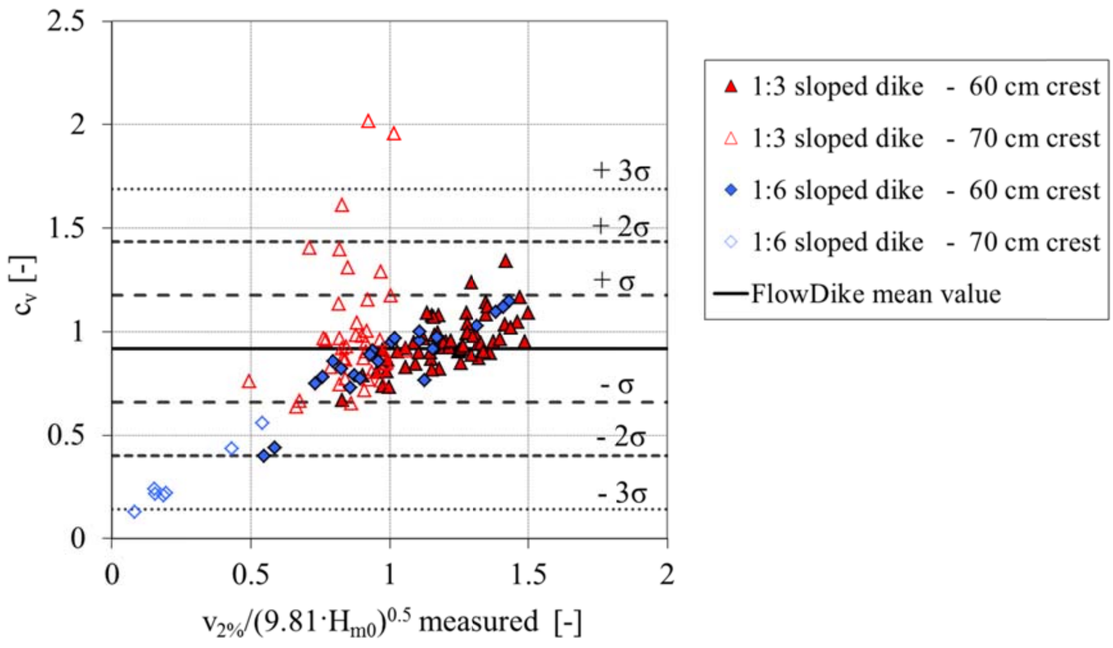

Figure 8.32 Coefficient c_v as a function of $v_{2\%}/(9.81 \cdot H_{m0})^{0,5}$ without tests with wind or flow depth under 1cm

Furthermore as a result of these distributions the data which are located outside the 3σ-interval are excluded from the following analysis and new mean values are determined.

To verify the coefficients for each dike configuration the average coefficient of each dike configuration and the average coefficient of all dike configurations are shown in Figure 8.33. The standard deviation refers to every single test. The dimension is declared and also presented in the figure (every test is depicted).

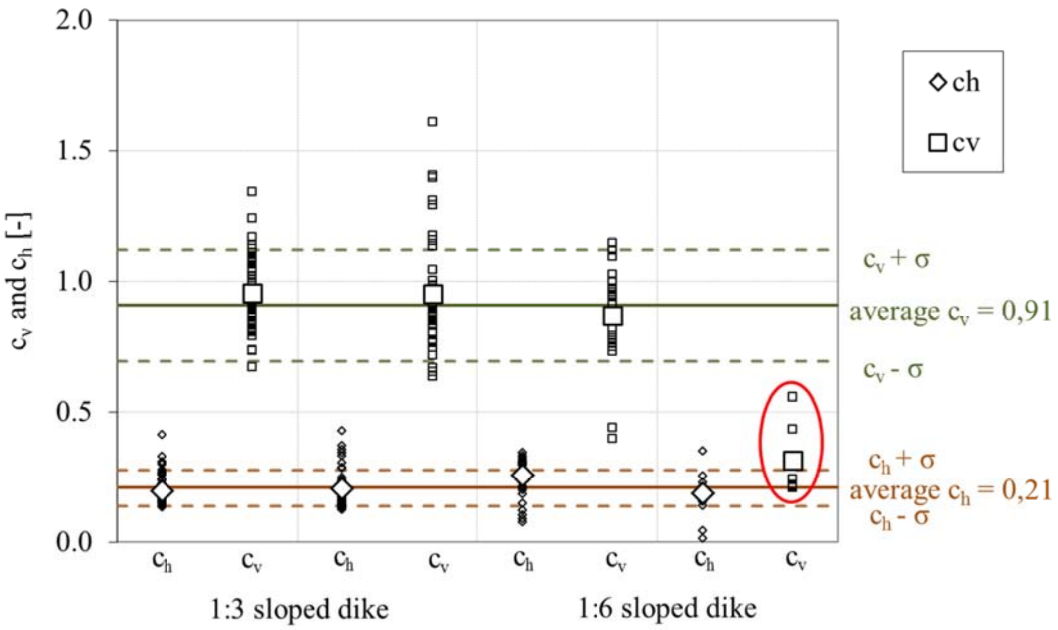

Figure 8.33 Average coefficients of every single dike configuration and of all configurations together

The coefficient c_v of the 1:6 sloped and 70 cm high dike give quite different values than the other dike configurations (cf. red-lined circle in Figure 8.34). Therefore this dike configuration will be omitted for the determination of the coefficient c_v. Figure 8.34 show the new distribution of coefficients and the final constant empirical coefficients c_h and c_v:

$c_h = 0.21$ and $c_v = 0.94$

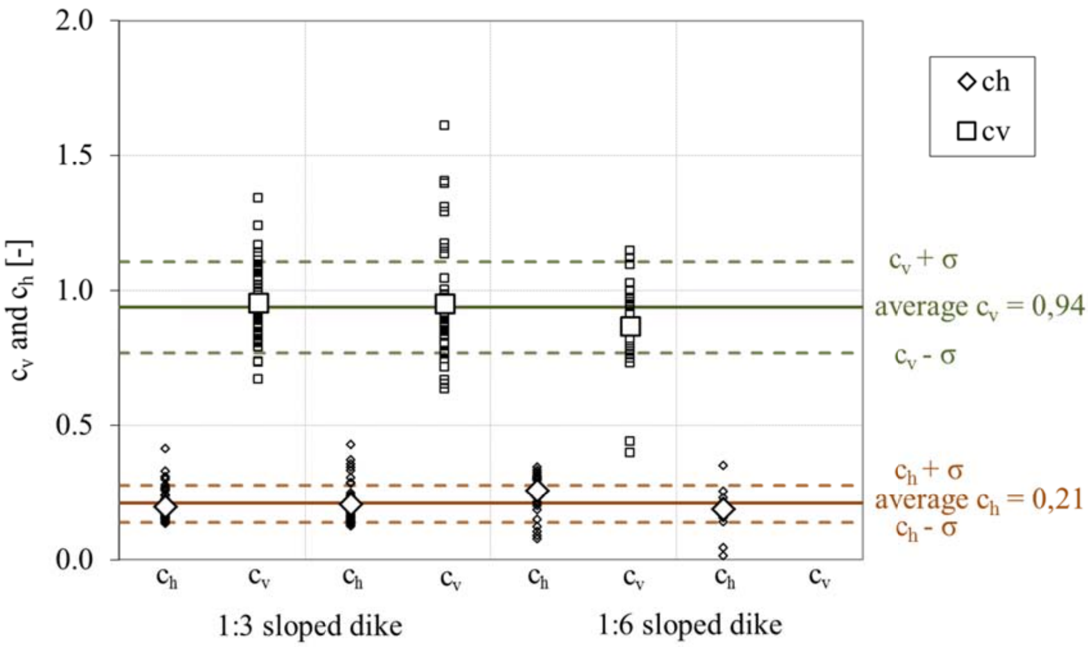

Figure 8.34 Average coefficients of every single dike configuration and of all configurations together excluding c_v of 1:6 sloped and 70 cm high dike

Comparing the new constant empirical coefficients c_h and c_v with the values from former investigation (cf. Figure 8.35) the coefficient $c_h = 0.21$ correspond well with the value by SCHÜTTRUMPF (2001) $c_h = 0.21$ and is slightly higher than the value by VAN GENT (2002) $c_h = 0.15$. The coefficient c_v for the results of FlowDike-D is lower than the coefficients by SCHÜTTRUMPF (2001) and VAN GENT (2002).

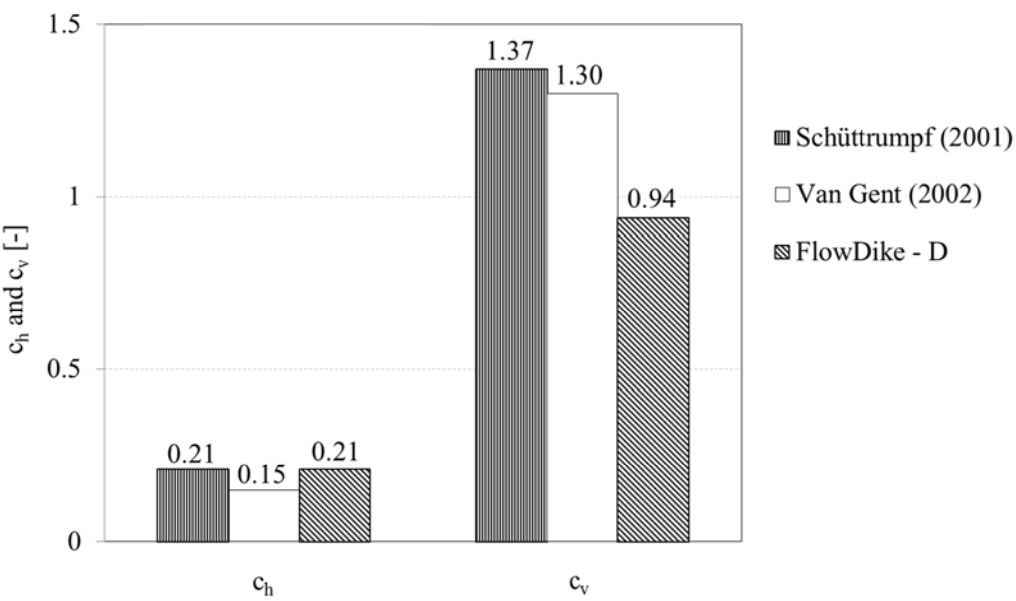

Figure 8.35 Coefficients c_h and c_v of former investigations compared with the new coefficients by FlowDike-D

According to the modification of empirical coefficients used in formula (5.31) and (5.32) by SCHÜTTRUMPF & VAN GENT (2003) it is possible to determine the flow depths and flow velocities on the seaward side.

With the new empirical coefficients c_h and c_v flow depths $h_{2\%}$ and flow velocities $v_{2\%}$ were calculated and plotted against the measured values (Figure 8.36). According to the modification of empirical coefficients used in formula by SCHÜTTRUMPF & VAN GENT (2003) it is possible to determine the flow depths and flow velocities on the seaward side of the crest exemplary on the 1:3 sloped dike. Further analysis considering the influence of current and wind on flow processes on dike crests has not been analyzed yet.

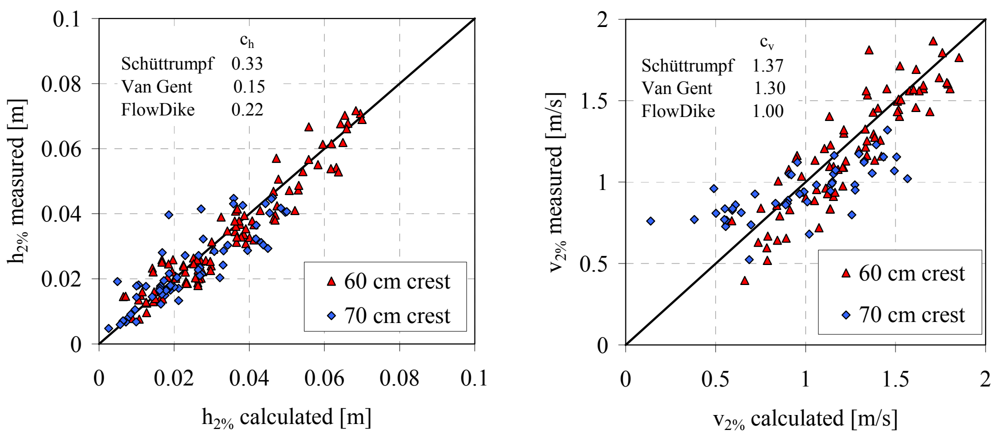

Figure 8.36 Measured and calculated flow depths $h_{2\%}$ and flow velocities $v_{2\%}$ on the seaward side of the dike crests using the new empirical coefficients, 1:3 sloped dike

8.5 Evaluation of single overtopping events

8.5.1 General

To determine the single overtopping events two methods can be used (cf. Figure 8.37):

- flow processes on the dike crest using the flow depth h and the flow velocities v
- load cell measurements

The measurements were carried out on a 60 cm high dike and a 70 cm high dike each with two load cells. Up to now only the 60 cm high dike will be considered because of the more significant flow processes. Furthermore only the measurements on the seaward site are analyzed yet.

To distinguish between the data of the two different measurement methods the indices "lc" (for the load cell method) and "vh" (for the flow process method) are included.

The following parameters will be used to describe the proceeding and the results:

q	overtopping rate [m³/(s·m)]
v	flow velocity on the dike crest [m/s]
h	flow depth on the dike crest [m]
V'	overtopping volume per meter wave [m³/m]

V overtopping volume per wave [m³]

Δt duration of a wave overtopping [s]

a correction factor [-]

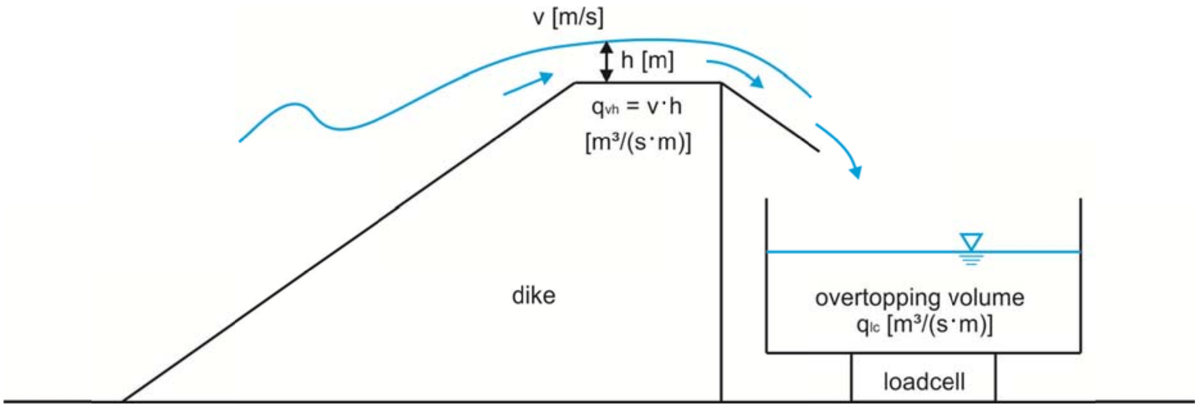

Figure 8.37 Overview of the different measurements

8.5.1.1 Methods

Overtopping volumes V_{vh} and flow rates q_{vh} by data of the wave gauge and the micro propeller

Per wave gauge the flow depth h is measured using a wave gauge and the flow velocity v is measured using a micro propeller. The product of these two parameters give the overtopping rate q_{vh}:

$$q_{vh} = v \cdot h \quad [\text{m}^3/(\text{sm})] \tag{8.6}$$

The duration of the overtopping event Δt_{vh} is deposited in the data of the wave gauge as well as of the micro propeller. The measurement of the wave gauge is used for further analyses to avoid impreciseness through the rotating of the micro propeller although the wave has passed.

The volume V_{vh}' per meter wave is determined as

$$V_{vh}^{'} = q_{vh} \cdot \Delta t_{vh} = v \cdot h \cdot \Delta t_{vh} \tag{8.7}$$

Overtopping volumes V_{lc} and flow rates q_{lc} by data of the load cells

The volume per meter wave V_{lc}' [m³/m] can be calculated by considering the channel width of the load cell of 0.1 m:

$$V_{lc}^{'} = \frac{V_{lc}}{0.1\,m} \tag{8.8}$$

The flow rate is determined by combining the measured time of the wave gauge Δt_{vh} with the volume of the load cells V_{lc}':

$$q_{lc,vh} = \frac{V_{lc}^{'}}{\Delta t_{vh}} \tag{8.9}$$

In summary there are determined two flow rates for each overtopping event q_{vh} and q_{lc} and two overtopping volumes V_{vh}' and V_{lc}'.

8.5.2 Data evaluation

The selecting of the needed measurements is described referring to the marked points in Figure 8.38.

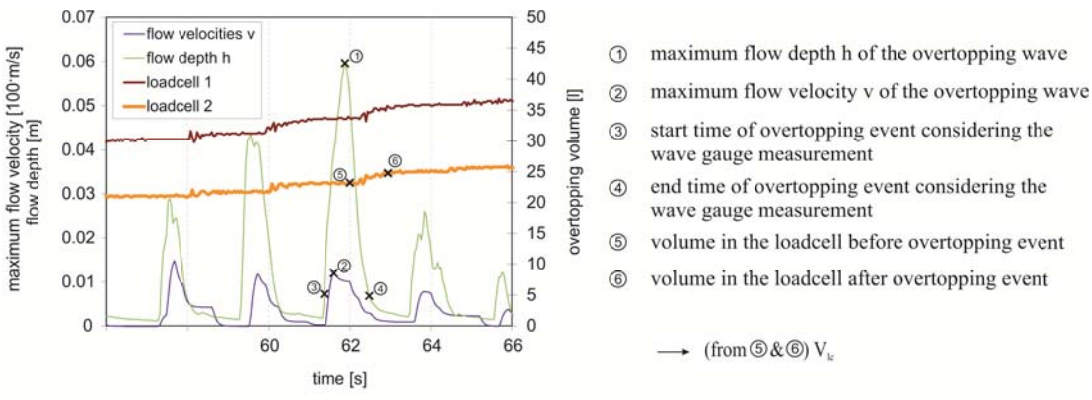

Figure 8.38 Signal of the overtopping measurements exemplary for the 1.3 sloped and 60 cm high dike

8.5.3 Results

Figure 8.39 and Figure 8.40 show the single overtopping volumes per meter dike length (left graph) and the overtopping rates per meter dike length (right graph) of the two analyzing methods against each other. The black graph is the so called ideal curve where both measurements are equal.

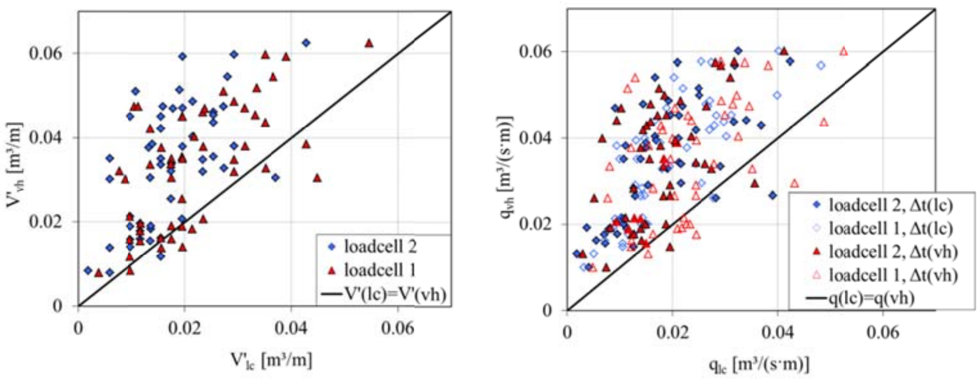

Figure 8.39 Overtopping volume V_{vh}' against V_{lc}' (left graph) and overtopping rate q_{vh} against q_{lc} (right graph), 1:3 sloped dike

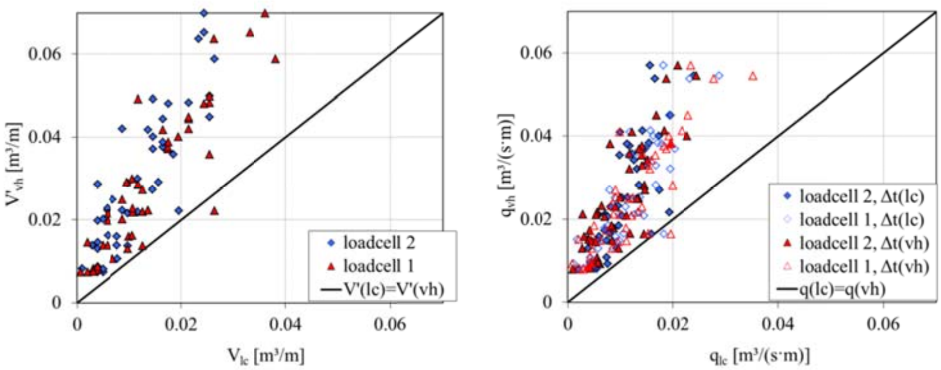

Figure 8.40 Overtopping volume V_{vh}' against V_{lc}' (left graph) and overtopping rate q_{vh} against q_{lc} (right graph), 1:6 sloped dike

The wave overtopping volumes based on flow processes on the dike crest seem to be overestimated because of using the maximum values for flow depth and flow velocity of each wave overtopping event. The correction factor a is determined by using the following ratios:

$$a_{vh} = \frac{q_{lc,vh}}{q_{vh}} \tag{8.10}$$

Considering the correction factor $a = 0.5$ (determined average), the overtopping rate q_{vh} and overtopping volume V_{vh}' are determined by formulae (8.11) and (8.12). Figure 8.41 and Figure 8.42 show the corrected data for the 1:3 and 1:6 sloped dike respectively.

$$q_{vh} = v \cdot h \cdot a \tag{8.11}$$

and

$$V_{vh}^{'} = q_{vh} \cdot \Delta t_{vh} \cdot a = v \cdot h \cdot \Delta t_{vh} \cdot a \tag{8.12}$$

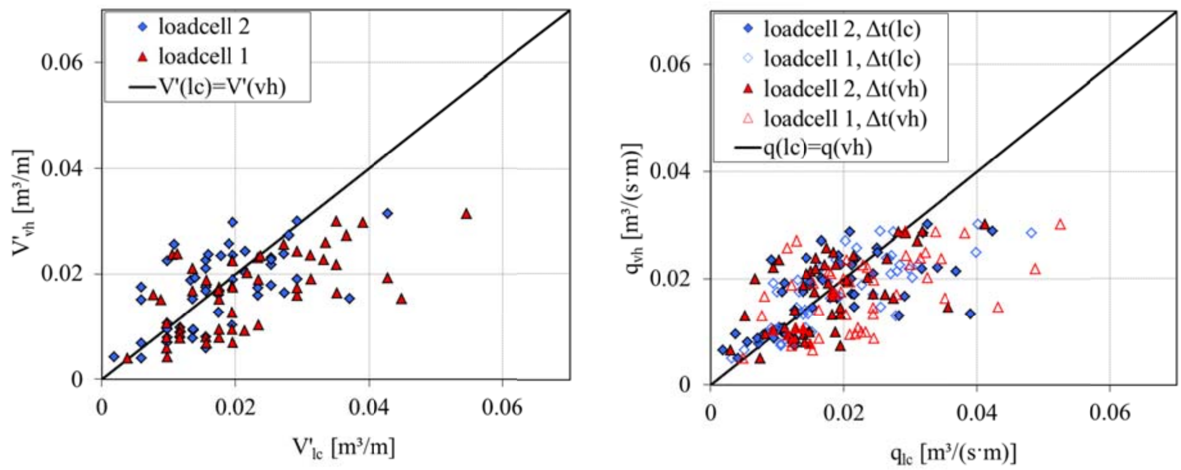

Figure 8.41 Overtopping volume V_{vh}' against V_{lc}' (left graph) and overtopping rate q_{vh} against q_{lc} (right graph) regarding correction factor a = 0.5; 1:3 sloped dike

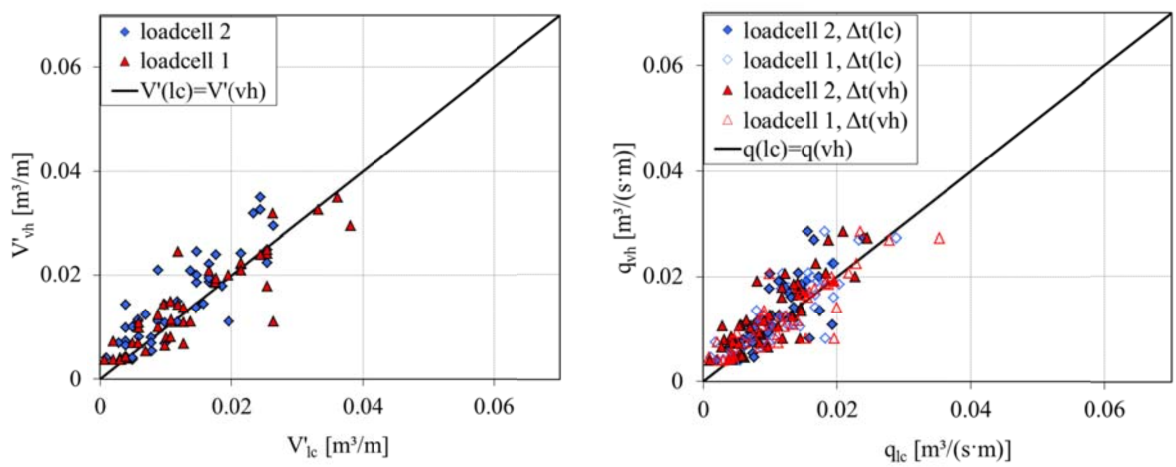

Figure 8.42 Overtopping volume V_{vh}' against V_{lc}' (left graph) and overtopping rate q_{vh} against q_{lc} (right graph) regarding correction factor a = 0.5; 1:6 sloped dike

9 Conclusion

The investigations of FlowDike 1 and FlowDike 2 concentrate on the effects of wind and parallel current on wave run-up and wave overtopping for perpendicular and oblique wave attack. These variables were two of the missing effects in freeboard design and therefore a main interest for design purposes. Model tests were carried out in the shallow water wave basin at DHI (Hørsholm, Denmark) and included the configuration of a 1:3 sloped dike (FlowDike 1) and a 1:6 sloped dike (FlowDike 2).

The tests on perpendicular wave attack without influencing parameter validated the existing wave overtopping formulae from the EUROTOP-MANUAL (2007). For both model tests the data points of the reference tests fit well within the 90% confidence interval of the formula.

All wind tests on wave overtopping confirmed the stated assumptions by GONZÁLEZ-ESCRIVA (2006) and DE WAAL ET AL. (1996) concerning the significant wind impact on small overtopping discharge. For high overtopping discharges practically no influence is noticeable as the data points for wind match those of the reference test, this validates the stated theory of WARD ET AL. (1996).

The influence of oblique waves on overtopping was analyzed as a last resort. In a first attempt the results found for both investigations validate the trend for obliqueness to reduce wave overtopping. The reduction factors found for FlowDike 1 validate well the regression trend found for former investigations.

For wave overtopping the combination of oblique wave attack and current parallel to the dike was analyzed by determine an influence factor $\gamma_{\beta,cu}$. Using therefore the relative wave period $T_{rel,m-1,0}$ instead of the absolute wave period $T_{abs,m-1,0}$ leads to rather high values and does not account the current influence on wave overtopping. Instead of that the influence-factor $\gamma_{\beta,cu}$ can be determined by using the angle of wave energy β_e instead of the angle of wave attack β.

The analysis of wave run-up was focused on the combined effect of oblique wave attack and current. A current seems to increase the effect of oblique wave attack which is stronger with a higher absolute value of the angle of wave attack.

The ongoing data analysis on wave run-up considering an advanced data extraction from video films considering 10 separate stripes of the run-up board provides new measurement results which will include in the data analysis in a next step.

According to the modification of empirical coefficients used in formulae by SCHÜTTRUMPF & VAN GENT (2003) it is possible to determine the flow depths and flow velocities on the seaward side of the crest. Further analysis considering the influence of current and wind on flow processes on dike crests will be presented in detail in the paper.

Two methods are used to determine the single overtopping events. Both methods, flow processes on the dike crest and load cell measurements, give better results for the analysis on the 1:6 sloped dike than on the 1.3 sloped dike.

10 References

Ahrens, J. P. and Heimbaugh, M. S. (1992): **Seawall overtopping model**, Proceedings of the 21st International Conference on Coastal Engineering

Aminti, P. and Franco, L. (1988): **Wave overtopping on rubble mound breakwaters**, Proceedings of the 21st International Conference on Coastal Engineering, pp. 770 - 781, New York, United States

Battjes, J. A. (1974): **Computation of set-up, longshore currents, run-up and overtopping due to wind-generated waves**, Vol. 74-2, Delft, Netherlands

Bradbury, A. P. and Allsop, N. W. H. (1988): **Hydraulic effects of breakwater crown walls**, Proceedings of conference on design of breakwaters, pp. 385 - 396, London

de Rouck, J., Troch, P., van de Walle, B., van Gent, M. R. A., van Damme, L., de Rond, J., Frigaard, P. and Murphy, J. (2002): **Wave run-up on sloping coastal structures prototype measurements versus scale model tests**, Proceedings of the international Conference on Breakwaters, coastal structures and coastlines, pp. 233 - 244, London, England

de Waal, J. P. and van der Meer, J. W. (1992): **Wave runup and overtopping on coastal structures**, Proceedings of the 23rd International Conference on Coastal Engineering, pp. 1772 - 1784

de Waal, J. P., Tönjes, P. and van de Meer, J. W. (1996): **Wave overtopping of vertical structures including wind effect**, Proceedings of the 25th International Conference on Coastal Engineering, pp. 2216 - 2229, Singapore, Singapore

EurOtop-Manual, Pullen, T., Allsop, N. W. H., Bruce, T., Kortenhaus, A., Schüttrumpf, H. and van der Meer, J. W. (2007): **Die Küste - EurOtop, wave overtopping of sea defences and related structures: Assessment manual**, Issue 73, Heide, Germany

Franco, L., de Gerloni, M. and van der Meer, J. W. (1994): **Wave overtopping on vertical and composite breakwaters**, Proceedings of the 24th International Conference on Coastal Engineering

Gibson, A. H. (1930): **The effect of surface waves on the discharge over weirs**, ICE Selected Engineering Papers, Vol. 1, Issue 99, pp. 5 - 18, London, UK

González-Escriva, J. A. (2006): **The role of wind in wave runup and wave overtopping of coastal structures**, Proceedings of the 30th International Conference, Vol. 5, pp. 4766 - 4778, Singapore, Singapore

Grüne, J. and Wang, Z. (2000): **Wave run-up on sloping seadykes and revetments**, Proceedings of the 27th International Conference, Singapore, Singapore

Hedges, T. S. (1987): **Combinations of Waves and Currents - An Introduction**, Proceedings of the Institution of Civil Engineers Part 1-Design and Construction, Vol. 82, pp. 567 - 585, London, England

Hedges, T. S. and Reis, M. T. (1998): **Random waves overtopping of simple sea walls: a new regression model**, Proceedings of the Institution of Civil Engineers.Water, maritime & energy, Vol. 130, Issue Telford, pp. 1 - 10, London, United Kingdom

Heyer, T. and Pohl, R. (2005): **Der Auflauf unregelmäßiger Wellen im Übergangsbereich zwischen branden und Schwingen**, Wasser und Abfall, Vol. 5, pp. 34 - 38, Sindelfingen, Germany

Holthuijsen, L. H. (2007): **Waves in oceanic and coastal waters**, New York, New York

Hunt, I. A. (1959): **Design of seawalls and breakwaters**, Journal of Waterway Port Coastal and Ocean Engineering-Asce, pp. 123 - 152, New York, New York

Juhl, J. and Sloth, P. (1994): **Wave overtopping of breakwaters under oblique waves**, Proceedings of the 24th International Conference on Coastal Engineering, pp. 1182 – 1196

Kortenhaus, A., Fröhle, P., Jensen, J., von Lieberman, N., Mai, S., Miller, C., Peters, K. and Schüttrumpf, H. (2009): **Probabilistische Bemessung von Bauwerken**, In:Hafenbautechnische Gesellschaft and Deutsche Gesellschaft für Geotechnik e.V., Unsere Gewässer - Forschungsbedarf aus Sicht der Praxis : eine Dokumentation von HTG und DGGT, Hamburg, pp. 109-122

Malcherek, A. (2010): **Gezeiten und Wellen - Die Hydromechanik der Küstengewässer**, Vieweg + Teubner

Oumeraci, H., Schüttrumpf, H., Sauer, W., Möller, J. and Droste, T. (2000): **Physical model tests on wave overtopping with natural sea states - 2D model tests with single, double and multi peak wave energy spectra**, Vol. LWI-Bericht 852, Braunschweig, Germany

Oumeraci, H., Möller, J., Schüttrumpf, H., Zimmermann, C., Daemrich, K.-F. and Ohle, N. (2002): **Schräger Wellenauflauf an Seedeichen**, Vol. LWI 881, FI 643/V, Braunschweig, Germany

Owen, M. W. (1980): **Design of seawalls allowing for wave overtopping**, Vol. EX 924, Wallingford, England

Owen, M. W. (1982): **The hydraulic design of sea-wall profiles**, pp. 185 - 192, London, England

Pedersen, J. and Burcharth, H. F. (1992): **Wave forces on crown walls**, Proceedings of the 23st international Conference on Coastal Engineering, New York, United States

Sawaragi, T., Deguchi, I. and Park, S.-K. (1988): **Reduction of wave overtopping rate by use of artificial reefs**, Proceedings of the 21st International Conference on Coastal Engineering, pp. 335 - 349, New York, United States

Schüttrumpf, H. (2001): **Wellenüberlaufströmung bei Seedeichen - Experimentelle und theoretische Untersuchungen**, Braunschweig, Germany

Schüttrumpf, H. and van Gent, M. R. A. (2003): **Wave overtopping at seadikes**, pp. 431 - 443, Vicksburg, MS

Smith, G. M., Seijffert, J. W. W. and van der Meer, J. W. (1994): **Erosion and overtopping of a**

grass dike large scale model tests, Proceedings of the 24th International Conference on Coastal Engineering, pp. 2639 - 2652

SPSS User´s Guide (2007): **SPSS Statistics Base 17.0 - User´s Guide**, (SPSS Inc.), Chicago, United States

Tautenhain, E., Kohlhase, S. and Partenscky, H. W. (1982): **Wave run-up at sea dikes under oblique wave approach**, Proceedings of the 18th International Conference on Coastal Engineering, pp. 804 - 810

Treloar, P. D. (1986): **Spectral wave refraction under the influence of depth and current**, Coastal Engineering, Vol. 9, Issue 5, pp. 439 - 452, Amsterdam, Netherlands

van der Meer, J. W. (1993): **Conceptual design of rubble mound breakwater**, Delft Hydraulics, Vol. 483

van der Meer, J. W. and Janssen, J. P. F. M. (1994): **Wave run-up and wave overtopping at dikes and revetments**, Delft, Netherlands

van der Meer, J. W. and Janssen, J. P. F. M.(1995): **Wave run-up and wave overtopping at dikes**, In: Wave forces on inclined and vertical wall structures, New York, New York, pp. 1-27

van Gent, M. R. A. (2002): **Wave overtopping events at dikes**, Proceedings of the 28th International Conference, Singapore

Wagner, H. and Bürger, W. (1973): **Kennwerte zur Seedeichbemessung**, Wasserwirtschaft Wassertechnik, Vol. 23, Issue 6, pp. 204 - 207, Berlin, Germany

Ward, D. L., Zhang, J., Wibner, C. G. and Cinotto, C. M. (1996): **Wind effects on runup and overtopping of coastal structures**, Proceedings of the 29th International Conference on Coastal Engineering, pp. 2206 - 2215, Singapore, Singapore

Wassing, F. (1957): **Model investigation on wave run-up carried out in the Netherlands during the past twenty years**, Issue 42, pp. 700 - 714

Glossary

Average wave: The average wave is a superposition of the incident and reflected wave and therefore it is the actual visible wave.

Breaking waves (plunging) and non-breaking waves (surging): A certain type of breaking is given by the combination of structure slope and wave steepness for the deep water conditions. On sloped structures it can be defined by the surf similarity parameter $\xi_{m-1,0}$ with breaking waves $\xi_{m-1,0} > 2 - 3$ and non-breaking waves $\xi_{m-1,0} > 2 - 3$. The transition between plunging and surging waves is known as collapsing.

Crossing analysis: For most of the processed data a crossing analysis (up or down crossing) was used in time domain. Both options use a defined crossing level within the raw data signal to detect single events and their parameter, such as peak to peak value or event duration. The difference between up or down crossing is the starting direction within the analysis, whether it starts to detect an event first when it is crossing the threshold in upward direction or downwards.

Exceedance curve: An exceedance curve is one tool to visualise the distribution of any parameter, such as run-up heights. The percentage of exceeding is calculated from the number of detected events related to the number of waves N. The curve simply relates the percentage of events to i.e. the run-up height.

Incident wave: The incident wave describes the wave coming from the sea before it hits the structure. In the model tests it is the incidental generated wave from the wave maker without reflection influences.

JONSWAP–spectra: The Joint North Sea Wave Project – spectra describes the empirical distribution of energy with frequency within the ocean. It is one of the most frequently applied spectra and was applied for many model tests before; thus it was used for comparability.

Long crested waves: Surface waves that are nearly two-dimensional, in that the crests appear very long in comparison with the wave length, and the energy propagation is concentrated in a narrow band around the mean wave direction. They do not exist in nature, but can be generated in the laboratory.

Oblique wave attack: Waves that strike the structure at an angle.

Perpendicular wave attack: Waves that strike the structure normally to its face.

Raleigh distribution: A Raleigh distribution is a continuous probability distribution that can be used to describe the fitting of a density function.

Reflection analysis: The reflection analysis done in frequency domain is used to determine the moments of spectral density for incident and reflected waves.

Reflection coefficient: The reflection coefficient is determined during reflection analysis and describes the intensity of a reflected wave relative to an incident wave.

Reflected wave: Waves that hit the structure and are reflected seaward with little or no breaking. The wave height and wave length decreases depending on the type of structure.

Return period: The average length of time between sea states of a given severity.

Significant wave height: The average height of the highest of one third of the waves in a given sea state.

Short crested waves: Waves that have a small extent in the direction perpendicular to the direction of propagation. Most waves in natural state are short-crested.

Spectral energy density: It describes how the energy (or variance) of a signal or a time series is distributed with frequency.

Wave run-up and wave overtopping: The run-up is the rush of water up a structure as a result of wave attack. Wave overtopping is the mean discharge of water in l/(s·m) that passes over a structure due to wave attack and should be limited to a tolerable amount.

Wave steepness: The wave steepness is defined as the ratio of wave height to wave length (H/L). It includes therefore information about the characteristic and history of the wave. Distinction can be made into swell sea (s_0 = 0.01) and wind sea (s_0 = 0.04 to 0.06).

Annex A Model set-up

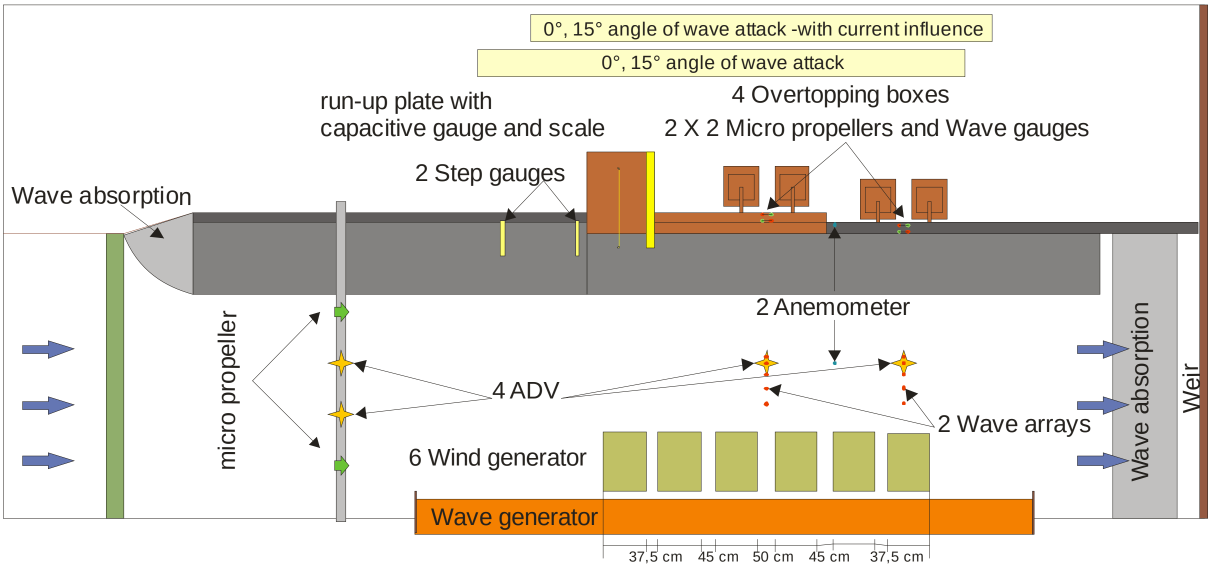

Figure-annex 1 Set-up 1 - angles of wave attack -15°,0° and +15° (1:3 sloped dike - FlowDike 1)

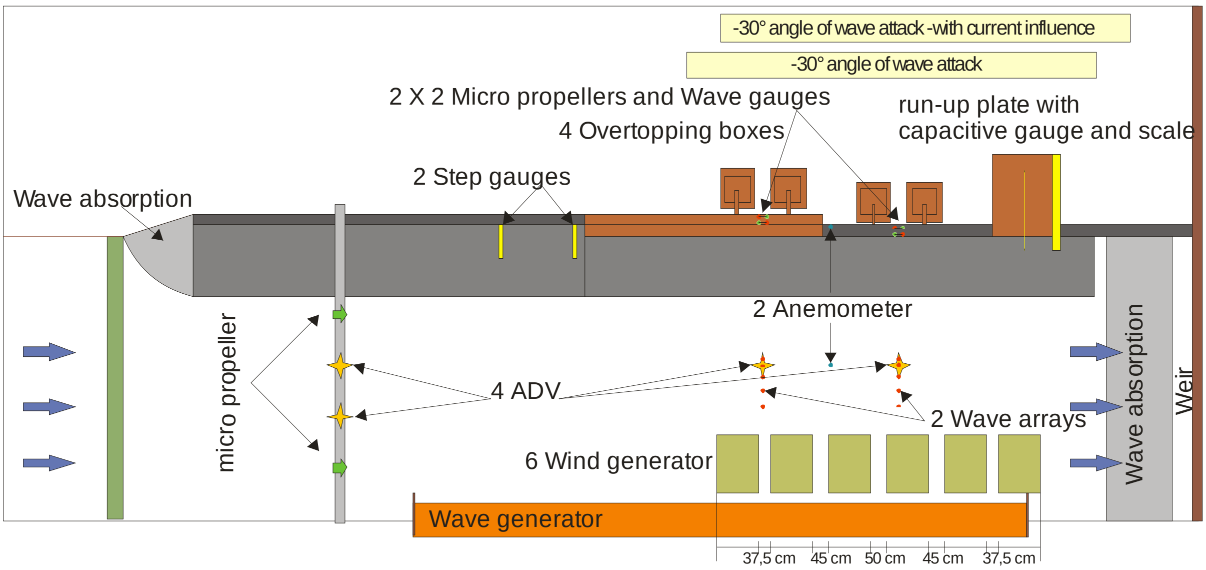

Figure-annex 2 Set-up 2 - angles of wave attack +30° (1:3 sloped dike - FlowDike 1)

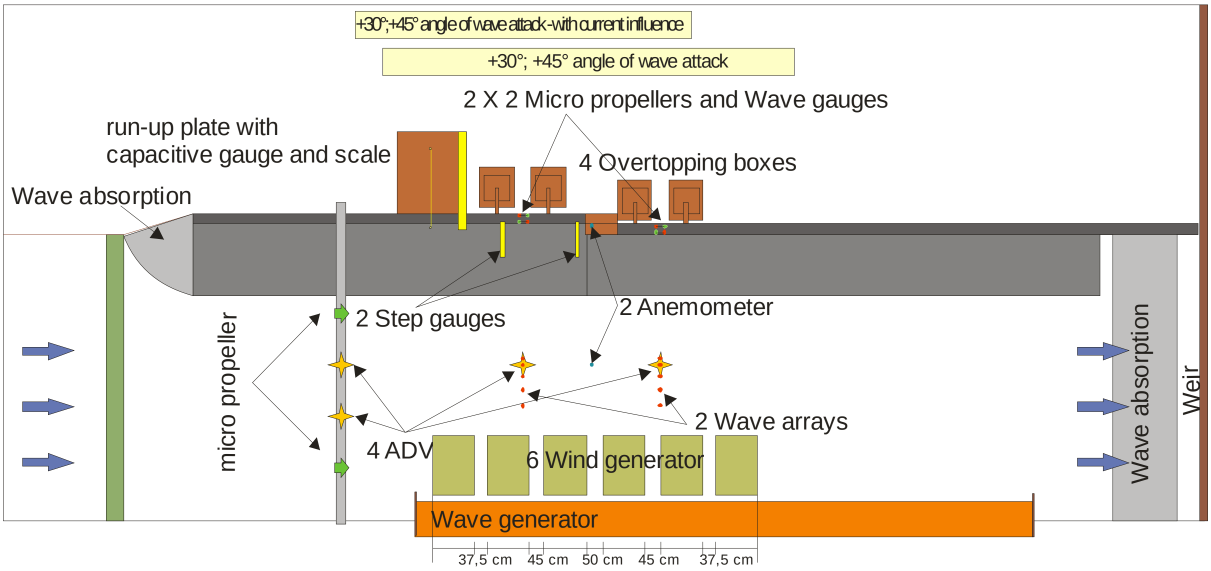

Figure-annex 3 Set-up 3 - angles of wave attack -30° and -45° (1:3 sloped dike - FlowDike 1)

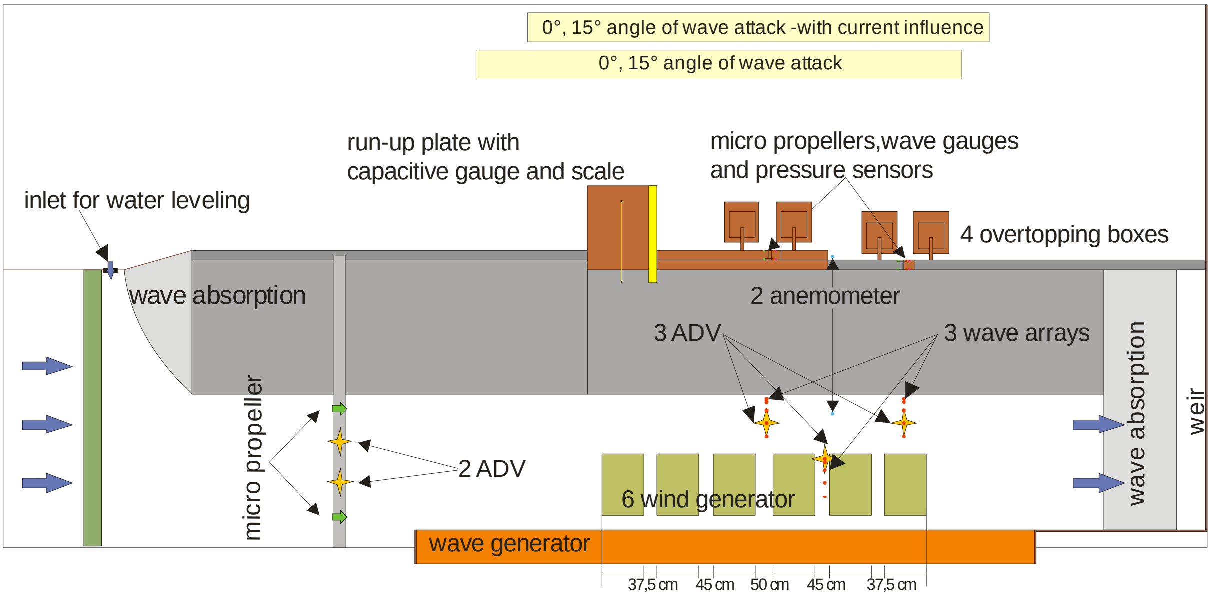

Figure-annex 4 Set-up 4 - angles of wave attack -15°, 0° and +15° (1:6 sloped dike - FlowDike 2)

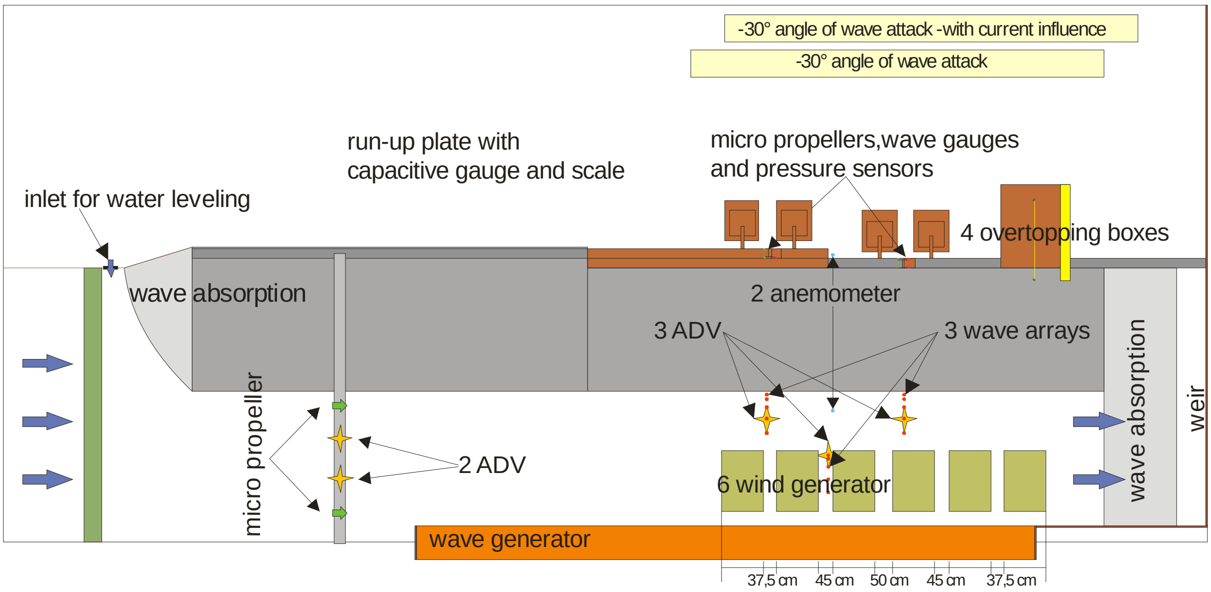

Figure-annex 5 Set-up 5 - angles of wave attack +30° (1:6 sloped dike - FlowDike 2)

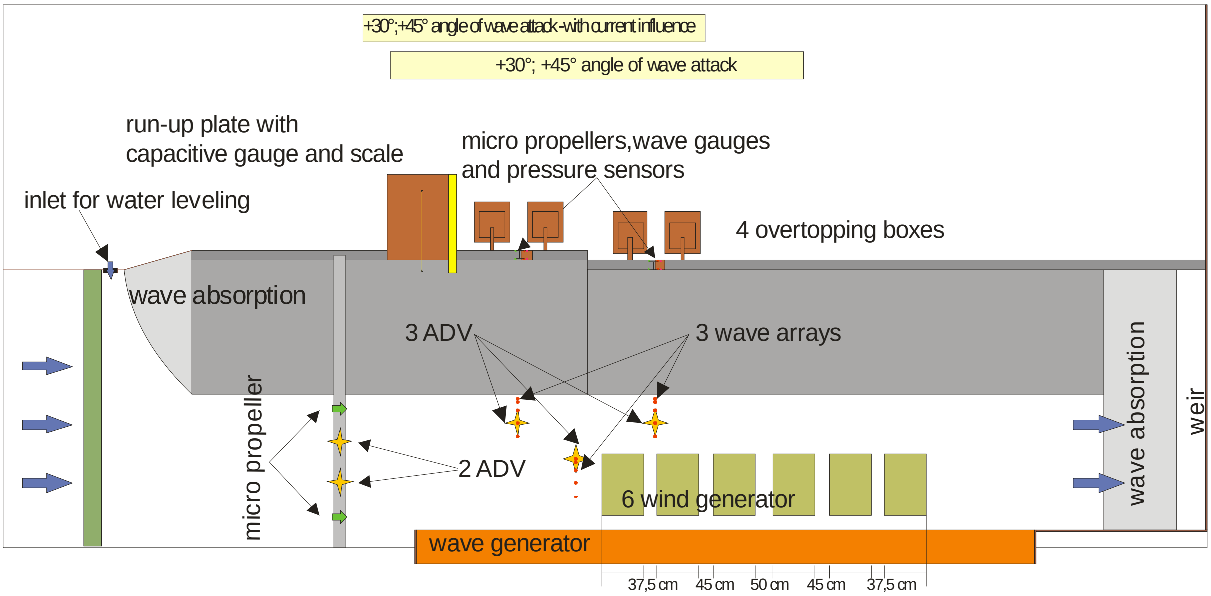

Figure-annex 6 Set-up 6 - angles of wave attack -30° and -45° (1:6 sloped dike - FlowDike 2)

Annex B Channel List - 1:3 sloped dike (FlowDike 1)

Table-annex 1 Channel list – 1:3 sloped dike (FlowDike 1)

channel number	**row in *.dfs0-file**	**item in wave syntheziser**	**Description**	**Position**	**Calibration curve**
1	2	1	air temperature		[°C]
2	3	2	water temperature		[°C]
3	4	3	air flow	behind the dike (landwardside)	50 Hz on wind generator correspond to 10 m/s 25 Hz on wind generator correspond to 5 m/s (20cm above 60 cm crest. 10 cm above 70 cm crest)
4	5	4	air flow	near ADV in front of 70 cm crest	
5	6	5	wave gauge in front of the 70 cm crest	position: 1.1 m (at dike side)	[m]
6	7	6		position: 1 m	[m]
7	8	7		position: 0.75 m	[m]
8	9	8		position: 0.4 m	[m]
9	10	9		position: 0 m (at wave machine side)	[m]
10	11	10	wave gauges in front of the 60 cm crest	position: 1.1 m (at dike side)	[m]
11	12	11		position: 1 m	[m]
12	13	12		position: 0.75 m	[m]
13	14	13		position: 0.4 m	[m]
14	15	14		position: 0 m (at wave machine side)	[m]
15	16	15	wave gauge	on landward side on the 70 cm crest	[m]
16	17	16	wave gauge	on seaward side on the 70 cm crest	[m]
17	18	17	wave gauge	on landward side on the 60 cm crest	[m]
18	19	18	wave gauge	on seaward side on the 60 cm crest	[m]
19	20	19	Vx - ADV (DHI)	near wave array in front of the 60 cm crest, wg13 (set-up 1, 2 + 3 until test 220) not used after test 220	[m/s]
20	21	20	Vy - ADV (DHI)		[m/s]
21	22	21	Vz - ADV (DHI)		[m/s]

22	23	22	Vx - SD12 (DHI)	near wave array in front of the 70 cm crest, wg5 (set-up 1, 2 + 3 until test 220) near wave array in front of the 60 cm crest, wg13 (from test 222)	[m/s]
23	24	23	Vy - SD12 (DHI)		[m/s]
25	25	24	Vx - ADV (RWTH)	in the middle of the beam (set-up 1, 2 + 3 until test 220) near wave array in front of the 70 cm crest, wg5 (from test 222)	[m/s]
26	26	25	Vy - ADV (RWTH)		[m/s]
27	27	26	Vz - ADV (RWTH)		[m/s]
28	28	27	Vx - ADV (RWTH)	in the middle of the beam	[m/s]
29	29	28	Vy - ADV (RWTH)		[m/s]
30	30	29	Vz - ADV (RWTH)		[m/s]
31	31	30	micro propeller	replaced ADV (19-21)	v = 0.8616 · signal
32	32	31	micro propeller	replaced ADV (22-24)	v = 1.09 · signal
33	33	32	micro propeller MiniWater 20	on landward side on the 70 cm crest	v = 0.8296 · signal
34	34	33	micro propeller MiniWater 20	on seaward side on the 70 cm crest	v = 0.4871 · signal
35	35	34	micro propeller MiniWater 20	on landward side on the 60 cm crest	v = 0.4687 · signal
36	36	35	micro propeller MiniWater 20	on seaward side on the 60 cm crest	v = 0.4913 · signal
37	37	36	load cell Vz	of the overtopping-box behind 70 cm crest, upstream	[kg]
38	38	37	wavegauge	in the overtopping-box behind 70 cm crest, upstream	[m]
39	39	38	load cell Vz	of the overtopping-box behind 70 cm crest, downstream	[kg]
40	40	39	wavegauge	in the overtopping-box behind 70 cm crest, downstream	[m]
41	41	40	load cell Vz	of the overtopping-box behind 60 cm crest, upstream	[kg]
42	42	41	wavegauge	in the overtopping-box behind 60 cm crest, upstream	[m]
43	43	42	load cell Vz	of the overtopping-box behind 60 cm crest, downstream	[kg]
44	44	43	wavegauge	in the overtopping-box behind 60 cm crest, downstream	[m]
45	45	44	pump	in the overtopping-box behind 70 cm crest, upstream (lc37)	q = 1.7845 * signal [l/s]
46	46	45	pump	in the overtopping-box behind 70 cm crest, downstream (lc39)	q = 1.401 * signal [l/s]
47	47	46	pump	in the overtopping-box behind 60 cm crest, upstream (lc41)	q = 1.5942 * signal [l/s]
48	48	47	pump	in the overtopping-box behind 60 cm crest, downstream (lc43)	q = 1.5943 * signal [l/s]

49	49	48	capacitive-gauge	on the run-up-board	set-up1: R = 0.3748 · signal + 0.1679 set-up1: R = 0.3674 · signal - 0.171 set-up1: R = 0.3708 · signal + 0.1647 R given in [m above water level]
50	50	49	pump	in the deep basin (to induce the flow)	
53	51	50	stepgauge	stepgauge at 50 m; 2 m (upstream)	
54	52	51	stepgauge		
55	53	52	stepgauge		
56	54	53	stepgauge		
57	55	54	stepgauge	stepgauge at 50 m; 2 m (downstream)	
58	56	55	stepgauge		
59	57	56	stepgauge		
60	58	57	stepgauge		

Annex C Channel list – 1:6 sloped dike (FlowDike 2)

Table-annex 2 Channel list – 1:3 sloped dike (FlowDike 1)

channel number	**row in *.dfs0-file**	**item in wave synthesizer**	**Description**	**Position**	**Calibration curve** **Unit**
1	2	1	water temperature		[°C]
2	3	2	air temperature		[°C]
3	4	3	air flow	behind dike	50 Hz on wind generator correspond to 10 m/s 25 Hz on wind generator correspond to 5 m/s (20cm above 60 cm crest. 10 cm above 70 cm crest)
4	5	4	air flow	near ADV in front of 70 cm crest	
5	6	5	wave gauges 50 cm away from wave generator	position: 1.1 m (at dike side)	[m]
6	7	6		position: 1 m	[m]
7	8	7		position: 0.75 m	[m]
8	9	8		position: 0.4 m	[m]
9	10	9		position: 0 m (at wave generator side)	[m]
10	11	10	wave gauges in front of the 60 cm crest	position: 1.1 m (at toe of the dike)	[m]
11	12	11		position: 1 m	[m]
12	13	12		position: 0.75 m	[m]
13	14	13		position: 0.4 m	[m]
14	15	14		position: 0 m (at wave generator side)	[m]
15	16	15	wave gauge	on landward side on the 70 cm crest	[m]
16	17	16	wave gauge	on seaward side on the 70 cm crest	[m]
17	18	17	wave gauge	on landward side on the 60 cm crest	[m]
18	19	18	wave gauge	on seaward side on the 60 cm crest	[m]
19	20	19	Vx - ADV (DHI)	near wave array in front of the 70 cm crest	[m/s]
20	21	20	Vy - ADV (DHI)		[m/s]
21	22	21	Vz - ADV (DHI)		[m/s]
22	23	22	Vx - SD-12 (DHI)	near wave array in front of the 70 cm crest	[m/s]

23	24	23	Vy - SD-12 (DHI)		[m/s]
24	25	24	Vz - SD-12 (DHI)		[m/s]
25	26	25	Vx - ADV (RWTH)	in the middle of the beam	[m/s]
26	27	26	Vy - ADV (RWTH)		[m/s]
27	28	27	Vz - ADV (RWTH)		[m/s]
28	29	28	Vx - ADV (RWTH)	in the middle of the beam	[m/s]
29	30	29	Vy - ADV (RWTH)		[m/s]
30	31	30	Vz - ADV (RWTH)		[m/s]
31	32	31	micro propeller	replaced ADV (19-21)	v = 0.8616 · signal [m/s]
32	33	32	micro propeller	replaced ADV (22-24)	v = 1.09 · signal [m/s]
33	34	33	micro propeller MiniWater 20	on seaward side on the 70 cm crest	v = 0.1932 · signal [m/s]
34	35	34	micro propeller MiniWater 20	on landward side on the 70 cm crest	v = 0.1518 · signal [m/s]
35	36	35	micro propeller MiniWater 20	on seaward side on the 60 cm crest	v = 0.2347 · signal [m/s]
36	37	36	micro propeller MiniWater 20	on landward side on the 60 cm crest	v = 0.1625 · signal [m/s]
37	38	37	load cell Vz	of the overtopping-box behind 70 cm crest, upstream	[kg]
38	39	38	wavegauge	in the overtopping-box behind 70 cm crest, upstream	[m]
39	40	39	load cell Vz	of the overtopping-box behind 70 cm crest, downstream	[kg]
40	41	40	wavegauge	in the overtopping-box behind 70 cm crest, downstream	[m]
41	42	41	load cell Vz	of the overtopping-box behind 60 cm crest, upstream	[kg]
42	43	42	wavegauge	in the overtopping-box behind 60 cm crest, upstream	[m]
43	44	43	load cell Vz	of the overtopping-box behind 60 cm crest, downstream	[kg]
44	45	44	wavegauge	in the overtopping-box behind 60 cm crest, downstream	[m]
45	46	45	pump	in the overtopping-box behind 70 cm crest, upstream	q = 1.73347 * signal [l/s]
46	47	46	pump	in the overtopping-box behind 70 cm crest, downstream	q = 1.59961 * signal [l/s]
47	48	47	pump	in the overtopping-box behind 60 cm crest, upstream	q = 1.67989 * signal [l/s]
48	49	48	pump	in the overtopping-box behind 60 cm crest, downstream	q = 1.74557 * signal [l/s]
49	50	49	capacitive-gauge	on the run-up-board	R given in [m above water level]

50	51	50	pump	in the deep basin (to induce the flow)	
51	52	51	wave gauges in front of the 70 cm crest	position: 1.1 m (at toe of the dike)	[m]
52	53	52		position: 1 m	[m]
53	54	53		position: 0.75 m	[m]
54	55	54		position: 0.4 m	[m]
55	56	55		position: 0 m (at wave generator side)	[m]
56	57	56	wave gauge	slope on 60 cm crest	[m]
57	58	57	wave gauge	slope on 70 cm crest	[m]
58	59	58	pressure sensor	on seaward side on the 70 cm crest	[m]
59	60	59	pressure sensor	on landward side on the 70 cm crest	[m]
60	61	60	pressure sensor	on seaward side on the 60 cm crest	[m]
61	62	61	pressure sensor	on landward side on the 60 cm crest	[m]
62	63	62	Vx vectrino		[m/s]
63	64	63	Vy vectrino		[m/s]
64	65	64	Vz vectrino		[m/s]

Annex D Wave conditions – Jonswap spectrum

Table-annex 3 Wave parameters, **flow depth d= 0.50 m, wave characteristics I** (1:3 sloped dike)

wave spectra	Hs [m]	Tp [s]	$T_{m-1,0} = \frac{T_p}{1.1}$ [s]	$L_{m-1,0} = \frac{g \cdot T_{m-1,0}}{2\pi} \cdot \tanh\left(\frac{2\pi}{L_{m-1,0}} \cdot d\right)$ [m]	steepness $s_{m-1,0} = \frac{H_s}{L_{m-1,0}}$ [-]	duration for 1000 waves [min]
w1	0.07	1.474	1.340	2.416	0.029	25
w2	0.07	1.045	0.950	1.379	0.051	18
w3	0.10	1.76	1.600	3.078	0.032	30
w4	0.10	1.243	1.130	1.862	0.054	21
w5	0.15	2.156	1.960	3.960	0.038	36
w6	0.15	1.529	1.390	2.545	0.059	26

Table-annex 4 Wave parameters, **flow depth d = 0.50 m, wave characteristics II** (1:3 and 1:6 sloped dike)

wave spectra	Hs [m]	Tp [s]	$T_{m-1,0} = \frac{T_p}{1.1}$ [s]	$L_{m-1,0} = \frac{g \cdot T_{m-1,0}}{2\pi} \cdot \tanh\left(\frac{2\pi}{L_{m-1,0}} \cdot d\right)$ [m]	steepness $s_{m-1,0} = \frac{H_s}{L_{m-1,0}}$ [-]	duration for 1000 waves [min]
w1	0.09	1.670	1.518	2.873	0.031	28
w2	0.09	1.181	1.074	1.710	0.053	20
w3	0.12	1.929	1.754	3.459	0.035	33
w4	0.12	1.364	1.240	2.154	0.056	23
w5	0.15	2.156	1.960	3.960	0.038	36
w6	0.15	1.525	1.386	2.535	0.059	26

Table-annex 5 Wave parameters, **flow depth d = 0.55 m wave characteristics I** (1:3 and 1:6 sloped dike)

wave spectra	Hs [m]	Tp [s]	$T_{m-1,0} = \frac{T_p}{1.1}$ [s]	$L_{m-1,0} = \frac{g \cdot T_{m-1,0}}{2\pi} \cdot \tanh\left(\frac{2\pi}{L_{m-1,0}} \cdot d\right)$ [m]	steepness $s_{m-1,0} = \frac{H_s}{L_{m-1,0}}$ [-]	duration for 1000 waves [min]
w1	0.07	1.474	1.340	2.478	0.028	25
w2	0.07	1.045	0.950	1.390	0.050	18
w3	0.10	1.76	1.600	3.180	0.031	30
w4	0.10	1.243	1.130	1.893	0.053	21
w5	0.15	2.156	1.960	4.113	0.036	36
w6	0.15	1.529	1.390	2.614	0.057	26

Table-annex 6 Wave parameters, **flow depth d = 0.55 m wave characteristics II** (1:6 sloped dike)

wave spectra	Hs [m]	Tp [s]	$T_{m-1,0} = \frac{T_p}{1.1}$ [s]	$L_{m-1,0} = \frac{g \cdot T_{m-1,0}}{2\pi} \cdot \tanh\left(\frac{2\pi}{L_{m-1,0}} \cdot d\right)$ [m]	steepness $s_{m-1,0} = \frac{H_s}{L_{m-1,0}}$ [-]	duration for 1000 waves [min]
w1	0.09	1.670	1.518	2.962	0.030	28
w2	0.09	1.181	1.074	1.734	0.052	20
w3	0.12	1.929	1.754	3.581	0.033	33
w4	0.12	1.364	1.240	2.201	0.055	23
w5	0.15	2.156	1.960	4.113	0.036	36
w6	0.15	1.525	1.386	2.605	0.058	26

Annex E Test program - 1:3 sloped dike (FlowDike 1)

Table-annex 7 Test program - 1:3 sloped dike, flow depth d = 0.50 m, wave characteristic I

testseries name	experiment date	wave direction [°] (+with current; - against current)	current [m/s]	wind speed [m/s]	wave spectra and its test number
s1_03_30_wi_00_00	02.02.09	0	0.30	0	w1 to w6 114, 115, 116, 117, 119, 120
s1_08_30_wi_49_00	03.02.09	0	0.30	10	w1, w3, w5 121, 122, 123
s1_19_30_wi_00_15m	03.02.09	+15	0.30	0	w1 to w6 124, 125, 126, 127, 128, 129
s1_16_30_wi_00_15p	04.02.09	-15	0.30	0	w1 to w6 131, 132, 133, 134, 135, 136
s1_08b_30_wi_25_00	04.02.09	0	0.30	5	w1, w3, w5 137, 138, 140
s1_01_00_wi_00_00	05.02.09	0	0.00	0	w1 to w6 144, 145, 146, 147, 148, 149
s1_06b_00_wi_25_00	05.02.09	0	0.00	5	w1, w3, w5 150, 151, 152
s1_06_00_wi_49_00	05.02.09	0	0.00	10	w1, w3, w5 153, 154, 155
s1_12_00_wi_00_15m	06.02.09	+15	0.00	0	w1 to w6 156, 157, 158, 159, 160, 161
s1_11_15_wi_00_00	06.02.09	0	0.15	0	w1 to w6 162, 163, 164, 165, 166, 167
s1_13_15_wi_00_15m	09.02.09	+15	0.15	0	w1 to w6 168, 169, 170
s1_15_15_wi_00_15p	09.02.09	-15	0.15	0	w1 to w6 174, 175, 176, 177, 178, 179
s2_02_00_wi_00_30m	11.02.09	+30	0.00	0	w1 to w6 180, 181, 182, 183, 184, 185
s2_07b_00_wi_25_30m	11.02.09	+30	0.00	5	w1, w3, w5 186, 187, 188
s2_07_00_wi_49_30m	11.02.09	+30	0.00	10	w1, w3, w5 189, 190, 191
s2_20_15_wi_00_30m	12.02.09	+30	0.15	0	w1 to w6 192, 193, 194, 195, 196, 197
s2_04_30_wi_00_30m	12.02.09	+30	0.30	0	w1 to w6 202, 203, 204, 205, 206, 207
s2_09b_30_wi_25_30m	13.02.09	+30	0.30	5	w1, w3, w5 208, 209, 210
s2_09_30_wi_49_30m	13.02.09	+30	0.30	10	w1, w3, w5 211, 212, 213
s3_18_00_wi_00_45p	17.02.09	-45	0.00	0	w1 to w5 215, 216, 217, 218, 220
s3_05_30_wi_00_30p	18.02.09	-30	0.30	0	w1 to w6 222, 223, 224, 225, 226, 227
s3_14_30_wi_00_45p	18.02.09	-45	0.30	0	w1 to w6 228, 229, 230, 231, 232, 233
s3_21_15_wi_00_30p	19.02.09	-30	0.15	0	w1 to w6 234, 235, 236, 237, 238, 239
s3_17_15_wi_00_45p	19.02.09	-45	0.15	0	w1 to w6 240, 241, 242, 243, 244, 245

Annex F Test program - 1:6 sloped dike (FlowDike 2)

Table-annex 8 Test program - 1:6 sloped dike

testseries name	experiment date	flow depth [m]	wave characteristic	wave direction [°] (+with current; - against current)	current [m/s]	wind speed [m/s]	wave spectra and its test number (wave condition wc I or wave condition wc II)
s4_01_00_wi_00_00	09_11_19	0.50	wc I	0	0	0	w1 to w6 425, 427, 426, 428, 429, 430
s4_01a_00_wi_00_00	09_11_23+24	0.55	wc II	0	0	0	w1 to w6 451, 452, 453, 454, 456, 457
s4_02_00_wi_25_00	09_11_18+19	0.50	wc I	0	0	5	w1, w3, w5 418, 419, 421
s4_03_00_wi_49_00	09_11_19	0.50	wc I	0	0	10	w1, w3, w5 422, 423, 424
s4_03a_00_wi_49_00	09_11_25	0.55	wc II	0	0	10	w1, w3, w5 464, 465, 466,
s4_04_30_wi_00_00	09_11_17	0.50	wc I	0	0.30	0	w1 to w6 411, 410, 409, 408, 407, 406
s4_04a_30_wi_00_00	09_11_25	0.55	wc II	0	0.30	0	w1 to w6 458, 459, 460, 461, 462, 463
s4_05_30_wi_49_00	09_11_18	0.55	wc II	0	0.30	10	w1, w3, w5 412, 413, 414
s4_06_30_wi_25_00	09_11_18	0.50	wc I	0	0.30	5	w1, w3, w5 415, 416, 417
s4_07_15_wi_00_00	09_11_26	0.55	wc II	0	0.15	0	w1 to w6 467, 468, 469, 470, 471, 472
s4_08_15_wi_49_00	09_11_26	0.55	wc II	0	0.15	10	w1, w3, w5 473, 474, 475
s4_10_40_wi_00_00	09_11_27	0.55	wc II	0	0.40	0	w1 to w6 480, 481, 482, 483, 484, 485
s4_11_40_wi_49_00	09_11_27	0.55	wc II	0	0.40	10	w1, w3, w5 488, 489, 490

testseries name	experiment date	flow depth [m]	wave characteristic	wave direction [°] (+with current; - against current)	current [m/s]	wind speed [m/s]	wave spectra and its test number (wave condition wc I or wave condition wc II)
s4_32_30_wi_00_15m	09_11_20	0.50	wc I	+15	0.30	0	w1 to w6 432, 433, 434, 435, 437, 438
s4_33_30_wi_00_15p	09_11_20	0.50	wc I	-15	0.30	0	w1 to w6 440, 441, 442, 443
s4_34_00_wi_00_15m	09_11_23	0.55	wc II	+15	0.00	0	w1 to w6 444, 445, 447, 448, 449, 450
s4_35_15_wi_00_00	09_11_26	0.55	wc I	0	0.15	0	w1, w2 476, 477
s4_36_40_wi_00_00	09_11_27	0.55	wc I	0	0.40	0	w1, w2 486, 487
s5_13_00_wi_00_30m	09_12_01+02+03	0.55	wc II	+30	0.00	0	w1 to w6 511, 512, 513, 517, 515, 516
s5_15_00_wi_49_30m	09_12_03	0.55	wc II	+30	0.00	10	w1, w3, w5 536, 537, 538
s5_16_40_wi_00_30m	09_12_01	0.55	wc II	+30	0.40	0	w1 to w6 501, 502, 503, 504, 505, 506
s5_17_40_wi_49_30m	09_12_01	0.55	wc II	+30	0.40	10	w1, w3, w5 508, 509, 510
s5_19_30_wi_00_30m	09_12_02	0.55	wc II	+30	0.30	0	w1 to w6 517, 518, 519, 520, 521, 522
s5_20_30_wi_49_30m	09_12_02	0.55	wc II	+30	0.30	10	w1, w3, w5 523, 524, 525
s5_22_15_wi_00_30m	09_12_03	0.55	wc II	+30	0.15	0	w1 to w6 530, 531, 532, 533, 534, 535
s6_25_00_wi_00_45p	09_12_08+09	0.55	wc II	-45	0.00	0	w1 to w6 613, 614, 615, 616, 617, 618
s6_26_15_wi_00_30p	09_12_07+08	0.55	wc II	-30	0.15	0	w1 to w6 607, 608, 609, 610, 611, 612
s6_27_15_wi_00_45p	09_12_07	0.55	wc II	-45	0.15	0	w1 to w6 601, 602, 603, 604, 605, 606
s6_28_30_wi_00_30p	09_12_08+09	0.55	wc II	-30	0.30	0	w1 to w6 625, 626, 627, 628, 629, 630

testseries name	**experiment date**	**flow depth [m]**	**wave characteristic**	**wave direction [°] (+with current; - against current)**	**current [m/s]**	**wind speed [m/s]**	**wave spectra and its test number (wave condition wc I or wave condition wc II)**
s6_29_30_wi_00_45p	09_12_08	0.55	wc II	-45	0.30	0	w1 to w6 619, 620, 621, 622, 623, 624
s6_30_40_wi_00_30p	09_12_10	0.55	wc II	-30	0.40	0	w1 to w6 637, 638, 639, 640, 641, 642
s6_31_40_wi_00_45p	09_12_09+10	0.55	wc II	-45	0.40	0	w1 to w6 631, 632, 633, 634, 635, 636

Annex G Calibration function - Micro propeller

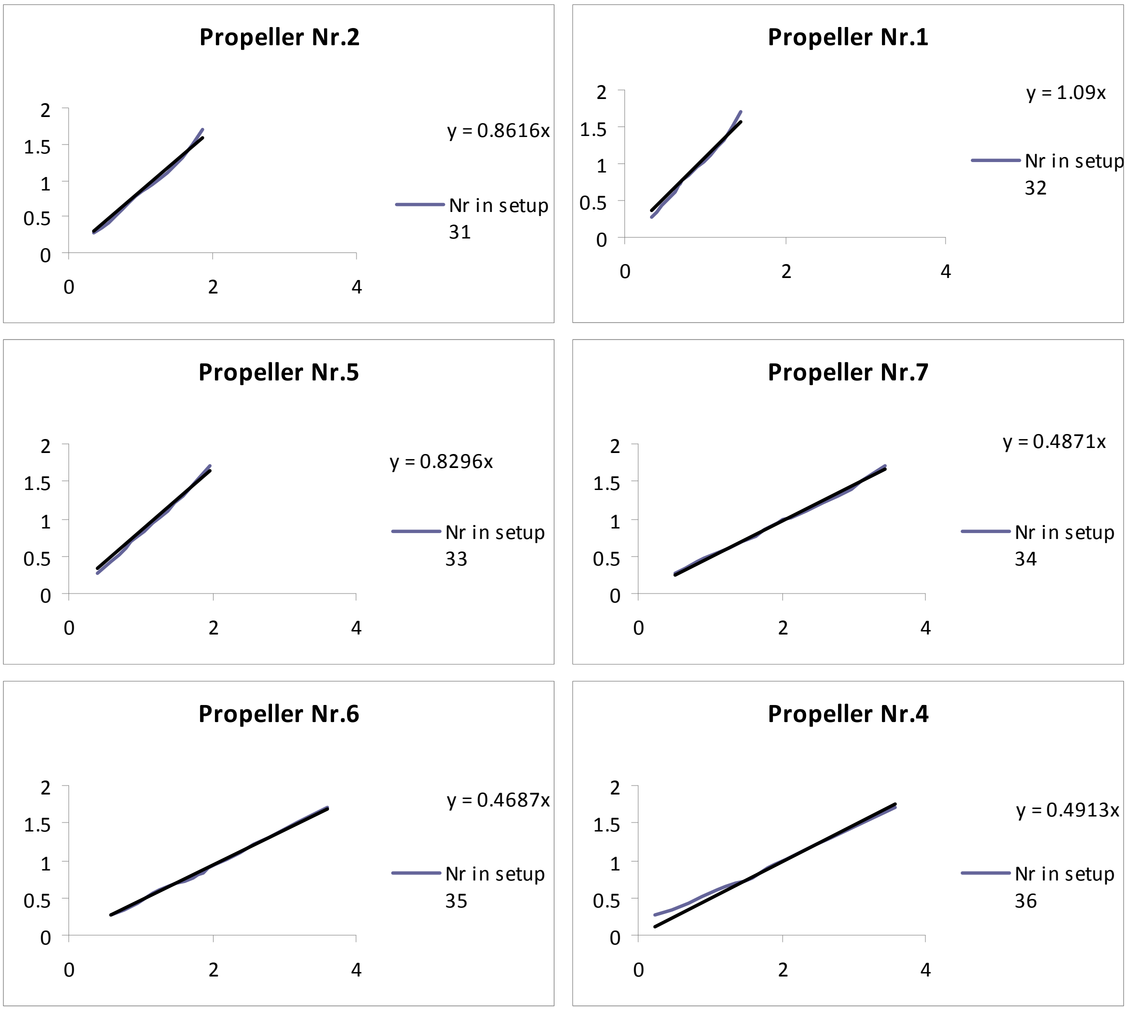

Figure annex 7 Calibration curves for micro propeller from TU Braunschweig

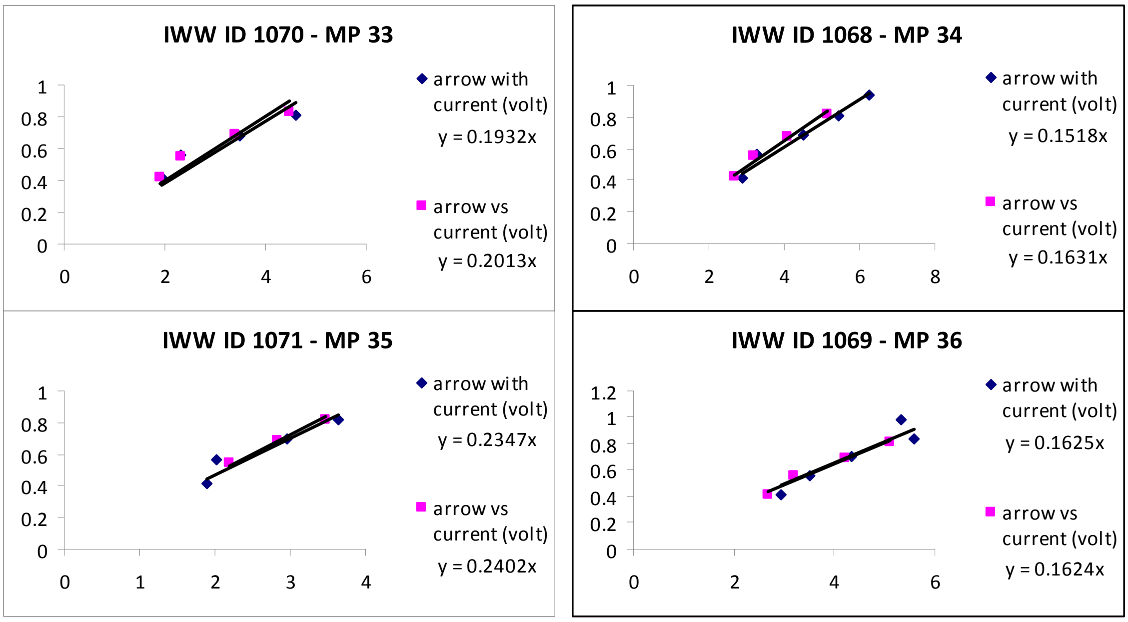

Figure-annex 8 Calibration curves for micro propeller of RWTH Aachen

Annex H Analyzed data - wave field – 1:3 sloped dike

Table-annex 9 Test program - 1:3 sloped dike, flow depth d = 0.50 m, wave characetristics I (wc I)

test-number	testseries name	at toe of 60 cm dike			at toe of 70 cm dike		
		H_{m0} [m]	T_p [s]	$T_{m-1,0}$ [s]	H_{m0} [m]	T_p [s]	$T_{m-1,0}$ [s]
144	s1_01_00_w1_00_00	0.0706	1.4629	1.3494	0.0680	1.4629	1.3271
145	s1_01_00_w2_00_00	0.0588	1.0503	1.0196	0.0649	1.0779	1.0116
198	s1_01_00_w3_00_00	0.1004	1.7809	1.5990	0.0950	1.7809	1.5762
199	s1_01_00_w4_00_00	0.0920	1.2800	1.1639	0.0945	1.2047	1.1451
200	s1_01_00_w5_00_00	0.1476	2.1558	1.8882	0.1399	2.1558	1.8722
201	s1_01_00_w6_00_00	0.1449	1.5170	1.4384	0.1407	1.5170	1.4148
114	s1_03_30_w1_00_00	0.0509	1.1703	1.0392	0.0538	1.1378	1.0333
115	s1_03_30_w2_00_00	0.0466	0.7877	0.7858	0.0493	0.7877	0.7870
116	s1_03_30_w3_00_00	0.0966	1.6384	1.4261	0.1043	1.5754	1.4287
117	s1_03_30_w4_00_00	0.1006	1.1703	1.0643	0.1038	1.1378	1.0574
119	s1_03_30_w5_00_00	0.1416	2.1558	1.8873	0.1409	2.1558	1.8584
120	s1_03_30_w6_00_00	0.1310	1.5170	1.4075	0.1394	1.5170	1.4055
153	s1_06_00_w1_49_00	0.0690	1.4629	1.3615	0.0672	1.4629	1.3335
154	s1_06_00_w3_49_00	0.0985	1.7809	1.6052	0.0936	1.7809	1.5757
155	s1_06_00_w5_49_00	0.1440	2.1558	1.8885	0.1348	2.1558	1.8709
150	s1_06b_00_w1_25_00	0.0693	1.4629	1.3583	0.0676	1.4629	1.3319
151	s1_06b_00_w3_25_00	0.0994	1.7809	1.6019	0.0940	1.7809	1.5737
152	s1_06b_00_w5_25_00	0.1467	2.1558	1.8893	0.1363	2.1558	1.8737
121	s1_08_30_w1_49_00	0.0496	1.2412	1.1161	0.0502	1.2412	1.1084
122	s1_08_30_w3_49_00	0.0929	1.7809	1.5663	0.0939	1.7809	1.5493
123	s1_08_30_w5_49_00	0.1447	2.1558	1.9173	0.1423	2.1558	1.8792
137	s1_08b_30_w1_25_00	0.0640	1.5170	1.2977	0.0684	1.4629	1.3118
138	s1_08b_30_w3_25_00	0.0947	1.7067	1.5782	0.0958	1.7809	1.5644

test-number	testseries name	at toe of 60 cm dike			at toe of 70 cm dike		
		H_{m0} [m]	T_p [s]	$T_{m-1,0}$ [s]	H_{m0} [m]	T_p [s]	$T_{m-1,0}$ [s]
140	s1_08b_30_w5_25_00	0.1404	2.1558	1.9110	0.1402	2.1558	1.8689
162	s1_11_15_w1_00_00	0.0651	1.4629	1.3187	0.0671	1.4124	1.3084
163	s1_11_15_w2_00_00	0.0663	1.0503	1.0152	0.0650	1.0240	1.0048
164	s1_11_15_w3_00_00	0.0997	1.7809	1.5933	0.0962	1.7809	1.5732
165	s1_11_15_w4_00_00	0.0907	1.2047	1.1270	0.0982	1.2800	1.1477
166	s1_11_15_w5_00_00	0.1509	2.1558	1.9067	0.1435	2.1558	1.8659
167	s1_11_15_w6_00_00	0.1395	1.5170	1.4266	0.1367	1.5170	1.4036
156	s1_12_00_w1_00_15m	0.0670	1.4629	1.2898	0.0747	1.4629	1.3191
157	s1_12_00_w2_00_15m	0.0728	1.0503	0.9865	0.0722	1.0240	0.9762
158	s1_12_00_w3_00_15m	0.0884	1.7067	1.4861	0.0960	1.7067	1.5004
159	s1_12_00_w4_00_15m	0.1008	1.2047	1.1361	0.0992	1.2412	1.1449
160	s1_12_00_w5_00_15m	0.1365	2.1558	1.8386	0.1332	2.1558	1.7817
161	s1_12_00_w6_00_15m	0.1343	1.5170	1.3844	0.1473	1.5170	1.4134
168	s1_13_15_w1_00_15m	0.0707	1.4124	1.3041	0.0692	1.4124	1.2971
169	s1_13_15_w2_00_15m	0.0697	1.0240	0.9793	0.0716	1.0503	0.9859
170	s1_13_15_w3_00_15m	0.0914	1.7067	1.4941	0.0931	1.7809	1.4929
171	s1_13_15_w4_00_15m	0.1037	1.2412	1.1520	0.1032	1.2412	1.1451
172	s1_13_15_w5_00_15m	0.1321	2.1558	1.7970	0.1273	2.1558	1.7801
173	s1_13_15_w6_00_15m	0.1412	1.5170	1.3935	0.1386	1.5754	1.3867
174	s1_15_15_w1_00_15p	0.0785	1.4629	1.3372	0.0713	1.4629	1.3118
175	s1_15_15_w2_00_15p	0.0710	1.0503	0.9988	0.0715	1.0503	0.9852
176	s1_15_15_w3_00_15p	0.1036	1.7809	1.5226	0.0940	1.7809	1.5084
177	s1_15_15_w4_00_15p	0.1074	1.2412	1.1698	0.0989	1.2800	1.1567
178	s1_15_15_w5_00_15p	0.1409	2.1558	1.7860	0.1323	2.1558	1.8015
179	s1_15_15_w6_00_15p	0.1525	1.5170	1.4042	0.1402	1.5170	1.4046
131	s1_16_30_w1_00_15p	0.0762	1.4629	1.3510	0.0706	1.5170	1.3333
132	s1_16_30_w2_00_15p	0.0692	1.0240	0.9893	0.0692	1.0240	0.9908

test-number	testseries name	at toe of 60 cm dike			at toe of 70 cm dike		
		H_{m0} [m]	T_p [s]	$T_{m-1,0}$ [s]	H_{m0} [m]	T_p [s]	$T_{m-1,0}$ [s]
133	s1_16_30_w3_00_15p	0.1068	1.7067	1.5540	0.0988	1.7067	1.5314
134	s1_16_30_w4_00_15p	0.0994	1.2412	1.1787	0.0972	1.2412	1.1655
135	s1_16_30_w5_00_15p	0.1474	2.1558	1.8346	0.1322	2.1558	1.8088
136	s1_16_30_w6_00_15p	0.1541	1.5170	1.4370	0.1465	1.5170	1.4381
124	s1_19_30_w1_00_15m	0.0710	1.5170	1.3281	0.0663	1.4629	1.2914
125	s1_19_30_w2_00_15m	0.0691	1.0240	0.9787	0.0696	1.0503	0.9855
126	s1_19_30_w3_00_15m	0.0948	1.7067	1.5225	0.0908	1.7809	1.5114
127	s1_19_30_w4_00_15m	0.0941	1.1703	1.1437	0.0958	1.2412	1.1380
128	s1_19_30_w5_00_15m	0.1234	2.0480	1.7655	0.1267	2.1558	1.7962
129	s1_19_30_w6_00_15m	0.1449	1.5170	1.4161	0.1322	1.5170	1.3897
180	s2_02_00_w1_00_30m	0.0810	1.4629	1.3234	0.0768	1.4629	1.3028
181	s2_02_00_w2_00_30m	0.0785	1.0503	0.9915	0.0805	0.9990	0.9895
182	s2_02_00_w3_00_30m	0.1077	1.7067	1.5331	0.1074	1.7809	1.5711
183	s2_02_00_w4_00_30m	0.1091	1.2800	1.1701	0.1112	1.2412	1.1571
184	s2_02_00_w5_00_30m	0.1444	2.0480	1.8459	0.1590	2.1558	1.8861
185	s2_02_00_w6_00_30m	0.1554	1.5170	1.4432	0.1635	1.5170	1.4158
202	s2_04_30_w1_00_30m	0.0717	1.4124	1.3305	0.0808	1.4629	1.3393
203	s2_04_30_w2_00_30m	0.0720	1.0240	1.0121	0.0743	1.0779	1.0389
204	s2_04_30_w3_00_30m	0.1056	1.7809	1.5945	0.1089	1.7067	1.5529
205	s2_04_30_w4_00_30m	0.1040	1.2800	1.1743	0.1114	1.2800	1.1972
206	s2_04_30_w5_00_30m	0.1527	2.1558	1.8652	0.1463	2.1558	1.8172
207	s2_04_30_w6_00_30m	0.1498	1.4629	1.4344	0.1556	1.4629	1.4273
189	s2_07_00_w1_49_30m	0.0808	1.4629	1.3274	0.0743	1.4629	1.3177
190	s2_07_00_w3_49_30m	0.1066	1.7067	1.5336	0.1054	1.7809	1.5813
191	s2_07_00_w5_49_30m	0.1418	2.0480	1.8460	0.1553	2.1558	1.8883
186	s2_07b_00_w1_25_30m	0.0807	1.4629	1.3233	0.0752	1.4629	1.3070
187	s2_07b_00_w3_25_30m	0.1069	1.7067	1.5317	0.1062	1.7809	1.5760

test-number	testseries name	at toe of 60 cm dike			at toe of 70 cm dike		
		H_{m0} [m]	T_p [s]	$T_{m-1,0}$ [s]	H_{m0} [m]	T_p [s]	$T_{m-1,0}$ [s]
188	s2_07b_00_w5_25_30m	0.1435	2.0480	1.8450	0.1576	2.1558	1.8871
211	s2_09_30_w1_49_30m	0.0714	1.4124	1.3344	0.0811	1.4629	1.3417
212	s2_09_30_w3_49_30m	0.1055	1.7809	1.6022	0.1092	1.7067	1.5555
213	s2_09_30_w5_49_30m	0.1513	2.1558	1.8688	0.1463	2.1558	1.8159
208	s2_09b_30_w1_25_30m	0.0720	1.4124	1.3317	0.0812	1.4629	1.3413
209	s2_09b_30_w3_25_30m	0.1058	1.7809	1.5978	0.1095	1.7067	1.5553
210	s2_09b_30_w5_25_30m	0.1519	2.1558	1.8654	0.1469	2.1558	1.8170
192	s2_20_15_w1_00_30m	0.0702	1.5170	1.3020	0.0832	1.5170	1.3265
193	s2_20_15_w2_00_30m	0.0790	1.0503	0.9998	0.0811	1.0779	1.0158
194	s2_20_15_w3_00_30m	0.1057	1.7809	1.5705	0.1147	1.7067	1.5430
195	s2_20_15_w4_00_30m	0.1078	1.2412	1.1530	0.1198	1.2047	1.1768
196	s2_20_15_w5_00_30m	0.1482	2.1558	1.8706	0.1580	2.1558	1.8391
197	s2_20_15_w6_00_30m	0.1487	1.5754	1.4374	0.1662	1.5170	1.4182
222	s3_05_30_w1_00_30p	0.0764	1.4629	1.3276	0.0707	1.4124	1.3361
223	s3_05_30_w2_00_30p	0.0748	1.0240	1.0217	0.0723	0.9990	1.0260
224	s3_05_30_w3_00_30p	0.1034	1.7809	1.5310	0.0999	1.7809	1.5597
225	s3_05_30_w4_00_30p	0.1045	1.2800	1.1906	0.0989	1.2047	1.1966
226	s3_05_30_w5_00_30p	0.1460	2.1558	1.8330	0.1550	2.1558	1.8948
227	s3_05_30_w6_00_30p	0.1514	1.5170	1.4638	0.1416	1.5170	1.4998
228	s3_14_30_w1_00_45p	0.0877	1.4124	1.3469	0.0962	1.3653	1.3540
229	s3_14_30_w2_00_45p	0.0812	1.0503	1.0622	0.0853	1.1070	1.0732
230	s3_14_30_w3_00_45p	0.1249	1.7809	1.5650	0.1302	1.7809	1.5468
231	s3_14_30_w4_00_45p	0.1155	1.3213	1.2162	0.1244	1.3213	1.2392
232	s3_14_30_w5_00_45p	0.1750	2.1558	1.8560	0.1668	2.1558	1.8396
233	s3_14_30_w6_00_45p	0.1284	1.4629	1.5008	0.1481	1.5170	1.4962
240	s3_17_15_w1_00_45p	0.0902	1.5170	1.3363	0.0975	1.4629	1.3348
241	s3_17_15_w2_00_45p	0.0885	1.0503	1.0260	0.0918	1.0240	1.0359

test-number	testseries name	at toe of 60 cm dike			at toe of 70 cm dike		
		H_{m0} [m]	T_p [s]	$T_{m-1,0}$ [s]	H_{m0} [m]	T_p [s]	$T_{m-1,0}$ [s]
242	s3_17_15_w3_00_45p	0.1255	1.7067	1.5409	0.1282	1.7067	1.5181
243	s3_17_15_w4_00_45p	0.1198	1.2412	1.1960	0.1276	1.2412	1.1970
244	s3_17_15_w5_00_45p	0.1753	2.1558	1.8442	0.1710	2.1558	1.8263
245	s3_17_15_w6_00_45p	0.1362	1.5754	1.4822	0.1384	1.5754	1.4718
215	s3_18_00_w1_00_45p	0.0965	1.4629	1.3101	0.0869	1.5170	1.3089
216	s3_18_00_w2_00_45p	0.0957	1.0503	1.0189	0.0937	1.0240	1.0070
217	s3_18_00_w3_00_45p	0.1232	1.7067	1.4837	0.1231	1.7809	1.5282
218	s3_18_00_w4_00_45p	0.1253	1.2047	1.1761	0.1264	1.2412	1.1660
220	s3_18_00_w5_00_45p	0.1575	2.1558	1.7751	0.1704	2.1558	1.8138
234	s3_21_15_w1_00_30p	0.0790	1.4629	1.3178	0.0787	1.4124	1.2868
235	s3_21_15_w2_00_30p	0.0790	1.0240	1.0021	0.0858	1.0240	1.0064
236	s3_21_15_w3_00_30p	0.1021	1.7067	1.5068	0.1033	1.7809	1.4957
237	s3_21_15_w4_00_30p	0.1084	1.2412	1.1724	0.1148	1.2047	1.1660
238	s3_21_15_w5_00_30p	0.1431	2.1558	1.8129	0.1475	2.1558	1.8249
239	s3_21_15_w6_00_30p	0.1512	1.5170	1.4390	0.1483	1.5170	1.4391

Annex I Analyzed data - wave field – 1:6 sloped dike

Table-annex 10 Test program - 1:6 sloped dike

test-number	testseries name	water depth [m]	wave characteristic wc I or wc II	in front of wave generator			at toe of 60 cm dike			at toe of 70 cm dike		
				H_{m0} [m]	T_p [s]	$T_{m-1,0}$ [s]	H_{m0} [m]	T_p [s]	$T_{m-1,0}$ [s]	H_{m0} [m]	T_p [s]	$T_{m-1,0}$ [s]
425	s4_01_00_w1_00_00	0.50	wc I	0.0658	1.5059	1.3736	0.0653	1.5059	1.3547	0.0698	1.4222	1.3496
427	s4_01_00_w2_00_00	0.50	wc I	0.0614	1.0240	0.9836	0.0633	1.0240	0.9968	0.0652	1.0240	1.0011
426	s4_01_00_w3_00_00	0.50	wc I	0.0995	1.7067	1.6411	0.0957	1.7067	1.6051	0.1024	1.7067	1.6125
428	s4_01_00_w4_00_00	0.50	wc I	0.0868	1.2190	1.1858	0.0946	1.2190	1.1780	0.0994	1.2190	1.1764
429	s4_01_00_w5_00_00	0.50	wc I	0.1538	2.1333	1.9538	0.1422	2.1333	1.8747	0.1522	2.1333	1.9465
430	s4_01_00_w6_00_00	0.50	wc I	0.1366	1.5059	1.4722	0.1349	1.5059	1.4332	0.1425	1.5059	1.4187
451	s4_01a_00_w1_00_00	0.55	wc II	0.0896	1.7067	1.5472	0.0865	1.6000	1.5275	0.0929	1.7067	1.5221
452	s4_01a_00_w2_00_00	0.55	wc II	0.0802	1.2190	1.1055	0.0849	1.2190	1.1159	0.0914	1.1636	1.1063
453	s4_01a_00_w3_00_00	0.55	wc II	0.1222	1.8286	1.7765	0.1146	1.8286	1.7364	0.1225	1.9692	1.7326
454	s4_01a_00_w4_00_00	0.55	wc II	0.1098	1.3474	1.2924	0.1110	1.2800	1.2720	0.1191	1.3474	1.2636
456	s4_01a_00_w5_00_00	0.55	wc II	0.1538	2.1333	1.9499	0.1429	2.1333	1.8882	0.1498	2.1333	1.9204
457	s4_01a_00_w6_00_00	0.55	wc II	0.1408	1.5059	1.4588	0.1384	1.5059	1.4266	0.1468	1.5059	1.4176
418	s4_02_00_w1_25_00	0.50	wc I	0.0649	1.5059	1.3616	0.0656	1.5059	1.3340	0.0694	1.4222	1.3290
419	s4_02_00_w3_25_00	0.50	wc I	0.0961	1.7067	1.6266	0.0937	1.7067	1.5797	0.0985	1.7067	1.5764
421	s4_02_00_w5_25_00	0.50	wc I	0.1537	2.1333	1.9587	0.1415	2.1333	1.8791	0.1523	2.1333	1.9447
422	s4_03_00_w1_49_00	0.50	wc I	0.0652	1.5059	1.3868	0.0652	1.5059	1.3640	0.0692	1.4222	1.3637
423	s4_03_00_w3_49_00	0.50	wc I	0.0999	1.7067	1.6533	0.0957	1.7067	1.6123	0.1033	1.7067	1.6214
424	s4_03_00_w5_49_00	0.50	wc I	0.1532	2.1333	1.9622	0.1408	2.1333	1.8812	0.1532	2.1333	1.9475
464	s4_03a_00_w1_49_00	0.55	wc II	0.0882	1.7067	1.5739	0.0861	1.6000	1.5315	0.0928	1.6000	1.5353
465	s4_03a_00_w3_49_00	0.55	wc II	0.1207	1.8286	1.8021	0.1122	1.8286	1.7404	0.1225	1.9692	1.7424
466	s4_03a_00_w5_49_00	0.55	wc II	0.1566	2.1333	1.9714	0.1409	2.1333	1.8966	0.1534	2.1333	1.9365
411	s4_04_30_w1_00_00	0.50	wc I	0.0640	1.4222	1.3204	0.0699	1.4222	1.3172	0.0723	1.5059	1.3579

test-number	testseries name	water depth [m]	wave characteristic wc I or wc II	in front of wave generator			at toe of 60 cm dike			at toe of 70 cm dike		
				H_{m0} [m]	T_p [s]	$T_{m-1,0}$ [s]	H_{m0} [m]	T_p [s]	$T_{m-1,0}$ [s]	H_{m0} [m]	T_p [s]	$T_{m-1,0}$ [s]
410	s4_04_30_w2_00_00	0.50	wc I	0.0631	1.0667	1.0510	0.0686	1.0240	1.0000	0.0654	1.0240	1.0795
409	s4_04_30_w3_00_00	0.50	wc I	0.0923	1.7067	1.5974	0.0948	1.7067	1.5640	0.1002	1.7067	1.6124
408	s4_04_30_w4_00_00	0.50	wc I	0.0954	1.2190	1.1526	0.0986	1.2190	1.1488	0.0950	1.2190	1.1883
407	s4_04_30_w5_00_00	0.50	wc I	0.1434	2.1333	1.9302	0.1444	2.1333	1.8734	0.1501	2.1333	1.9922
406	s4_04_30_w6_00_00	0.50	wc I	0.1308	1.5059	1.4179	0.1415	1.5059	1.3985	0.1457	1.5059	1.4772
458	s4_04a_30_w1_00_00	0.55	wc II	0.0813	1.7067	1.5293	0.0839	1.6000	1.5049	0.0889	1.7067	1.5154
459	s4_04a_30_w2_00_00	0.55	wc II	0.0848	1.1636	1.1110	0.0855	1.2190	1.1056	0.0905	1.1636	1.1068
460	s4_04a_30_w3_00_00	0.55	wc II	0.1190	1.9692	1.7985	0.1168	1.9692	1.7592	0.1249	1.9692	1.7550
461	s4_04a_30_w4_00_00	0.55	wc II	0.1056	1.3474	1.2673	0.1136	1.3474	1.2691	0.1211	1.3474	1.2659
462	s4_04a_30_w5_00_00	0.55	wc II	0.1538	2.1333	1.9781	0.1511	2.1333	1.9211	0.1571	2.1333	1.9402
463	s4_04a_30_w6_00_00	0.55	wc II	0.1309	1.5059	1.4372	0.1388	1.5059	1.4134	0.1480	1.5059	1.4117
412	s4_05_30_w1_49_00	0.55	wc II	0.0621	1.4222	1.3244	0.0663	1.5059	1.3294	0.0700	1.4222	1.3352
413	s4_05_30_w3_49_00	0.55	wc II	0.0901	1.7067	1.6039	0.0898	1.7067	1.5738	0.0964	1.7067	1.5752
414	s4_05_30_w5_49_00	0.55	wc II	0.1404	2.1333	1.9312	0.1371	2.1333	1.8786	0.1443	2.1333	1.9164
415	s4_06_30_w1_25_00	0.50	wc I	0.0624	1.4222	1.3200	0.0665	1.5059	1.3240	0.0707	1.4222	1.3320
416	s4_06_30_w3_25_00	0.50	wc I	0.0903	1.8286	1.6016	0.0902	1.7067	1.5697	0.0969	1.7067	1.5722
417	s4_06_30_w5_25_00	0.50	wc I	0.1414	2.1333	1.9318	0.1380	2.1333	1.8778	0.1450	2.1333	1.9142
467	s4_07_15_w1_00_00	0.55	wc II	0.0839	1.6000	1.5486	0.0830	1.7067	1.5153	0.0884	1.6000	1.5202
468	s4_07_15_w2_00_00	0.55	wc II	0.0803	1.1636	1.0994	0.0842	1.1636	1.1078	0.0888	1.2190	1.1089
469	s4_07_15_w3_00_00	0.55	wc II	0.1198	1.9692	1.8043	0.1150	1.9692	1.7600	0.1215	1.9692	1.7530
470	s4_07_15_w4_00_00	0.55	wc II	0.1039	1.3474	1.2749	0.1126	1.3474	1.2760	0.1174	1.3474	1.2670
471	s4_07_15_w5_00_00	0.55	wc II	0.1558	2.1333	1.9805	0.1472	2.1333	1.9182	0.1532	2.1333	1.9421
472	s4_07_15_w6_00_00	0.55	wc II	0.1351	1.5059	1.4524	0.1369	1.5059	1.4158	0.1428	1.5059	1.4177
473	s4_08_15_w1_49_00	0.55	wc II	0.0840	1.6000	1.5549	0.0828	1.7067	1.5231	0.0882	1.6000	1.5279
474	s4_08_15_w3_49_00	0.55	wc II	0.1197	1.9692	1.8084	0.1144	1.9692	1.7688	0.1213	1.9692	1.7629
475	s4_08_15_w5_49_00	0.55	wc II	0.1559	2.1333	1.9809	0.1470	2.1333	1.9263	0.1534	2.1333	1.9491
480	s4_10_40_w1_00_00	0.55	wc II	0.0789	1.7067	1.5182	0.0853	1.6000	1.5183	0.0877	1.7067	1.5160

test-number	testseries name	water depth [m]	wave characteristic wc I or wc II	in front of wave generator			at toe of 60 cm dike			at toe of 70 cm dike		
				H_{m0} [m]	T_p [s]	$T_{m-1,0}$ [s]	H_{m0} [m]	T_p [s]	$T_{m-1,0}$ [s]	H_{m0} [m]	T_p [s]	$T_{m-1,0}$ [s]
481	s4_10_40_w2_00_00	0.55	wc II	0.0829	1.2190	1.1212	0.0856	1.1636	1.1112	0.0896	1.1636	1.1090
482	s4_10_40_w3_00_00	0.55	wc II	0.1134	1.9692	1.7912	0.1158	1.9692	1.7548	0.1230	1.9692	1.7523
483	s4_10_40_w4_00_00	0.55	wc II	0.1093	1.3474	1.2733	0.1130	1.3474	1.2688	0.1194	1.4222	1.2707
484	s4_10_40_w5_00_00	0.55	wc II	0.1479	2.1333	1.9785	0.1497	2.1333	1.9210	0.1546	2.1333	1.9438
485	s4_10_40_w6_00_00	0.55	wc II	0.1280	1.5059	1.4292	0.1380	1.5059	1.4198	0.1465	1.5059	1.4088
488	s4_11_40_w1_49_00	0.55	wc II	0.0793	1.7067	1.5281	0.0850	1.6000	1.5297	0.0883	1.6000	1.5209
489	s4_11_40_w3_49_00	0.55	wc II	0.1133	1.9692	1.8032	0.1151	1.9692	1.7676	0.1234	1.9692	1.7600
490	s4_11_40_w5_49_00	0.55	wc II	0.1479	2.1333	1.9877	0.1495	2.1333	1.9315	0.1554	2.1333	1.9511
432	s4_32_30_w1_00_15m	0.50	wc I	0.0652	1.4222	1.3675	0.0648	1.4222	1.3582	0.0666	1.5059	1.3601
433	s4_32_30_w2_00_15m	0.50	wc I	0.0577	1.0667	1.0088	0.0589	1.0240	1.0085	0.0626	1.0240	1.0063
434	s4_32_30_w3_00_15m	0.50	wc I	0.0821	1.7067	1.5290	0.0865	1.7067	1.5515	0.0897	1.7067	1.5346
435	s4_32_30_w4_00_15m	0.50	wc I	0.0864	1.2800	1.1876	0.0896	1.2190	1.1822	0.0925	1.2800	1.1721
437	s4_32_30_w5_00_15m	0.50	wc I	0.1229	2.1333	1.8240	0.1228	2.1333	1.7823	0.1403	2.1333	1.8995
438	s4_32_30_w6_00_15m	0.50	wc I	0.1344	1.5059	1.4375	0.1335	1.5059	1.4172	0.1424	1.5059	1.4201
440	s4_33_30_w3_00_15p	0.50	wc I	0.1051	1.7067	1.6110	0.0993	1.7067	1.5908	0.1026	1.7067	1.5656
441	s4_33_30_w4_00_15p	0.50	wc I	0.0933	1.2800	1.2051	0.0941	1.2190	1.1909	0.1001	1.2190	1.1835
442	s4_33_30_w5_00_15p	0.50	wc I	0.1565	2.1333	1.8908	0.1363	2.1333	1.8171	0.1416	2.1333	1.8313
443	s4_33_30_w6_00_15p	0.50	wc I	0.1537	1.5059	1.4778	0.1442	1.5059	1.4457	0.1555	1.5059	1.4257
444	s4_34_00_w1_00_15m	0.55	wc II	0.0796	1.6000	1.5099	0.0873	1.7067	1.5303	0.0890	1.6000	1.5193
445	s4_34_00_w2_00_15m	0.55	wc II	0.0838	1.2190	1.1215	0.0819	1.1636	1.1213	0.0869	1.1636	1.1194
447	s4_34_00_w3_00_15m	0.55	wc II	0.1067	1.9692	1.7640	0.1127	1.9692	1.7362	0.1168	1.9692	1.7551
448	s4_34_00_w4_00_15m	0.55	wc II	0.1090	1.3474	1.2631	0.1082	1.3474	1.2797	0.1167	1.3474	1.2750
449	s4_34_00_w5_00_15m	0.55	wc II	0.1403	2.1333	1.9740	0.1394	2.1333	1.8840	0.1539	2.1333	1.9745
450	s4_34_00_w6_00_15m	0.55	wc II	0.1304	1.5059	1.4127	0.1389	1.5059	1.4322	0.1472	1.5059	1.4144
476	s4_35_15_w1_00_00	0.55	wc II	0.0643	1.5059	1.3516	0.0677	1.4222	1.3331	0.0695	1.5059	1.3339
477	s4_35_15_w2_00_00	0.55	wc II	0.0652	1.0240	0.9826	0.0656	1.0240	0.9818	0.0696	1.0240	0.9790
486	s4_36_40_w1_00_00	0.55	wc II	0.0642	1.4222	1.3297	0.0675	1.5059	1.3327	0.0725	1.4222	1.3443

test-number	testseries name	water depth [m]	wave characteristic wc I or wc II	in front of wave generator			at toe of 60 cm dike			at toe of 70 cm dike		
				H_{m0} [m]	T_p [s]	$T_{m-1,0}$ [s]	H_{m0} [m]	T_p [s]	$T_{m-1,0}$ [s]	H_{m0} [m]	T_p [s]	$T_{m-1,0}$ [s]
487	s4_36_40_w2_00_00	0.55	wc II	0.0650	1.0240	0.9960	0.0669	1.0240	0.9852	0.0696	1.0240	0.9833
511	s5_13_00_w1_00_30m	0.55	wc II	0.0854	1.7067	1.5558	0.0796	1.7067	1.5517	0.0878	1.7067	1.5593
512	s5_13_00_w2_00_30m	0.55	wc II	0.0737	1.1636	1.1434	0.0778	1.1636	1.1379	0.0789	1.1636	1.1393
513	s5_13_00_w3_00_30m	0.55	wc II	0.1082	1.9692	1.7383	0.1164	1.9692	1.7969	0.1178	1.9692	1.7524
514	s5_13_00_w4_00_30m	0.55	wc II	0.1029	1.4222	1.3144	0.1006	1.3474	1.2829	0.1049	1.3474	1.2960
515	s5_13_00_w5_00_30m	0.55	wc II	0.1239	2.1333	1.8695	0.1461	2.1333	1.9454	0.1374	2.1333	1.9244
516	s5_13_00_w6_00_30m	0.55	wc II	0.1355	1.5059	1.4565	0.1265	1.5059	1.4409	0.1339	1.5059	1.4465
536	s5_15_00_w1_49_30m	0.55	wc II	0.0821	1.7067	1.5608	0.0778	1.7067	1.5557	0.0848	1.7067	1.5644
537	s5_15_00_w3_49_30m	0.55	wc II	0.1043	1.9692	1.7466	0.1130	1.9692	1.8022	0.1155	1.9692	1.7626
538	s5_15_00_w5_49_30m	0.55	wc II	0.1226	2.1333	1.8765	0.1442	2.1333	1.9431	0.1368	2.1333	1.9259
501	s5_16_40_w1_00_30m	0.55	wc II	0.0703	1.7067	1.5760	0.0813	1.7067	1.5678	0.0737	1.6000	1.5103
502	s5_16_40_w2_00_30m	0.55	wc II	0.0680	1.1636	1.1583	0.0721	1.1636	1.1423	0.0782	1.1636	1.1684
503	s5_16_40_w3_00_30m	0.55	wc II	0.1035	1.9692	1.7966	0.1111	1.9692	1.7548	0.1016	1.9692	1.7470
504	s5_16_40_w4_00_30m	0.55	wc II	0.0922	1.3474	1.3024	0.1010	1.3474	1.3012	0.1055	1.3474	1.2932
505	s5_16_40_w5_00_30m	0.55	wc II	0.1277	2.1333	1.9382	0.1375	2.1333	1.8625	0.1263	2.1333	1.9453
506	s5_16_40_w6_00_30m	0.55	wc II	0.1120	1.6000	1.4528	0.1298	1.5059	1.4513	0.1263	1.5059	1.4053
508	s5_17_40_w1_49_30m	0.55	wc II	0.0704	1.7067	1.5824	0.0822	1.7067	1.5698	0.0746	1.6000	1.5113
509	s5_17_40_w3_49_30m	0.55	wc II	0.1029	1.9692	1.7977	0.1118	1.9692	1.7592	0.1027	1.9692	1.7477
510	s5_17_40_w5_49_30m	0.55	wc II	0.1271	2.1333	1.9404	0.1382	2.1333	1.8621	0.1281	2.1333	1.9491
517	s5_19_30_w1_00_30m	0.55	wc II	0.0713	1.6000	1.5480	0.0802	1.7067	1.5754	0.0768	1.6000	1.5165
518	s5_19_30_w2_00_30m	0.55	wc II	0.0708	1.2190	1.1576	0.0695	1.1636	1.1386	0.0743	1.1636	1.1593
519	s5_19_30_w3_00_30m	0.55	wc II	0.0994	1.9692	1.7621	0.1107	1.9692	1.7723	0.1033	1.9692	1.7319
520	s5_19_30_w4_00_30m	0.55	wc II	0.0950	1.3474	1.2955	0.0999	1.4222	1.2999	0.1073	1.3474	1.3018
521	s5_19_30_w5_00_30m	0.55	wc II	0.1214	2.1333	1.9048	0.1398	2.1333	1.8843	0.1252	2.1333	1.9230
522	s5_19_30_w6_00_30m	0.55	wc II	0.1140	1.6000	1.4385	0.1292	1.5059	1.4496	0.1321	1.5059	1.4153
523	s5_20_30_w1_49_30m	0.55	wc II	0.0715	1.6000	1.5529	0.0813	1.7067	1.5758	0.0768	1.6000	1.5163
524	s5_20_30_w3_49_30m	0.55	wc II	0.0993	1.9692	1.7680	0.1114	1.9692	1.7738	0.1035	1.9692	1.7342

test-number	testseries name	water depth [m]	wave characteristic wc I or wc II	in front of wave generator			at toe of 60 cm dike			at toe of 70 cm dike		
				H_{m0} [m]	T_p [s]	$T_{m-1,0}$ [s]	H_{m0} [m]	T_p [s]	$T_{m-1,0}$ [s]	H_{m0} [m]	T_p [s]	$T_{m-1,0}$ [s]
525	s5_20_30_w5_49_30m	0.55	wc II	0.1213	2.1333	1.9102	0.1404	2.1333	1.8859	0.1254	2.1333	1.9253
530	s5_22_15_w1_00_30m	0.55	wc II	0.0779	1.6000	1.5387	0.0778	1.7067	1.5769	0.0820	1.7067	1.5413
531	s5_22_15_w2_00_30m	0.55	wc II	0.0734	1.1636	1.1488	0.0681	1.1636	1.1332	0.0741	1.1636	1.1400
532	s5_22_15_w3_00_30m	0.55	wc II	0.1003	1.9692	1.7247	0.1125	1.9692	1.8012	0.1104	1.9692	1.7398
533	s5_22_15_w4_00_30m	0.55	wc II	0.1003	1.3474	1.2972	0.0972	1.3474	1.2922	0.1062	1.4222	1.3025
534	s5_22_15_w5_00_30m	0.55	wc II	0.1188	2.1333	1.8662	0.1432	2.1333	1.9267	0.1301	2.1333	1.9092
535	s5_22_15_w6_00_30m	0.55	wc II	0.1271	1.5059	1.4398	0.1284	1.5059	1.4497	0.1369	1.5059	1.4322
613	s6_25_00_w1_00_45p	0.55	wc II	0.0868	1.7067	1.5968	0.0819	1.7067	1.6142	0.0771	1.7067	1.5552
614	s6_25_00_w2_00_45p	0.55	wc II	0.0701	1.2190	1.1733	0.0702	1.2190	1.1486	0.0751	1.1636	1.1608
615	s6_25_00_w3_00_45p	0.55	wc II	0.1185	1.9692	1.8004	0.1256	1.9692	1.8328	0.1124	1.8286	1.7857
616	s6_25_00_w4_00_45p	0.55	wc II	0.1061	1.3474	1.3380	0.0970	1.3474	1.3107	0.1044	1.3474	1.3060
617	s6_25_00_w5_00_45p	0.55	wc II	0.1471	2.1333	1.9359	0.1514	2.1333	1.9599	0.1407	2.1333	1.9801
618	s6_25_00_w6_00_45p	0.55	wc II	0.1380	1.6000	1.4758	0.1287	1.6000	1.4754	0.1284	1.5059	1.4297
607	s6_26_15_w1_00_30p	0.55	wc II	0.0838	1.7067	1.5466	0.0823	1.7067	1.5344	0.0867	1.6000	1.5510
608	s6_26_15_w2_00_30p	0.55	wc II	0.0759	1.1636	1.1414	0.0798	1.1636	1.1525	0.0808	1.1636	1.1521
609	s6_26_15_w3_00_30p	0.55	wc II	0.1080	1.8286	1.7595	0.1115	1.9692	1.7661	0.1181	1.9692	1.7901
610	s6_26_15_w4_00_30p	0.55	wc II	0.1068	1.3474	1.3047	0.1116	1.3474	1.3013	0.1103	1.4222	1.3026
611	s6_26_15_w5_00_30p	0.55	wc II	0.1353	2.1333	1.9403	0.1413	2.1333	1.9224	0.1563	2.1333	1.9753
612	s6_26_15_w6_00_30p	0.55	wc II	0.1337	1.5059	1.4493	0.1349	1.5059	1.4359	0.1427	1.5059	1.4391
601	s6_27_15_w1_00_45p	0.55	wc II	0.0821	1.7067	1.6194	0.0821	1.7067	1.5765	0.0839	1.7067	1.5848
602	s6_27_15_w2_00_45p	0.55	wc II	0.0669	1.1636	1.1623	0.0707	1.1636	1.1650	0.0701	1.1636	1.1741
603	s6_27_15_w3_00_45p	0.55	wc II	0.1209	1.9692	1.8506	0.1149	1.9692	1.7967	0.1116	1.9692	1.7862
604	s6_27_15_w4_00_45p	0.55	wc II	0.0938	1.3474	1.3306	0.1011	1.4222	1.3232	0.1026	1.3474	1.3346
605	s6_27_15_w5_00_45p	0.55	wc II	0.1546	2.1333	1.9978	0.1394	2.1333	1.9440	0.1376	2.1333	1.9761
606	s6_27_15_w6_00_45p	0.55	wc II	0.1296	1.5059	1.4975	0.1313	1.5059	1.4662	0.1323	1.5059	1.4664
625	s6_28_30_w1_00_30p	0.55	wc II	0.0872	1.7067	1.5727	0.0848	1.6000	1.5414	0.0879	1.6000	1.5696
626	s6_28_30_w2_00_30p	0.55	wc II	0.0753	1.1636	1.1566	0.0822	1.1636	1.1436	0.0777	1.1636	1.1645

test-number	testseries name	water depth [m]	wave characteristic wc I or wc II	in front of wave generator			at toe of 60 cm dike			at toe of 70 cm dike		
				H_{m0} [m]	T_p [s]	$T_{m-1,0}$ [s]	H_{m0} [m]	T_p [s]	$T_{m-1,0}$ [s]	H_{m0} [m]	T_p [s]	$T_{m-1,0}$ [s]
627	s6_28_30_w3_00_30p	0.55	wc II	0.1134	1.8286	1.7818	0.1159	1.9692	1.8005	0.1210	1.9692	1.8012
628	s6_28_30_w4_00_30p	0.55	wc II	0.1043	1.3474	1.3217	0.1104	1.3474	1.2937	0.1114	1.3474	1.3203
629	s6_28_30_w5_00_30p	0.55	wc II	0.1407	2.1333	1.9542	0.1537	2.1333	1.9767	0.1632	2.1333	1.9929
630	s6_28_30_w6_00_30p	0.55	wc II	0.1370	1.6000	1.4803	0.1349	1.5059	1.4416	0.1455	1.5059	1.4528
619	s6_29_30_w1_00_45p	0.55	wc II	0.0761	1.7067	1.6128	0.0907	1.7067	1.5904	0.0878	1.7067	1.6270
620	s6_29_30_w2_00_45p	0.55	wc II	0.0638	1.1636	1.1874	0.0710	1.2190	1.1863	0.0648	1.2190	1.2070
621	s6_29_30_w3_00_45p	0.55	wc II	0.1169	1.9692	1.8643	0.1156	1.9692	1.7761	0.1185	1.9692	1.8044
622	s6_29_30_w4_00_45p	0.55	wc II	0.0964	1.3474	1.3424	0.1073	1.3474	1.3480	0.1006	1.3474	1.3566
623	s6_29_30_w5_00_45p	0.55	wc II	0.1549	2.1333	2.0352	0.1398	2.1333	1.9454	0.1459	2.1333	1.9816
624	s6_29_30_w6_00_45p	0.55	wc II	0.1245	1.5059	1.4989	0.1431	1.5059	1.4890	0.1357	1.6000	1.5079
637	s6_30_40_w1_00_30p	0.55	wc II	0.0847	1.6000	1.5851	0.0851	1.7067	1.5664	0.0882	1.6000	1.5822
638	s6_30_40_w2_00_30p	0.55	wc II	0.0743	1.1636	1.1713	0.0805	1.1636	1.1506	0.0755	1.1636	1.1754
639	s6_30_40_w3_00_30p	0.55	wc II	0.1185	1.8286	1.8094	0.1197	1.9692	1.8182	0.1254	1.9692	1.8084
640	s6_30_40_w4_00_30p	0.55	wc II	0.1059	1.4222	1.3421	0.1081	1.3474	1.3125	0.1113	1.3474	1.3358
641	s6_30_40_w5_00_30p	0.55	wc II	0.1487	2.1333	1.9792	0.1578	2.1333	2.0076	0.1652	2.1333	1.9978
642	s6_30_40_w6_00_30p	0.55	wc II	0.1362	1.5059	1.4902	0.1337	1.5059	1.4674	0.1452	1.5059	1.4616
631	s6_31_40_w1_00_45p	0.55	wc II	0.0786	1.6000	1.6201	0.0905	1.7067	1.5913	0.0873	1.7067	1.6476
632	s6_31_40_w2_00_45p	0.55	wc II	0.0616	1.1636	1.2011	0.0756	1.2190	1.2009	0.0610	1.2190	1.2264
633	s6_31_40_w3_00_45p	0.55	wc II	0.1115	1.9692	1.8604	0.1204	1.9692	1.7791	0.1218	1.9692	1.8376
634	s6_31_40_w4_00_45p	0.55	wc II	0.0949	1.3474	1.3651	0.1132	1.3474	1.3492	0.0980	1.3474	1.3814
635	s6_31_40_w5_00_45p	0.55	wc II	0.1503	2.1333	2.0496	0.1460	2.1333	1.9582	0.1548	2.1333	2.0029
636	s6_31_40_w6_00_45p	0.55	wc II	0.1282	1.5059	1.5140	0.1440	1.5059	1.4847	0.1363	1.5059	1.5240

Annex J Test-diary – run-up videos

Table-annex 11 Model tests and associated films (AVI-file 101 to 152)

AVI Nr	Date	Set-up	Test Label	File name	Comment	Remarks
101	29. Jan	1	RW1.1		Regular Waves	-
102	29. Jan	1	RW1.2		Regular Waves	pumps switched off too late at first pumping
103	29. Jan	1	RW1.3		Regular Waves	-
104	29. Jan	1	RW1.4		Regular Waves	-
105	29. Jan	1	RW1.5		Regular Waves	pump (channel 46) started too late, water beside channels into collecting tank
106	29. Jan	1	RW1.6		Regular Waves	water beside channels into collecting tank, plug of platform 1 unplugged (current supply) for about 3 sec., possibly affected channels: microprops, stepgauges, ADV RWTH, capacitive gauge, pump (channel 48) ran dry on last pumping
107	30. Jan	1	RW6.1		Regular Waves; error in the anemometer; replaced with 108	temp up to 14.5, delete values during data acquisition: channels 3, 4, 33; changed range of airflow from 0-5m/s and 0-10V to 0-20m/s and 0-10V; added amplifiers for the 4 small props to reduce 10V to 5V ; repetition in test no 108
108	30. Jan	1	RW6.2		Regular Waves; replaces 107	
109	30. Jan	1	RW6.3		Regular Waves	-
110	30. Jan	1	RW6.4		Regular Waves	delete values channel 56 (step gauge 50,2m)
111	30. Jan	1	RW6.5		Regular Waves	container not empty before test was started
112	30. Jan	1	RW6.6		Regular Waves	pump 46 accidentially started, turned off imediately
113	30. Jan	1	RW6.7		Regular Waves	-
114	02. Feb.	1	T3.1	s1_03_30_w1_00	shorter Wave Period	Gauges on dike and overtopping co,ntainers calibrated with water from behind the dike; distance between WG on crest: 0.6m ->0.3m, 0.7m ->0.29m
115	02. Feb.	1	T3.2	s1_03_30_w2_00	shorter Wave Period	see test 114
116	02. Feb.	1	T3.3	s1_03_30_w3_00	shorter Wave Period	-
117	02. Feb.	1	T3.4	s1_03_30_w4_00	shorter Wave Period	-
118					replaced with 119; shorter Wave Period	delete values on wave gauges; splash into tank -> mounting splash board; repetition in test 119
119	02. Feb.	1	T3.5	s1_03_30_w5_00	replaces 118; shorter Wave Period	delete values on wave gauges; splash into tank -> mounting splash board; repetition in test 119
120	02. Feb.	1	T3.6	s1_03_30_w6_00	shorter Wave Period	-
121	03. Feb.	1	T8.1	s1_08_30_w1_49		
122	03. Feb.	1	T8.2	s1_08_30_w2_49		
123	03. Feb.	1	T8.3	s1_08_30_w3_49	AVI truncated (last 5 minutes)	
124	03. Feb.	1	T19.1	s1_19_30_w1_00_-15		Hs changed to 0.07m for Wave 1
125	03. Feb.	1	T19.2	s1_19_30_w2_00_-15		Hs changed to 0.07m for Wave 2
126	03. Feb.	1	T19.3	s1_19_30_w3_00_-15		
127	03. Feb.	1	T19.4	s1_19_30_w4_00_-15		
128	03. Feb.	1	T19.5	s1_19_30_w5_00_-15	not recorded	at 26:30 and 31:40 minutes, water besides the channel for loadcell 39
129	03. Feb.	1	T19.6	s1_19_30_w6_00_-15	not recorded	
130					Test x ADV; not recorded	only current to check ADV signals
131	04. Feb.	1	T16.1	s1_16_30_w1_00_+15	AVI truncated	ADV + SD moved closer to gauges
132	04. Feb.	1	T16.2	s1_16_30_w2_00_+15		
133	04. Feb.	1	T16.3	s1_16_30_w3_00_+15		
134	04. Feb.	1	T16.4	s1_16_30_w4_00_+15		
135	04. Feb.	1	T16.5	s1_16_30_w5_00_+15		waves touching windmaker (?)
136	04. Feb.	1	T16.6	s1_16_30_w6_00_+15		pump 47 ran dry at about 8:30 min
137	04. Feb.	1	T8b.1	s1_08b_30_w4_25	restarted	
138	04. Feb.	1	T8b.3	s1_08b_30_w5_25		
139					replaced with 140; error in Water Gauges; AVI deleted	recalibration of gauges 5 - 14 to a range of 0.4m (change of calibration factor + voltage: 2.5V -> 0.1m); correction of calibration factors for gauges in overtoppingtanks (-> now 0.04, before 0.0025); repetition of test in test 140
140	04. Feb.	1	T8b.5	s1_08b_30_w6_25	replaces 139; new position of the Videocamera (mark "2")	repetition of test 139
141					Calibration of capitive gauge	regular waves for calibration of capacitive gauge
142					Calibration of capitive gauge	regular waves for calibration of capacitive gauge
143					Calibration of capitive gauge	regular waves for calibration of capacitive gauge
144	05. Feb.	1	T1.1	s1_01_00_w1_00	longer Video because replacing USB cable	Testseries 1 with JONSWAP not regular waves
145	05. Feb.	1	T1.2	s1_01_00_w2_00		
146	05. Feb.	1	T1.3	s1_01_00_w3_00		
147	05. Feb.	1	T1.4	s1_01_00_w4_00		
148	05. Feb.	1	T1.5	s1_01_00_w5_00		
149	05. Feb.	1	T1.6	s1_01_00_w6_00		
150	05. Feb.	1	T6b.1	s1_06b_00_w1_25		
151	05. Feb.	1	T6b.2	s1_06b_00_w2_25		
152	05. Feb.	1	T6b.3	s1_06b_00_w3_25		pumps 46,47 ran dry at about 11:55; recognized, that there is no signal from prop 34 -> solution: amp. Turned off an on again

Table-annex 1 Model tests and associated films (AVI-file 153 to 201)

AVI Nr	Date	Set-up	Test Label	File name	Comment	Remarks
153	05. Feb.	1	T6.1	s1_06_00_w4_49		
154	05. Feb.	1	T6.2	s1_06_00_w5_49		
155	05. Feb.	1	T6.3	s1_06_00_w6_49	replaces the 155a = no data saved	
155,5					no data saved; replaced with 155	
156	06. Feb.	1	T12.1	s1_12_00_w1_00_-15	new casette - first on the casette	
157	06. Feb.	1	T12.2	s1_12_00_w2_00_-15	only avi	
158	06. Feb.	1	T12.3	s1_12_00_w3_00_-15	only avi	
159	06. Feb.	1	T12.4	s1_12_00_w4_00_-15	only avi	
160	06. Feb.	1	T12.5	s1_12_00_w5_00_-15	only avi	
161	06. Feb.	1	T12.6	s1_12_00_w6_00_-15	only avi	
162	06. Feb.	1	T11.1	s1_11_15_w1_00	second on the casette	
163	06. Feb.	1	T11.2	s1_11_15_w2_00	third on the casette - end	
164	06. Feb.	1	T11.3	s1_11_15_w3_00	new casette - first on the casette	after this test offset factor for ADV (19-21) changed from -100 to -1; effect on all test since change from cm to m
165	06. Feb.	1	T11.4	s1_11_15_w4_00	second on the casette	
166	06. Feb.	1	T11.5	s1_11_15_w5_00	third on the casette	pump 47 ran dry at about 5:30 min
167	06. Feb.	1	T11.6	s1_11_15_w6_00	new casette - first on the casette	pump 47 was stopped after end of waves
168	09. Feb.	1	T13.1	s1_13_15_w1_00_-15	only avi	
169	09. Feb.	1	T13.2	s1_13_15_w2_00_-15	only avi	
170	09. Feb.	1	T13.3	s1_13_15_w3_00_-15	only avi	
171	09. Feb.	1	T13.4	s1_13_15_w4_00_-15	only avi	
172	09. Feb.	1	T13.5	s1_13_15_w5_00_-15	only avi	
173	09. Feb.	1	T13.6	s1_13_15_w6_00_-15	only avi	
174	09. Feb.	1	T15.1	s1_15_15_w1_00_+15	second on the casette	
175	09. Feb.	1	T15.2	s1_15_15_w2_00_+15	third on the casette	
176	09. Feb.	1	T15.3	s1_15_15_w3_00_+15	new casette - first on the casette	
177	09. Feb.	1	T15.4	s1_15_15_w4_00_+15	second on the casette	Wavemakerfile is recorded with 15.3 -> testno 177
178	09. Feb.	1	T15.5	s1_15_15_w5_00_+15	third on the casette	
179	09. Feb.	1	T15.6	s1_15_15_w6_00_+15	new casette - first on the casette	repeat this testseries with setup3, because overtopping on 60 cm crest can not be measured (waves out of range)
180	11. Feb.	2	T2.1	s2_02_00_w1_00_-30	second on the casette	micropropeller not in wave direction, but 0 degree
181	11. Feb.	2	T2.2	s2_02_00_w2_00_-30	third on the casette	micropropeller not in wave direction, but 0 degree
182	11. Feb.	2	T2.3	s2_02_00_w3_00_-30	new casette - first on the casette	direction of micropropeller changed to -30 degree
183	11. Feb.	2	T2.4	s2_02_00_w4_00_-30	second on the casette	
184	11. Feb.	2	T2.5	s2_02_00_w5_00_-30	third on the casette	
185	11. Feb.	2	T2.6	s2_02_00_w6_00_-30	new casette - first on the casette	
186	11. Feb.	2	T7b.1	s2_07b_00_w1_25_-30	second on the casette	
187	11. Feb.	2	T7b.2	s2_07b_00_w3_25_-30	third on the casette, long video because of test restart	
188	11. Feb.	2	T7b.3	s2_07b_00_w5_25_-30	new casette - first on the casette	
189	11. Feb.	2	T7.1	s2_07_00_w1_49_-30	second on the casette	
190	11. Feb.	2	T7.2	s2_07_00_w3_49_-30	third on the casette	
191	11. Feb.	2	T7.3	s2_07_00_w5_49_-30	new casette - first on the casette	
192	12. Feb.	2	T20.1	s2_20_15_w1_00_-30	second on the casette	
193	12. Feb.	2	T20.2	s2_20_15_w2_00_-30	third on the casette	
193.5	12. Feb.	2	T20.3	s2_20_15_w3_00_-30	194a: wavemaker stopped during the test,replaced with 194, new casette	
194	12. Feb.	2	T20.3	s2_20_15_w3_00_-30	second on the casette	breaking waves on downstream edge of the wavemaker, wavemaker stopped, new offsetscan because temperature has changed, test repeated with same testno
195	12. Feb.	2	T20.4	s2_20_15_w4_00_-30	third on the casette	
196	12. Feb.	2	T20.5	s2_20_15_w5_00_-30	new casette - first on the casette	
197	12. Feb.	2	T20.6	s2_20_15_w6_00_-30	second on the casette	
198					rerun 146	repeating test s1_01_00_w3_00 (microprop did not work there
199					rerun 147	
200					rerun 148	overflow of overtopping tank during first time pumping, pump 43 switched on too late
201					rerun 149	pump 48 pumped too long once

Table-annex 12 Model tests and associated films (AVI-file 202 to 247)

AVI Nr	Date	Set-up	Test Label	File name	Comment	Remarks
202	12. Feb.	2	T4.1	s2_04_30_w1_00_-30	second on the casette, (with 191)	
203	12. Feb.	2	T4.2	s2_04_30_w2_00_-30	new casette - first on the casette	
204	12. Feb.	2	T4.3	s2_04_30_w3_00_-30	second on the casette	
205	12. Feb.	2	T4.4	s2_04_30_w4_00_-30	third on the casette - end (started twice)	
206	12. Feb.	2	T4.5	s2_04_30_w5_00_-30	new casette - first on the casette	
207	12. Feb.	2	T4.6	s2_04_30_w6_00_-30	second on the cassette - end (2x)	test was repeated, data was overwritten
208	13. Feb.	2	T9b.1	s2_09b_30_w1_25_-30	new casette - first on the casette	
209	13. Feb.	2	T9b.3	s2_09b_30_w3_25_-30	second on the casette	
210	13. Feb.	2	T9b.5	s2_09b_30_w5_25_-30	third on the casette	
211	13. Feb.	2	T9.1	s2_09_30_w1_49_-30	new casette - first on the casette	
212	13. Feb.	2	T9.3	s2_09_30_w3_49_-30	second on the casette	
213	13. Feb.	2	T9.5	s2_09_30_w5_49_-30	third on the casette	
214					missing DFS0	
215	18. Feb.	3	T18.1	s3_18_00_w1_00_+45	new casette - first on the casette	
216	18. Feb.	3	T18.2	s3_18_00_w2_00_+45	second on the casette	
217	18. Feb.	3	T18.3	s3_18_00_w3_00_+45	third on the casette	
218	18. Feb.	3	T18.4	s3_18_00_w4_00_+45	new casette - first on the casette	
219					replaced with 220	Wavemaker stopped after 21 min repetition in test 220
220	18. Feb.	3	T18.5	s3_18_00_w5_00_+45	second on the casette	repeating test 219
221					wavemaker stopped during the test, no existing data, test left out	new testseries with 40 degree angle, -> 45 did not work (breaking waves at the paddle); 40 Degree did not work as well, dataacquisition not started
222	19. Feb.	3	T5.1	s3_05_30_w1_00_+30	new casette - first on the casette	changed ADV positions: SD12 to WG array (10-14), ADV RWTH (25-27) to WG array (5-9), ADV DHI (19-21) not in use anymore
223	19. Feb.	3	T5.2	s3_05_30_w2_00_+30	second on the casette	
224	19. Feb.	3	T5.3	s3_05_30_w3_00_+30	third on the casette	
225	19. Feb.	3	T5.4	s3_05_30_w4_00_+30	new casette - first on the casette	
226	19. Feb.	3	T5.5	s3_05_30_w5_00_+30	second on the casete	pump 47 interrupted too late 12:10 min
227	19. Feb.	3	T5.6	s3_05_30_w6_00_+30	third on the casette	
228	20. Feb.	3	T14.1	s3_14_30_w1_00_+45	new casette - first on the casette	
229	20. Feb.	3	T14.2	s3_14_30_w2_00_+45	second on the casette	
230	20. Feb.	3	T14.3	s3_14_30_w3_00_+45	third on the casette	
231	20. Feb.	3	T14.4	s3_14_30_w4_00_+45	new casette - first on the casette	
232	20. Feb.	3	T14.5	s3_14_30_w5_00_+45	second on the casete	
233	20. Feb.	3	T14.6	s3_14_30_w6_00_+45	third on the casette	without absorbtion
234	18. Feb.	3	T21.1	s3_21_15_w1_00_+30	new casette - first on the casette	before test: changed mircopropeller ports 31 and 34, it seems as if port 4 of the amplifier is not working right, also changed cables at the cabinett
235	18. Feb.	3	T21.2	s3_21_15_w2_00_+30	second on the casette	
236	18. Feb.	3	T21.3	s3_21_15_w3_00_+30	third on the casette	
237	18. Feb.	3	T21.4	s3_21_15_w4_00_+30	new casette - first on the casette	
238	18. Feb.	3	T21.5	s3_21_15_w5_00_+30	second on the casette	
239	18. Feb.	3	T21.6	s3_21_15_w6_00_+30	third on the casette	
240	19. Feb.	3	T17.1	s3_17_15_w1_00_+45	new casette - first on the casette	
241	19. Feb.	3	T17.2	s3_17_15_w2_00_+45	second on the casette	
242	19. Feb.	3	T17.3	s3_17_15_w3_00_+45	third on the casette	
243	19. Feb.	3	T17.4	s3_17_15_w4_00_+45	new casette - first on the casette	
244	19. Feb.	3	T17.5	s3_17_15_w5_00_+45	second on the casette	
245	19. Feb.	3	T17.6	s3_17_15_w6_00_+45	third on the casette	without absorbtion
246	20.Feb.	3	T23.3	s3_23_00_w3_00_+30MD	only AVI, multidirectional	multi directional waves
247	20.Feb.	3	T23.5	s3_23_00_w5_00_+30MD	only AVI, multidirectional	multi directional waves
-	18. Feb.	3	T18.6	s3_18_00_w6_00_+45		

FlowDike-D

Freibordbemessung von Ästuar- und Seedeichen unter Berücksichtigung von Wind und Strömung

Zusammenstellung der aus dem Projekt resultierten Veröffentlichungen
März 2011

Dipl.-Ing. Stefanie Lorke[1]
Dr.-Ing. Antje Bornschein[2]
Univ.-Prof. Dr.-Ing. Holger Schüttrumpf[1]
Prof. Dr.-Ing. habil. Reinhard Pohl[2]

Aachen und Dresden, März 2011

[1] Institut für Wasserbau und Wasserwirtschaft (IWW), RWTH Aachen
[2] Institut für Wasserbau und Technische Hydromechanik (IWD), TU Dresden

Veröffentlichungen

Brüning, A.; Gilli, S.; Lorke, S.; Pohl, R.; Schlüter, F.; Spano, M.; van der Meer, J.; Werk, S.; Schüttrumpf, H. (2009); FlowDike - Investigating the effect of wind and current on wave run-up and wave overtopping; 4th SCACR - International Short conference on APPLIED COASTAL RESEARCH, Barcelona

Brüning, A.; Gilli, S.; Lorke, S.; Pohl, R.; Schlüter, F.; Spano, M.; van der Meer, J.; Werk, S.; Schüttrumpf, H. (2010); FlowDike - Investigating the effect of wind and current on wave run-up and wave overtopping; Hydralab III Joint User Meeting, Hannover

Lorke, S., Brüning, A.; Bornschein, A.; Gilli, S.; Pohl, R.; Spano, M.; van der Meer, J.; Werk, S.; Schüttrumpf, H. (2010); On the effect of wind and current on wave run-up and wave overtopping; 32nd International Conference on Coastal Engineering. Shanghai

Lorke, S.; Schüttrumpf, H.; Bornschein, A.; Pohl, R.; van der Meer, J. W. (2010): FlowDike-D: Freibord-bemessung von Ästuar- und Seedeichen unter Berücksichtigung von Wind und Strömung. KFKI aktuell, Ausgabe 02/2010

Pohl, R. (2010); Neue Aspekte der Freibordbemessung an Fluss- und Ästuardeichen; Wasserbauliche Mitteilungen des Institutes für Wasserbau und Technische Hydromechanik der Technischen Universität Dresden, Heft 40, S. 467 - 478 (nicht beigefügt)

Rahlf, H.; Schüttrumpf, H. (2010); Critical overtopping rates for Brunsbüttel lock; 32nd International Conference on Coastal Engineering. Shanghai

Schüttrumpf, H. (2009) Wellenüberlauf an Deichen - Stand der Wissenschaft und aktuelle Untersuchungen. 3. Siegener Symposium "Sicherung von Dämmen, Deichen und Stauanlagen". Tagungsband

Van der Meer, J.; Hardeman, B.; Steendam, G.J.; Schüttrumpf, H.; Verheij, H. (2010) Flow depths and velocities at crest and inner slope of a dike, in theory and with the wave overtopping simulator. 32nd International Conference on Coastal Engineering. Shanghai

FLOWDIKE
INVESTIGATING THE EFFECT OF WIND AND CURRENT ON WAVE RUN-UP AND WAVE OVERTOPPING

Anja Brüning[1]; Stefano Gilli[2]; Stefanie Lorke[3]; Reinhard Pohl[4]; Flemming Schlütter[5]; Miroslav Spano[6]; Jentsje van der Meer[7]; Stefan Werk[8] and Holger Schüttrumpf[9]

Abstract: This study describes the experimental work and preliminary results of investigations made on the effects of wind and currents on wave run-up and wave overtopping. The tests were carried out in the shallow water wave basin at the DHI (Hørsholm / Denmark). A detailed description of the set-up and measurements will be given followed by a parametric and a regression analysis which aims at the development of reduction factors for wind, current and obliquity. This is done with respect to the existent design formulae in the Eurotop-Manual (2007) and the results are discussed with regard to former investigations.

INTRODUCTION

In the past, a variety of structures was built to protect the hinterland during high water levels from coastal flooding or river flooding. Common use in practice is the application of smooth sloped dikes as well as steep or vertical walls. Today the knowledge of the design water level, wind surge, wave run- up and/or wave

---

1 Institute for Hydraulic Engineering and Water Resources Management; RWTH Aachen University, Mies-van-der-Rohe-Str. 1; 52056 Aachen; Germany
anja_bruening@gmx.de
2 Institute for Hydraulic Engineering and applied Hydromechanics; TU Dresden; Germany
3 Institute for Hydraulic Engineering and Water Resources Management; RWTH Aachen University; Germany
4 Institute for Hydraulic Engineering and applied Hydromechanics; TU Dresden; Germany
5 DHI; Agern Allé 5,DK-2970 Hørsholm; Denmark
6 Brno University of Technology, Faculty of Civil Engineering, Veveri 95, 60200 Brno; Czech Republic
7 Van der Meer Consulting B.V;. P.O. Box 423; 8440 AK Heerenveen; The Netherlands
8 Leichtweiß-Institute for Hydraulic Engineering; Beethovenstr. 51°; 38106 Braunschweig; Germany
9 Institute for Hydraulic Engineering and Water Resources Management; RWTH Aachen University, Mies-van-der-Rohe-Str. 1; 52056 Aachen; Germany
schuettrumpf@iww.rwth-aachen.de

overtopping is used to determine the crest height of these structures. Due to the choice of the return interval of the design water level, the uncertainties in applied formulae for wave run-up or wave overtopping as well as the incoming wave parameters, wave overtopping can not be avoided.

Relevant for the freeboard design in wide rivers, estuaries and at the coast are the incoming wave parameters at the toe of the structure. These are influenced by local wind fields and strong currents - occurring at high water levels mostly parallel to the structure. Earlier investigations did not consider the combined effects of wind and current on wave run-up and wave overtopping. Only few papers, dealing either with wind effects or current influence, are published.

In 2006 Gonzalez-Escriva mentioned that strong winds may have multiple effects on wave run-up and wave overtopping (deformation of incoming wave field, generation and transport of spray, direct influence on wave run-up and wave overtopping). Especially for small overtopping rates and vertical structures the effect of wind might be significant (de Waal et al., 1996). On the other hand, the influence of wind can be neglected for high overtopping rates and/or low wind velocities (Ward et al., 1996). But it has to be stated that the information on wind influence is still scarce.

By now, no systematic investigations are available on the effect of currents on wave run-up and wave overtopping. Jensen and Frigaard (2000) performed a small number of model tests as a part of the EU-Opticrest project to investigate the influence of introducing an along shore current on wave run-up for a model of the Zeebrugge breakwater site. The results indicate an increase of the wave run-up height of about 20% by introducing a current of 1m/s in the model.

To achieve an improved design of structures the effects of wind and currents should not be neglected, otherwise the lack of knowledge results in too high and expensive structures, or in an under design of the flood protection structure which increases the risk of flooding. Therefore the objective of the EU-Hydralab-FlowDike-Project is to investigate the effects of wind and current within experimental tests. Data from former investigations like the KFKI[10] projects “Oblique wave attack at sea dikes”, “Loading of the inner slope of sea dikes by wave overtopping” and the CLASH-database are used to compare and integrate the test results in already existent design approaches.

EXPERIMENTAL SETUP

Configuration

The model tests were conducted in the shallow water wave basin of the DHI in Hørsholm (Denmark). The basin has a length of 35 m, a width of 25 m and can be flooded to a maximum water depth of 0.9 m. Along the east side (35 m in length) the basin is equipped with a multidirectional wave maker composed of 36-segments. The 0.5 m wide and 1.2 m high segments can be programmed to generate, multidirectional, long or short crested waves. Dynamic wave absorption for reflected waves is integrated in the wave generation with the DHI software by an automatic control system called Active Wave Absorption Control System (AWACS). For further absorption of reflection and diffraction effects gravel and metallic wave absorbers are placed on the edges of the dike.

The wave field containing incident and reflected waves as well as a directional spreading is determined by two arrays of 5 wave gauges (with a length of 60 cm) and an

10 KFKI – German Coastal Engineering Research Council (GCERC)

Acoustic Doppler Velocity Meter (ADV) respectively Minilab SD-12. An overview given in Fig. 1 demonstrates that each of them is orthogonally aligned between the wave maker and the overtopping unit per dike crest. The surface elevation is determined by wave gauges as a change of conductivity between two electronic wires. They should be calibrated for a constant water temperature at least once a day. Hereby a calibration factor of 10 cm/1 Volt is used.

To provide aligned streamlines within the channel three rows of beverage crates are used to straighten the inflow. For constant water depth of 0.5 m within the channel a stabilised current of approx. 0.3 m/s is achieved with a maximum pump capacity of 1.2 m³/s. The second investigated current of 0.15 m/s is adjusted by reducing the pump capacity to approx. 0.6 m³/s and raising the weir position from 32.16 cm to 38.66 cm above the ground.

The wind is generated by six wind generators placed on metal stands (80 cm high) in front of the wave generator. Therefore two different frequencies are set to produce a homogenous wind field with a maximum velocity of 10 m/s (49 Hz) and a lower one of 5 m/s (25 Hz).

Data collection is simplified by using the DHI Wave Synthesizer with an acquisition frequency of 25 Hz. All acquired data are stored in dfs0- and daf-files and calibration is easily set for most instrumentation in the user interface.

This study focuses on a dike structure with a slope of 1:3. The toe of the structure is situated in a distance of 6.5 m from the wave machine. It has an over all length of 26.5 m which is necessary to generate a homogeneous wave field in front of the dike for all investigated parameter combinations. The backside and crest of the dike are brick-built with a width of 0.3 m and its core is out of compacted gravel covered with 50 mm concrete. In order to acquire wave overtopping data for freeboard heights of 0.1 m and 0.2 m the dike is divided in two sections. The first 15 m upstream the weir, the dike has a crest height of 60 cm and 11.5 m further up the crest level is 70 cm from the basin floor. A variable crest extends the 70 cm crest 7 m further downstream. This additional part made of plywood is used to change the set-up configuration during the test programme.

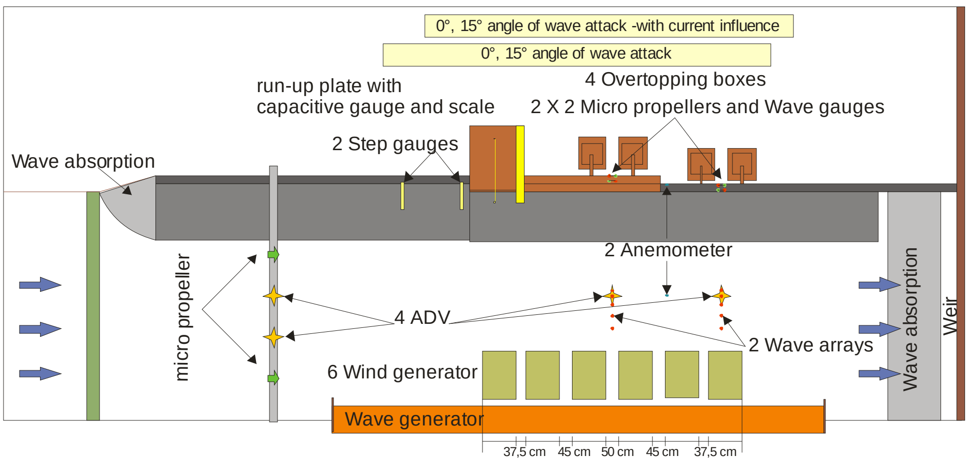

Fig. 1. Overview of the model with instruments and flow direction

A “run-up plate” of plywood (2 m x 2.5 m) is mounted on the concrete crest for the wave run-up measurement by a capacity gauge and video analysis. To prevent different roughness coefficients on the variable crest, the run-up plate and in the gap between concrete and plywood, a polish with sand is used.

The cross section for the wave overtopping unit is given in Fig. 2. For sampling of the overtopping volume a plywood channel is mounted at the landward edge of the crest and leads the incoming water directly into one of the four overtopping tanks. Two tanks are installed per section (60 cm and 70 cm crest) and the amount of water is measured by load cells and wave gauges. Dry boxes are constructed to prevent the tanks and load cells from uplift when the basin is flooded.

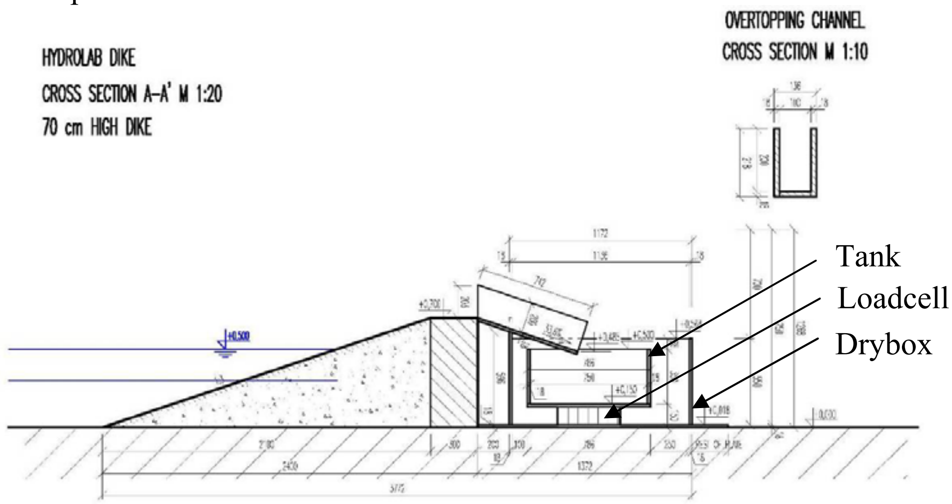

Fig. 2. Cross section of overtopping unit for the 70cm crest

Procedure

The test programme covers model tests on wave set-up, wave run-up and wave overtopping, with and without currents and with and without wind for different wave conditions. Short crested waves were generated for normal or oblique wave attack, respectively. Acquired raw data conduce to determine the degree of dependence of wave run-up and wave overtopping on wind, currents and incoming wave parameters.

A JONSWAP spectrum ($\gamma = 3.3$) is generated and controlled by using the Wave Synthesizer where a file for all six wave spectra could be stored. One test series was foreseen to contain all six wave spectra, differing from each other in significant wave height H_s, peak period T_p and Steepness s_0 as illustrated in Table 1.

Table 1. Jonswap Wave spectra – Parameters

Wave spectra	H_s [m]	T_p [s]	Steepness s_0 [-]	Duration [min]	No. of Waves
1	0.07	1.474	0.025	23	1021
2	0.07	1.045	0.05	16	1002
3	0.1	1.76	0.025	27	1004
4	0.1	1.243	0.05	19	1001
5	0.15	2.156	0.025	33	1002
6	0.15	1.529	0.05	24	1027

The testing time was optimised by dividing the dike in three separate parts to perform wave run- up and wave overtopping at the same time. Furthermore the domain of fully developed sea state is limited by the length of the wave maker. Thus with the influence of current and angle of wave attack the section for a reliable measurement of run-up and overtopping on the dike is restricted. Three different set-up configurations are installed to cover the effective measurement range for all angles of wave attack issued within the test programme. The change of set-up is not avoidable and the test programme has to be optimised for the parameters of interest. A detailed overview of the final test programme is given in Table 2.

Table 2. Final Test Programme

Testseries	**Wave direction** [°]	**Current** [m/s]	**Wind speed** [m/s]	**Wave spectra** (ref. to Table 1)
Set-up 1				
T3	0	0.3	0	1 to 6
T8	0	0.3	10	1, 3, 5
T19	-15	0.3	0	1 to 6
T16	15	0.3	0	1 to 6
T8b	0	0.3	5	1, 3, 5
T1	0	0	0	1 to 6
T6b	0	0	5	1, 3, 5
T6	0	0	10	1, 3, 5
T12	-15	0	0	1 to 6
T11 = T3b	0	0.15	0	1 to 6
T13	-15	0.15	0	1 to 6
T15	15	0.15	0	1 to 6
Set-up 2				
T2	-30	0	0	1 to 6
T7b	-30	0	5	1, 3, 5
T7	-30	0	10	1, 3, 5
T20	-30	0.15	0	1 to 6
T4	-30	0.3	0	1 to 6
T9b	-30	0.3	5	1, 3, 5
T9	-30	0.3	10	1, 3, 5
Set-up 3				
T18	45	0	0	1 to 6
T5	30	0.3	0	1 to 6
T14	45	0.3	0	1 to 6
T21	30	0.15	0	1 to 6
T17	45	0.15	0	1 to 6

EVALUATION OF MEASURED DATA

An evaluation of the measured raw data of the wave field, overtopping and run-up is done to analyse and present the results in order to develop or modify the existent design formulae. As described previously the raw data are available from a digitalisation with $\Delta t = 0.04$ sec ($f_s = 25$Hz). In order to reduce their extent to characteristic parameters, analyses driven by time domain or by frequency domain are used. In the following only the analysis of the wave field and wave overtopping will be discussed, since detailed run-up analysis will be done in the near future.

Determining the wave field in time domain, a zero-down crossing is applied, whereby single wave events are defined. From the certain quantity (No. of waves) of the wave height H, related average values for the maximum wave height H_{max} (peak to peak decomposition) and the mean wave period $T_{p,mean}$ (event duration), can be calculated. These values are the average of all wave gauges contributing to one of the wave arrays. Other characteristic wave height parameters in time domain, such as $H_{1/3}$, have not been analysed yet.

In frequency domain the wave parameters are analysed using a reflection analysis, wherein the reflection coefficient Cr is determined at the same time. The time-series of water level elevation is transformed and analysed by a FOURIER-transformation giving the spectral energy density S(f) for incident and reflected wave and their average. Based on the moments m_n of the spectral densities, characteristic wave parameters such as $H_{m0} = 4\ (m_0)^{1/2}$ or T_p can be calculated. Since $T_{-1,0}$ could not be calculated with the applied software, the clear relation between spectral and peak period $T_p = 1.1 * T_{-1,0}$ is used (Eurotop-Manual, 2007).

The overtopping is calculated by adding the lost pump volumes (recalculation from known capacity and working period) to the collected amount within the tank. By dividing the overtopping amount by the channel width of 0.118 m and the testing duration an average overtopping rate q in [l/s m] is determined.

For data analysis the following parameters were distinguished to be analysed in a first step:

- Evaluation from wave measurements:
  - Frequency domain: H_{m0}; T_p, $T_{0,1}$; $T_{0,2}$; T_p; Cr, $T_{-1,0}$
  - Time domain: H_{max}, $T_{p,mean}$, No. of waves
  - Plots: time series, energy density, reflection function
- Analysis from wave overtopping:
  - Time domain: overtopping waves for 0.1 m/0.2 m freeboard, q
  - Plots: time series, exceedance curves

PRELIMINARY RESULTS

Remarks

The tests were carried out with short crested waves using a JONSWAP spectrum. According to the test set up in Fig. 1 wave run-up and wave overtopping were measured in separate sections in the middle of the dike to avoid the influence of edge effects. As described in the previous chapter wave field analysis are implemented in time and frequency domain. Existent approaches and theoretical investigations are used to verify and compare the data.

Wave field

To validate the application of a homogenous JONSWAP spectrum, the results from reflection and crossing analysis are evaluated. From the reflection analysis which is performed in frequency domain, the plotted distribution of energy density in Fig. 3 corresponds to the theoretical assumption for a JONSWAP spectrum to be single peaked.

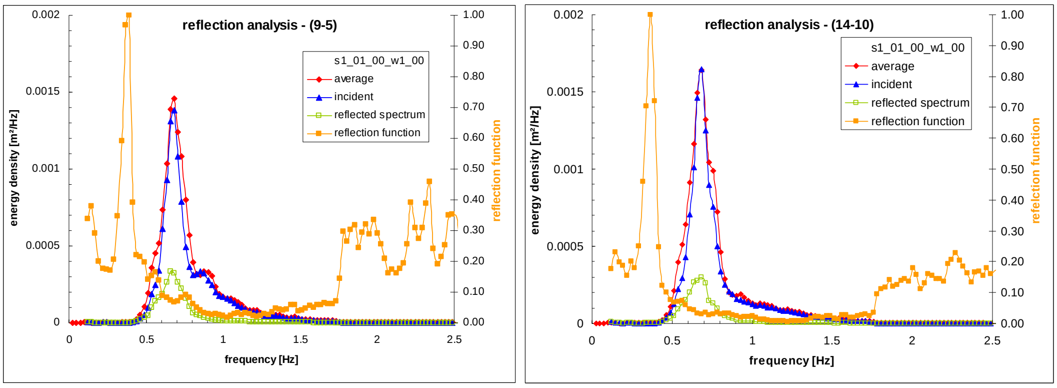

Fig. 3. Results for spectral energy density (frequency domain) for wave array 9-5 (left) and wave array 14-10 (right)

Fig. 4 depicts the Raleigh distribution of wave heights for both wave arrays, as it is common for JONSWAP spectra. The abscissa is fitted to a Raleigh scale; this is the reason why a linear distribution is noticeable. The similarity of their shape indicates the homogeneous arrangement for both crest heights.

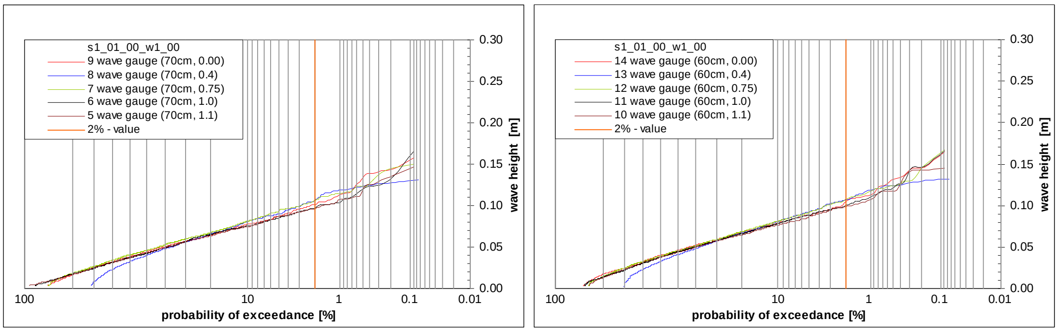

Fig. 4. Linear distribution of wave height H_{m0} over a Raleigh scale for a Jonswap spectrum for wave array 9-5 (left) and wave array 14-10 (right)

Homogeneity of wind field

To prove a homogeneous distributed wind field along the dike, the wind velocity for two different frequencies are measured with a propeller within defined distances. Reflection effects induced by the water surface and parallel flow from adjacent generators are observed by an increase of the velocity range.

In Fig. 5 and Fig. 6 the results for 49 Hz and 25 Hz are plotted along the dike. The wind velocity is assumed to be 10 m/s respectively 5 m/s in the following analyses.

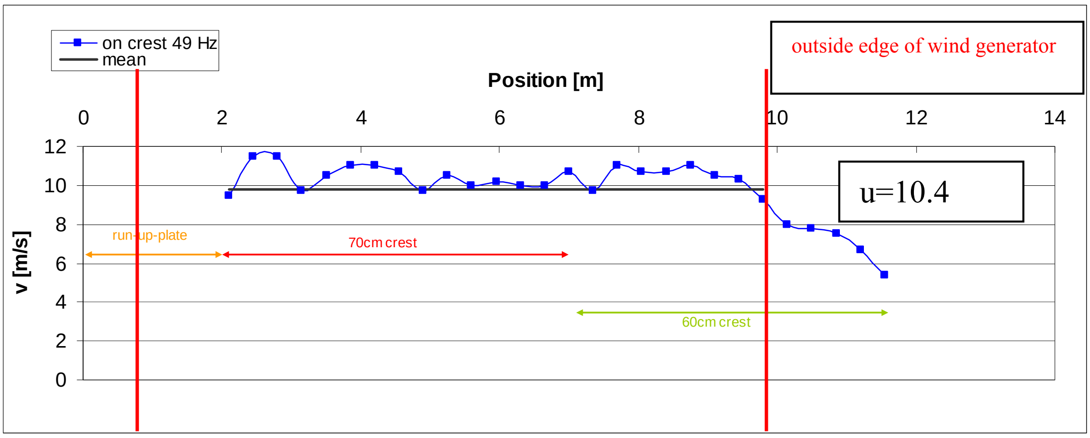

Fig. 5. Wind velocity distribution for a frequency of 49 Hz

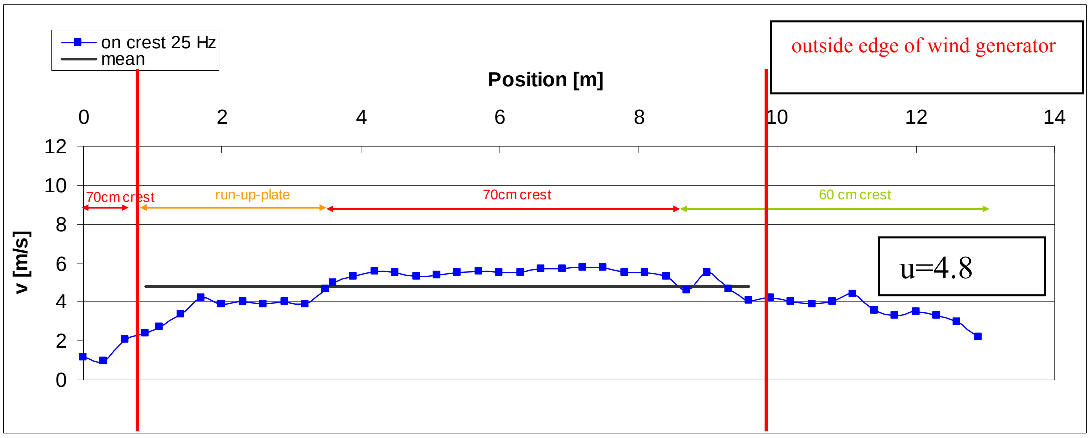

Fig. 6. Wind velocity distribution for a frequency of 25 Hz

Wave overtopping tests

The objective of the wave overtopping tests is to study the influence of currents and wind on the average wave overtopping rate q. Furthermore, the influence of oblique wave attack is identified and compared to former investigations by Oumeraci et al. (2001). Wave overtopping tests were performed corresponding to the test programme listed in Table 2. Using dimensionless factors for the average wave overtopping rate and a dimensionless freeboard height, presented in the Eurotop-Manual (2007), all four overtopping tanks for both crest heights could be included in the analysis. The dimensionless factors correspond to an exponential relationship used for the design formula of the average overtopping rate.

$$Q_* = Q_0 \cdot \exp(-b \cdot R_*) \qquad (1)$$

with: Q_0, b = dimensionless factors

Formulas for breaking ($\xi_{m\,1,0} < 2$; (2)) and non-breaking ($\xi_{m-1,0} \geq 2$; (3)) conditions determine the dimensionless parameters Q_* and R_* :

$$Q_* = \frac{q}{\sqrt{g \cdot H_{m0}{}^3}} \cdot \sqrt{\frac{s_{m-1,0}}{\tan\alpha}} \; ; \; R_* = \frac{R_C}{H_{m0}} \cdot \frac{\sqrt{s_{m-1,0}}}{\tan\alpha} \qquad (2)$$

with: $$\frac{1}{\xi_{m-1,0}} = \frac{\sqrt{s_{m-1,0}}}{\tan\alpha}$$

$$Q_* = \frac{q}{\sqrt{g \cdot H_{m0}{}^3}} \; ; \; R_* = \frac{R_C}{H_{m0}} \qquad (3)$$

where: Q_* = dimensionless overtopping rate; R_* = dimensionless freeboard; H_{m0} = significant wave height; $s_{m-1,0}$ = steepness; $\xi_{m-1,0}$ = Iribarren number (surf similarity parameter); α = angle of slope

Reduction factors for obliqueness and current (γ_θ; γ_C) and in case of the wind influence an increasing factor (γ_W) can be investigated by comparison of the different exponential coefficients b (see formula (4)). The coefficient b is obtained using a regression analysis for the test series of the decisive parameter, e.g. in Fig. 7 and Fig. 8 the corresponding graphs for current influence are shown. Therefore the distinction is made between breaking and non breaking waves.

$$\gamma_{\Theta,C,W} = \frac{b(\theta,C,W)}{b(\theta,C,W=0)} \qquad (4)$$

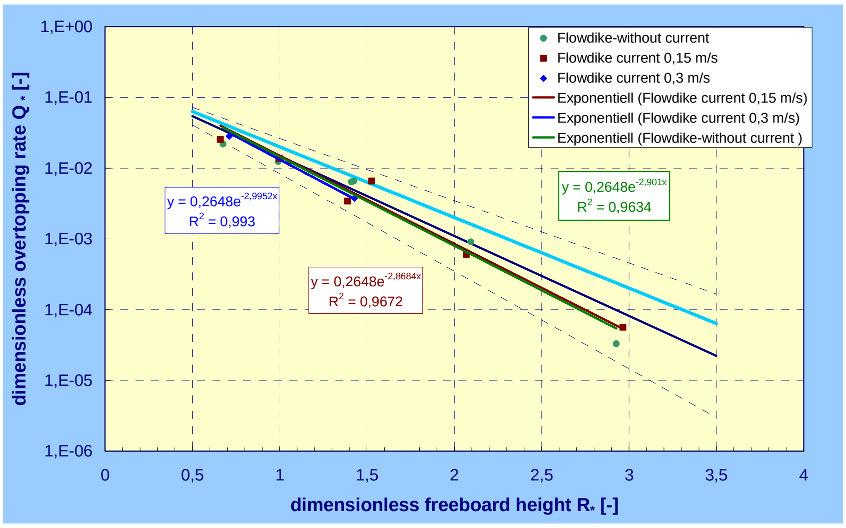

Fig. 7. Wave overtopping data influenced by current (non-breaking)

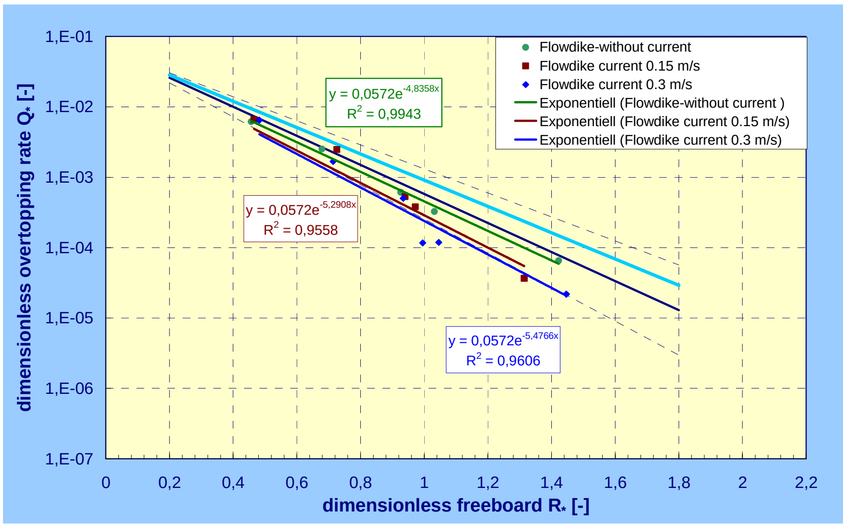

Fig. 8.Wave overtopping data influenced by current (breaking waves)

In Table 3 the calculated factors for all influencing parameters are summarised. It has to be mentioned, that all parameters included in the analyses are average values along the dike (average overtopping rate of two tanks per crest and characteristic wave parameters for each crest determined by the corresponding wave array). Furthermore, these results are preliminary and more detailed analyses will follow.

Validating the setup for oblique waves, the resulting reduction factors are compared with results from former investigations by Oumeraci et al. (2001) in Fig. 9.

Table 3. Factors for obliquity, current and wind influence

Breaking Waves			**Non-breaking Waves**		
θ	**b**	**γ_θ**	**θ**	**b**	**γ_θ**
0°	-4.8358	1.000	0°	-2.901	1.000
-15°	-5.1857	0.933	-15°	-3.016	0.962
-30°	-6.2685	0.771	-30°	-3.419	0.848
45°	-8.03	0.602	45°	No data	no data
Current	**b**	**γ_C**	**Current**	**B**	**γ_C**
0m/S	-4.8358	1.000	0m/S	-2.901	1.000
0.15m/s	-5.291	0.914	0.15m/s	-2.868	1.011
0.3m/S	-5.477	0.883	0.3m/S	-2.995	0.969
Wind	**b**	**γ_W**	**Wind**	**B**	**γ_W**
0m/S	-4.8358	1.000	0m/S	-2.901	1.000
5m/s	no data	no data	5m/s	-2.757	1.052
10m/S	no data	no data	10m/S	-2.730	1.063

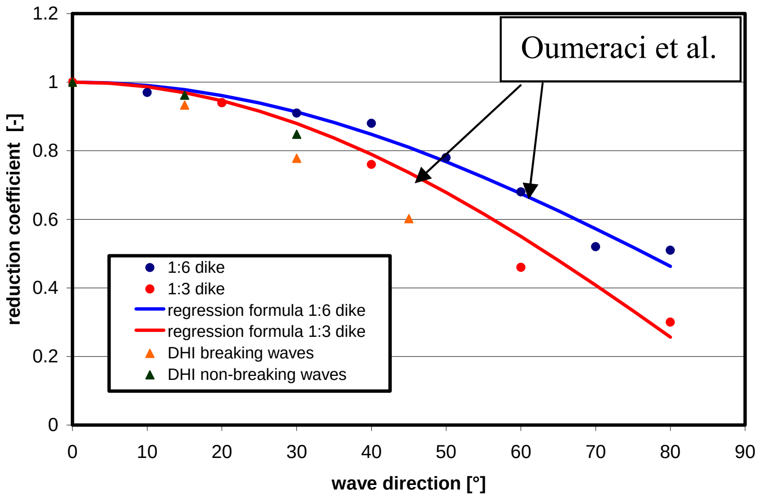

Fig. 9. Comparison of reduction coefficients

CONCLUSIONS

In the past a large variety of investigations concerning wave run-up and wave overtopping has been performed. Given by the diversity of influencing factors, uncertainties will still remain which have to be considered in the design of dikes in estuarine and coastal areas. Therefore, model tests are conducted in order to indicate these parameters. Parallel current and wind are two of the missing effects in freeboard design; hence model tests were performed in a shallow water wave basin at DHI (Denmark). The investigations carried out on a 1:3 sloped dike, used a JONSWAP spectrum with short crested waves.

As main objective of these tests can be declared:

- the influence of dike parallel currents on wave run-up and wave overtopping
- the influence of wind on wave run-up and wave overtopping, due to the direct influence by friction

First analysis covering the distribution of the wave field and the wind approved the sea state to be a JONSWAP spectrum and that the applied wind field is homogeneous. The model tests on wave overtopping confirmed the stated assumptions by Gonzalez-Escriva and de Waal concerning the significant wind impact on overtopping. Furthermore, the influence of oblique waves on overtopping has been validated. Preliminary correction factors (γ_θ; γ_C; γ_W) were designated for each influencing parameter of this validation. It can be stated that increasing overtopping volumes were determined for wind application, as well as decreasing volumes for test series with currents or oblique waves.

Finally the combined effects for wind, current and obliquity is still a matter of further analysis, especially the adoption of the factors by formulas has to be investigated. In addition, more theoretical work is required to determine the effect of currents on wave evolution and the resulting wave run-up and wave overtopping processes.

ACKNOWLEDGEMENTS

The model tests were conducted by RWTHUG in the Shallow Water Basin at DHI, Denmark, under Contract Number 022441 of the European Community- Structuring the European Research Area- Research Infrastructures. The financial contribution from the EC is appreciated.

The preparation of the model tests and the data analysis was supported by the German Coastal Engineering Research Council (GCERC/KFKI) and funded by the German Ministry of Education and Research (BMBF) under 03KIS075-076 "Freibordbemessung von See-, Ästuar- und Flussdeichen".

The additional testing week for extension of the number of tests was funded by Deltares.

The authors gratefully acknowledge this support, as well as the contributions of other colleagues in this research project, especially Jens Kirkegaard and Jesper Fuchs from the DHI in Hørsholm, Denmark.

REFERENCES

Eurotop-Manual (2007) "European Overtopping Manual", Eds Pullen, T., Allsop, N.W.H., Bruce, T., Kortenhaus, A, Schuttrumpf, H. & van der Meer, J.W., www.overtopping-manual.com

Gonzalez-Escriva, J.A. (2006) The role of wind in wave run-up and overtopping of coastal structures. Proc. 30th Int. Conf. on Coastal Engineering. San Diego

Jensen, M.S. and Frigaard, P. (2000) Zeebrugge model: Wave runup under simulated prototype storms (II) and The influence on wave run-up introducing a current. Report Hydraulics and Coastal Engineering Laboratory. Aalborg University. OPTICREST-project.

Oumeraci, H.; Schüttrumpf, H. & Möller, J. (2001): Influence of Oblique Wave Attack on Wave Run-up and Wave Overtopping - 3 D Model Tests at NRC/Canada with long and short crested Waves.

Oumeraci, H.; Schüttrumpf, H.; SAUER, W.; MÖLLER, J. & DROSTE, T. (2001): Physical Model Tests on Wave overtopping with Natural Sea States- 2 D Model Tests with single, double and multi peak wave energy spectra.

Waal, J.P.; Tönjes, P.; van der Meer, J.W. (1996) Wave overtopping of vertical structures including wind effect. Proc. 25th Int. Conf. on Coastal Engineering. Orlando. pp. 2216-2229

Ward, D.L.; Zhang, J.; Wibner, C. and Cinotto, C.M. (1996) Wind effects on run-up and overtopping of coastal structures. Proc. 25th Int. Conf. on Coastal Engineering. Orlando. pp. 2206-2215

Van der Meer, J.W.; Tönjes, P. & de Waal, J. (1998): A code for dike height design and examination. Proceedings Int. Conf. on Coastlines, Structures and Breakwaters. (Ed. N.W.H. Allsop) Thomas Telford. London

FLOWDIKE
INVESTIGATING THE EFFECT OF WIND AND CURRENT ON WAVE RUN-UP AND WAVE OVERTOPPING

Anja Brüning(1); Stefano Gilli(2); Stefanie Lorke(3); Reinhard Pohl(4); Flemming Schlütter(5); Miroslav Spano(6); Jentsje van der Meer(7); Stefan Werk(8) and Holger Schüttrumpf(9)

(1) Institute for Hydraulic Engineering and Water Resources Management; RWTH Aachen University, Germany, e-mail: anja_bruening@gmx.de
(2) Institute for Hydraulic Engineering and applied Hydromechanics; TU Dresden; Germany
(3) Institute for Hydraulic Engineering and Water Resources Management; RWTH Aachen University; Germany
(4) Institute for Hydraulic Engineering and applied Hydromechanics; TU Dresden; Germany
(5) DHI; Denmark
(6)Brno University of Technology, Faculty of Civil Engineering,; Czech Republic
(7) Van der Meer Consulting B.V Heerenveen; The Netherlands
(8) Leichtweiß-Institute for Hydraulic Engineering; Braunschweig; Germany
(9) Institute for Hydraulic Engineering and Water Resources Management; RWTH Aachen University,; Germany, e-mail: schuettrumpf@iww.rwth-aachen.de

This study describes the experimental work and preliminary results of investigations made on the effects of wind and currents on wave run-up and wave overtopping. The tests were carried out in the shallow water wave basin at the DHI (Hørsholm / Denmark). A detailed description of the set-up and measurements will be given followed by a parametric and a regression analysis which aims at the development of reduction factors for wind, current and obliquity. This is done with respect to the existent design formulae in the Eurotop-Manual (2007) and the results are discussed with regard to former investigations.

1. INTRODUCTION

In the past, a variety of structures was built to protect the hinterland during high water levels from coastal flooding or river flooding. Common use in practice is the application of smooth sloped dikes as well as steep or vertical walls. Today the knowledge of the design water level, wind surge, wave run-up and/or wave overtopping is used to determine the crest height of these structures. Due to the choice of the return interval of the design water level, the uncertainties in applied formulae for wave run-up or wave overtopping as well as the incoming wave parameters, wave overtopping can not be avoided.

Relevant for the freeboard design in wide rivers, estuaries and at the coast are the incoming wave parameters at the toe of the structure. These are influenced by local wind fields and strong currents - occurring at high water levels mostly parallel to the structure. Earlier investigations did not consider the combined effects of wind and current on wave run-up and wave overtopping. Only few papers, dealing either with wind effects or current influence, are published (see references).

2. EXPERIMENTAL SETUP

The model tests were conducted in the shallow water wave basin of the DHI in Hørsholm (Denmark). The basin has a length of 35 m, a width of 25 m and can be flooded to a maximum water depth of 0.9 m. Along the east side (35 m in length) the basin is equipped with a multidirectional wave maker composed of 36-segments. The 0.5 m wide and 1.2 m high segments can be programmed to generate, multidirectional, long or short crested waves. Dynamic wave absorption for reflected waves is integrated in the wave generation with the DHI software by an automatic control system called Active Wave Absorption Control System (AWACS). For further absorption of reflection and diffraction effects gravel and metallic wave absorbers are placed on the edges of the dike.

This study focuses on a dike structure with a slope of 1:3. The toe of the structure is situated in a distance of 6.5 m from the wave machine (Fig. 1). It has an over all length of 26.5 m which is necessary to generate a homogeneous wave field in front of the dike for all investigated parameter combinations. The backside and crest of the dike are brick-built with a width of 0.3 m and its core is out of compacted gravel covered with 50 mm concrete. In order to acquire wave overtopping data for freeboard heights of 0.1 m and 0.2 m the dike is divided in two sections. The first 15 m upstream the weir, the dike has a crest height of 60 cm and 11.5 m further up the crest level is 70 cm from the basin floor. A variable crest extends the 70 cm crest 7 m further downstream. This additional part made of plywood is used to change the set-up configuration during the test programme.

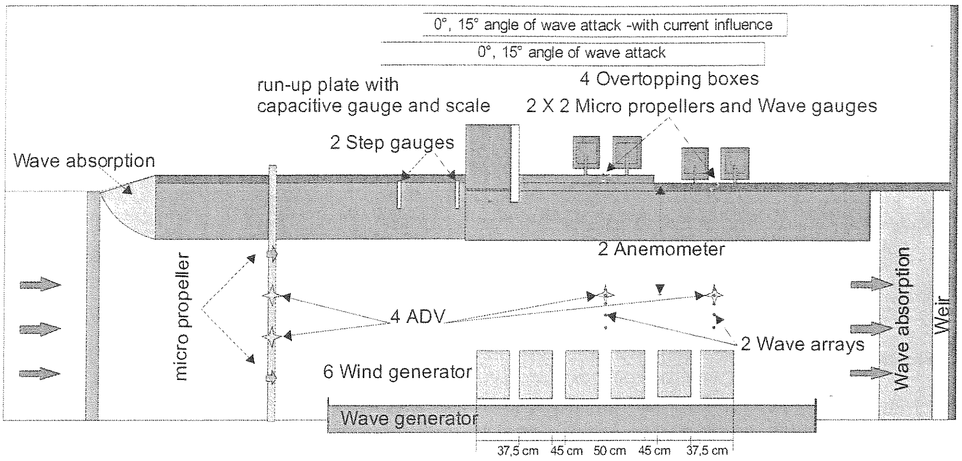

Fig. 1. Overview of the model with instruments and flow direction

The cross section for the wave overtopping unit is given in Fig. 2. For sampling of the overtopping volume a plywood channel is mounted at the landward edge of the crest and leads the incoming water directly into one of the four overtopping tanks. Two tanks are installed per section (60 cm and 70 cm crest) and the amount of water is measured by load cells and wave gauges. Dry boxes are constructed to prevent the tanks and load cells from uplift when the basin is flooded.

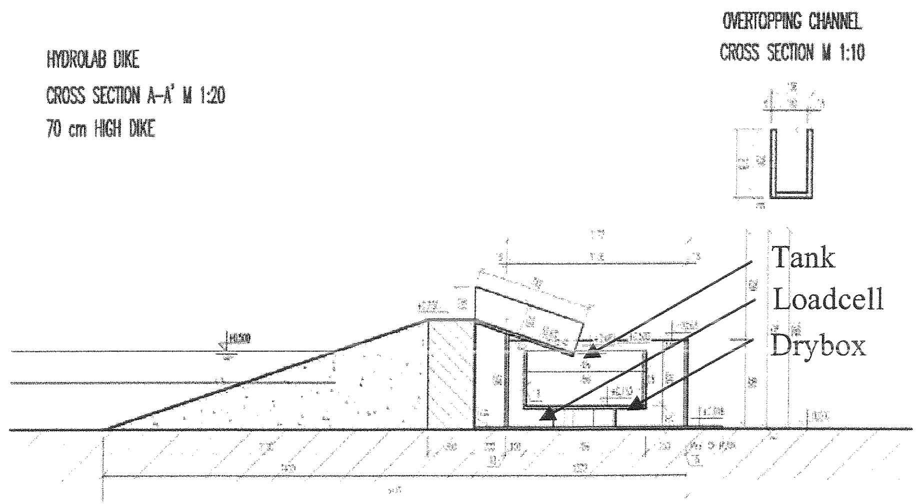

Fig. 2. Cross section of overtopping unit for the 70cm crest

3. PRELIMINARY RESULTS

Remarks

The tests were carried out with short crested waves using a JONSWAP spectrum. According to the test set up in Fig. 1 wave run-up and wave overtopping were measured in separate sections in the middle of the dike to avoid the influence of edge effects. As described in the previous chapter wave field analysis are implemented in time and frequency domain. Existent approaches and theoretical investigations are used to verify and compare the data.

Wave overtopping tests

The objective of the wave overtopping tests is to study the influence of currents and wind on the average wave overtopping rate q. Furthermore, the influence of oblique wave attack is identified and compared to former investigations by Oumeraci et al. (2001). Wave overtopping tests were performed in addition to wave run-up tests. Using dimensionless factors for the average wave overtopping rate and a dimensionless freeboard height, presented in the Eurotop-Manual (2007), all four overtopping tanks for both crest heights could be included in the analysis. The dimensionless factors correspond to an exponential relationship used for the design formula of the average overtopping rate.

$$Q_* = Q_0 \cdot \exp(-b \cdot R_*) \tag{1}$$

with: Q_0, b = dimensionless factors.

Reduction factors for obliqueness and currents (γ_θ; γ_C) and in case of the wind influence an increasing factor (γ_W) can be investigated by comparison of the different exponential coefficients b (see formula (2)). The coefficient b is obtained using a regression analysis for the test series of the decisive parameter, e.g. in Fig. 3 the corresponding graphs for current influence are shown. A distinction is also made between breaking and non breaking waves.

$$\gamma_{\Theta,C,W} = \frac{b(\theta,C,W)}{b(\theta,C,W=0)} \tag{2}$$

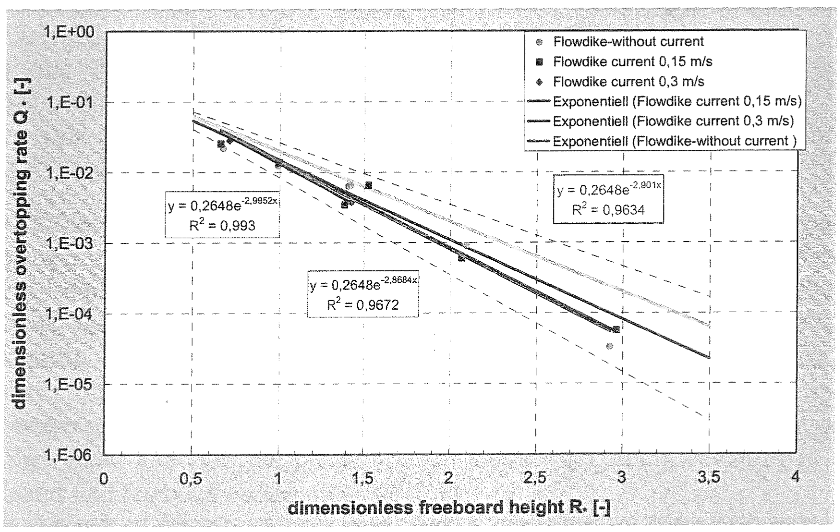

Fig. 3. Wave overtopping data influenced by current (non-breaking)

4. CONCLUSIONS

In the past a large variety of investigations concerning wave run-up and wave overtopping has been performed. Given by the diversity of influencing factors, uncertainties will still remain which have to be considered in the design of dikes in estuarine and coastal areas. Therefore, model tests are conducted in order to indicate these parameters. Parallel current and wind are two of the missing effects in freeboard design; hence model tests were performed in a shallow water wave basin at DHI (Denmark). The investigations carried out on a 1:3 sloped dike, used a JONSWAP spectrum with short crested waves.

The influence of oblique waves on overtopping has been validated. Preliminary correction factors (γ_θ; γ_C; γ_W) were designated for each influencing parameter of this validation. It can be stated that increasing overtopping volumes were determined for wind application, as well as decreasing volumes for test series with currents or oblique waves.

Finally the combined effects for wind, current and obliquity is still a matter of further analysis, especially the adoption of the factors by formulas has to be investigated. In addition, more theoretical work is required to determine the effect of currents on wave evolution and the resulting wave run-up and wave overtopping processes.

REFERENCES

Eurotop-Manual (2007) "European Overtopping Manual", Eds Pullen, T., Allsop, N.W.H., Bruce, T., Kortenhaus, A, Schuttrumpf, H. & van der Meer, J.W., www.overtopping-manual.com

Gonzalez-Escriva, J.A. (2006) The role of wind in wave run-up and overtopping of coastal structures. Proc. 30th Int. Conf. on Coastal Engineering. San Diego

Oumeraci, H.; Schüttrumpf, H. & Möller, J. (2001): Influence of Oblique Wave Attack on Wave Run-up and Wave Overtopping - 3 D Model Tests at NRC/Canada with long and short crested Waves.

Waal, J.P.; Tönjes, P.; van der Meer, J.W. (1996) Wave overtopping of vertical structures including wind effect. Proc. 25th Int. Conf. on Coastal Engineering. Orlando. pp. 2216-2229

Ward, D.L.; Zhang, J.; Wibner, C. and Cinotto, C.M. (1996) Wind effects on run-up and overtopping of coastal structures. Proc. 25th Int. Conf. on Coastal Engineering. Orlando. pp. 2206-2215

Van der Meer, J.W.; Tönjes, P. & de Waal, J. (1998): A code for dike height design and examination. Proceedings Int. Conf. on Coastlines, Structures and Breakwaters. (Ed. N.W.H. Allsop) Thomas Telford. London

ON THE EFFECT OF CURRENT
ON WAVE RUN-UP AND WAVE OVERTOPPING

Stefanie Lorke[1]; Anja Brüning[1]; Jentsje van der Meer[2], Holger Schüttrumpf[1], Antje Bornschein[3]; Stefano Gilli[3]; Reinhard Pohl[3]; Miroslav Spano[4]; Jaromír Říha[4], Stefan Werk[5]; Flemming Schlütter[6]

Intention of the project FlowDike-D is to quantify the impacts of current and wind on wave run-up and wave overtopping and to consider these processes in existing design formulae for estuarine, river and sea dikes. Physical model tests were carried out in the shallow water basin at DHI (Hørsholm/Denmark) for two different dike geometries (1:3 and 1:6 sloped dike). The paper introduces the model setup and test programme followed by a short description of the applied instrumentation. The test results for wave run-up and wave overtopping with oblique and non-oblique wave attack, but without current, correspond well with existing formulae from the EurOtop-Manual (2007). The influence of current parallel to the dike combined with different angles of wave attack on wave overtopping and wave run-up has been quantified. A distinction was made between wave attack with and against the current.

Keywords: wave run-up, wave overtopping, physical model test, waves, current, dike, EurOtop-Manual

INTRODUCTION

Different types of structures, like smooth sloped dikes, are built worldwide to protect adjacent areas from river or coastal flooding during high water levels. In estuaries and along the coast the effect of tidal and storm induced current combined with local wind fields can influence the incoming wave parameters at the dike toe. Furthermore, the wave run-up height and the overtopping amount of water are influenced by the named parameters. Better understanding of wave run-up and wave overtopping processes on dikes leads to an improved design of the dike. The lack of knowledge in this research field may result either in too high and expensive flood protection structures or in a higher risk of flooding because of weak designs.

To consider two new aspects - a current parallel and a wind perpendicular to the dike line - physical model tests were performed within two test phases in 2009 at DHI in Hørsholm, Denmark. In the first test phase (EU-Hydralab-FlowDike project) a 1:3 sloped dike was investigated, while a 1:6 sloped dike was tested in the second test phase (BMBF-KFKI-FlowDike-D project). The compilation of both test phases, using the results for the 1:3 dike as well as the results for the 1:6 dike, is done within the FlowDike-D-project.

The main intention of these tests was to determine the run-up height and overtopping amount of water depending on current and wind and combining these parameters with different angles of wave attack. Tests were performed using two dike slopes at two different dike heights each. The four resulting dike configurations were exposed to six different wave conditions. Additionally, flow velocities and flow depths have been measured on the dike crests.

EXPERIMENTAL SETUP

General Configuration

Figure 1 gives an overall view of the model setup in the 35 m wide shallow water basin at DHI. The 16 m wide wave generator is able to create multidirectional wave spectra as well as long-crested waves. The wind generator was installed in front of and above the wave generator to create a wind field with velocities up to 10 m/s at the dike crest. The 26 m long concrete dike was placed opposite of the wave wordgenerator. The dike was divided into two parts with different crest levels. With this setup it was possible to measure the wave overtopping rate for two different freeboard heights.

[1] Institute for Hydraulic Engineering and Water Resources Management (IWW), RWTH Aachen University, Mies-van-der-Rohe-Strasse 1, 52056 Aachen, Germany; lorke@iww.rwth-aachen.de; anja_bruening@gmx.de; schuettrumpf@iww.rwth-aachen.de
[2] Van der Meer Consulting B.V;. P.O. Box 423, 8440 AK Heerenveen, The Netherlands; jm@vandermeerconsulting.nl
[3] Institute of Hydraulic Engineering and Technical Hydromechanics (IWD), TU Dresden, 01062 Dresden, Germany; antje.bornschein@tu-dresden.de; Stefano.Gilli@tu-dresden.de; Reinhard.Pohl@tu-dresden.de
[4] Faculty of Civil Engineering, Brno University of Technology, Veveri 95, 602 00 Brno, Czech Republic; spano.m@fce.vutbr.cz; riha.j@fce.vutbr.cz
[5] Leichtweiß-Institute for Hydraulic Engineering and Water Resources (LWI), Department of Hydromechanics and Coastal Engineering, TU Braunschweig, Beethovenstr. 51a, 38106 Braunschweig; Germany; s.werk@tu-bs.de
[6] Danish Hydraulic Institute (DHI), Agern Allé 5, 2970 Hørsholm, Denmark; fls@dhigroup.com

The wave overtopping volume was measured using two overtopping boxes for each dike section. Overtopping was measured by weighing the overtopping water, which enables a wave by wave analysis. A wave run-up board was located beside the overtopping boxes. An intake basin which was filled by a deep well water pump was located upstream of the wave basin (on the left side in Figure 1). At the boundary between the intake basin and the wave basin a flow straightener was installed. This installation ensured a flow direction parallel to the dike and a uniform inflow across the flow cross-section. The outflow of the wave basin was regulated by a weir with an adjustable crest height to enable different current velocities parallel to the dike. In front of the weir a wave absorber made of perforated metal plates was installed to avoid wave reflection.

While testing water was in front and behind the dike. An opening near the inflow (see Figure 1) allowed the overtopped water to flow back and to ensure a constant water depth in front of the dike.

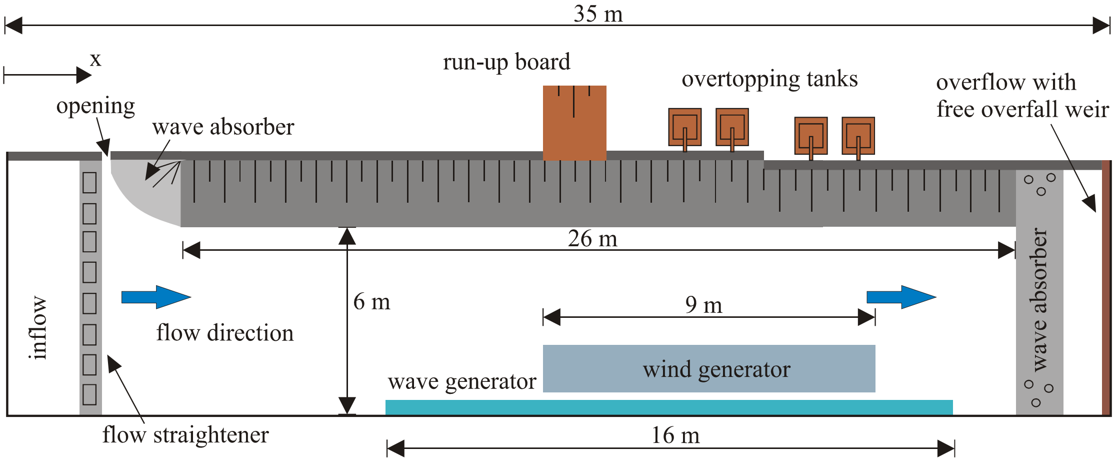

Figure 1. Topview of the model setup, 1:3 slope

TEST PROGRAMME

The test programme covered model tests with and without current and with and without wind for normal and oblique wave attack. Six different long-crested waves using a Jonswap spectrum were applied. Table 1 presents a summary of the test programme. Normal wave attack is defined with an angle of β = 0°. Positive angles of wave attack are in the direction of the current, while negative angles of wave attack are directed against the current.

Table 1. Summary of the test programme and test configurations

freeboard height R_C [m]	1:3 dike: 0.10 and 0.20 1:6 dike: 0.05 and 0.15							
wave spectrum	longcrested waves using a Jonswap spectrum							
wave height H_s [m] and wave period T_p [s]	1:3 dike:	H_s	0.07	0.07	0.10	0.10	0.15	0.15
		T_P	1.474	1.045	1.76	1.243	2.156	1.529
	1:6 dike:	H_s	0.09	0.09	0.12	0.12	0.15	0.15
		T_P	1.67	1.181	1.929	1.364	2.156	1.525
angle of wave attack β [°]	-45 -30 -15 0 +15 +30							
current v_x [m/s]	0.00 0.15 0.30 0.40 (only 1:6 dike)							
wind u (at the dike crest) [m/s]	0 5 (only 1:3 dike)10							

INSTRUMENTATION

Wave field

The wave generator created long-crested waves using a Jonswap spectrum. The wave field was measured by two wave arrays of 5 wave gauges and a current meter each. Both wave arrays were located at the dike toe, one for each crest elevation. During the tests with the 1:6 sloped dike an additional wave array was installed directly in front of the wave generator to analyze the evolution of the wave field in the wave basin. The wave arrays were aligned orthogonal between the wave generator and the dike. The sampling rate for all measuring devices was 25 Hz (1:3 dike) and 40 Hz (1:6 dike).

Wave run-up

A 2 m wide and 2.5 m long plywood plate was installed as an extension of the dike slope in order to measure the wave run-up height (see Figure 2). The surface of the plywood plate was covered with sand which was fixed by means of shellac to provide a surface roughness similar to a concrete slope.

Two methods were applied to measure the wave run-up height. First, a capacitive run-up gauge on the run-up-board was used. The capacitive gauge was mounted in the middle of the run-up-plate. Second, a video camera recorded the wave run-up process. Therefore, an adhesive tape with a black/yellow gauge was fixed to the wave run-up plate. The wave run-up board was enlightened by a spotlight to ensure better contrast during the video recordings. The emitted beams of light met the optical axis of the digital cameras within an angle of 120°. For synchronizing all measurements a digital radio controlled clock with a 0.4 m x 0.4 m display was positioned on the left side of the run-up plate.

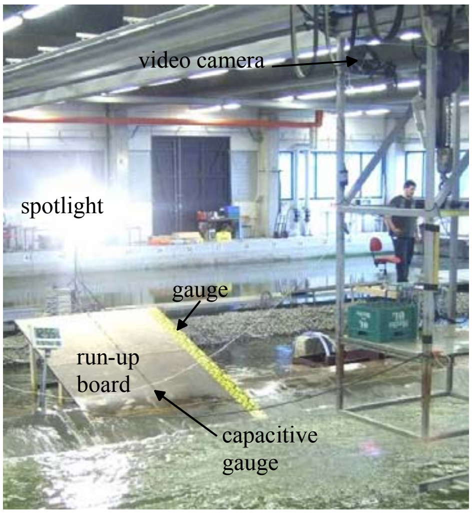

Figure 2. Wave run-up unit, 1:3 dike

Wave overtopping

The cross-section of an overtopping unit is sketched in Figure 3. On the left hand side the 1:3 sloped dike and the water level in front of the dike is shown. On the right hand side, the overtopping unit has been placed. A 0.1 m wide overflow channel was connected with the dike crest and led the overtopping water to the inner box of the overflow unit. The inner box had a total volume of 0.66 m³ and was weighed by a pressure cell. Because of the flooded wave basin also behind the dike, it was necessary to place the inner box in a water-tight external box.

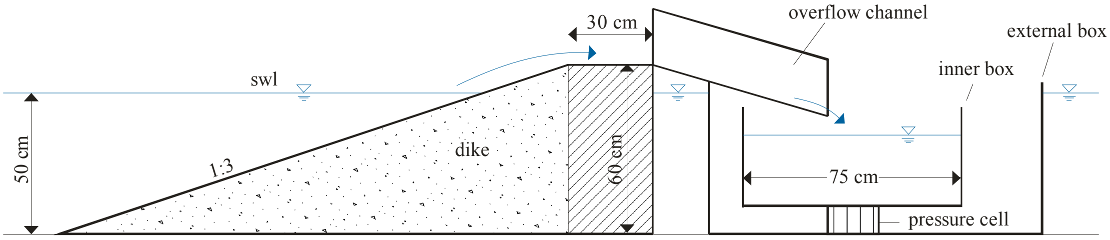

Figure 3. Cross-section of the overtopping unit on the 1:3 sloped dike

One of the four overtopping units (two behind each dike height) is shown in Figure 4. The photo was taken from the rear of the dike. At the photo the water flows from the back crest via the overflow channel into the inner box. Depending on the incoming wave field in front of the dike, the overtopping tanks were sometimes too small to capture the full amount of water for a single test. Then the tanks had to be emptied several times during the test duration of about 30 minutes. Hence, a pump with a predetermined flow was placed in each tank. All pumps (each of them in one of the inner boxes of the four overtopping units) had been connected with the data acquisition system. From the pumping curve and the start and end time of pumping, the lost amount of water could be recalculated to get the whole overtopping volume. An additional pump is located in each external box.

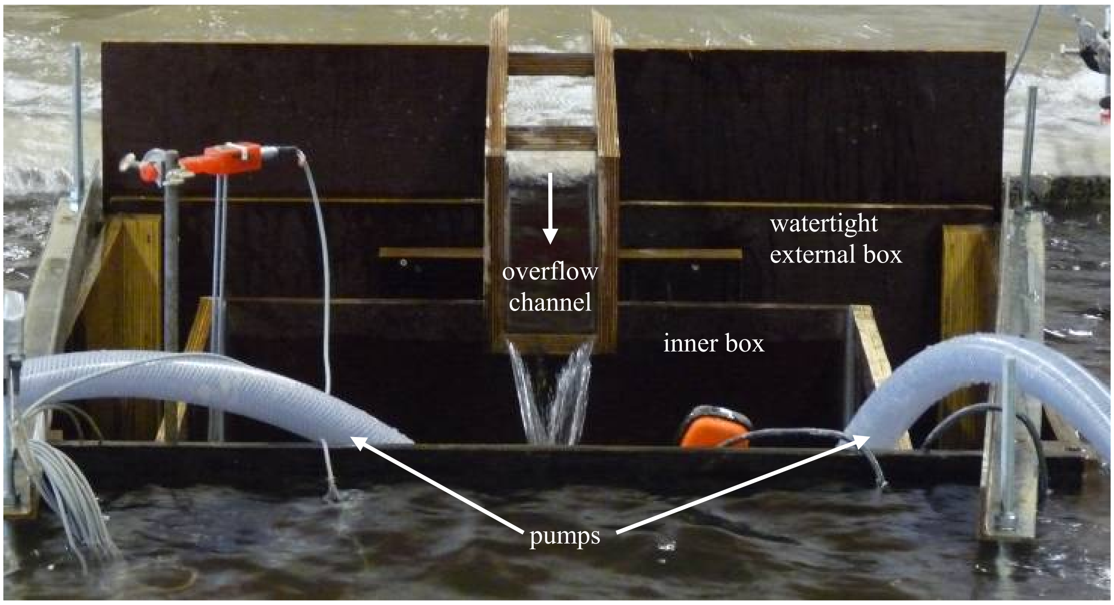

Figure 4. Overtopping unit seen from behind the dike

THEORY - WAVE AND CURRENT INTERACTION

The model tests were performed with and without a current parallel to the dike. Since the wave propagation is different in flowing water and in still water, it is required to interpret the following results with respect to the interaction of waves and current (Treloar, 1986). Two main aspects have to be considered while interpreting the results:

- current induced shoaling: absolute and relative wave parameters
- current induced wave refraction: energy propagation

The wave propagation path can be divided into two parts. The first part reaches from the wave generator to the dike toe. The second part extends from the dike toe to the dike crest. The first part from the wave generator to the dike toe can be determined using the following formulae for the two aspects:

Absolute and relative wave parameters

If a wave propagates on a current, a distinction has to be made between relative and absolute wave parameters and can be described by using the wave celerity. The relative wave celerity is the celerity relative to an observer who moves with the current, while the absolute celerity is defined as the velocity compared to a stationary observer and the ground, respectively.

The wave arrays in front of the dike measured the wave field with its absolute parameters. According to Hedges (1987), Treloar (1986) and Holthuijsen (2007) waves act only with its relative parameters. To determine the relative wave period $T_{rel,m-1,0}$ from the measured absolute wave period $T_{abs,m-1,0}$, the absolute angular frequency ω_{abs} has to be equalized to the sum of the relative angular frequency ω_{rel} and the corresponding constituent of the current ($k \cdot v_n$) (cf. Holthuijsen, 2007):

$$\omega_{abs} = \omega_{rel} + k \cdot v_n = \sqrt{gk \cdot \tanh(k \cdot d)} + k \cdot v_n \qquad (1)$$

with

ω_{abs} absolute angular frequency [rad/s]
ω_{rel} relative angular frequency [rad/s]
k wave number [rad/m]
v_n current velocity in the direction of wave propagation [m/s]
d flow depth [m]

The absolute angular frequency is defined as:

$$\omega_{abs} = \frac{2\pi}{T_{abs,m-1,0}} \qquad (2)$$

with the absolute spectral period $T_{abs,m-1,0}$ (EurOtop 2007)

$$T_{abs,m-1,0} = \frac{T_P}{1.1} \qquad (3)$$

with T_P spectral peak period [s]

By using eq. (1) and (2), the wave number k can be determined iteratively by using the measured absolute wave period $T_{abs,m-1,0}$, the known flow depth d and the current velocity in the direction of wave propagation v_n (cf. Figure 5):

$$v_n = v_x \cdot \sin\beta \qquad (4)$$

with the current velocity parallel to the dike v_x and the angle of wave attack relative to the normal of the dike β.

The relative angular frequency ω_{rel} results in

$$\omega_{rel} = \sqrt{g \cdot k \cdot \tanh(k \cdot d)} \qquad (5)$$

and leads to the relative wave period $T_{rel,m-1,0}$:

$$T_{rel,m-1,0} = \frac{2\pi}{\omega_{rel}} \qquad (6)$$

The relative wave period $T_{rel,m-1,0}$ decreases when the wave propagates against the current and increases by wave propagation with the current (cf. formula (1) and (4)).

Angle of wave energy

Figure 5 shows schematically the combination of the two vectors for the current and the wave direction for negative (left) and positive (right) angles of wave attack. The dashed arrow describes the relative direction of the wave attack generated by the wave generator and the corresponding angle β. The dotted arrow indicates the direction of the current parallel to the dike. According to Holthuijsen (2007) the current does not change the angle of wave attack but its energy direction by the combination of the two vectors current velocity v_x and relative group velocity $c_{g,rel}$ marked with the corresponding arrow. As shown in Figure 5, negative angles of wave attack lead to a smaller absolute value of the angle of wave energy β_e whereas positive angles of wave attack lead to a higher angle of wave energy β_e than the angle of wave attack β.

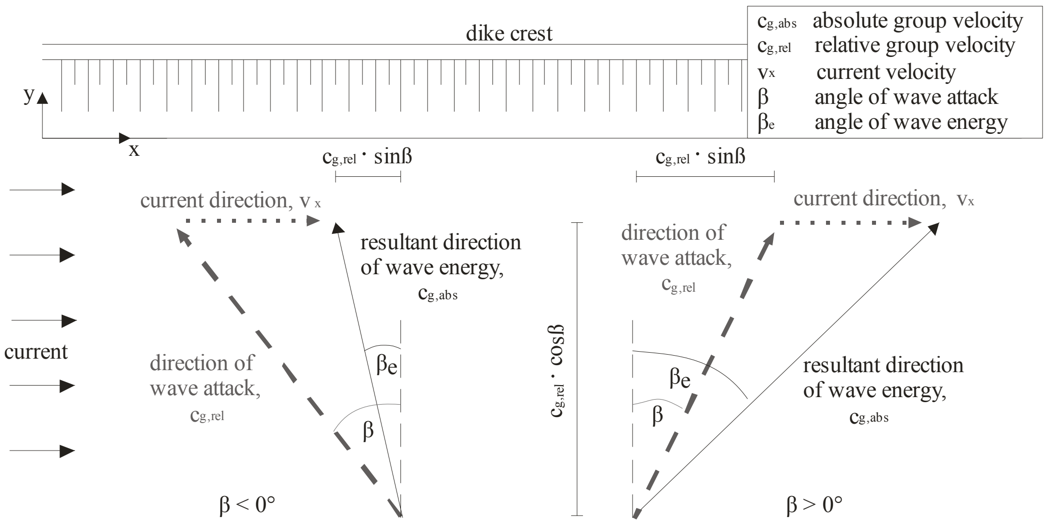

Figure 5. Interaction between wave direction and current

With the help of Figure 5 the angle of wave energy β_e is determined by the relative group velocity $c_{g,rel}$, the angle of wave attack β and the current velocity v_x by the trigonometrical function:

$$\tan\beta_e = \frac{c_{g,rel} \cdot \sin\beta + v_x}{c_{g,rel} \cdot \cos\beta} \qquad (7)$$

Herein the relative group velocity $c_{g,rel}$ is determined by the following formula:

$$c_{g,rel} = \frac{\partial\omega}{\partial k} = \frac{\partial\left(\sqrt{g \cdot k \cdot \tanh(k \cdot d)}\right)}{\partial k} \tag{8}$$

which leads to:

$$c_{g,rel} = 0.5 \cdot \frac{\omega_{rel}}{k}\left(1 + \frac{2 \cdot k \cdot d}{\sinh(2 \cdot k \cdot d)}\right) \tag{9}$$

METHOD OF ANALYSIS

The EurOtop-Manual (2007) has been used to analyse the data and to derive influencing factors including current. The EurOtop-Manual (2007) distinguishes between formulae for wave run-up and wave overtopping, for breaking and non-breaking wave conditions.

Wave run-up

Usually the influence of different factors on wave run-up height could be determined using a formula which was originally suggested by Hunt (1959) and than upgraded in EurOtop-Manual (2007) with different correction parameters:

$$\frac{R_{u2\%}}{H_{m0}} = c_1 \cdot \gamma_b \cdot \gamma_f \cdot \gamma_\beta \cdot \xi_{m-1,0} \tag{10}$$

with its maximum:

$$\frac{R_{u2\%}}{H_{m0}} = \gamma_f \cdot \gamma_\beta \cdot \left(c_2 - \frac{c_3}{\sqrt{\xi_{m-1,0}}}\right) \tag{11}$$

with

- $R_{u2\%}$ wave run-up height which will be exceeded by 2% of all wave run-ups [m]
- γ_b parameter which covers the influence of a berm [-]
- γ_f parameter which covers the influence of surface roughness [-]
- γ_β parameter which covers the influence of wave direction (angle β) [-]
- $\xi_{m-1,0}$ breaker parameter based on $s_{m-1,0}$ [-]
- $s_{m-1,0}$ wave steepness based on H_{m0} and $L_{m-1,0}$ [-]
- $L_{m-1,0}$ deep water wave length based on $T_{m-1,0}$ [m]
- $T_{m-1,0}$ spectral wave period [s]
- H_{m0} significant wave height from spectral analysis [m]

The empirical parameters c_1, c_2 and c_3 are dimensionless and defined as follow:

$$c_2 = c_1 \cdot \xi_{tr} + c_3 / \xi_{tr} \tag{12}$$

with

- ξ_{tr} surf parameter describing the transition between breaking and non breaking waves [-]

For a prediction of the average run-up height $R_{u2\%}$ the following values $c_1 = 1.65$, $c_2 = 4.0$ and $c_3 = 1.5$ should be used.

Wave overtopping

Formulae (13) can be used to calculate the average overtopping discharge q per meter dike length for given geometry and wave condition. As the non breaking condition the overtopping discharge limits to a maximum value, see formula (14). The smallest value of both equations should be taken as the result.

Breaking wave conditions:

$$\frac{q}{\sqrt{g \cdot H_{m0}^{3}}} = \frac{0.067}{\sqrt{\tan\alpha}} \cdot \gamma_b \cdot \xi_{m-1,0} \cdot \exp\left(-4.75 \frac{R_C}{\xi_{m-1,0} \cdot H_{m0} \cdot \gamma_b \cdot \gamma_f \cdot \gamma_\beta \cdot \gamma_\upsilon}\right) \quad (13)$$

With a maximum for non breaking wave conditions:

$$\frac{q}{\sqrt{g \cdot H_{m0}^{3}}} = 0.2 \cdot \exp\left(-2.6 \frac{R_C}{H_{m0} \cdot \gamma_f \cdot \gamma_\beta}\right) \quad (14)$$

with

- q mean overtopping discharge per meter structure width [m³/s/m]
- α slope of the front face of the structure [°]
- R_c crest freeboard of structure [m]
- γ_υ correction factor for a vertical wall on the slope [-]

Furthermore, reduction factors for wave overtopping for obliqueness γ_β can be determined by comparing the exponential coefficients b_β for oblique wave attack ($\beta \neq 0$) and normal wave attack ($\beta = 0$):

$$\gamma_\beta = \frac{b_{\beta=0}}{b_\beta} \quad (15)$$

A new reduction factor $\gamma_{\beta,cu}$ is introduced in the same way to take the influence of current v_x into account:

$$\gamma_{\beta,cu} = \frac{b_{\beta=0,cu=0}}{b_{\beta,cu}} \quad (16)$$

FIRST RESULTS

Definitions and Remarks

- Reference tests are defined as tests with perpendicular wave attack, without current and without wind but with different wave parameters.
- Normal wave attack is equivalent to a wave angle of $\beta = 0°$.
- Wave attack along with the current is described by positive angles of wave attack, whereas wave attack against the current gives negative angles.
- The 1:3 sloped dike was analyzed for breaking and non breaking waves, while the 1:6 sloped dike was investigated only for breaking waves, as for such a gentle slope only breaking conditions were present.
- Changes of wave heights due to current are measured by the wave gauges at the toe of the dike.

Wave run-up

To validate the overall model setup, results from reference tests (1:3 dike as well as 1:6 dike) are compared to data of former investigations. Figure 6 shows calculated values of relative wave run-up height $R_{u2\%}/H_{m0}$ versus breaker parameter $\xi_{m-1,0}$. Several functions of former investigations have been added to the figure including equation (10) and (11) by EurOtop-Manual (2007). Values for H_{m0} were obtained analysing measurement results of the wave array which was situated closer to the run-up plate. Values for wave run-up height were measured by the capacitive gauge.

Relative wave run-up of reference model test is little lower than expected by EurOtop 2007. This is explicable because the function of EurOtop-Manual (2007) is only valid for smooth dike slopes. The rougher surface of the dike slope in the model setup causes slightly lower wave run-up heights. Breaker parameter $\xi_{m-1,0}$ is greater than 0.8 for 1:6 dike model tests and greater than 1.5 for the 1:3 dike model tests.

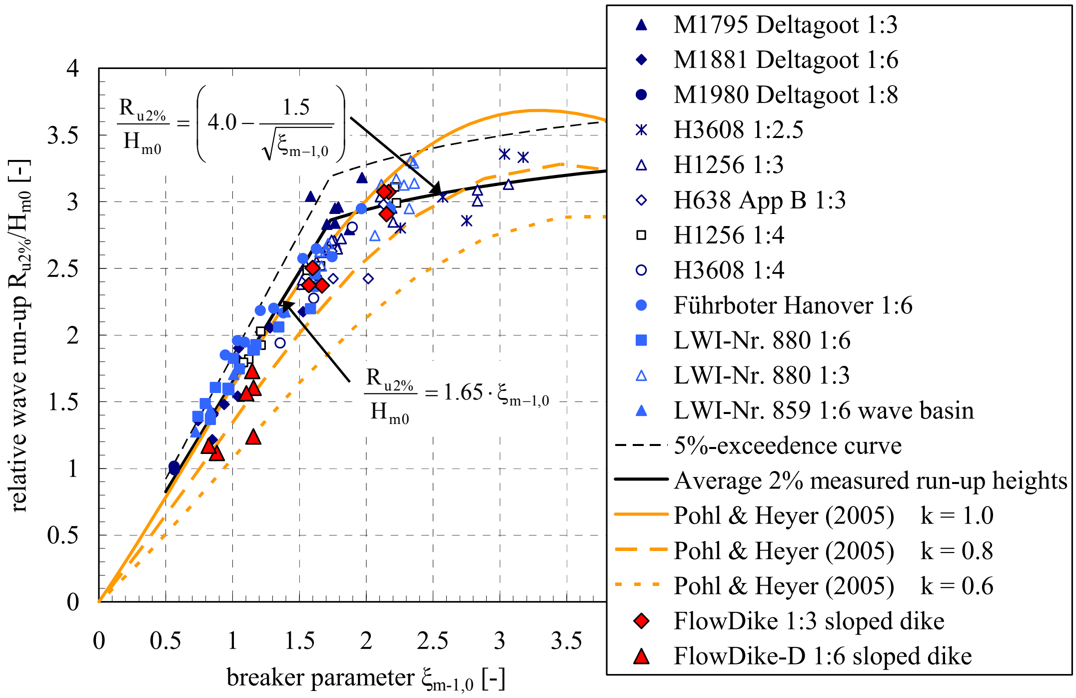

Figure 6. Relative wave run-up height $R_{u2\%}/H_{m0}$ versus breaker parameter $\xi_{m-1,0}$ – comparison between reference tests and former investigations from the EurOtop-Manual (2007)

It was expected that the wave run-up considering oblique wave attack is lower than wave run-up with orthogonal wave direction. In addition decreasing wave run-up height because of a dike parallel current was anticipated. In order to determine an average reduction factor γ_β as the ratio between relative run-up heights of model tests with oblique wave attack, current and/or wind against relative run-up height of the reference test linear regression was used as one can see in Figure 7. The factor γ_β is equal to the slope of the regression line.

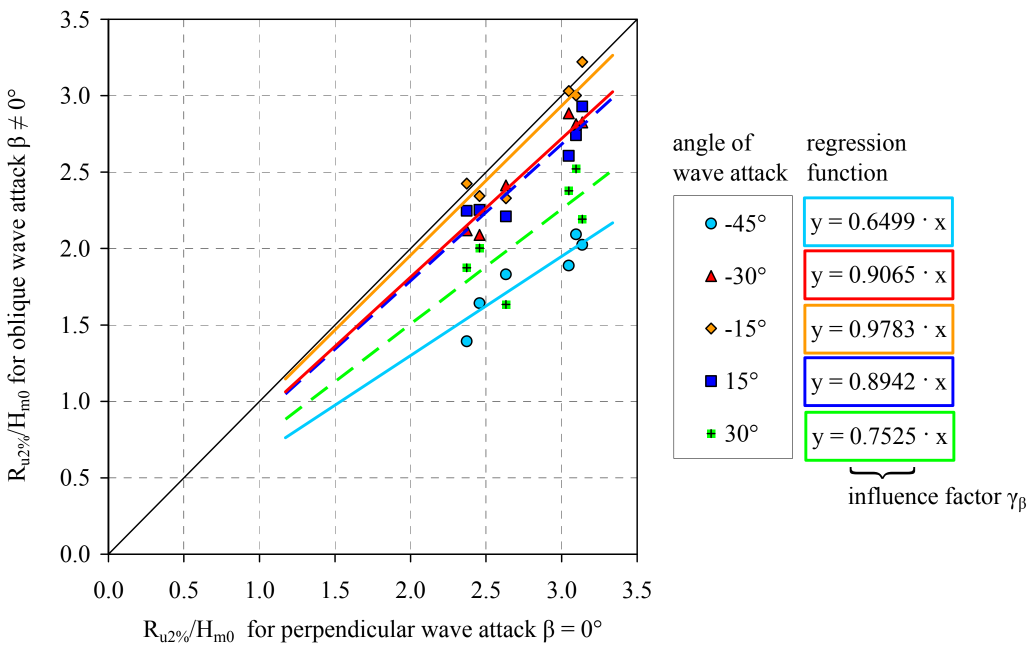

Figure 7. Relative wave run-up height: comparison between reference tests (β = 0) and model tests with oblique wave attack (current velocity v_x = 0.15 m/s)

The reduction factors of measurement analysis analogue to Figure 7 are expected to be dependent of the angle of wave attack. This is presented in Figure 8 together with some empirical functions (Oumeraci et al., 2001). It must be pointed out that the older functions were developed for wave run-up without current. On the one hand the formula of Wagner & Bürger (1973) agrees to the own results for smaller values of β. On the other hand the bigger the angle of wave attack the bigger the discrepancy to the values on the basis of measurements. These factors correspond to the formula given by De Waal and Van der Meer (1992):

for $\beta < -10°$ and $\beta > 10°$ $\qquad \gamma_\beta = \cos^2(|\beta| - 10) \qquad$ (17)

for $-10° < \beta > 10°$ $\qquad \gamma_\beta = 1 \qquad$ (18)

The de Waal & Van der Meer formula refers only to the test results without current and is valid for $\beta \leq 40$ considering the model tests.

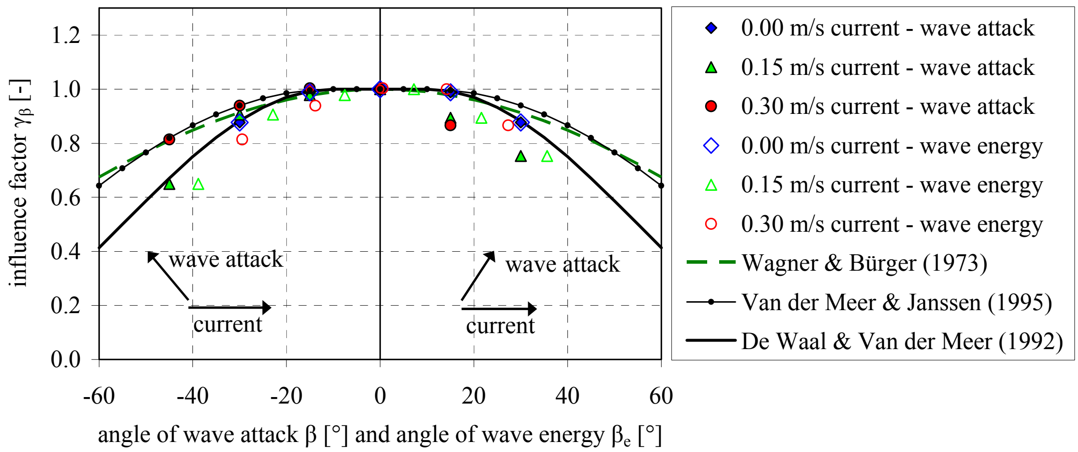

Figure 8. Factor γ_β versus angle of wave attack β and angle of wave energy β_e: test results and empirical functions, wave run-up, 1:3 sloped dike

In applying the influence of dike parallel current on the 1:3 sloped dike by using the angle of wave energy β_e (formula (7)) instead of the angle of wave attack β the formulae (17) and (18) show a good agreement with results of tests with a dike parallel current too. This confirms the approach to include the influence of dike parallel current considering its effects on characteristics of incoming waves.

Wave overtopping

Reference tests

Figure 9 shows the results of the reference tests for the 1:3 and 1:6 sloped dikes for breaking waves. In Figure 10 the regression curve for non-breaking waves for the 1:3 dike is given. All regression lines of the two dike slopes (dotted graph (1:3 dike) and dashed graph (1:6 dike)) are slightly lower than the recommended formula of the EurOtop-Manual (2007), but still lying within the confidence interval of 5%. In the following analysis the inclination of the graph of the corresponding reference test is used to determine the influence factors γ_i for the three different conditions:

- 1:3 dike for breaking wave conditions
- 1:3 dike for non-breaking wave conditions
- 1:6 dike for breaking wave conditions

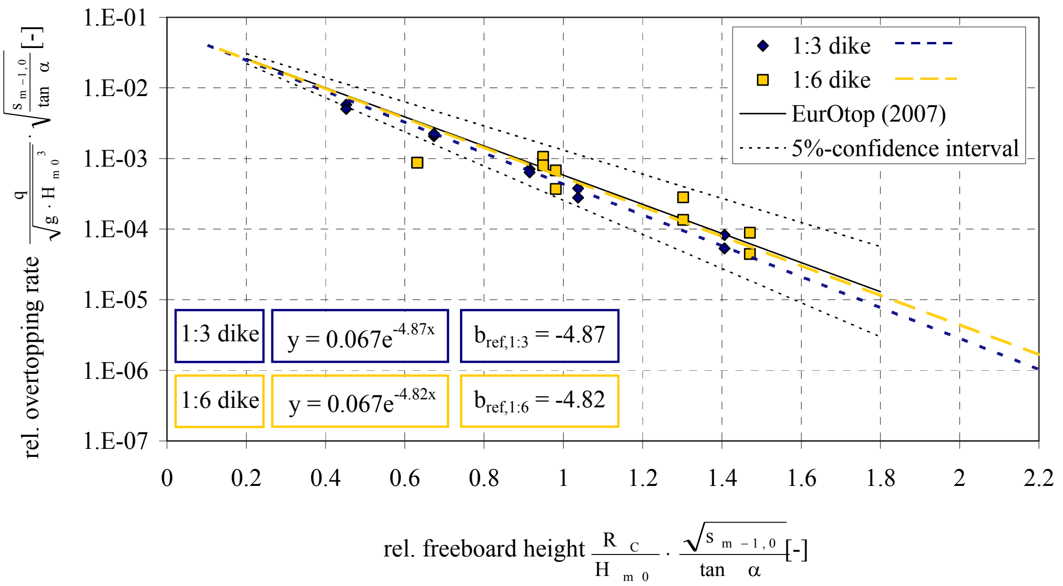

Figure 9. Relative overtopping rate - reference tests for breaking wave conditions (1:3 dike, 1:6 dike)

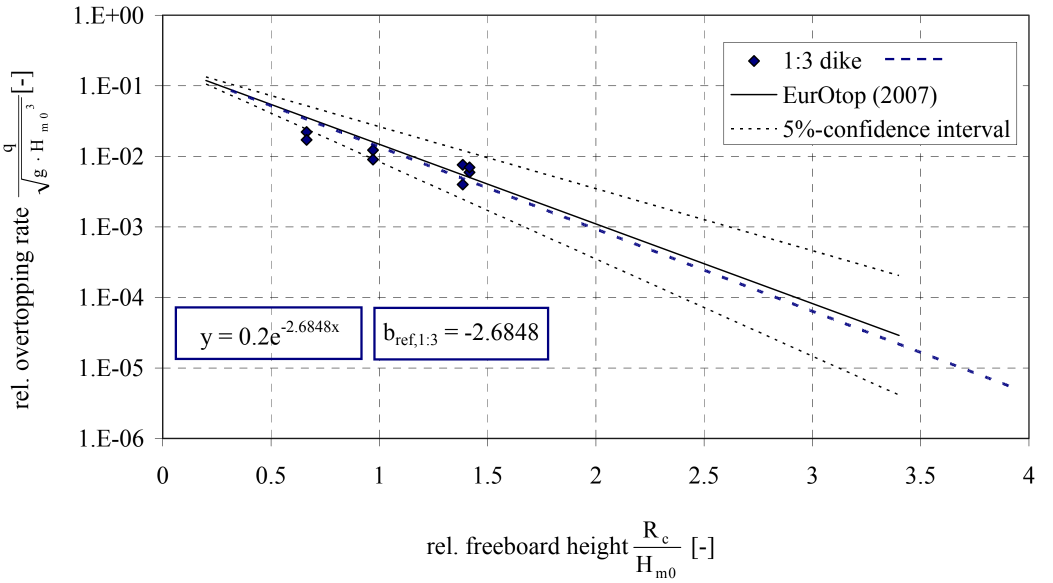

Figure 10. Relative overtopping rate - reference test for non-breaking wave conditions (1:3 dike)

The following paragraphs describe the analysis of the different influencing factors γ_β and $\gamma_{\beta,cu}$ (see formulae (15) to (16)) implicating the theory described above.

Oblique wave attack

Previous investigations by Wassing (1957), Tautenhain (1982), Oumeraci et al. (2001) and De Waal and van der Meer (1992) resulted in different formulae for the reduction factor γ_β. The De Waal & Van der Meer formula was selected due to the availability of recent and comprehensive data. Moreover, it was used for comparison purposes in the present study. In Figure 11 the angle of wave attack is given on the x-axis. The corresponding influence factors γ_β for the different angles of wave attack are given on the y-axis. The graph shows the recommended line from the EurOtop-Manual (2007). The influence factors γ_β of the 1:3 and the 1:6 sloped dike are shown by the diamond shaped and quadrat data points, respectively. These factors correspond to the formula given by De Waal and Van der Meer (1992) above (formulae (17) and (18)). The reduction factors for the 1:3 dike are a little bit lower than for the 1:6 dike. This can be explained by a slightly higher refraction of the waves between the dike toe and the point of wave breaking for the 1:6 dike (cf. Ohle et al., 2002).

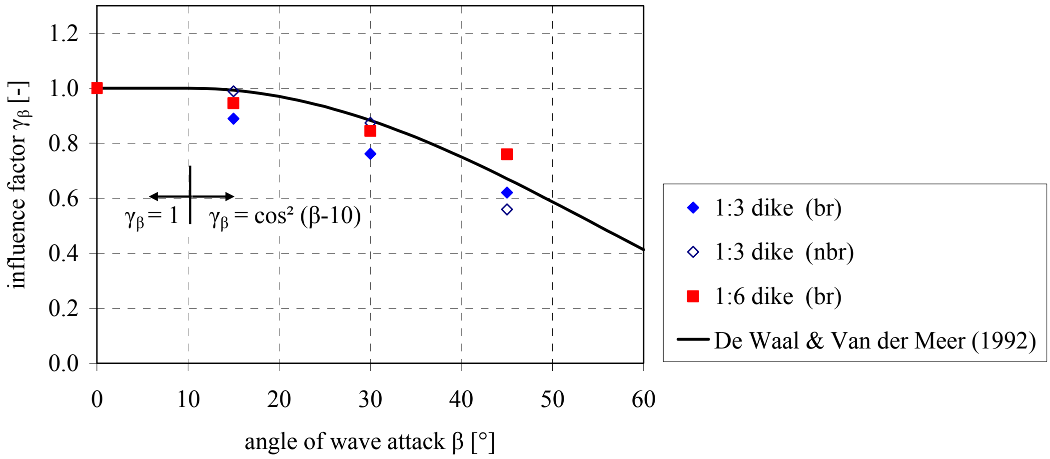

Figure 11. Influence of angle of wave attack on wave overtopping

Combination oblique wave attack and current

In a first step, a characteristic factor was applied to determine the influence of a combination of oblique waves and current parallel to the dike structure. The absolute wave parameters are used. A distinction was made between the results for the 1:3 sloped dike for breaking and non breaking waves (see Figure 12 and Figure 13) and the results for the breaking waves on the 1:6 sloped dike (see Figure 14). The diamonds show the influence factors for tests without current. An increase of the influence factor for increasing current velocity, shown by the triangles (0.15 m/s), circles (0.30 m/s) and squares (0.40 m/s only 1:6 dike), is noticeable except for the -15° and 30° tests for non-breaking waves (1:3 dike) and for the 30° test for breaking waves (1:6 dike). For normal wave attack the 1:3 dike for breaking wave conditions a decrease of the influence factor and consequently an increasing wave overtopping rate is noticeable for increasing current velocities.

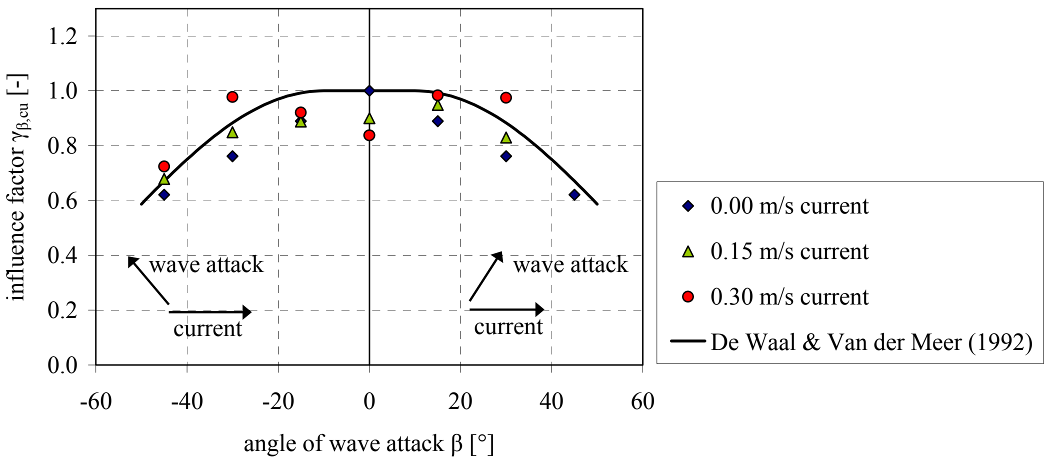

Figure 12. Current influence on wave overtopping, 1:3 dike, breaking waves

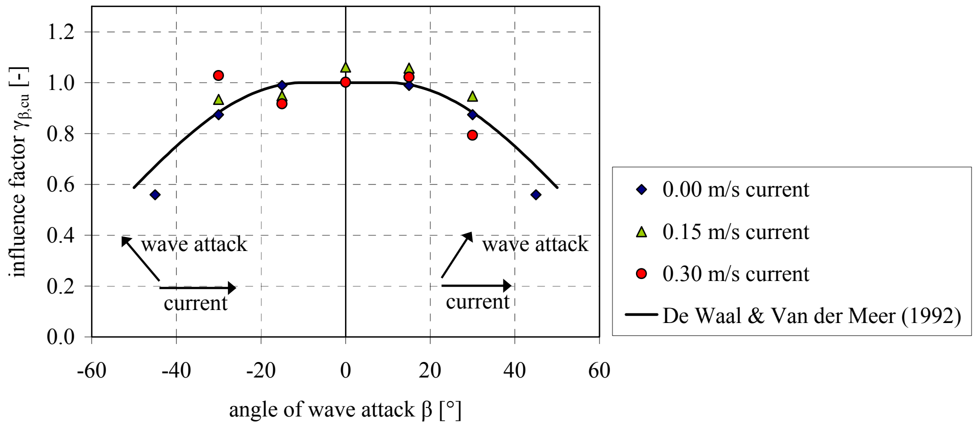

Figure 13. Current influence on wave overtopping, 1:3 dike, non breaking waves

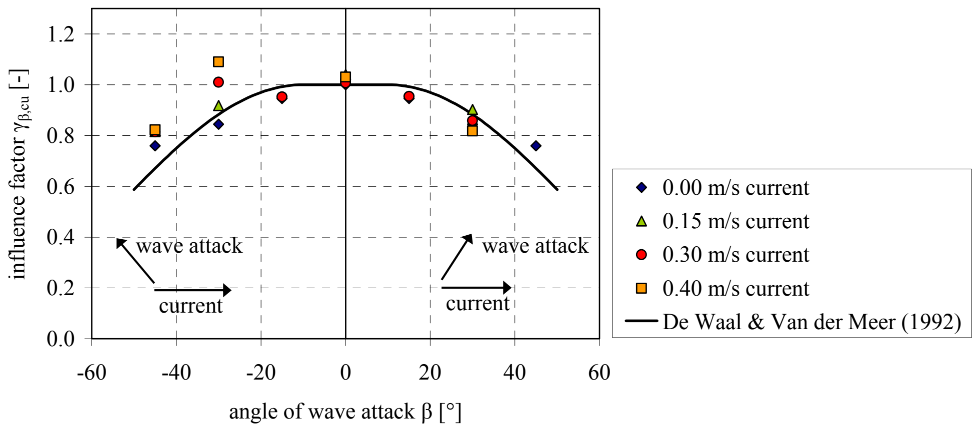

Figure 14. Current influence on wave overtopping, 1:6 dike, breaking waves

For non-breaking waves the relative overtopping rate and the relative freeboard height is determined independent of the wave period (cf. Figure 9 and 10). Hence using the relative wave period only changes the influence factor $\gamma_{\beta,cu}$ for breaking wave conditions and not for non-breaking conditions. The corresponding graphs are given below for the 1:3 and the 1:6 sloped dike (Figure 15 and 16). The filled data points are results considering the absolute wave period $T_{abs,m-1,0}$. The non-filled data points are determined by using the relative wave period $T_{rel,m-1,0}$. The influence factor decreases for positive angles of wave attack. For negative angles of wave attack the relative wave periods become smaller. Consequently the influence factors increase to high values and can not be used for describing the influence of current.

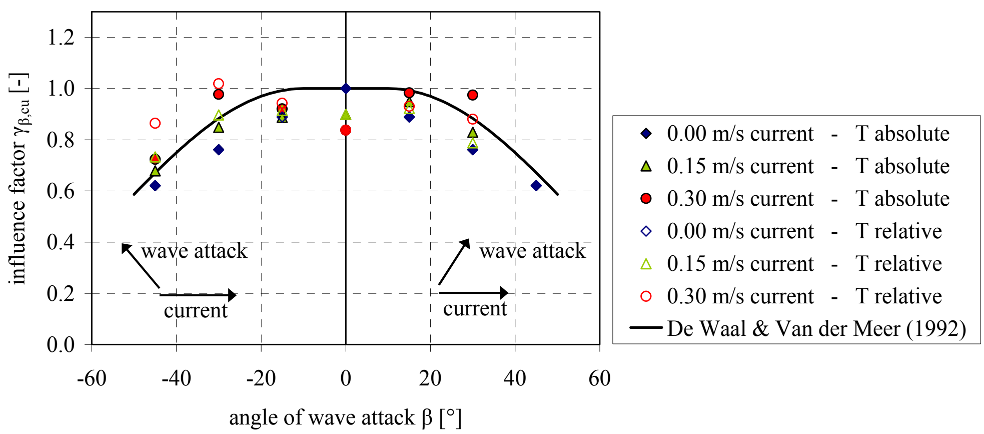

Figure 15. Current influence on wave overtopping including the relative wave period, 1:3 dike, br. waves

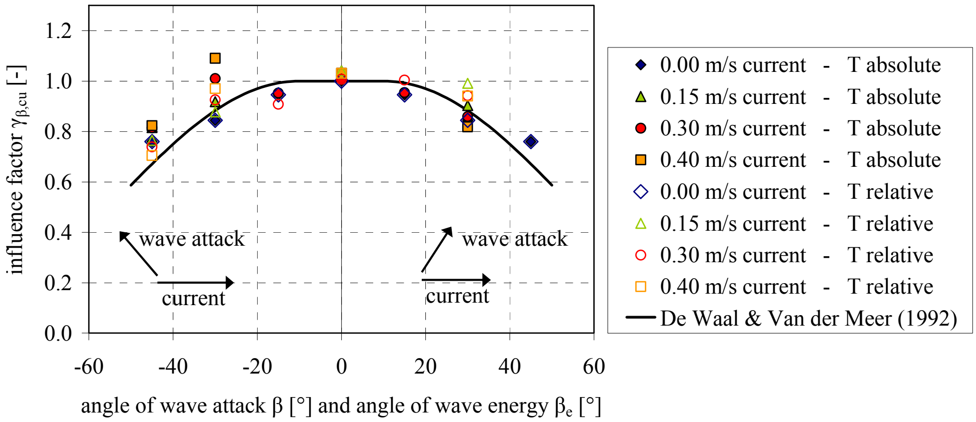

Figure 16. Current influence on wave overtopping including the relative wave period, 1:6 dike, br. waves

In the following, the theory of the wave energy direction is applied to the test results in Figure 17 to 19 for the 1:3 and 1:6 sloped dike for breaking and non-breaking (only 1:3 dike) waves. The filled data points are plotted against the angle of wave attack β whereas the non-filled data points are plotted against the angle of wave energy β_e. The data using the direction of wave energy are arranged further to the right than the data points that consider only the wave direction and not its energy direction and correspond fairly well to the graph of De Waal & Van der Meer (1992).

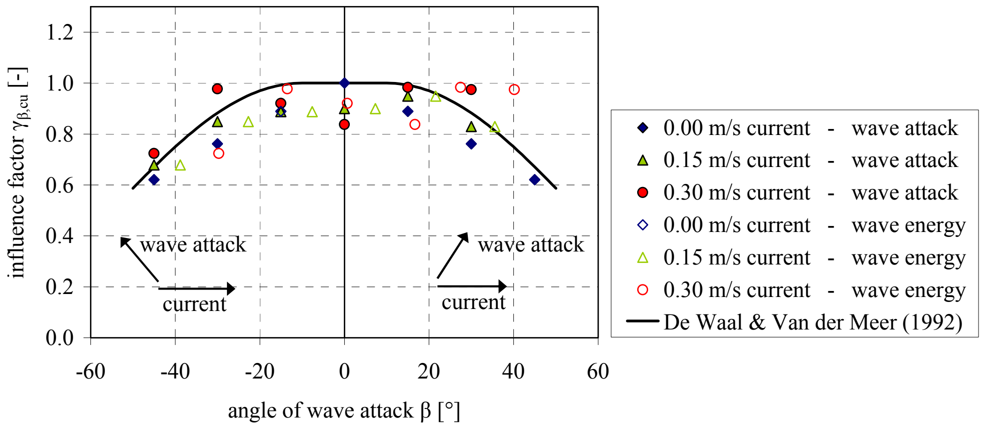

Figure 17. Current influence on wave overtopping including the angle of wave energy, 1:3 dike, br. waves

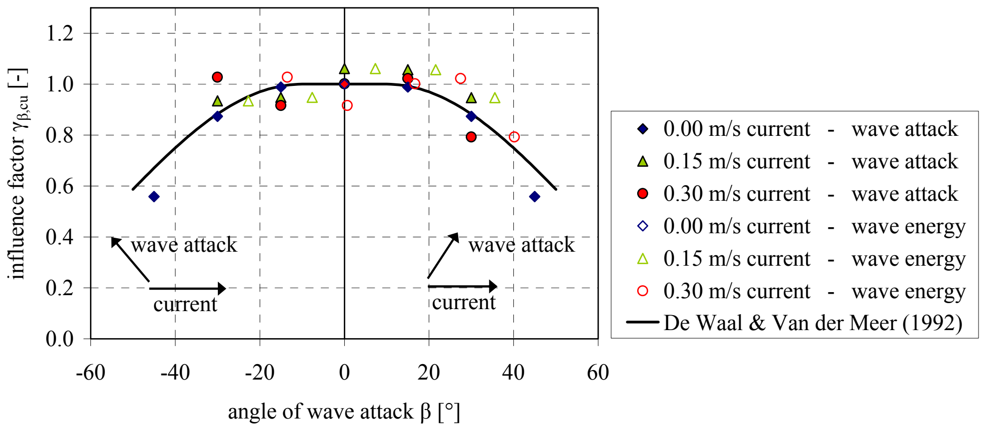

Figure 18. Current influence on wave overtopping incl. the angle of wave energy, 1:3 dike, non-br. waves

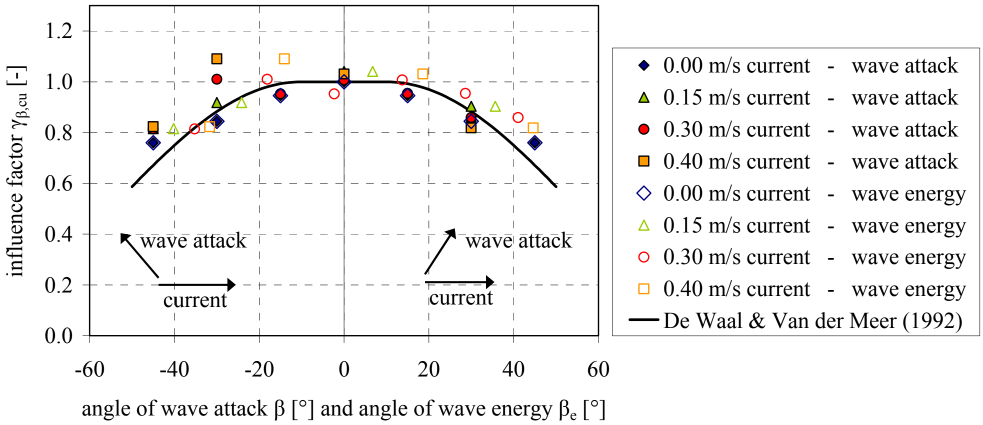

Figure 19. Current influence on wave overtopping including the angle of wave energy, 1:6 dike, br. waves

CONCLUSION AND RECOMMENDATIONS

The influence of current combined with different angles of wave attack on wave run-up and wave overtopping has been studied experimentally. The experimental study included two smooth dike slopes (1:3 and 1:6) and six different wave parameters. Oblique wave attack and current velocities parallel to the dike line have been combined in different test configurations.

The results for oblique and non-oblique wave attack agree well with the formula given by De Waal and Van der Meer (1992). The consideration of current along the dike line combined with normal wave attack leads to decreasing average wave run-up heights and overtopping-rates.

For wave overtopping the combination of oblique wave attack and current parallel to the dike was analysed by determine an influence factor $\gamma_{\beta,cu}$. Using therefore the relative wave period $T_{rel,m-1,0}$ instead of the absolute wave period $T_{abs,m-1,0}$ leads to rather high values and does not account the current influence on wave overtopping. Instead of that the influence-factor $\gamma_{\beta,cu}$ can be determined by using the angle of wave energy β_e instead of the angle of wave attack β.

In upcoming studies the influence of currentom wave run-up and wave overtopping will be investigated in ore detail. In addition the wave behaviour on the dike crest by analysing single wave events has to be determined as well as the flow processes on the dike crest in the presence of current and oblique waves.

ACKNOWLEDGMENT

The first part of the results was obtained from model tests carried out within the EU-Hydralab-project FlowDike (contract no. 022441), which enable researchers from different countries to use large scale facilities in Europe. The FlowDike-project has been a cooperation of three German Universities (RWTH Aachen University, TU-Dresden and TU-Braunschweig), the Czech Brno University of Technology, the University of Valencia (Spain) and VanderMeer Consulting B.V.. The second part of the results was obtained within a project supported by the German Ministry of Education and Research (BMBF) within the research project FlowDike-D and is a cooperation of RWTH Aachen University (reference number: 03KIS075), TU-Dresden (reference number: 03KIS076) and VanderMeer Consulting B.V..

Both test phases were combined within the project FlowDike-D. Rijkswaterstaat funded in both project phases some additional tests to complete the dataset with important test configurations.

REFERENCES

Ahrens, J.P. 1981: Irregular wave runup on smooth slopes. *Coastal Engineering Technical Aid No. 81-17.* U.S.Army Corps of Engineers. CERC, Ft. Belvoir, Va. 22060.

De Waal, J. P., Van der Meer, J. W. 1992: Wave run-up and overtopping on coastal structures. *Proceedings of the 23th International Conference on Coastal Engineering.* pp. 1758-1771. Venice, Italy.

EurOtop-Manual. 2007: European Overtopping Manual, *www.overtopping-manual.com*. Eds Pullen, T., Allsop, N.W.H., Bruce, T., Kortenhaus, A, Schüttrumpf, H., Van der Meer, J.W.. Heide, Germany.

Hedges, T. S. 1987: Combinations of waves and currents: an introduction. *Proceedings of Institution of Civil Engineers 82*, pp. 567-585.

Holthuijsen, L. H. 2007: Waves in oceanic and coastal waters. *Cambridge Univ. Press*. U. Kingdom.
Hughes, S.A. 2003: Estimating irregular wave runup on smooth, impermeable slopes. U.S. Army Engineer Research and Development Center. Vicksburg, MS, United States.
Hunt, I.A. 1959. Design of seawalls and breakwaters. *Proceedings ASCE Journal of waterways, harbor and coastal engineering division*. Volume 85. pp. 123 ff. Galveston, U.S.
Ohle, N., Möller, J., Schüttrumpf, H., Daemrich, K.-F., Oumeraci, H., Zimmermann, C. 2002: The influence of refraction and shoaling on wave run-up under oblique waves. *Proceedings of the 28th International Conference Coastal Engineering.* pp. 885-894. Cardiff, U.K.
Oumeraci, H., Schüttrumpf, H., Möller, J., Zimmermann, C., Daemrich, K.-F., Ohle, N. 2001: Influence of oblique wave attack on wave run-up and wave overtopping - 3D Model Tests at NRC/Canada with long and short crested waves- . Hannover, Germany.
Pohl, R., Heyer, T. 2005: Der Auflauf unregelmäßiger Wellen im Übergangsbereich zwischen Branden und Schwingen. *Wasser und Abfall*. pp. 34 - 38. Germany.
Schüttrumpf, H., Oumeraci, H. 2005: Layer thicknesses and velocities of wave overtopping flow at seadikes. *Coastal Engineering.* Vol. 52, Issue: 6, pp. 473-495. Amsterdam, The Netherlands.
Tautenhain, E., Kohlhase, S., Partenscky, H. W. 1982: Wave run-up at sea dikes under oblique wave approach. *Proceedings of the 18th International Conference on Coastal Engineering.* pp. 804-810. Cape Town, South Africa.
Treloar, P.D. 1986: Spectral wave refraction under the influence of depth and current. *Coastal Engineering 9.* pp. 439-452. Amsterdam, The Netherlands.
Van der Meer, J.W., Janssen, J. 1995. Wave run-up and wave overtopping at dikes. *Wave forces on Inclined and vertical wall structures.* pp. 1-27. New York, United States.
Van der Meer, J.W. 2010. Hydralab - FlowDike. Influence of current on wave run-up and wave overtopping, Detailed analysis on the influence of current on wave overtopping. *Project Report vdm08310, version 1.0.* Van der Meer Consulting. The Netherlands (unpubl. - subm. to the EU).
Wagner, H. 1968: Kennzeichnung der Wellenauflaufhöhe an geraden, glatten, undurchlässigen Böschungen im brandenden Bereich. *Wasserwirtschaft Wassertechnik.*Volume 18.
Wagner, H., Bürger, W. 1973. Kennwerte zur Seedeichbemessung. *Wasserwirtschaft Wassertechnik (WWT).* Volume 23. Issue 6. pp. 204-207.
Wassing, F. 1957: Model investigations of wave run-up carried out in the Netherlands during the last twenty years. *Proceedings of the 6th International Conference on Coastal Engineering*. Gainsville, Florida.

Kuratorium für Forschung im Küsteningenieurwesen

KFKI aktuell

Editorial

Küstenschutz – eine Daueraufgabe

Küstenschutz ist Voraussetzung für die Erhaltung und Entwicklung des Lebens- und Wirtschaftsraumes der ca. 1,1 Mio. ha Niederungsgebiete an Nord- und Ostsee. Das Bundesministerium für Ernährung, Landwirtschaft und Verbraucherschutz (BMELV) fühlt sich als Sachwalter innerhalb der Bundesregierung insbesondere für die ländlichen Räume, aber auch für die im Tidebereich liegenden Städte zuständig. Deshalb werden im Rahmen der Gemeinschaftsaufgabe "Verbesserung der Agrarstruktur und des Küstenschutzes" (GAK) jedes Jahr entsprechende Bundesmittel zur Verfügung gestellt.

Die Durchführung der Küstenschutzmaßnahmen ist Sache der Länder; sie legen auch die Prioritäten fest. Der Bund erstattet ihnen 70% der Ausgaben im Rahmen der GAK. Bund und Küstenländer haben sich in Stichworten auf folgende grundlegende finanzierungsfähige Küstenschutzstrategie verständigt:

- Sorgfältige Beobachtung und Bewertung der hydromorphologischen Änderungen und der Klimaänderungen an der Küste, Entwicklung von Folgeszenarien; (Forschungsaktivitäten im Rahmen des KFKI);
- Gewährleistung eines bestimmten Schutzstandards der Küstenniederungsgebiete (kein absoluter Schutz möglich);
- Grundsätzlich keine Rückverlegung oder Aufgabe von Deichen (linienhafter Küstenschutz), aber auch keine Landgewinnung durch Vordeichungen;
- zweite Deichlinien schaffen, wo dies möglich ist (flächenhafter Küstenschutz);
- neue Deichprofile so anlegen, dass spätere Anpassungen problemlos möglich sind (Flexibilisierung);
- sonstige Küstenschutzbauwerke statisch so ausrichten, dass spätere signifikante Erhöhungen noch möglich sind;
- Sandvorspülungen als "weiche" Küstenschutzmaßnahme weiter betreiben;
- Schutz der Inseln und Halligen weiter fördern, da auch sie dem Schutz der Festlandsküste dienen;
- vordringliche Küstenschutzmaßnahmen zuerst durchführen (Prioritäten setzen).

Diese Strategie hat sich bewährt, denn sie hat ganz unspektakulär dazu geführt, dass, obwohl noch nicht einmal alle geplanten Maßnahmen nach der verheerenden Sturmflut vom Februar 1962 durchgeführt sind, die nachfolgenden, noch höheren Sturmfluten von 1976, 1990, 1994 oder 2007 keine wesentlichen Schäden angerichtet haben.

Im Zeitraum von 1973 bis 2009 hat der Bund zusammen mit den Küstenländern über 4 Mrd. € in den Küstenschutz investiert. Darüber hinaus hat der Planungsausschuss am 20. Januar 2009 den Sonderrahmenplan "Maßnahmen des Küstenschutzes in Folge des Klimawandels" beschlossen, mit dem der Bund den Küstenländern in den Jahren 2009 bis 2025 zusätzlich jährlich 25 Mio. €, insgesamt also 380 Mio. €, zur Verfügung stellt. Somit können die Küstenländer bis 2025 jährlich rund 182 Mio. € Gesamtinvestitionsmittel für Küstenschutzmaßnahmen verbauen und das auch bei gekürztem Mittelvolumen der GAK. Damit hat die Bundesregierung auf die Forderungen der Küstenländer reagiert, sich noch stärker als bisher an den Investitionskosten für Küstenschutzmaßnahmen zu beteiligen.

Die Länder können auch ELER-Mittel (Europäischer Landwirtschaftsfonds für die Entwicklung des ländlichen Raums) der EU verwenden. Sie sind auch daran interessiert, entsprechende Mittel nach 2013 für den Küstenschutz einzusetzen. Der Bund unterstützt dieses Anliegen.

Es ist in den vergangenen 30 Jahren schon vieles geschehen, es bleibt aber auch noch etliches zu tun, und zwar nicht nur in der praktischen Abwicklung von Baumaßnahmen, sondern auch im Forschungsbereich. In diesem Zeitraum sind etwa 80 Projekte vorrangig mit Mitteln des Bundesministerium für Bildung und Forschung (BMBF) mit Erfolg gefördert worden, und es besteht zweifellos weiterhin ein erheblicher Forschungsbedarf, um die im Küstenraum ablaufenden Prozesse noch besser verstehen und darauf richtig reagieren zu können. Küstenschutzmaßnahmen und Sicherung des Seeverkehrs kosten viel Geld. Deshalb ist jeder Erkenntnisgewinn aus der angewandten Forschung zu nutzen, um zu sachgerechten, wirtschaftlichen und damit nachhaltigen Lösungen zu kommen.

Ich denke, die Politik ist sensibilisiert, und die Weichen sind gestellt - soweit es möglich war -, um den Küstenschutz auch in Zukunft nicht als Selbstzweck, sondern zum Wohle der an der Küste lebenden Menschen voranzubringen.

MinR Dr.-Ing. Eiko Lübbe | Bundesministerium für Ernährung, Landwirtschaft und Verbraucherschutz
Postfach 140270 | 53107 Bonn | 415@bmelv.bund.de

Verbundprojekt davon aus, dass eine Kombination von Datenanalysemethoden, von "bottom up" Methoden (prozessbasiertes physikalisches Verhalten, partielle DGL) und von "top down" Methoden (am bekannten Systemzustand orientiert) erforderlich ist. Die im Verbundprojekt vereinten Teilprojekte lassen sich in diese Methodenvielfalt einordnen. Zu den erforderlichen Grundlagen gehört ein umfassendes Bodenmodell, für das im Rahmen des Verbundprojekts vorhandene Daten (Sedimentologie, Bathymetrie, Sohlformen, im Ansatz auch Bauwerke,...) integriert und neue Daten aufgenommen werden. Das Bodenmodell wird mit innovativer Informationstechnik für die Aufgaben in der morphodynamischen Analyse und Prognose genutzt. Nach Auffassung des Autors ist dies eine sehr wichtige, über das Ende des Verbundprojekts hinaus reichende Kernaufgabe. Weiterhin gehört zu den erforderlichen Datengrundlagen eine umfassende Datenbasis zur Ozeanografie und Hydrologie der Nordsee, insbesondere der Deutschen Bucht einschließlich der besonderen Verhältnisse in den Tideflüssen und Watteinzugsgebieten. Das Bodenmodell und die ozeanographisch-hydrologische Datenbasis unterstützen im Verbundprojekt verschiedene Ansätze für die o.g. datenorientierten Analysemethoden (statistische, räumliche und zeitliche Analysen, Sedimentbilanzen) und die „top down" Methoden (z.B. Formanalysen, Analysen für Geometrie- und Tide-Kennwerte, Analysen zur Asymmetrie von Tidekennwerten).

Zur Diagnose des noch verborgenen Wirkungsgefüges, das sich über verschiedene Kombinationen der Raum- und Zeitskalen erstrecken kann, werden verschiedene prozessbasierte Modelle genutzt. Sie orientieren sich je nach angestrebter Auflösung der Raum- und Zeitskalen an unterschiedlichen Graden in der detaillierten Beschreibung der physikalischen Prozesse. Im Hinblick auf die eingesetzten Simulationsverfahren bzw. Simulationsbausteine kann grundsätzlich die folgende Einteilung kommuniziert werden:

Hydrodynamik: Wasserstände, Durchflussmengen, Strömungen (auch Dichte-, Sekundär- oder Zirkulationsströmungen), Wellen, Seegang sowie Bodenschubspannungen aus Strömung und Seegang

- Advektion und turbulente Diffusion gelöster und partikulärer Stoffe: Salz, verschiedene Fraktionen suspendierter Feststoffe, Sinkgeschwindigkeiten der Feststoffe
- Partikel Tracking: Nachverfolgung einzelner Partikel im Wasserkörper
- Sedimenttransport am Gewässerboden: residuelle Transporte, charakteristische Transportbänder, Erosions- und Sedimentationsgebiete
- Morphodynamik: Evolution der Gewässersohle in Wechselwirkung mit der Belastung

Aus einer Kombination der genannten Methoden soll im Verbundprojekt das Systemverständnis für die langfristige Morphodynamik in der Deutschen Bucht gewonnen werden. In diesem Zusammenhang ist der Gültigkeitsbereich der Modellergebnisse auf Grundlage von einer Validierungsstrategie und von Validierungsrechnungen mit Bezug auf verfügbare Validierungsdaten zu analysieren und zu dokumentieren.

Mit dem Verbundprojekt sollen letztendlich integrierte Datengrundlagen und Werkzeuge geschaffen werden, mit denen Fragestellungen zur Sediment- und Morphodynamik innerhalb der Deutschen Bucht und in den Gewässern entlang der Deutschen Bucht mit einem integrierten Ansatz bearbeitet werden können. Für den im Verbundprojekt gewählten integrierten Bearbeitungsansatz steht die Abbildung 1.

FlowDike-D (03KIS075-76)

Freibordbemessung von Ästuar- und Seedeichen unter Berücksichtigung von Wind und Strömung

Stefanie Lorke
Univ.-Prof. Dr.-Ing. Holger Schüttrumpf

Rheinisch-Westfälische Technische Hochschule (RWTH) Aachen, Lehrstuhl und Institut für Wasserbau und Wasserwirtschaft (IWW)

Antje Bornschein
Stefano Gilli
apl. Prof. Dr.-Ing. habil. Reinhard Pohl

Technische Universität Dresden, Institut für Wasserbau und Technische Hydromechanik (IWD)

Dr. Jentsje van der Meer

Van der Meer Consulting B.V., Heerenveen, Niederlande

Einführung

Eine Vielzahl von Schäden an See- und Ästuardeichen ist auf den Wellenüberlauf zurückzuführen. Daher sind für die Freibordbemessung von Deichen der Wellenauflauf und -überlauf maßgebende Bemessungsgrößen. Der Wellenauflauf und Wellen-

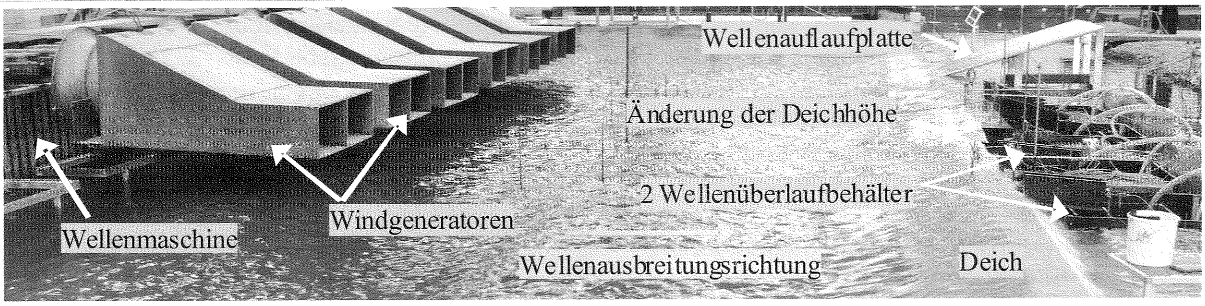

Abbildung 1:
Versuchsaufbau, 1:3 geneigter Deich

überlauf wird unter Berücksichtigung der Deichgeometrie sowie der Wellenhöhe, der Wellenperiode und der Wellenangriffsrichtung berücksichtigt (vgl. EurOtop-Manual, 2007). Eine durch die Tide induzierte deichparallele Strömung sowie lokale Windfelder werden bislang in diesen Bemessungsformeln nicht berücksichtigt. Ziel des Projektes FlowDike-D ist die Untersuchung des Wellenauflaufs und -überlaufs beeinflusst durch Strömung und Wind in Kombination mit unterschiedlichen Wellenangriffsrichtungen sowie die Implementierung dieser Erkenntnisse in bestehende Bemessungsformeln für die Wellenauflaufhöhe und die -überlaufrate.

Modellversuche

Für die Untersuchung dieser zwei Aspekte - deichparallele Strömung und senkrecht auf den Deich treffender Wind - wurden im Jahr 2009 in zwei Testphasen physikalische Modellversuche im Wellenbecken des DHI in Hørsholm (Dänemark) durchgeführt. In der ersten Testphase (im Rahmen des EU-Hydralab-Projektes HYIII-DHI-5, Vertragsnr.: 022441) wurde der genannte Einfluss an einem 1:3 geneigten Deich untersucht, während in der zweiten Testphase ein 1:6 geneigter Deich getestet wurde. Das FlowDike-D-Projekt ist vom Bundesministerium für Bildung und Forschung (BMBF) gefördert und stellt eine Kooperation der RWTH Aachen (03KIS075), der TU Dresden (03KIS076) und VanderMeer Consulting B.V. dar. Ziel des Verbundprojektes ist zum einen die Bestimmung der Wellenauflaufhöhe und der Wellenüberlaufrate in Abhängigkeit von Wellenangriffsrichtung, Strömung und Wind. Zum anderen sollen die einzelnen Überlaufereignisse identifiziert und die zugehörigen Strömungsprozesse auf der Deichkrone quantifiziert werden. Neben den zwei unterschiedlichen Deichneigungen wurden die Versuche mit je zwei Kronenhöhen durchgeführt. Die sich daraus ergebenden vier Deichformen wurden mit Wellen eines Jonswap-Spektrums belastet. Abbildung 1 zeigt den Modellversuch im Wellenbecken des DHI. Links in Abbildung 1 sind die Wellenmaschine sowie die Windgeneratoren zu erkennen. Die durch die Parameter Wind, Strömung und Wellenangriffsrichtung beeinflussten Wellen trafen bzw. überströmten den Deich (rechts im Bild). Dabei wurde die Wellenüberlaufrate mittels zwei Wellenüberlaufbehältern je Deichkronenhöhe gemessen. Zur Bestimmung der Wellenauflaufhöhe wurde eine 2 m breite Wellenauflaufplatte installiert.

Ergebnisse

Die Versuchsergebnisse zeigen, dass mit zunehmendem Wellenangriffswinkel die Wellenüberlaufrate abnimmt. Ein Windfeld auf der Deichkrone führt zu einer erhöhten Wellenüberlaufrate, insbesondere bei kleinen Überlaufraten. Diese Aussagen stimmen mit früheren Untersuchungen überein (De Waals und Van der Meer, 1992; Waal, 1996; Ward, 1996).

In weiteren Versuchen wurde der Einfluss der Strömung auf die Wellenentwicklung untersucht, die sich durch das strömungsinduzierte Shoaling und die strömungsinduzierte Refraktion bestimmen lässt. Dieser Einfluss ist in den bestehenden Bemessungsformeln für den Wellenauflauf und den Wellenüberlauf des EurOtop-Manuals (2007) noch nicht enthalten. Für die Berücksichtigung unterschiedlicher Wellenangriffsrichtungen wird bisher ein Einflussfaktor γ_β verwendet. Im FlowDike-Projekt wurde der Einflussfaktor $\gamma_{\beta,cu}$ eingeführt, der den Einfluss der Strömung kombiniert mit der Wellenangriffsrichtung auf den Wellenauflauf und den Wellenüberlauf beschreibt. Der Einflussfaktor $\gamma_{\beta,cu}$ wird nun nicht mehr allein von dem Wellenangriffwinkel bestimmt, sondern von dem Energiewinkel der Welle, der sich aufgrund der Strömung von dem Wellenangriffswinkel unterscheidet. Aus den Untersuchungen wurden daher die Einflussfaktoren $\gamma_{\beta,cu}$ für unterschiedliche Energiewinkel der Welle ermittelt. Es zeigt sich eine gute Übereinstimmung mit der Formel nach de Waal & Van der Meer (1992), die noch keine Strömung entlang des Deiches berücksichtigt hat.

Referenzen

De Waal, J. P., Van der Meer, J. W. (1992): Wave run-up and overtopping on coastal structures. Proceedings of the 23th International Conference on Coastal Engineering, 1758-1771. Venice, Italy.

EurOtop-Manual (2007): European Overtopping Manual, www.overtopping-manual.com. Eds. Pullen, T., Allsop, N.W.H., Bruce, T., Kortenhaus, A., Schüttrumpf, H., van der Meer, J. W.. Die Küste, 73.

Waal, J.P.; Tönjes, P.; van der Meer, J.W. (1996): Wave overtopping of vertical structures including wind effect. Proc. 25th Int. Conf. on Coastal Engineering, 2216-2229, Orlando.

Ward, D.L., Zhang, J., Wibner, C. and Cinotto, C.M. (1996): Wind effects on run-up and overtopping of coastal structures. Proc. 25th Int. Conf. on Coastal Engineering, 2206-2215, Orlando.

AMSeL(03KIS068)

Ermittlung des MSL (Mean Sea Level) und Analyse von hochaufgelösten Tidewasserständen an der deutschen Nordseeküste: MSL + Trends Nordsee

Meeresspiegeländerungen in der Deutschen Bucht

Prof. Dr.-Ing. Jürgen Jensen
Thomas Wahl
Dr.-Ing. Torsten Frank

Universität Siegen, Forschungsinstitut Wasser und Umwelt, Abteilung Wasserbau und Hydromechanik

Zielsetzung

Eines der Hauptziele des KFKI-Forschungsvorhabens AMSeL bestand in der Analyse der beobachteten Änderungen des relativen mittleren Meeresspiegels (engl. Relative Mean Sea Level, RMSL) entlang der Deutschen Nordseeküste. Im Rahmen des Projektes wurde im Detail untersucht, (i) welchen mittel- bis langfristigen Veränderungen der RMSL in der Vergangenheit (ca. 150 Jahre) unterworfen war, (ii) ob eine Beschleunigung in den Beobachtungsdaten zu erkennen ist, (iii) ob es signifikante Unterschiede in der RMSL-Entwicklung entlang der deutschen Nordseeküste gibt und (iv) ob die durchgeführten Analysen der Beobachtungsdaten in irgendeiner Weise zur Erarbeitung belastbarer regionaler Meeresspiegelszenarien beitragen können.

Daten und Methodik

Insgesamt wurden 13 Pegel, mit langen qualitativ hochwertigen Zeitreihen in die Analysen einbezogen (siehe Abbildung 1). Alle verwendeten Datensätze wurden um die im KFKI-Projekt IKÜS (Wanninger et al., 2010) ermittelten Pegeloffsets korrigiert.

Für die Untersuchungen wurden soweit möglich hoch aufgelöste Datensätze (mind. Stundenwerte) verwendet. Aus diesen Daten resultieren zunächst für viele Pegel vergleichsweise kurze (10-12 Jahre) RMSL-Zeitreihen. Diese wurden mit Hilfe des k-Wert-Verfahrens mit den lange zurückreichenden Tidehalbwasser-Zeitreihen (aus Mittelung der Tidehoch- und Tideniedrigwasser) kombiniert. Die dazu verwendeten k-Werte wurden zunächst mittels verschiedener Testverfahren auf Sationarität geprüft. Die so generierten langen RMSL-Zeitreihen wurden durch Anpassung parametrischer (z.B. Polynome 1. Ordnung) und nicht-paramterischer Funktionen (hier: Singuläre Systemanalyse, SSA) analysiert bzw. geglättet. Während die Ergebnisse der Anpassung parametrischer Funktionen einen direkten Vergleich zulassen und die Funktionen selbst extrapolierbar sind, erlauben nicht-paramterische Funktionen eine deutlich bessere Anpassung an die Beobachtungsdaten und Beschleunigungsphasen können belastbarer detektiert werden. Im Rahmen des AMSeL-Vorhabens wurde eine Methode entwickelt (Monte-

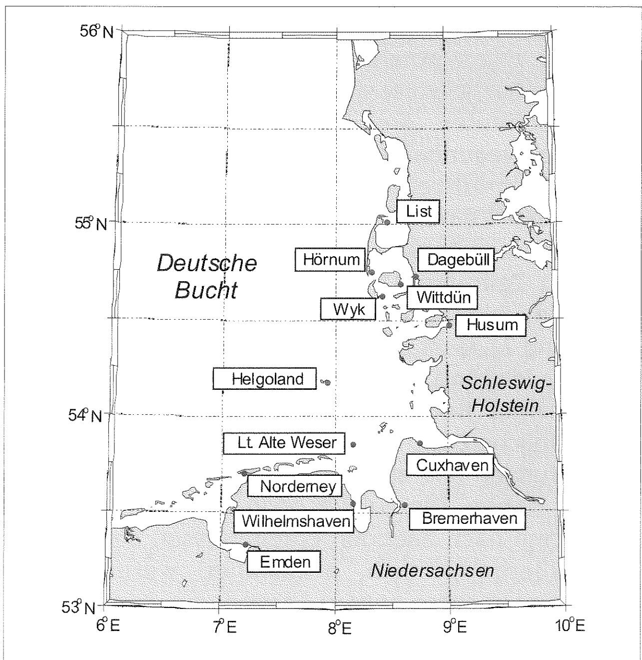

Abbildung 1:
Untersuchungsgebiet und berücksichtigte Pegel

Ocean (Frankreich) koordiniert. In MyOcean werden von meteorologischen und ozeanographischen Institutionen, Forschungseinrichtungen und Firmen vier Themen-bereiche bearbeitet. Anwendungsbeispiele sind u.a. Beiträge zur Sicherheit im Seeverkehr, die Unterstützung von Offshore-Aktivitäten, präventive Methoden gegen Ölverschmutzungen, das Management mariner Ressourcen, Wasserqualitätsmonitoring zum Schutz der Meeresumwelt, Klimaüberwachung und saisonale Vorhersagen.

In MyOcean gibt es 12 Produktionseinheiten, die aus 5 thematischen Zentren für Beobachtungsdaten (4 Zentren für Fernerkundungsdaten und ein Insitu-Datenzentrum) sowie 7 Vorhersagezentren (6 regionale und 1 globales Zentrum) bestehen. Alle Produktionseinheiten sind zur kontinuierlichen, offenen und kostenlosen Lieferung von Basisdaten zum physikalischen Zustand und zum Ökosystem des Meeres verpflichtet. Nutzer der MyOcean-Produkte sind europäische Organisationen (EEA, EMSA, HELCOM, OSPAR, ICES u.a.) sowie unterschiedliche Institutionen der EU-Mitgliedsstaaten. Da die Basisdaten von MyOcean eher großräumig bis mesoskalig sind, müssen diese für spezielle Anwendungen und Anforderungen von Endnutzern noch von weiteren Dienstleistern zu sogenannten "Downstream Services" weiterverarbeitet werden.

Deutsche Partner in MyOcean sind das Bundesamt für Seeschifffahrt und Hydrographie (BSH), das Leibniz Institut für Meereswissenschaften an der Universität Kiel (IfM GEOMAR) sowie die Firma Brockmann Consult. Schwerpunkte der BSH-Beteiligung liegen bei den Insitu-Beobachtungsdaten sowie bei Modellierungsaktivitäten in den Vorhersagezentren für die Ostsee und den NW-Schelfbereich. Beim Vorhersagezentrum Ostsee ist das BSH als Partner eines Konsortiums von 4 Ostseeanliegerstaaten (DMI, BSH, SMHI, FMI) direkt an der Produktion beteiligt. Derzeit wird im Konsortium ein neues physikalisch-biogeochemisches Ostseemodell HBM (HIROMB-BOOS-Model) entwickelt, welches zentral gepflegt und von den Partnern mit unterschiedlichen Randbedingungen angetrieben wird. Hierdurch wird die Grundlage für ein Ensemble-Vorhersagesystem in der Ostsee geschaffen. Das Vorhersagezentrum für das Nordwestschelfgebiet wird vom UK Met. Office betrieben, hier liegen Schwerpunkte der BSH-Aktivitäten im Bereich Validation und Qualitätskontrolle. Das BSH koordiniert außerdem das Insitu-Datenmanagement für den Nordwestschelfbereich. Für den Ostseeraum hat diese Aufgabe das SMHI (Schweden) übernommen.

In MyOcean wurde ein zentraler und einheitlicher Zugang zu Diensten und Produkten unter ***www.myocean.eu.org*** eingerichtet. Bei den bereits seit Start des Projektes existierenden 128 Version 0-Produkten ist jedoch nur in wenigen Fällen ein direkter "Download" vom Web-Portal möglich, in den meisten Fällen müssen noch die Produktionszentren kontaktiert werden. Nach Registrierung als MyOcean-Nutzer bzw. dem Abschluss eines Service Level Agreements (SLA) können dann Daten von ftp- oder OpenDAP-Servern heruntergeladen werden. In der nächsten Version 1, die Ende 2010 vorliegen soll, sollen alle Produkte direkt über das MyOcean-Portal erhältlich sein.

Von Besonderer Bedeutung für das Projekt MyOcean ist die Einbeziehung und Anbindung von Nutzern. In der ersten Jahreshälfte 2010 wurden bereits von über 70 Nutzern mehr als 600 Produkte angefordert sowie ca. 20 SLAs mit sogenannten "Core Usern", zu denen auch das BSH gehört, unterzeichnet.

Die Weiterentwicklung und operationelle Implementierung der Basisdienste soll in einem Folgeprojekt erfolgen, welches im 7. Rahmenprogramm der EU bis November 2010 ausgeschrieben ist und den Zeitraum 2012 bis 2014 abdecken wird. In dem Folgeprojekt von MyOcean sollen neue Produkte erstellt, die Qualität der Basisdienste gesteigert und der Zugang zu Produkten sowie die Nutzeranbindung weiter verbessert werden. Herausforderungen und Unsicherheiten bestehen derzeit noch bei der langfristigen Finanzierung der GMES Basisdienste nach 2014.

Referenz

Bahurel, P., F. Adragna, M. J. Bell, F. Jacq, J. A. Johannessen, P.-Y. Le Traon, N. Pinardi, J. She (2009): Monitoring and Forecasting Core Services, The European MyOcean Example. Proceedings of OceanObs'09: Sustained Ocean Observations and Information for Society, Venice, Italy, 21-25 September 2009, ESA Publication WPP-30.

Impressum

Kuratorium für Forschung im Küsteningenieurwesen
c/o Bundesanstalt für Wasserbau | Wedeler Landstraße 157 | 22559 Hamburg

KFKI-Geschäftsstelle | t +49 (0) 40-81908-392 | f +49 (0) 40-81908-578 | kfki-sekretariat@baw.de | www.kfki.de

KFKI-Bibliothek | t +49 (0) 40-81908-378 | kfki-bibliothek@baw.de | webOPAC http://vzb.baw.de

Online Ressource: http://d-nb.info/995087016

CRITICAL OVERTOPPING RATES FOR BRUNSBÜTTEL LOCK

H. Rahlf[1]; H. Schüttrumpf[2];
[1]Federal Waterways Engineering and Research Institute; E-Mail: holger.rahlf@.baw.de;
[2]RWTH Aachen University; E-Mail: schuettrumpf@iww.rwth-aachen.de;

INTRODUCTION

The Kiel Canal connects the Elbe estuary at Brunsbüttel with the Kiel bight over a length of appr. 100 km. Thereby, it represents a direct connection between North and Baltic Sea and is the most frequented artificial waterway of the world. More than 43,000 ships pass the canal every year (for comparison: 14,000 ships pass the Panama canal every year). The canal is protected by four locks on both sides (Brunsbüttel and Kiel) to avoid high water level variations and currents in the canal. Brunsbüttel lock is situated in the tidal estuary Elbe with severe storm surges coming from the North Sea. Therefore, Brunsbüttel lock must be designed to withstand high storm surges and a design water level of 6.10 mNN.

Wave overtopping is one of the relevant stresses for Brunsbüttel lock gates. Present critical overtopping rates are not applicable for this specific lock situation. Therefore, the objective of the present case study was (i) to derive lock specific critical overtopping rates, (ii) to determine the relevant overtopping rates under design sea states and (iii) to determine new crest levels for the lock gates and the training dikes in a probabilistic way.

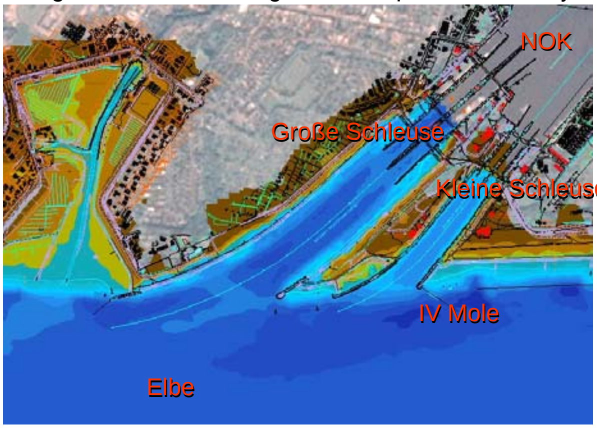

Fig. 1: Map of Brunsbüttel lock

NEW CRITICAL OVERTOPPING RATES

Critical overtopping rates for Brunsbüttel lock differ significantly from other critical overtopping rates (see: Eurotop-Manual, 2007: www.overtopping-manual.com). The Eurotop-manual presents critical overtopping rates for the safety of coastal structures like dikes and embankments, for the safety of persons and cars and finally for the safety of structures like buildings behind a dike. These critical overtopping rates can not be applied for Brunsbüttel lock due to the available high water storage volume behind the structure, the layout of a lock with three steel gates and training dikes on both sides of the lock and finally the strength of the steel structures. Therefore, six new critical overtopping parameters were identified and determined resulting in new critical overtopping rates. The following table gives an overview of the new critical overtopping rates which were proposed to apply for the redesign of Brunsbüttel lock:

(a) critical overtopping rate for connecting and training dikes = 2 l/(sm)
(b) critical overtopping rate for the safety of operations in the lock = 96 $m^3/(s)$
(c) critical overflow rate into the Kiel Canal due to high water level in the Elbe estuary = 937 $m^3/(s)$
(d) critical overtopping rate for the stability of the lock gates = 50 l/(sm)
(e) critical overtopping rate for the safety of the locks = 50 l/(sm)
(f) critical overtopping rate for the accessibility of the traffic control centre = 2 l/(sm)

Note that these (partly rather high) overtopping rates depend also on the operation of the lock itself and the large storage volume of the Kiel Canal.

Fig. 2: gate of the small lock

DETERMINATION OF OVERTOPPING RATES

The overtopping rates were determined on the basis of the Eurotop-manual (http://www.overtopping-manual.com). The crest level of the gates is 5.70 mNN and thus below design water level (6.10 mNN). Therefore, the case of combined wave overtopping and overflow had to be considered resulting in combined overtopping/overflow rates of 1.09 m^3/sm. The freeboads of the training and connecting dikes are in between R_C=0.0 m and R_C=0.98 m and thus resulting in very high overtopping rates of up to 1.07 $m^3/(sm)$.

PROHABILISTIC CREST LEVEL DESIGN

The overtopping rates were determined following the recommendations for probabilistic design of the Eurotop-manual. Two values were identified: The input parameters (wave height, wave period and wave direction) were calculated considering uncertainties. Therefore, the $q_{50\%}$ gives the average overtopping rate and the $q_{98\%}$ gives an upper limit of wave overtopping. The difference between both values is regarded as the uncertainty of the calculation.

CONCLUSION

Available critical overtopping rates are not suitable for all design situations of coastal structures. New lock specific critical overtopping rates were derived and recommended for application for Brunsbüttel lock. In such a case it is possible to increase the critical overtopping limits significantly in comparison to traditional structures. The crest level of Brunsbüttel lock was left low compared to the training and connecting dikes resulting in an economic but safe structure. The large storage volume of the Kiel Canal was taken into account.

Beitrag zum 3. Siegener Symposium „Sicherung von Dämmen, Deichen und Stauanlagen“ (12 und 13.3.2009)

Wellenüberlauf an Deichen – Stand der Wissenschaft und aktuelle Untersuchungen

Prof. Dr.-Ing. Holger Schüttrumpf
Institut für Wasserbau und Wasserwirtschaft, RWTH Aachen, Mies-van-der-Rohe-Str. 1; 52056 Aachen, Tel.: 0241-8025262, E-Mail: schuettrumpf@iww.rwth-aachen.de

1 Einleitung

Fluss-, See- und Ästuardeiche schützen große Landflächen vor den Gefahren durch Hochwässer und Sturmfluten. Besonders beeindruckend ist die Bedeutung der Deiche am Beispiel der zu schützenden Fläche sowie der geschützten Bevölkerung im Küstenbereich (Tab. 1). Hier schützen mehr als 1473 km See- und Ästuardeiche mehr als 2,3 Mio. Personen. Allein in Hamburg werden Werte von 10 Mrd. Euro durch Hochwasserschutzmaßnahmen – insbesondere durch Deiche – geschützt. Dies bedeutet aber auch, dass die Funktionsfähigkeit der Deiche bei extremen Sturmfluten gewährleistet sein muss und dass die wirkenden Kräfte und Belastungen bei Sturmflut als Grundlage für eine sichere Deichbemessung bekannt sein müssen.

Tab. 1: Übersicht über Deichlängen, geschützte Flächen und geschützte Bevölkerung für See- und Ästuardeiche (Schüttrumpf, 2008)

Bundesland	Deichlänge (1. Deichlinie)	Geschützte Fläche	Geschützte Bevölkerung
Niedersachsen (inkl. Inseln)	645 km	6,600 km^2	1,200,000
Schleswig-Holstein	527 km	3,800 km^2	345,000
Bremen	74 km	360 km^2	570,000
Hamburg	77.5 km	270 km^2	180,000
Mecklenburg-Vorpommern	150 km	1020 km^2	90,000

Insbesondere an der Küste und in den Ästuaren – aber auch an den großen Flüssen (z.B. Niederrhein) – stellt die dynamische Belastung der Deiche durch Wellenüberlauf bei extremen Wasserständen und Seegang eine Gefährdung der Deiche dar. Analysen der Deichschäden in Zusammenhang mit der großen Hollandsturmflut im Jahr 1953, der Hamburg-Sturmflut im Jahr 1962, der beiden Sturmflutereignisse im Jahr 1976 aber auch des Hurrikans Katrina im Jahr 2005 zeigen, dass viele Deiche durch Wellenüberlauf zerstört wurden und schließlich versagt haben (Schüttrumpf u. Oumeraci, 2004). Durch den Wellenüberlauf infiltriert Wasser in die Grasnarbe und weicht diese auf. Die Grasnarbe verliert ihre Festigkeit und beginnt sich zu verformen. Bei weiterer Wellenüberlaufbelastung kommt es schließlich zu einem Abrutschen der Grasnarbe (Weissmann, 2003). Zusätzlich wirkt durch die Wellenüberlaufströmung eine Schubspannung auf die Grasnarbe, erodiert u.U. einzelne Bodenteilchen und legt damit die Graswurzeln frei. Auch dieser Erosionsmechanismus kann zu einem Versagen der Binnenböschung und somit zum Deichbruch führen (Abb. 1).

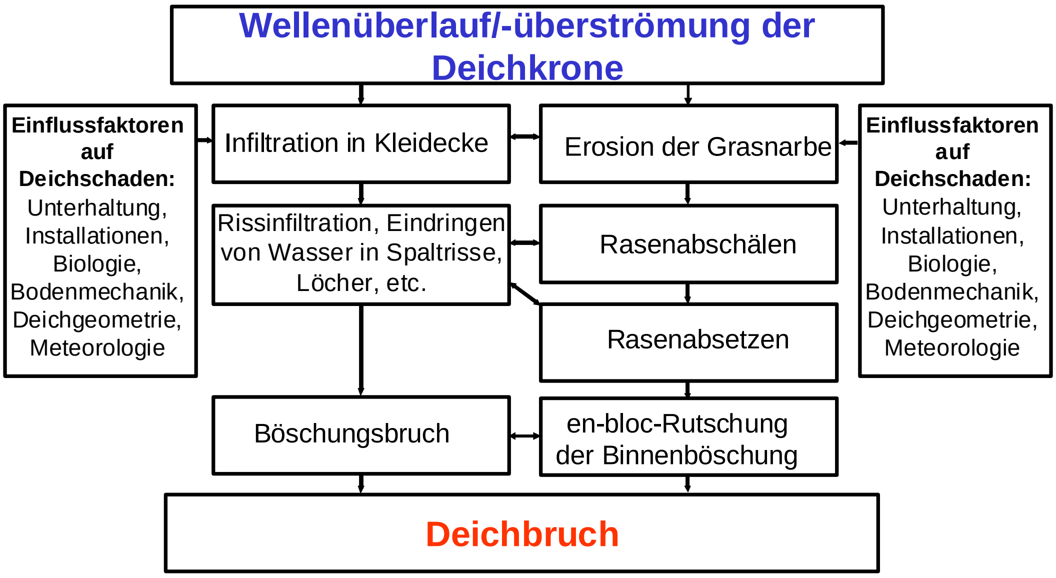

Abb. 1: Versagen der Binnenböschung infolge Wellenüberlauf (Schüttrumpf, 2004)

Bis in die 80-iger Jahre war es das Ziel der Deichbemessung, Wellenüberlauf vollständig zu vermeiden und die Deiche wurden nur auf Wellenauflauf bemessen. Daher hat sich die Forschung über viele Jahrzehnte nur mit dem Wellenauflauf und nicht mit dem Thema Wellenüberlauf beschäftigt. Grundlegende Untersuchungen zur Bestimmung des Wellenauflaufs an Deichen wurden von Wassing (1957), Hunt (1959), Battjes (1974) und Führböter (1991) durchgeführt.
Aufgrund der Unsicherheiten in der Festlegung der Bemessungsgrößen (Wasserstand, Wellenparameter) sowie der Erkenntnis, dass ein maximaler Wasserstand weder statistisch noch physikalisch bestimmt werden kann, gehen heutige Bemessungsphilosophien von der Festlegung eines Bemessungswasserstandes mit vorgegebener Eintrittswahrscheinlichkeit aus. Wellenüberlauf ist somit möglich und im Rahmen einer Deichbemessung im Vergleich mit zulässigen bzw. kritischen Wellenüberlaufraten zu berücksichtigen.
Um ein Versagen einer Deichbinnenböschung infolge Wellenüberlauf und damit einen Deichbruch zu vermeiden, ist einerseits eine genaue Kenntnis der physikalischen Prozesse bei Wellenüberlauf sowie der relevanten Parameter erforderlich. Andererseits sind kritische Wellenüberlaufraten als zulässige Grenzwerte zu bestimmen.
Ziel der vorliegenden Arbeit ist es, den Wissenstand zum Wellenüberlauf sowie die maßgebenden Prozesse und Mechanismen kurz darzustellen. In diesem Zusammenhang wird auch auf das Eurotop-Manual (Pullen et al., 2007) verwiesen, das den derzeitigen Wissensstand zusammenfasst und national wie international für viele Wellenauflauf- und Wellenüberlaufberechnungen verwendet wird. Abschließend wird ein kurzer Ausblick auf weiteren Forschungsbedarf sowie aktuelle Untersuchungen zum Thema Wellenüberlauf gegeben, die noch nicht im Eurotop-Manual enthalten sind.

2 Parameter des Wellenüberlaufs

Maßgebende physikalische Größe zur Bestimmung der Wellenüberlaufbelastung ist die mittlere Wellenüberlaufrate q [l/(sm)]. Die mittlere Wellenüberlaufrate q stellt eine stark gemittelte Größe dar und beschreibt die Wellenüberlaufmenge V, die während der Zeit t_{ges} über den Deich strömt. Es gilt somit:

$$q = \frac{V}{t_{ges}}$$

Üblicherweise wird als Referenzzeit t_{ges} hier die Versuchsdauer angesetzt. Erste Untersuchungen zum Wellenüberlauf an Deichen und zur Bestimmung der mittleren Wellenüberlaufrate q wurden in Deutschland von Tautenhain (1981) und in England von Owen (1980) durchgeführt. Ziel dieser Untersuchungen war die Bestimmung der mittleren Wellenüberlaufrate q [l/(sm)] als Funktion der Seegangsparameter und der Geometrie des Hochwasserbauwerks (Abb. 2).

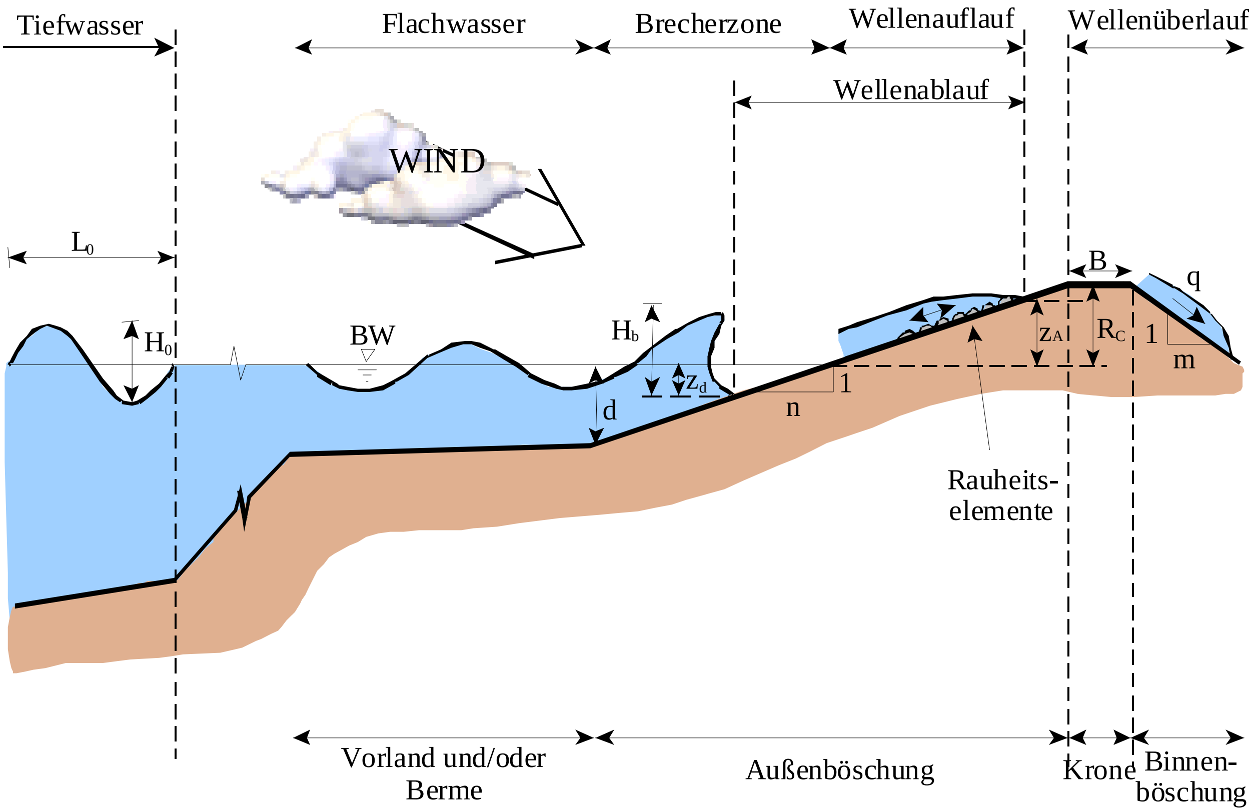

Abb. 2: Einflussparameter auf den Wellenauflauf und Wellenüberlauf (Schüttrumpf, 2001)

Owen hat auf der Grundlage experimenteller Untersuchungen an steil geneigten Ufermauern zwischen 1:n=1:1 und 1:n=1:5 erstmals den exponentiellen Zusammenhang zwischen dimensionsloser Überlaufrate Q* und dimensionsloser Freibordhöhe R* nachgewiesen. Tautenhain hat experimentelle Untersuchungen an einem 1:6 geneigten Seedeich durchgeführt und die Abhängigkeit der mittleren Wellenüberlaufrate q von der Wellenauflaufhöhe R dargestellt. Weitere Untersuchungen zur Bestimmung der mittleren Wellenüberlaufrate q wurden z.B. von Van der Meer u. Janssen (1995), Van Gent (1999) und Schüttrumpf (2001) durchgeführt. Außerdem folgten eine Vielzahl von Untersuchungen, um die Wirkung verschiedener Einflussfaktoren auf die mittlere Wellenüberlaufrate q zu ermitteln.

- Einfluss der Wellenangriffsrichtung (z.B. Van der Meer et al., 1998; Schüttrumpf et al., 2003)
- Einfluss der Böschungsrauheit (z.B. Szmytkiewicz et al., 1994; Schulz, 1992)
- Einfluss von Bermen (z.B. Van der Meer et al., 1998)
- Einfluss von Kronenmauern (z.B. Schüttrumpf et al., 2001)
- Einfluss von Wind (z.B. Ward et al., 1996; Brüning et al., 2009)

Der Stand der Wissenschaft zur Ermittlung der mittleren Wellenüberlaufrate ist im Eurotop-Manual (Pullen et al., 2007) zusammengefasst.

Mittlere Wellenüberlaufraten sind für die Bestimmung der Wellenüberlaufbelastung aber nur bedingt geeignet, da sie weder die Strömungsbelastung noch die Infiltrationsbelastung einzelner Wellen beschreiben. Für die Beschreibung der Wellenüberlaufbelastung sind somit die Strömungsgrößen des Wellenüberlaufs, d.h. die Strömungsgeschwindigkeiten und die Schichtdicken einzelner überlaufender Wellen geeigneter (Abb. 3). Untersuchungen zur Bestimmung der Strömungsgrößen des Wellenüberlaufs wurden bislang von Van Gent (2002) und Schüttrumpf (2001) durchgeführt. Schüttrumpf (2001) und Van Gent (2002) zeigen, dass die Wellenüberlaufströmung durch die Parameter Strömungsgeschwindigkeit des Wellenüberlaufs und Schichtdicke des Wellenüberlaufschwalls beschrieben werden kann. Eine Unterteilung in die drei Bereiche Deichaußenböschung, Deichkrone und Deichbinnenböschung ist dazu erforderlich, um in jedem Teilbereich Strömungsgeschwindigkeit v und Schichtdicke h zu ermitteln.

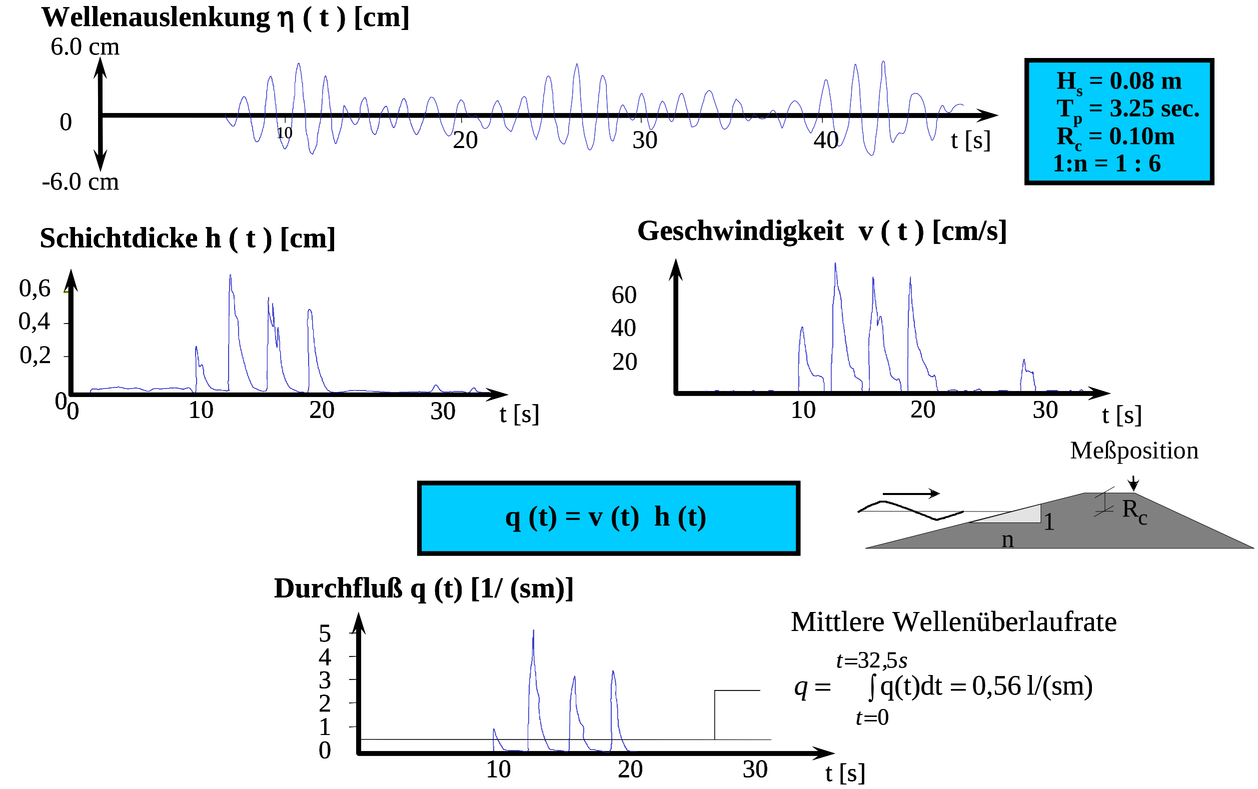

Abb. 3: Definition der Wellenüberlaufparameter (Schüttrumpf, 2001)

3 Eurotop-Manual

Der Wissensstand zum Thema Wellenüberlauf wurde auf der Grundlage nationaler und internationaler Forschungsprojekte in den vergangenen Jahren signifikant verbessert und erweitert. Beispiele für entsprechende Forschungsprojekte sind die beiden EU-Forschungsvorhaben OPTICREST und CLASH, die Untersuchungen in Großbritannien (z.B. VOWS-Projekt), aber insbesondere auch die BMBF-KFKI-Forschungsprojekte „Schräger Wellenauflauf an Deichen“ und „Belastung der Binnenböschung von Seedeichen“. Neu- und Weiterentwicklungen des Wissenstandes wurden insbesondere hinsichtlich der folgenden Themen erzielt:

- Ansätze zur Ermittlung mittlerer Wellenüberlaufraten für verschiedene Bauwerkstypen (Deiche, Ufermauern, senkrechte und geschüttete Wellenbrecher, HWS-Wände, etc.)
- Ansätze zur Berücksichtigung von Einflussfaktoren auf den Wellenüberlauf (Rauheit, Bermen, Schräger Wellenauflauf/-überlauf, Wind, Naturspektren, Kronenmauern)

- Ansätze zur Beschreibung der Wellenüberlaufströmung (Schichtdicken, Überlaufgeschwindigkeiten)
- Methoden zur Ermittlung mittlerer Wellenüberlaufraten (z.B. CLASH-Database, Neural Network, etc.)
- Ermittlung des Gefahrenpotentials durch Wellenüberlauf (kritische Wellenüberlaufraten, kritische Überlaufgeschwindigkeiten)
- Untersuchungen zum Einfluss von Maßstabs- und Modelleffekten auf den Wellenüberlauf
- Berücksichtigung von Unsicherheiten bei der Bemessung auf Wellenauflauf und -überlauf
- Probabilistische Ansätze zur Bemessung von Hochwasser- und Küstenschutzbauwerken

Aufgrund der zahlreichen Weiter- und Neuentwicklungen zum Wellenüberlauf mussten die vorhandenen Richtlinien und Empfehlungen zum Wellenauflauf/Wellenüberlauf in Deutschland, den Niederlanden und Großbritannien aktualisiert werden:

- Großbritannien: Design and Assessment Manual Wave Overtopping of Seawalls (Besley, 1999);
- Niederlande: Technical Report Wave Run-up and Wave Overtopping at dikes (van der Meer, 2002)
- Deutschland: Kapitel 4 der Empfehlungen des Arbeitsausschusses Küstenschutzwerke (EAK, 2002).

Da nationale Überarbeitungen der jeweiligen Richtlinien und Empfehlungen sehr zeit- und kostenintensiv sind und Synergieeffekte der jeweiligen nationalen Forschungsschwerpunkte nicht oder nur begrenzt genutzt werden können, haben die Environmental Agency (UK), Rijkswaterstaat (NL) und das Kuratorium für Forschung im Küsteningenieurwesen sowie der HTG-Ausschuss für Küstenschutzwerke (D) die Erarbeitung eines europäischen Wellenüberlaufhandbuchs unter Leitung von HR Wallingford im Rahmen des Eurotop-Projektes vereinbart. Im Folgenden soll das europäische Wellenüberlaufhandbuch kurz mit „*Eurotop-Manual*“ bezeichnet werden. Weitere Partner im Eurotop-Projekt waren neben HR Wallingford auch INFRAM (NL), die Bundesanstalt für Wasserbau (D) sowie die Universitäten von Edinburgh (UK) und Braunschweig (D). Ergänzende Beiträge zum *Eurotop-Manual* kamen vom *Steering Committee* (Projektbegleitende Lenkungsgruppe) sowie von Fachkollegen aus Italien und Dänemark.

Der vorliegende Beitrag soll einen Überblick über die Schwerpunkte des *Eurotop-Manuals* geben. Die vollständige Fassung wurde vom Kuratorium für Forschung im Küsteningenieurwesen im Heft 73 der Küste gedruckt bzw. steht auf www.overtopping-manual.com zum Download zur Verfügung steht.

Das Eurotop-Manual besteht aus zwei Teilen:

- *Eurotop-Manual* (das eigentliche Handbuch)
- *Calculation Tool* (internet-basierte Berechnungshilfe)

Das *Eurotop-Manual* (Abb. 4) selber besteht aus ca. 200 Seiten Text und ist unterteilt in die folgenden Kapitel:

Kapitel 1: Einleitung
Kapitel 2: Wasserstände und Wellenbedingungen
Kapitel 3: Zulässige Wellenüberlaufraten
Kapitel 4: Ermittlung des Wellenüberlaufs

Kapitel 5: Deiche und geneigte Ufermauern
Kapitel 6: Schüttsteinböschungen
Kapitel 7: Vertikale Bauwerke

Abb. 4: Eurotop-Manual (www.overtopping-manual.com)

Das *Eurotop-Manual* beschreibt die verfügbaren Methoden zur Ermittlung von Wellenauflauf und Wellenüberlauf für Hochwasser- und Küstenschutzbauwerke. Hierbei handelt es sich einerseits um die klassischen Wellenüberlaufformeln, die sehr intensiv diskutiert werden, aber auch um Methoden wie Neuronale Netze, die Clash-Datenbank, das Verfahren PC-Overtop, experimentelle und numerische Verfahren. Das Eurotop-Manual empfiehlt Methoden zur Ermittlung mittlerer Wellenüberlaufraten, maximaler Wellenüberlaufvolumina und des Anteils überlaufender Wellen. Für ausgewählte Bauwerke werden auch Ansätze zur Ermittlung von Überlaufgeschwindigkeiten und Schichtdicken des Wellenauflauf- und Wellenüberlaufschwalls empfohlen. Das Handbuch soll dem planenden Ingenieur außerdem Hilfestellung geben, die zulässigen Wellenüberlaufraten unter Bemessungsbedingungen festzulegen und dann auf der Grundlage der verfügbaren Ansätze nachzuweisen, dass die zulässigen Wellenüberlaufraten nicht überschritten werden.

Das *Eurotop-Manual* beschränkt sich in diesem Zusammenhang auf drei grundlegende Bauwerkstypen, die einen Großteil der Hochwasser- und Küstenschutzanlagen in Europa abdecken:

- Flach geneigte Deichböschungen und flach geneigte Ufermauern
- Schüttsteinböschungen und andere flach geneigte Böschungen mit rauer Oberfläche

- Vertikale Wände und steile Böschungen

Bei der Wellenüberlaufberechnung sind Unsicherheiten sowohl in den Eingangsparametern (Wellenparameter, geometrische Parameter) als auch in den Wellenüberlaufmodellen selber zu berücksichtigen. Daher wurde das Wellenüberlaufhandbuch so aufbereitet, dass sowohl eine deterministische als auch eine probabilistische Ermittlung des Wellenüberlaufs möglich ist. Entsprechende Ansätze werden getrennt dargestellt, und am Ende jedes Bauwerkskapitels (Kapitel 5, 6, 7 des Eurotop-Manuals) werden Empfehlungen zum Umgang mit den verschiedenen Unsicherheiten gegeben.

Ergänzt wird der Textteil um Informationen zur Struktur des *Calculation Tools* sowie zu Rechenbeispielen. Mit dem Calculation Tool sind die Autoren des Eurotop-Manuals neue Wege gegangen. Planenden und beratenden Ingenieuren werden durch das Calculation Tool Werkzeuge frei im Internet zur Verfügung gestellt, mit denen die Ermittlung der Wellenüberlaufparameter sehr einfach möglich ist.

Die erste Internet-Seite des *Calculation Tools* stellt eine Liste der wesentlichen Bauwerkstypen und der möglichen Methoden zur Wellenüberlaufermittlung dar. Um den Wellenüberlauf für ein bestimmtes Bauwerk zu berechnen, ist lediglich auf die Liste der Methoden rechts vom Bauwerk zu clicken, um zur Eingabeseite zu gelangen (Abb. 5).

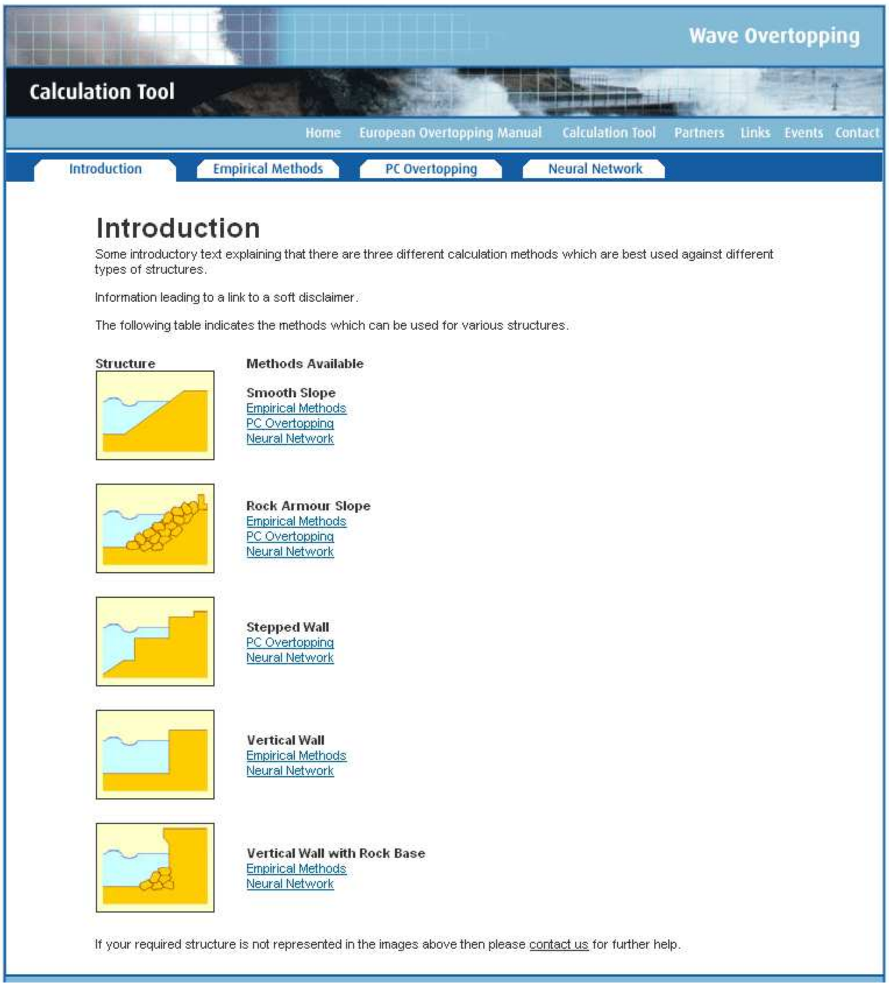

Abb. 5: Calculation Tool – Introduction (Schüttrumpf et al., 2007)

Wurde ein Bauwerk ausgewählt (hier: flach geneigte Böschung), die Methode gewählt (hier: *Empirical Calculator*), so müssen nur noch die Eingabeparameter in die entsprechenden Boxen eingetragen werden (Abb. 6). Durch Click auf den Button „Calculate Overtopping Rate“ wird die mittlere Wellenüberlaufrate berechnet. Auch ist eine Unterscheidung zwischen einer deterministischen und einer probabilistischen Berechnung möglich.

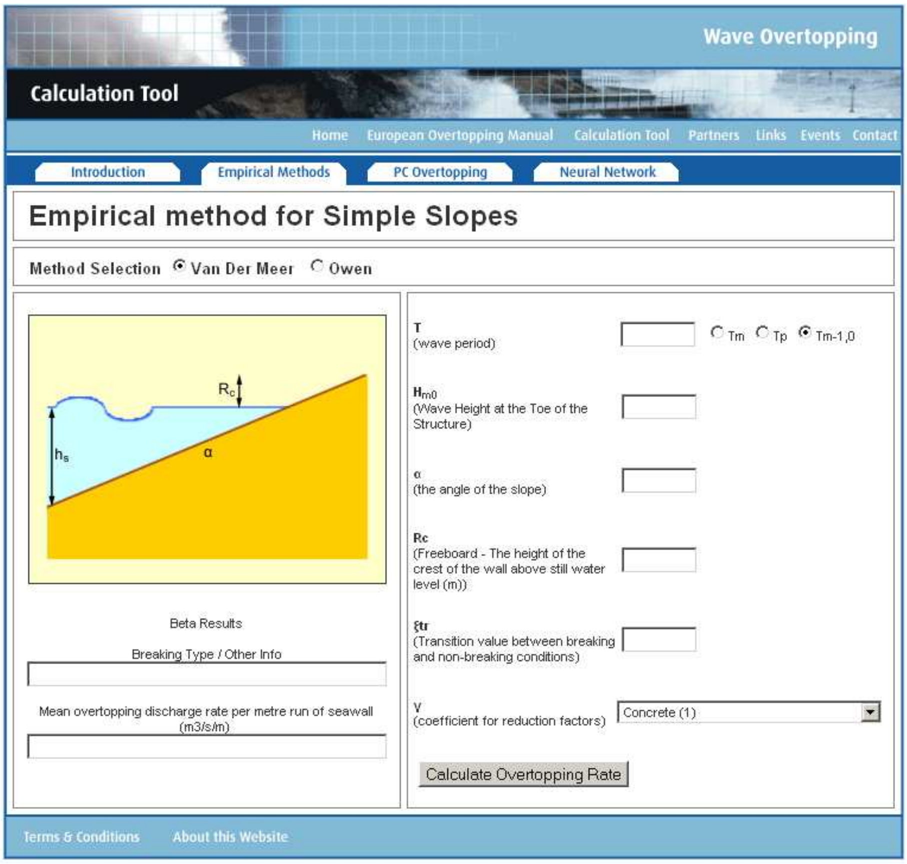

Abb. 6: Empirical Calculator für einfache Böschungen (Schüttrumpf et al., 2007)

4 Neue Wellenüberlaufuntersuchungen

4.1 Veranlassung

Viele experimentelle und numerische Untersuchungen wurden wie bereits erwähnt in den letzten Jahren durchgeführt. Trotzdem besteht nach wie vor ein hoher Forschungsbedarf, um die Wellenüberlaufprozesse exakt zu beschreiben. Während bisherige Untersuchungen zur Ermittlung von Wellenüberlaufparametern wie mittlerer Wellenüberlaufraten und Strömungsgrößen des Wellenüberlaufs überwiegend in Wellenkanälen durchgeführt wurden, gewinnt die Beschreibung der dreidimensionalen Prozesse zunehmend an Bedeutung.

Im Rahmen des vom BMBF geförderten Flowdike-Projektes (BMBF-03-KIS-075) werden aktuell die Wirkung von Wind und küstenparalleler Strömung auf den Wellenüberlauf in einem Wellenbecken bei Richtungsseegang untersucht.

Wind hat unterschiedliche Wirkungen auf den Wellenauflauf und den Wellenüberlauf. Einerseits führt Wind zu einer Deformation des Wellenfeldes, zur Entwicklung und zum Transport von Gischt, andererseits wirken windinduzierte Schubspannungen direkt auf den Wellenauflauf- und Wellenüberlaufschwall (Gonzalez-Escriva, 2006). Daher sollte der Windeinfluss bei typischen Bemessungsbedingungen nicht vernachlässigt werden. Insbesondere für kleine Wellenüberlaufraten an vertikalen Wänden zeigen Waal et al. (1996) einen signifikanten Einfluss des Windes. Andererseits haben Untersuchungen an geneigten Böschungen gezeigt, dass Wind bei hohen Wellenüberlaufraten und niedrigen

Windgeschwindigkeiten vernachlässigt werden kann (Ward et al., 1996). Eine besondere Schwierigkeit bei experimentellen Untersuchungen zum Windeinfluss besteht insbesondere in der exakten Ermittlung des Windeinflusses aufgrund von Modell- und Maßstabseffekten bei der Skalierung des Windes (Yamashiro et al. ,2006).
Andererseits wurden bislang keine systematischen Untersuchungen durchgeführt, um den Einfluss einer küstenparallelen Strömung auf den Wellenauflauf und Wellenüberlauf zu quantifizieren. Bislang haben nur Jensen and Frigaard (2000) einige wenige Modellversuche durchgeführt (ca. 10 Versuche), um den Einfluss einer küstenparallelen Strömung auf den Wellenauflauf für ein maßstäbliches Modell des Wellenbrechers in Zeebrugge zu bestimmen. Die Ergebnisse dieser Modellversuche zeigen eine Erhöhung der Wellenauflaufhöhen um rd. 20% bei einer küstenparallelen Strömung von 1m/s im Modell.
Die kombinierte Wirkung von Strömungs- und Windeffekten auf den Wellenauflauf und Wellenüberlauf wurde bislang ebenfalls noch nicht untersucht. Daher stellen experimentelle Untersuchungen zum Einfluss von Strömung und Wind auf den Wellenauf- und Wellenüberlauf ein wichtiges Thema für eine verlässliche Bemessung von Hochwasserschutzbauwerken dar.

4.2 Versuchsaufbau und Versuchsprogramm

Die experimentellen Untersuchungen zum Einfluss von Strömung und Wind auf den Wellenauflauf und Wellenüberlauf wurden im Shallow Water Wave Basin von DHI in Dänemark an einer einfachen 1:3 geneigten Böschung durchgeführt. Der Deich war in drei Bereiche unterteilt (Abb. 6), um aufgrund unterschiedlicher Deichkronenhöhen Wellenauflauf- und Wellenüberlaufuntersuchungen gleichzeitig durchführen zu können (Brüning et al., 2009).

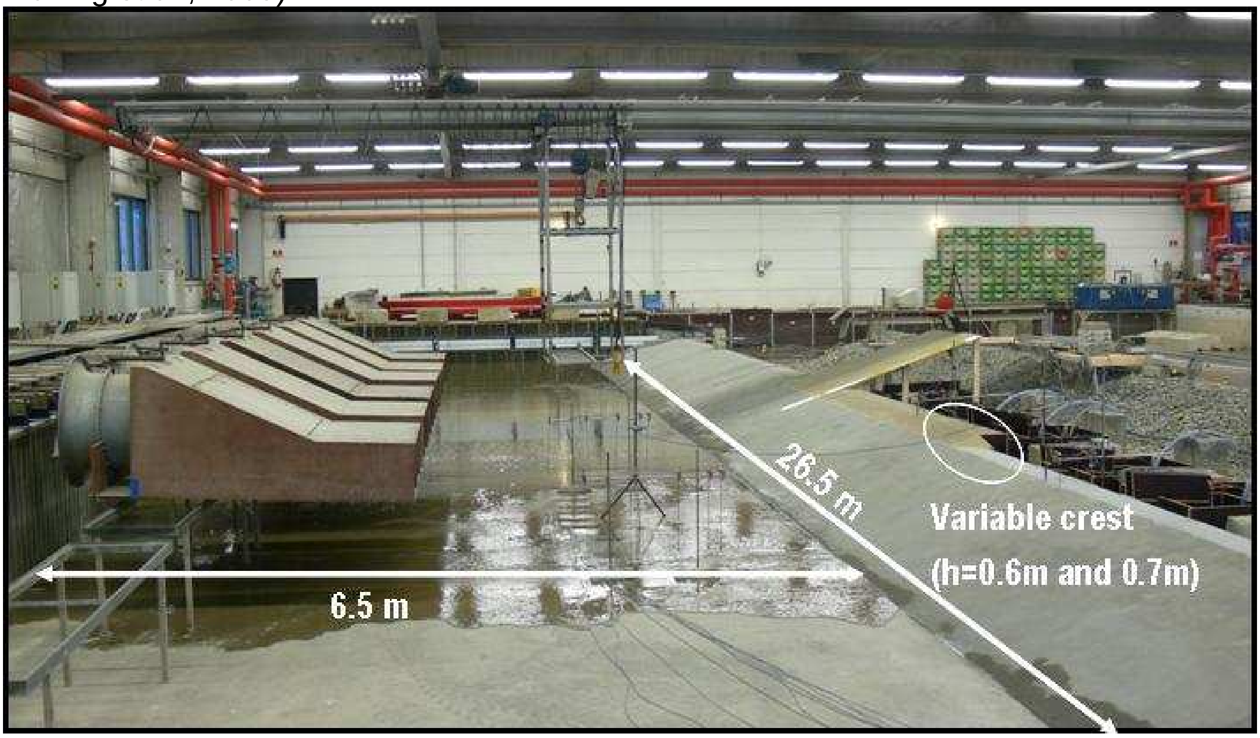

Abb. 6: Versuchsaufbau (Brüning et al., 2009)

Das Versuchsprogramm umfasste Modellversuche zum Wellenauflauf und Wellenüberlauf mit und ohne Strömungen aber auch mit und ohne Wind für unterschiedliche Wellenbedingungen (normaler Wellenangriff, schräger Wellenangriff, kurzkämmiger Seegang). Die Wellen-, Wellenauflauf-, Wellenüberlauf- und Strömungsparameter wurden an verschiedenen Positionen vor dem Deich und auf dem Deich gemessen. Eine genaue

Beschreibung der Versuchsrandbedingungen kann Brüning et al. (2009) entnommen werden.

4.3 Erste Ergebnisse

Die mittlere Wellenüberlaufrate q kann üblicherweise auf der Grundlage einer exponentiellen Gleichung beschrieben werden.

$$Q_* = Q_0 \cdot \exp(-b \cdot R_*)$$

In dieser Gleichung beschreibt Q_* die dimensionslose Wellenüberlaufrate, Q_0 die dimensionslose Wellenüberlaufrate für eine Freibordhöhe R_C=0, b einen empirischen Faktor zur Berücksichtigung geometrischer oder sonstiger Randbedingungen und R_* die dimensionslose Freibordhöhe.

Das Eurotop-Manual empfiehlt folgende Funktionen zur Bestimmung der mittleren Wellenüberlaufrate q für flach geneigte Böschungen:

$$\frac{q}{\sqrt{g \cdot H_{m0}^3}} = \frac{0.067}{\sqrt{\tan\alpha}} \gamma_b \cdot \xi_{m-1,0} \cdot \exp\left(-4.75 \frac{R_C}{\xi_{m-1,0} \cdot H_{m0} \cdot \gamma_b \cdot \gamma_f \cdot \gamma_\beta \cdot \gamma_v}\right)$$

mit einem Maximum von: $\frac{q}{\sqrt{g \cdot H_{m0}^3}} = 0.2 \cdot \exp\left(-2.6 \frac{R_C}{H_{m0} \cdot \gamma_f \cdot \gamma_\beta}\right)$

In dieser Funktion stellen q die mittlere Wellenüberlaufrate, g die Erdbeschleunigung, H_{m0} die Wellenhöhe, $\tan\alpha$ die Neigung der Außenböschung, γ_b den Reduktionsfaktor zur Berücksichtigung einer Berme, γ_f den Reduktionsfaktor zur Berücksichtigung der Böschungsrauheit, γ_β den Reduktionsfaktor zur Berücksichtigung der Wellenangriffsrichtung, γ_v den Reduktionsfaktor zur Berücksichtigung einer Kronenmauer, R_C die Freibordhöhe und $\xi_{m-1,0}$ die Brecherkennzahl unter Berücksichtigung der Wellenperiode $T_{m-1,0}$ dar.

Die Zuverlässigkeit dieser Funktion wird dadurch beschrieben, dass die beiden Koeffizienten 4,75 und 2,6 als Mittelwert einer Normalverteilung mit der Standardabweichung 0,5 bzw. 0,35 angesetzt werden.

Um den Einfluss von Strömung und Welle zu bestimmen, wurde die traditionelle Vorgehensweise gewählt, d.h. die Überlaufparameter mit Einfluss von Strömung oder Wind wurden ins Verhältnis zu den gleichen Modellversuchen ohne Wind bzw. Strömungseinfluss gesetzt. Auf dieser Grundlage wurden drei Reduktionsfaktoren für die Bestimmung des Einflusses der Wellenangriffsrichtung (γ_θ), den Einfluss einer küstenparallelen Strömung (γ_θ) und den Einfluss des Windes (γ_W) ermittelt. Es gilt:

$$\gamma_\theta = \frac{b(\theta)}{b(\theta = 0)}; \gamma_C = \frac{b(C)}{b(C = 0)}; \gamma_W = \frac{b(W)}{b(W = 0)}$$

Tab. 2 gibt einen Überblick über die drei Reduktionsfaktoren für brechende und nicht brechende Wellen. Abb. 7 zeigt beispielhaft die Vorgehensweise zur Bestimmung des Einflussfaktors für die Strömungsgeschwindigkeit auf der Grundlage der Versuchsergebnisse im Shallow Water Wave Basin. Weitere Details der experimentellen Untersuchungen können Brüning et al. (2009) entnommen werden.

Tab. 2: Reduktionsfaktoren zur Bestimmung des Einflusses von Strömung, Wind und Wellenangriffsrichtung

Breaking Waves			**Non-breaking Waves**		
Θ	**b**	γ_Θ	**angle**	**b**	γ_Θ
0°	-4,8358	1,000	0°	-2,901	1,000
-15°	-5,1857	0,933	-15°	-3,016	0,962
-30°	-6,2685	0,771	-30°	-3,419	0,848
45°	-8,03	0,602	45°	no data	no data
current	**b**	γ_C	**current**	**b**	γ_C
0m/S	-4,8358	1,000	0m/S	-2,901	1,000
0.15m/s	-5,291	0,914	0.15m/s	-2,868	1,011
0.3m/S	-5,477	0,883	0.3m/S	-2,995	0,969
wind	**b**	γ_W	**wind**	**b**	γ_W
0m/S	-4,8358	1,000	0m/S	-2,901	1,000
5m/s	no data	no data	5m/s	-2,757	1,052
10m/S	no data	no data	10m/S	-2,730	1,063

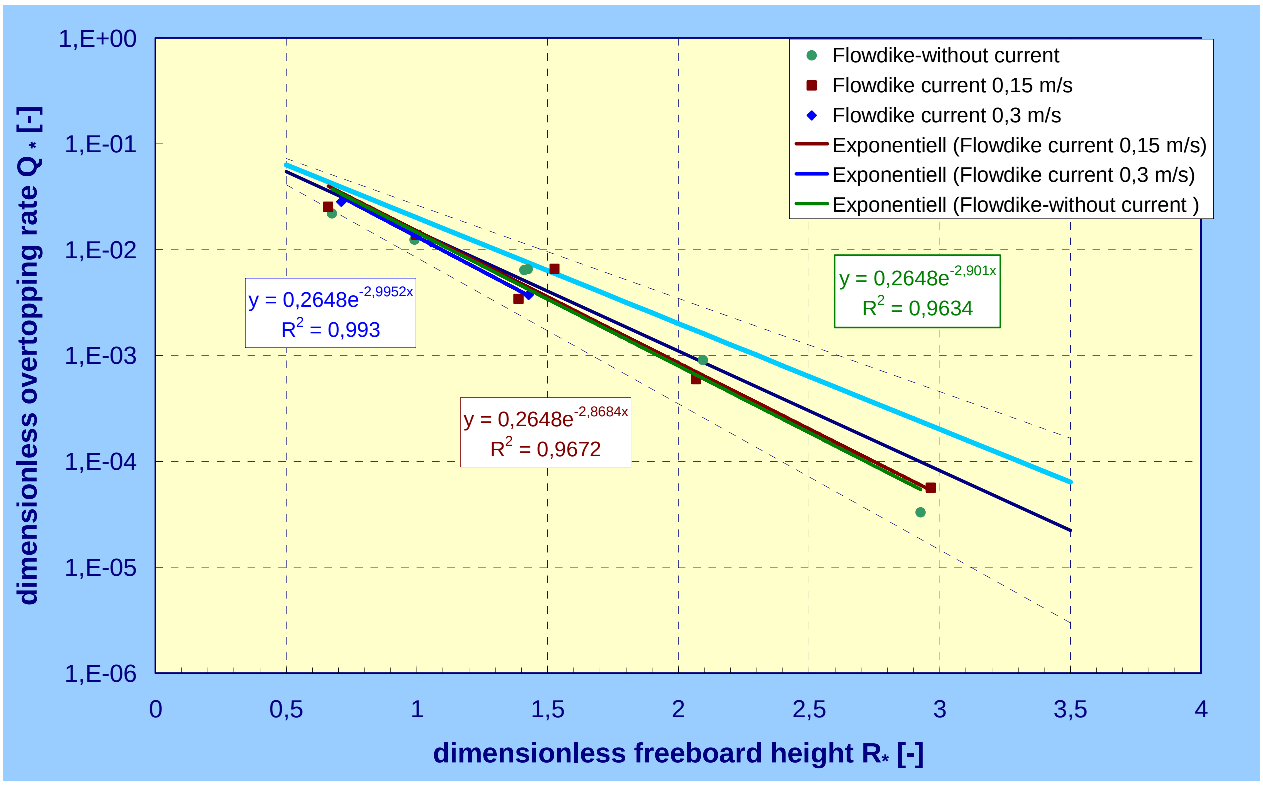

Abb. 7: Einfluss der Strömungsgeschwindigkeit auf den Wellenüberlauf

5 Zusammenfassung

Die Bemessung der Deiche auf Wellenüberlauf ist von hoher Bedeutung für die Sicherheit überflutungsgefährdeter Bereiche. Daher hat sich die Forschung in den vergangenen Jahren sehr intensiv mit dem Thema Wellenüberlauf beschäftigt und eine Vielzahl unterschiedlicher Ansätze und Methoden zur Bestimmung der Wellenüberlaufparameter entwickelt. Eine gute Übersicht des Wissensstandes zum Wellenüberlauf liefert das Eurotop-Manual, das in Zusammenarbeit britischer, niederländischer und deutscher Fachkollegen entstanden ist. Das Eurotop-Manual wird weltweit für viele Planungs- und Bemessungsaufgaben von Deichen eingesetzt und steht frei im Internet zur Verfügung.
Trotz der zahlreichen Untersuchungen zum Thema gibt es weiterhin Forschungsbedarf. Exemplarisch werden im Rahmen dieses Beitrags erste Ergebnisse dreidimensionaler Untersuchungen in einem Wellenbecken zur Bestimmung des Einflusses von Wind und küstenparalleler Strömung auf den Wellenauflauf und Wellenüberlauf dargestellt.

6 Schriftttum

Battjes, J.A. (1974) Surf Similarity. Proc. 14th Int. Conf. On Coastal Engineering. Kopenhagen. S. 466-480

Brüning, A.;Gilli, S.; Lorke, S.; Pohl, R.; Schlütter, F.; Spano, M.; van der Meer, J.; Werk, S.; Schüttrumpf, H. (2009) Flowdike – Investigating the effect of wind and current on wave run-up and wave overtopping. Proceedings 4th SCACR-Conference Barcelona

Führböter, A. (1991) Wellenbelastung von Deich- und Deckwerksböschungen. Jahrbuch der Hafenbautechnischen Gesellschaft. Bd. 46. S. 225-282

Gonzalez-Escriva, J.A. (2006) The role of wind in wave run-up and overtopping of coastal structures. Proc. 30th Int. Conf. on Coastal Engineering. San Diego

Hunt, A. (1959) Deesign of Seawalls and Breakwaters. Journal of the waterways and harbours division. S. 123-152

Jensen, M.S. and Frigaard, P. (2000) Zeebrugge model: Wave runup under simulated prototype storms (II) and The influence on wave run-up introducing a current. Report Hydraulics and Coastal Engineering Laboratory. Aalborg University. OPTICREST-project.

Owen, M.W. (1980) Design of Seawalls allowing for Wave Overtopping. Report No. EX 924. HR Wallingford

Pullen, T.; Allsop, W.; Bruce, T.; Kortenhaus, A.; Schüttrumpf, H.; Van der Meer, J.W. (2007) Eurotop – Wave overtopping of sea defences and related structures: Assessment Manual. Die Küste. H. 73. Verlag: Boyens Medien GmbH & Co. KG. Heide i. Holstein

Schulz, K.P. (1992) Maßstabseffekte beim Wellenauflauf auf glatten und rauhen Böschungen. Mitteilungen des Leichtweiß-Instituts für Wasserbau. H. 120

Schüttrumpf, H. (2001) Wellenüberlaufströmung bei Seedeichen – Experimentelle und theoretische Untersuchungen. Dissertation. Leichtweiß-Institut für Wasserbau.

Schüttrumpf, H.; Oumeraci, H.; Thorenz, F.; Möller, J. (2001) Reconstruction and Rehabilitation of a historical Seawall at Norderney. Proceedings Coastlines, Structures and Breakwaters Conference. London. Thomas-Telford-Verlag. 257-268

Schüttrumpf, H.; Barthel, V.; Ohle, N.; Möller, J.; Daemrich, K.-F. (2003) Run-up of Oblique Waves on Sloped Structures. COPEDEC VI. Colombo, Sri Lanka

Schüttrumpf, H.; Oumeraci, H. (2004) Learning from Sea Dike Failures. PIANC-Bulletin N^{o} 117, S. 47-60

Schüttrumpf, H.; Kortenhaus, A.; Van der Meer, J.; Pullen, T.; Allsop, W.; Bruce, T. (2007) Eurotop – Das europäische Wellenüberlaufhandbuch – Eine Kurzfassung. Die Küste. H. 72. Verlag: Boyens Medien GmbH & Co KG. Heide i. Holstein

Schüttrumpf, H. (2008) Sea dikes in Germany. Die Küste H. 74. S. 189-199. Verlag: Boyens Medien GmbH & Co. KG. Heide i. Holstein.

Szmytkiewicz, M.; Zeidler, R. und Pilarczyk, K. (1994) Irregular wave run-up on composite rough slopes. Coastal Dynamics. S. 599-613

Tautenhain, E. (1981) Der Wellenüberlauf an Seedeichen unter Berücksichtigung des Wellenauflaufs. Mitt. des Franzius-Instituts. H. 53. S. 1-245

Van der Meer, J.W. und Janssen, P.F.M. (1995) Wave Run-up and Wave Overtopping at Dikes. ASCE book on “Wave forces on inclined and vertical wall structures”. Ed. Z. Demirbilek.

Van der Meer, JK.W.; Tönjes, P.; de Waal, J. (1998) A code for dike heigt design and examination. Proceedings Int. Conf. On Coastlines, Structures and Breakwaters. (Ed. N.W.H. Allsop) Thomas Telford. London.

Van Gent, M.R.A. (1999) Physical Model Investigations on Coastal Structures with shallow foreshores – 2D model tests with single and double peaked wave energy spectra. Delft Hydraulics. Report H. 3608

Van Gent, M.R.A. (2002) Wave overtopping events at dikes. Proc. 28th Int. Conf. On Coastal Engineering. Cardiff. pp. 2203-2215

Waal, J.P.; Tönjes, P.; van der Meer, J.W. (1996) Wave overtopping of vertical structures including wind effect. Proc. 25th Int. Conf. on Coastal Engineering. Orlando.

Wassing, F. (1957) Model investigations of wave run-up carried out in the Netherlands during the last twenty years. Proc. 6th Int. Conf. On Coastal Eng. Gainesville. S. 700-714

Ward, D.L.; Zhang, J.; Wibner, C. und Cinotto, C.M. (1996) Wind effects on runup and overtopping of coastal structures. Proc. 25th Ing. Conf. On Coastal Engineering. Orlando. S. 2206-2215

Weissmann, R. (2003) Die Widerstandsfähigkeit von Seedeichbinnenböschungen gegenüber ablaufendem Wasser. Dissertation. Mitteilungen aus dem Fachgebiet Grundbau und Bodenmechanik der Universität Duisburg-Essen. H. 30. Verlag Glückauf GmbH

Yamashiro, M.; Yoshida, A.; Hashimoto, H.; Irie, I. (2006) Conversion ratio of wind velocity from prototype to experimental model on wave overtopping. Proc. 30th Int. Conf. on Coastal Engineering. San Diego. California. Pp. 4753-4765

FLOW DEPTHS AND VELOCITIES AT CREST AND INNER SLOPE OF A DIKE, IN THEORY AND WITH THE WAVE OVERTOPPING SIMULATOR

Jentsje W. van der Meer[1], Bianca Hardeman[2], Gosse-Jan Steendam[3], Holger Schüttrumpf[4] and Henk Verheij[5],

Wave overtopping discharges at coastal structures are well described in the EurOtop Manual (2007), including the distribution of overtopping wave volumes. Each volume that overtops a dike or levee will have a certain flow velocity and depth record in time, often given by the maximum velocity and flow depth. This paper describes some further development of the theory on flow depth and velocities on the crest, but will also show an inconsistency with respect to the mass balance. The second part of the paper gives an analysis of measured values on real dikes, simulated by the Wave Overtopping Simulator. It gives also the method of "cumulative hydraulic load" to compare overtopping discharges for different wave conditions. A large wave height with less overtopping waves, but larger overtopping wave volumes, is more damaging than a small wave height with more, but smaller overtopping volumes, even if the overtopping discharge is similar. The reasons to develop the cumulative hydraulic load have been compared with the recently in the US developed method of erosional equivalence.

Keywords: dikes, levees, overtopping, flow depth, flow velocity, wave overtopping simulator, erosional index

INTRODUCTION

Small and large scale model testing is often applied to measure wave overtopping at coastal structures. This wave overtopping determines the crest height of dikes, levees, breakwaters and other structures. Severe wave overtopping may damage the crest and landward side of the dike or levee by the overtopping flow. The mean discharge, q, and the distribution of overtopping wave volumes describe the wave overtopping for a main part. But each overtopping volume gives a flow depth and flow velocity at the crest and landward slope and each volume has a certain overtopping duration.

The Wave Overtopping Simulator (Van der Meer et al. 2006, 2007, 2008, 2009) simulates the overtopping wave tongues at the crest of a real dike and the development has been based on existing theory of flow depths and flow velocities. It appears, however, that this existing theory leads to a discrepancy and this discrepancy will be described in the paper.

It is not easy to measure flow depth and flow velocity in reality on a dike as the flow is very turbulent and a lot of air is entrapped. This is in contrast to small scale model testing. Conventional instruments seem not to be able to measure the flow accurately and therefore new, practical and robust, instruments have been developed. Measurements performed in March 2010 will be described and analyzed.

Finally, the effect of wave overtopping cannot be described by the wave overtopping discharge only. Severe (sea) wave conditions may give the same overtopping discharge as for much milder (river) wave conditions. In the first situation less waves overtop, but the overtopping wave volume (and consequently flow depth and velocity) is larger than for the mild condition, where many waves overtop with small overtopping wave volumes. A parameter or erosional index has to be developed which must be able to describe the different behaviour. This paper presents the "cumulative hydraulic load" and this has been compared with the developed theory on "erosional equivalence" by Dean et al. (2010).

FLOW DEPTH AND FLOW VELOCITY

Distribution of Overtopping Wave Volumes

Wave overtopping discharges at all kind of coastal structures are well described in the EurOtop Manual (2007), including the distribution of overtopping wave volumes. The overtopping discharge, q, is simply the total volume of overtopped water (per unit length) in a certain duration, divided by this duration. There will be a certain number of overtopping waves that produce a distribution of overtopping wave volumes. The distribution is characterized by many small overtopping waves and a few much larger ones, see also the EurOtop Manual (2007). The distribution can be described by:

[1] Van der Meer Consulting BV, P.O. Box 423, 8440 AK, Heerenveen, NL, jm@vandermeerconsulting.nl
[2] Rijkswaterstaat, Centre for Water Management; NL; bianca.hardeman@rws.nl
[3] Infram; NL; gosse.jan.steendam@infram.nl
[4] University of Aachen, DE; schuettrumpf@iww.rwth-aachen.de
[5] Delft University of Technology and Deltares; NL; henk.verheij@deltares.nl

$$P_V = P(\underline{V} \leq V) = 1 - \exp\left[-\left(\frac{V}{a}\right)^{0.75}\right] \quad (1)$$

$$a = 0.84 \cdot T_m \cdot \frac{q}{P_{ov}} = 0.84 \cdot T_m \cdot q \cdot N_w / N_{ow} = 0.84 \cdot q \cdot t / N_{ow} \quad (2)$$

P_V = probability of the overtopping volume $\underline{V}$ being smaller than V
V = overtopping wave volume (m^3/m)
T_m = mean wave period (s)
q = mean overtopping discharge (m^3/s per m width)
N_w = number of incident waves
N_{ow} = number of overtopping waves
t = duration of test or storm (s)

The overtopping wave volumes in reality occur randomly in time. Figures 1 and 2 show the overtopping wave volumes in time as they were simulated by the Wave Overtopping Simulator. Tests were performed with 0.1; 1; 5; 10; 30; 50 and 75 l/s per m overtopping discharge and each test condition was kept for 6 hours. The difference between Figures 1 and 2 is that Figure 1 was produced for a significant wave height of 1 m (river dikes), peak period of 4 s, and Figure 2 for a wave height of 3 m (sea waves), peak period of 6.9 s. There is a large difference between the two conditions, in number of overtopping waves and overtopping wave volumes, caused by the difference in wave heights and periods.

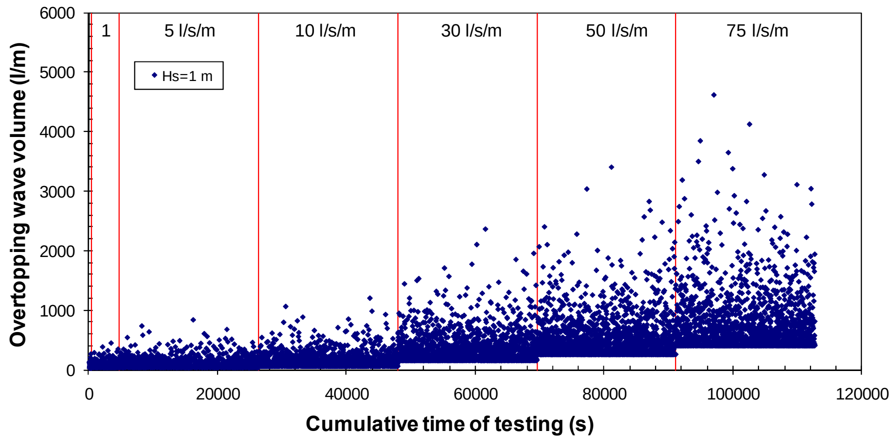

Figure 1. Overtopping wave volumes for various discharges and H_s = 1 m with T_p = 4 s

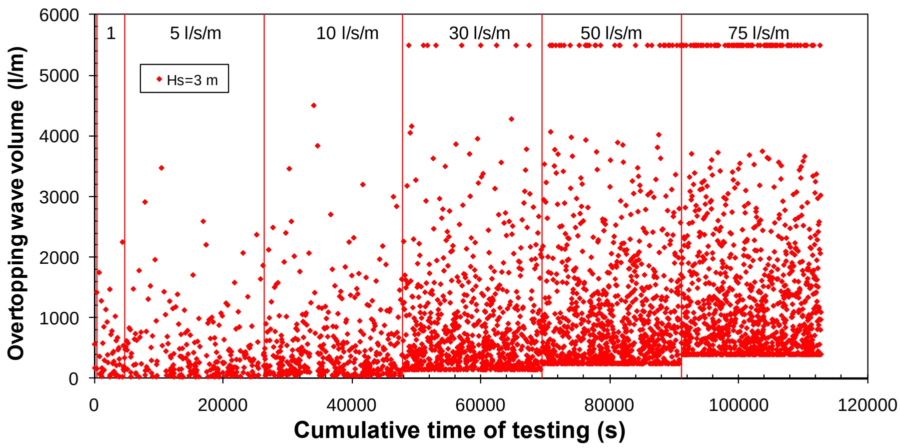

Figure 2. Overtopping wave volumes for various discharges and H_s = 3 m with T_p = 6.9 s

Existing Equations of Flow Depth and Flow Velocity

Equations for flow depth and velocity have been based on physical model investigations like by Schüttrumpf (2001, 2005) and Van Gent (2002), published as a joined paper in Schüttrumpf and Van Gent (2003). The problem at that time was that the flow depth predicted by Schüttrumpf was twice the one by Van Gent. For this reason the Wave Overtopping Simulator in 2006 was designed on flow velocity and not on flow depth. The EurOtop Manual (2007) also gives the equations.

Bosman et al. (2008) investigated this discrepancy and discovered that the difference in predicted flow depth could possibly be explained by the different seaward slopes (1:4 and 1:6) used by the different authors. He used a sinα to combine the equations. Bosman also studied flow depth and flow velocity on the crest of a dike or levee, and finally he looked at the flow time.

The basic equations for (maximum) flow depth and velocity are:

$$h_{2\%}(x_c=0) = c_{A,h}\ (R_{u2\%} - R_c) \qquad (3)$$

$$u_{2\%}(x_c=0) = c_{A,u}\ (g(R_{u2\%} - R_c))^{0.5} \qquad (4)$$

where:

$h_{2\%}$= flow depth exceeded by 2% of the incident waves [m]
$u_{2\%}$= flow velocity exceeded by 2% of the incident waves [m/s]
x_c= location on the crest (x_c=0 is the transition from seaward slope to the crest) [m]
$c_{A,h}$= coefficient for the flow depth [-]
$c_{A,u}$= coefficient for the flow velocity [-]
$R_{u2\%}$= 2% wave run-up level [m]
R_c = crest freeboard (vertical distance between crest and stil water level)) [m]

The coefficients where found as in Table 1. The Overtopping Simulator was designed with $c_{A,u}$ = 1.35.

Table 1. Coefficients in Equations (3) and (4)

Author	$c_{A,h}$	$c_{A,u}$
Schüttrumpf (2001,2005)	0.33	1.37
Van Gent (2002)	0.15	1.33
Bosman (2007)	$0.010/\sin^2\alpha$	$0.30/\sin\alpha$
Bosman (2007) 1:4	0.17	1.24
Bosman (2007) 1:6	0.37	1.82

Flowdike developments

The Flowdike project has been executed under the European Union programme Hydalab III. The objective was to investigate the influence of currents along a dike on wave run-up and wave overtopping. Leading partner was the University of Aachen in Germany. The tests were performed in the wave-current basin of the Danish Hydraulic Institute, DHI, at Hørsholm, see Figure 3.

Figure 3. Overall view of the Flowdike model with two crest heights and the run-up board.

The experimental investigations were performed for a simple 1:3 slope, typical for river dikes. The slope was divided into two separate parts to perform wave run-up and wave overtopping tests at the same time. The overtopping tests were performed on slope sections with crest freeboards of 0.1 m and 0.2 m. The crest width was 0.30 m. Flow velocities and flow depths were measured at the transition from seaward slope to the crest and 0.30 m behind this point, at the end of the crest.

The slope of 1:3 is steeper than the slopes of Van Gent (1:4) and Schüttrumpf (1:6). Bosman et al. (2008) used a sinα in his equations (Equations 3 and 4), which for fairly gentle slopes is almost equal to the more often used cotα. The extra data by the Flowdike project showed that the flow depth $h_{2\%}$ could not be described by Equation (3) as the data for the 1:3 slope fell in between the data for the 1:4 and 1:6 slope. But the influence of slope angle was clearly visible for the flow velocity $u_{2\%}$. Figure 4 gives all data for the flow depth and Figure 5 for the flow velocity. Note that data with "Conf. A-D'" belong to Van Gent (2002).

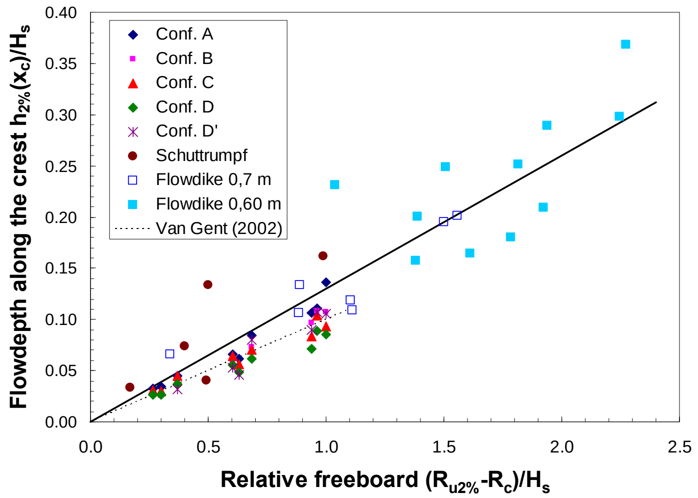

Figure 4. Flow depth at the landward crest, including Flowdike data.

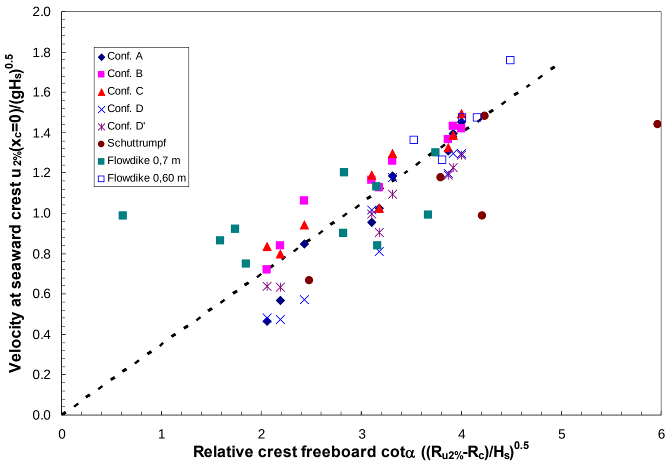

Figure 5. Flow velocity at the seaward crest, including the seaward slope cotα.

The analysis led to the following summary of equations for flow velocity and flow depth on and along the crest of a dike, with a smooth slope. The flow depth reduces directly behind the seaward crest and remains then almost constant along the crest. This flow depth along the crest is given in Figure 4 and Equation 5. The flow depth at the seaward crest is 50% larger than given in Equation 5.

$$h_{2\%}(x_c) = 0.13\ (R_{u2\%} - R_c) \qquad (5)$$

The flow velocity on the seaward crest is given in Figure 5 and can be described by Equation 6:

$$u_{2\%}(x_c{=}0) = 0.35 \cot\alpha\ (g(R_{u2\%} - R_c))^{0.5} \qquad (6)$$

The decay of flow velocity along the crest is given by Equation 7:

$$u_{2\%}(x_c)/u_{2\%}(x_c=0) = \exp(-1.4\ x_c\ /\ L_{m-1,0}) \qquad (7)$$

Discrepancy in equations

By assuming a Rayleigh distribution for the flow velocity (Equation 6) and flow depth (Equation 5) the velocity and flow depth can be calculated for each overtopping wave volume with a certain probability of exceedance. Such calculations lead to graphs of flow velocity or flow depth versus overtopping wave volume. Figure 6 gives these graphs for an 8 ft (2.4 m) wave condition.

Curves are found for each overtopping discharge, which ranges from 0.1 - 2.0 cfs/ft (almost equal to 10 - 200 l/s per m). But the curves deviate from each other and for the same overtopping wave volume lower flow velocities and flow depths are found if the overtopping discharge increases. And the same happens for the flow duration. This is physically not possible as a decrease in flow velocity should result in an increase in flow depth or flow duration (mass balance).

It must be concluded that present knowledge and prediction formulae for flow velocity, flow depth and flow duration do not yet give consistent answers. More research is required to solve this discrepancy and probably the flow depth and velocity must become more dependent on wave period. Also the assumption about both flow depth and flow velocity having a Rayleigh distribution may be questioned.

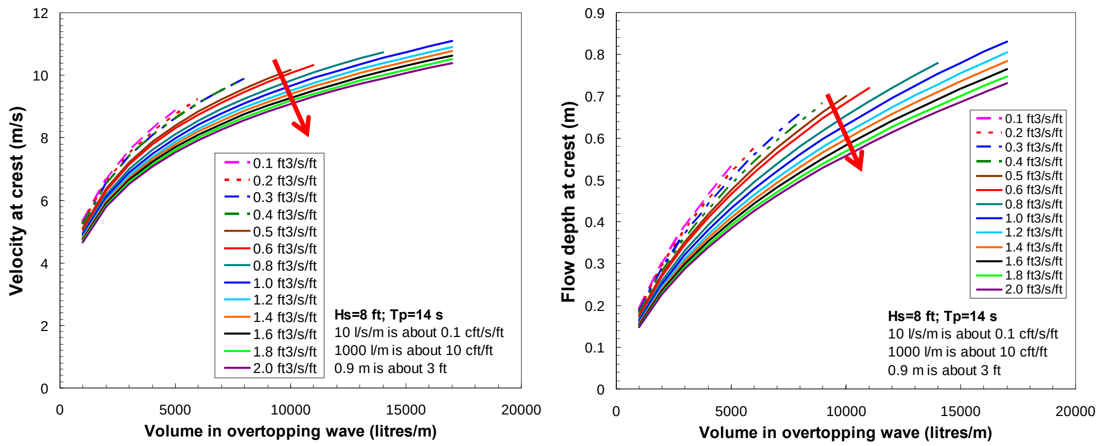

Figure 6. Flow velocity and flow depth at the seaward crest versus overtopping wave volume for a condition of H_{m0} = 8 ft (2.4 m) and T_p = 14 s. A similar volume may gave different values.

HYDRAULIC MEASUREMENTS ON A REAL DIKE

Test Set-up

The actual tests on erosion resistance of a sandy river dike have been described by Steendam et al. (2010). A special test was performed on a separate dike section, where the purpose was to measure hydraulic parameters only like flow depth, velocity and overtopping duration. The test consisted of three times repeated overtopping wave volumes, which increased in time from 200 l/m to 5,500 l/m (the maximum capacity of the Wave Overtopping Simulator).

Five "surf boards" were placed along the slope, see Figure 7. These surfboards are able to measure the flow depths (see Van der Meer et al. 2009). They are hinged on one side and the rotation of the surfboard, floating on top of the flow, is measured by a potentiometer. A new development is the use of a "paddle wheel" in this surfboard to measure the flow velocity. This paddle wheel is often used in small boats to measure their velocity in the water. As this was a new development and results were not guaranteed, only three paddle wheels were bought and installed. Two were installed in surfboards and one upside down on a plate in the soil. This last one measured the flow directly at the bottom, the others at the top of the flow.

Measurements were made from the inner crest line (at the transition to the landward slope) and 12 m along the slope. The slope was not completely straight, the upper part was 1:3.7 and the lower part 1:5.2. Surfboard 1 was located at the crest and surfboard 5 at the down slope.

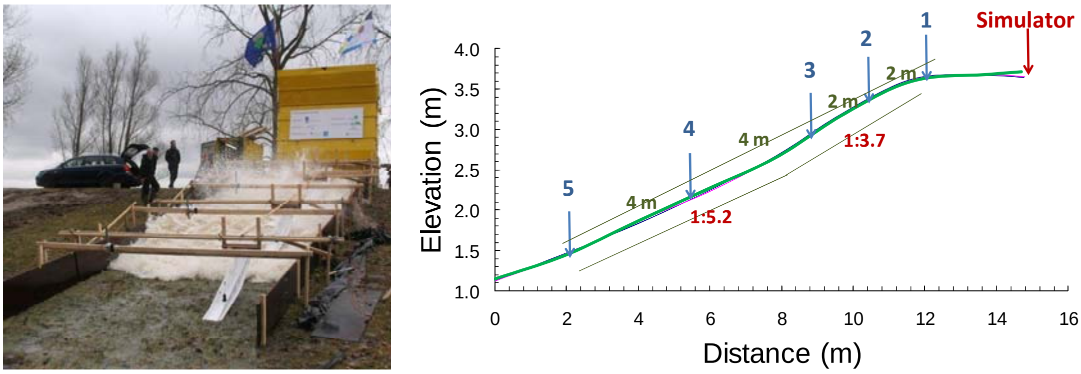

Figure 7. Test set-up with five surfboards for special measurements of flow depth, flow velocity and overtopping duration.

Measured records

The first analysis of measurements was to see what kind of records were obtained and if they made sense. Figure 8 shows the flow depth along the slope for an overtopping wave volume of 3000 l/m and the flow velocity along the slope for a volume of 1000 l/m. In general nice signals were recorded.

The (maximum) flow depth seems to decrease a little along the slope. The flow velocity for the paddle wheel at surfboard 3 and at the same location at the soil start at the same time, but the flow velocity at the soil is a little smaller as it is in the boundary layer of the flow.

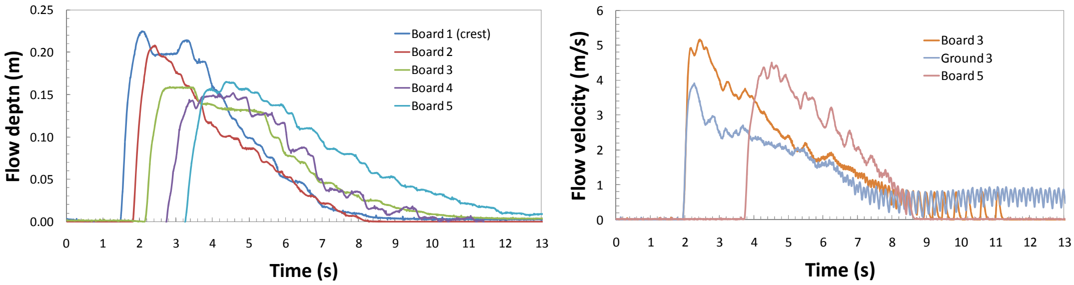

Figure 8. Records of flow depth and flow velocity along the slope.

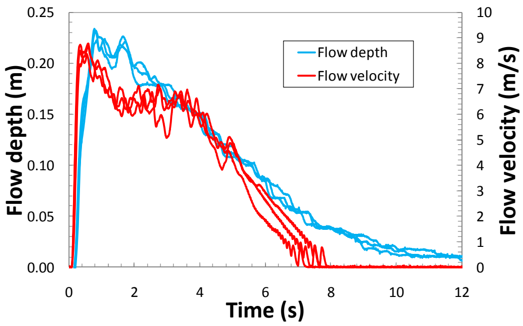

Figure 9 shows records of the flow depth and flow velocity for surfboard 5 (see Figure 7 for the location). The records are shown for an overtopping wave volume of 5000 l/m and for three waves that were repeated. The graph shows that a similar overtopping wave volume gives similar records and that the repeatability of the measurements is quite good.

Figure 9. Records for three overtopping wave volumes of 5000 l/m.

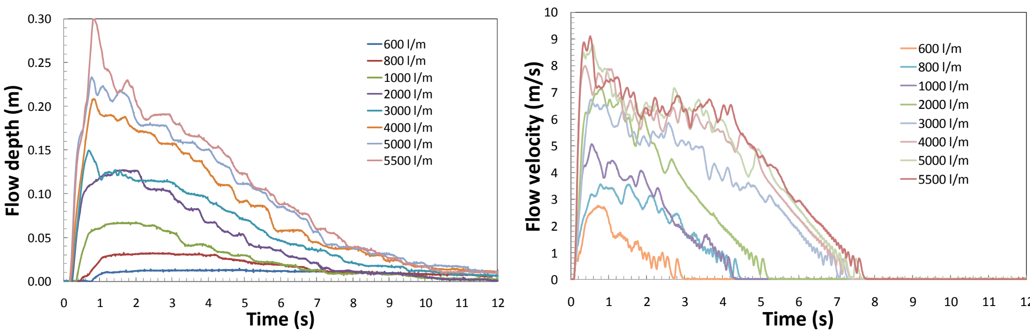

Figure 10. Flow depths and flow velocities for different overtopping wave volumes (surfboard 5).

Figure 10 was composed by putting the records of various overtopping wave volumes in one graph. The graphs show the development in flow depth and flow velocity from small overtopping wave volumes to the largest ones of 5,500 l/m. They were measured at surfboard 5. Flow depth increases with increasing volume, where the rise time to the peak is very short. Note that the overtopping time for small overtopping volumes is quite large. In fact these small overtopping volumes slow down along the grassed slope, a phenomenon that cannot or hardly be reproduced in a small scale model.

Also the flow velocities increase with increasing overtopping wave volumes. Maximum velocities of 9 m/s were reached. The paddle wheel reaches its maximum within tenths of seconds and responds very quickly. The overtopping durations measured with the paddle wheel seem shorter than measured for flow depth. The reason is that the paddle wheel was mounted a little above the ground and was not able to measure velocities in small flow depths. Where the surfboard measures flow depths of a few centimeters, the paddle wheel becomes dry.

Analysis of measurements

Figure 11 gives the (maximum) flow depth, h, versus the released overtopping wave volumes and for all five surfboards along the slope. The flow depth at the crest and also directly behind the crest is larger than further down the slope. It remains the same from 8-12 m from the crest, which may be explained by the changing slope angle after surfboard 3, see also Figure 7. The flow depth at the crest, mainly fitted on the larger overtopping wave volumes, can be given as (note coefficient 0.133 is not dimensionless):

$$h = 0.133\ V^{0.5} \qquad \text{(h in m; V in m}^3\text{/m)} \qquad (8)$$

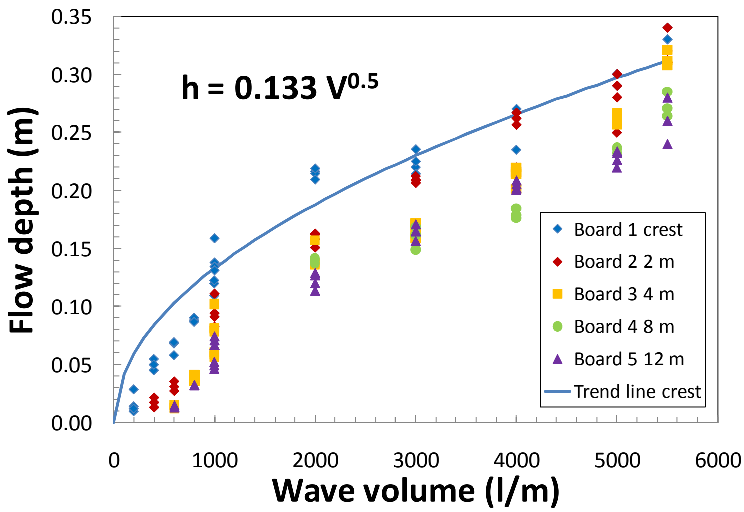

Figure 11. Flow depths along the slope as function of overtopping wave volumes.

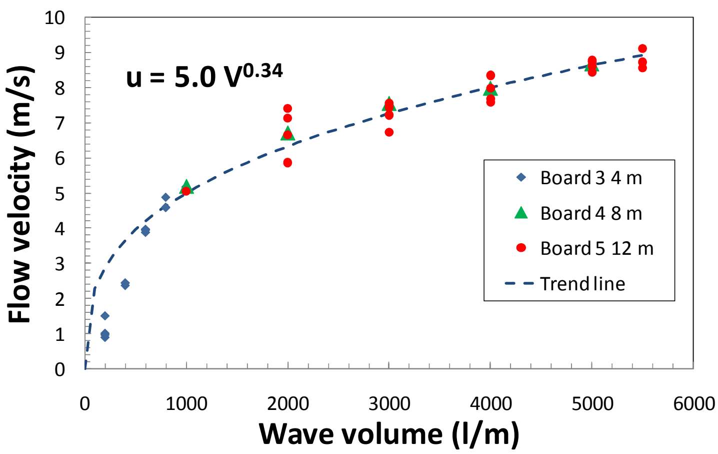

Figure 12. Flow velocities along the slope as function of overtopping wave volumes.

A similar graph was made in Figure 12, but now for the (maximum) flow velocities, u. There were only a few paddle wheels, but it seems that the velocity along the slope did not change significantly. All measurements form together a nice line and can be given by:

$$u = 5.0\ V^{0.34} \qquad \text{(u in m/s; V in m}^3\text{/m)} \qquad (9)$$

The paddle wheels in the surfboard measured the flow velocity on top of the flow. One paddle wheel was mounted upside down in the soil, in a flat and smooth plate. This paddle wheel measures part of the boundary layer and a comparison with the velocity on top of the flow may indicate the size of the boundary layer. Figure 13 is similar to Figure 12, but now the measurements at the ground/soil have been added.

For velocities up to 3 m/s (wave overtopping volumes up to 500 l/m) there is no difference between the ground level and the top of the flow. There is hardly a boundary layer in that case and the measured velocities can be considered as the depth-averaged velocities. For larger velocities and overtopping wave volumes it is clear that the velocity at ground level is smaller than at the top of the flow. Maximum velocities at ground level are about 5 m/s and at the top of the flow about 9 m/s.

But still 5 m/s is a large velocity very close to the ground level (the paddle wheel measures about 5 mm flow). It can be concluded that when flow velocities are smaller than 3 m/s (flow depths smaller than about 0.05 m), there is no boundary layer of significance. For larger velocities and flow depths it seems that the boundary layer is not much larger than a few centimeters, as the velocity in the first 5 mm from ground level is already 60-70% of the velocity at the top of the flow.

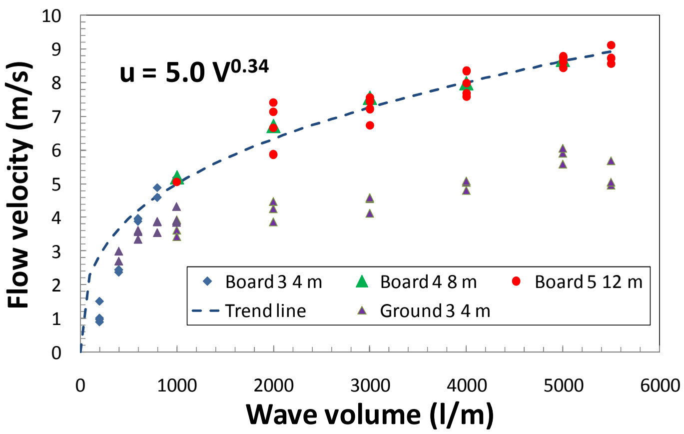

Figure 13. Flow velocities along the slope as function of overtopping wave volumes and compared with flow velocities at ground level.

It has been very difficult to measure flow velocities of overtopping water at real dikes and the surfboard with paddle wheel is a promising development. Another way of measuring the velocity is to measure the front velocity of the overtopping wave. Van der Meer et al. (2009) used a high speed camera to determine this front velocity. But the question that remains is whether the front velocity is equal to the maximum velocity in the flow and/or equal to the depth-averaged velocity.

With the surfboards and paddle wheels it is possible to measure velocity directly, but also front velocities can be calculated as the time difference of the wave front arriving at the paddle wheels or surfboards can be determined (and combined with the known distance between two instruments).

It appeared, after in depth analysis, that every surfboard has its own characteristics when the flow hits the surfboard. As the rise time in tenths of seconds is important and the rising of the surfboard was not identical for each surfboard, it was not possible to determine the front velocities from the flow depth measurements. Only if the distance between the surfboards was large enough, a reliable front velocity could be established. This was the case between surfboards 3 and 5, which were 8 m apart.

In a few measurements there were paddle wheels at surfboards 4 and 5 and the distance was here 4 m. Paddle wheels respond quickly and are good instruments to look at front velocities.

The front velocities as calculated between surfboards 4 and 5 (flow depth record) and between paddle wheels in surfboards 4 and 5 (velocity record) have been given in Figure 14. The curve in Figure 14 is not a fit to the data, but gives the (maximum) measured flow velocities, given by Eq. 9.

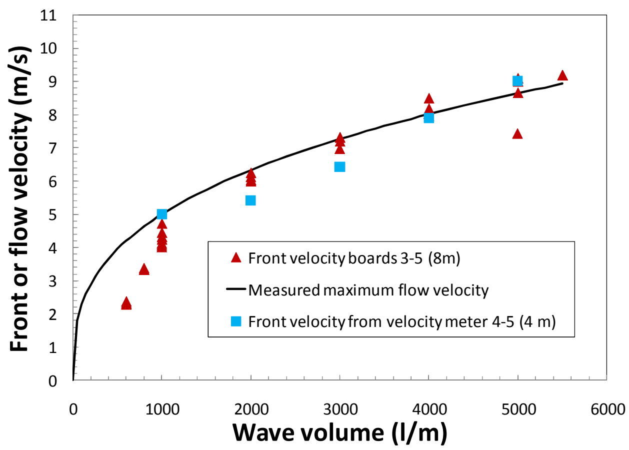

Figure 14. Front velocities calculated from flow depth and flow velocity records, compared with Eq. (9).

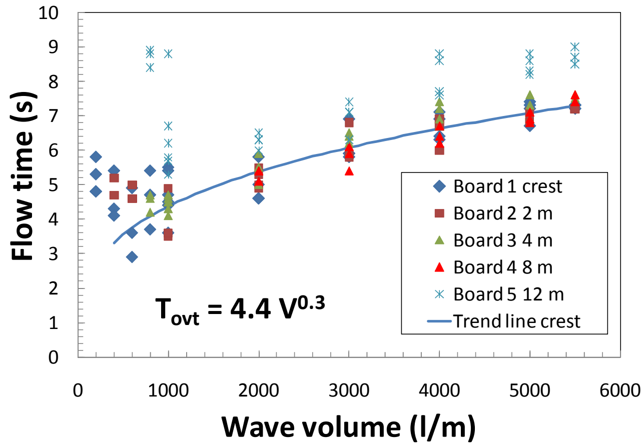

Figure 15. Overtopping durations, T_{ovt}, established from the flow depth records.

The curve in Figure 14 presents nicely the data points. It leads to the important conclusion that front velocities represent well the velocity at the top of the flow as well as the depth-averaged velocity in the layer, as a boundary layer will be very small.

Overtopping durations can be established from the flow depth records. It was hard to determine the overtopping durations for small overtopping wave volumes as water is still flowing a little along the grassed slope when the actual wave has passed already. Also small overtopping wave volumes slowed down the slope and although they were visible at the crest, they were not observed 12 m further down the slope.

Figure 15 gives the overtopping durations, T_{ovt}, as they were established from the various flow depth records. There is quite some scatter for overtopping volumes smaller than 1000 l/m, as explained above, but there is a nice trend for larger volumes. The data points show that there is hardly a change in overtopping duration for the first 8 m on the slope, but there is a slight increase between surfboard 4 and 5 along the more gentle slope. The overtopping duration at the crest can well be described by:

$$T_{ovt} = 4.4\ V^{0.3} \qquad (T_{ovt} \text{ in s; V in m}^3\text{/m}) \qquad (10)$$

Note that the coefficients in Equations 8-10 are not dimensionless. These three equations give (maximum) flow depth, (maximum) flow velocity and overtopping duration, all three as a function of the overtopping volume. There is also a physical relationship between these variables (mass balance) as integration of flow depth, multiplied by flow velocity (= discharge) over time gives the volume. It is a fairly good assumption that the records of an overtopping wave volume have a triangular shape, see also Figure 10.

This leads then to the following physical relationship, based on the mass balance:

$$V = 1/3\ h\ u\ T_{ovt} \qquad (11)$$

Combining Equations 8-10 leads to the following equation:

$$V^{1.14} = 0.34\ h\ u\ T_{ovt} \qquad (12)$$

The power coefficient of 1.14 in Equation 12 is not equal to 1.0 as in Equation 11, but is still close to it, representing a fairly straight line. For a volume of 1 m^3/m there is almost a perfect match between the coefficients 1/3 and 0.34. Equations 8-10 were established independently and based on the similarity between Equations 11 and 12 it can be concluded that Equations 8-10 as a combination fullfill fairly well the requirements for the mass balance.

EROSIONAL INDICES

The first three years of testing in the Netherlands with the Wave Overtopping Simulator was done for an assumed wave condition of H_s = 2 m and T_p = 5.7 s, being an average wave condition for the Dutch dikes. But estuaries, rivers and small lakes may have design conditions which are smaller, whereas dikes directly facing the North Sea may have larger conditions. It is the crest freeboard that governs the actual overtopping discharge, but the wave conditions determine how overtopping occurs. Larger waves give larger overtopping volumes, but less overtopping waves. From that point of view the overtopping discharge does not describe the full story of wave overtopping, see also Figs. 2 and 3.

The objective of tests with the Wave Overtopping Simulator is to test the erosional strength of the crest and landward slope against wave overtopping. But do different wave conditions indeed give different moments for damage or failure of the grass? Tests performed in February and March 2010 at the Vechtdijk near Zwolle were performed with different wave conditions, in order to establish the influence of wave climate on erosional resistance. The tests have been described by Steendam et al. (2010). The wave conditions are given in Table 2 and can be characterized by wave heights of 1 m, 2 m and 3 m. A wave height of 1 m gives almost two times more incident waves in 6 hours than a wave height of 3 m.

Table 2. Wave conditions simulated at the Vechtdijk, Zwolle

Seaward slope 1:4	***Wave height H_s***		
Test duration 6 hours	**1 m**	**2 m**	**3 m**
Peak period T_p (s)	4.0	5.7	6.9
Mean period T_m (s)	3.3	4.7	5.8
Number of waves N_w	6545	4596	3724
Run-up, $Ru_{2\%}$ (m)	1.99	3.98	5.94

Table 3. Wave overtopping for three wave heights		*Mean overtopping discharge q (l/s per m)*					
		0.1	*1*	*5*	*10*	*30*	*50*
H_s = 1 m	*Crest freeboard R_c (m)*	2.24	1.63	1.2	1.02	0.73	0.6
	Percentage overtopping waves P_{ov}	0.7	7.2	24	35.7	59	70
	Number overtopping waves N_{ow}	45	471	1573	2336	3861	4583
	Maximum overtopping volume V_{max} (l/m)	256	440	831	1197	2359	3401
H_s = 2 m	*Crest freeboard R_c (m)*	5.06	3.84	2.98	2.61	2.03	1.76
	Percentage overtopping waves P_{ov}	0.2	2.7	11.4	18.9	36.6	47
	Number overtopping waves N_{ow}	9	126	525	867	1683	2160
	Maximum overtopping volume V_{max} (l/m)	769	1222	2018	2697	4707	6387
H_s = 3 m	*Crest freeboard R_c (m)*	7.98	6.16	4.89	4.35	3.48	3.08
	Percentage overtopping waves P_{ov}	0.085	1.49	7.05	12.3	26.1	34.9
	Number overtopping waves N_{ow}	3	55	262	456	972	1300
	Maximum overtopping volume V_{max} (l/m)	1424	2254	3478	4509	7375	9709

The three wave conditions give different overtopping parameters, like the crest freeboard, percentage of overtopping waves, number of overtopping waves and largest overtopping wave volume, all related to a certain overtopping discharge. All these values have been given in Table 3. A wave height of 1 m, for example, gives for an overtopping discharge of 10 l/s per m 2336 overtopping waves in 6 hours. For a 3 m wave height this reduces to 456 overtopping waves, which is only 20% of the number for 1 m waves, but the overtopping discharge is the same. It is clear that the larger wave height will then give larger overtopping volumes, which in this example is 4.5 m^3/m as largest volume for a 3 m wave height and only 1.2 m^3/m for a 1 m wave height.

The Vechtdijk was a 100% sandy dike, covered with only 0.15 m of soil and grass. It was expected that failure of the grass would certainly be achieved for each of the wave conditions and probably for different overtopping discharges. This was, however, not always the case due to early failure of a tree in the slope and a particular transition (see Steendam 2010) and it was not always possible to reach failure of the grassed slope itself.

It became also clear that it is not so easy to decide when a grassed slope has start of damage, developing damage or failure. Failure is the most easy definition: the sand core underneath the soil layer becomes free and damage develops fast. Start of damage would actually be the first small hole in the grass cover and this is not a consistent parameter as it may depend on the existence or non-existence of one weak spot on a fairly large surface. A more consistent definition would be "various damaged locations", meaning that it does not depend solely on one weak spot. In the case the grassed slope did not fail the condition "no failure" became also a criterion.

In summary the following damage criteria were used:

- First damage (Figure 16)
- Various damaged locations (Figure 17)
- Failure (Figure 18)
- Non-failure after testing (Figure 19)

Figure 16. First damage.

Figure 17. Various damaged locations

Figure 18. Failure.

Figure 19. Non-failure after testing

The theory of shear stress with a threshold was taken as a basis for development, see also Hoffmans et al. (2008). The development, however, took place at the same time when Dean et al. (2010) worked on their erosional equivalence, but it was not yet published at that time. Dean et al. (2010) considered three possible developments, which in essence can be described as follows:

$$\text{Erosion due to excess velocity: } E = K\,\Sigma((u - u_c)\,t) \qquad [\text{m/s}] \qquad (13)$$

$$\text{Erosion due to excess shear stress: } E = K\,\Sigma((u^2 - u^2_c)\,t) \qquad [\text{m}^2/\text{s}] \qquad (14)$$

$$\text{Erosion due to excess of work: } E = K\,\Sigma((u^3 - u^3_c)\,t) \qquad [\text{m}^3/\text{s}] \qquad (15)$$

In all cases the velocity of the overtopping wave plays a role and a critical velocity, which should be exceeded before erosion will take place. In the equations also the time that the critical velocity is exceeded, is important.

The analysis of the Vechtdijk results had as basis Equation 14 (Hoffmans et al. 2008). The testing showed indeed that only waves of a certain volume (or velocity) damaged the slope. Smaller volumes did not contribute to the development of damage. This confirms the use of a threshold like u_c. But one main modification was made, based on observed behaviour during testing. In Equations 13-15 the time that u_c is exceeded is taken into account. The origin of this comes from tests with continuous overflow, where indeed time, or the duration that the flow is present, is important.

But (severe) wave overtopping is different from continuous overflow. First of all, velocities in an overtopping wave are much larger than velocities in continuous overflow, for the same discharge. Secondly, the duration that u_c is exceeded in an overtopping wave is quite short, in the order of 1-3 s, and this duration is fairly constant and in total much shorter than for continuous overflow.

The observation of overtopping waves has taught us that a wave front rushes over the slope with large velocity. Within tenths of seconds (see Figure 10) the maximum velocity is reached. The grass feels this as a kind of "impact" and it is this impact that causes initiation or further development of damage. It is believed that this impact is more important than the duration of the overtopping wave above a certain threshold. For this reason Equation 14 was rewritten to an erosional index called "cumulative hydraulic load", where the actual time or duration for an overtopping wave was omitted:

$$\text{Cumulative hydraulic load: } \Sigma(u^2 - u^2_c) \qquad [\text{m}^2/\text{s}^2] \qquad (16)$$

With known distributions of overtopping wave volumes (Eqs. 1 and 2) and known velocities per overtopping wave volume (Eq. 9) it is possible to calculate the cumulative hydraulic load for each wave overtopping condition, or a number of tests, to a certain moment when a damage criterion is reached. And the cumulative hydraulic load depends of course on the critical velocity u_c that is taken.

The main question is then: what is the critical velocity, u_c, that brings the damage observed for different hydraulic regimes, together?

The four damage criteria (see Figures 16-19) were taken for all tests and the results were compared for critical velocities of 0; 3.1; 4.0; 5.0 and 6.3 m/s, which are in accordance with overtopping wave volumes of 0; 0.25; 0.5; 1 and 2 m^3/m. Figures 20-22 give the comparison for the extremes (0 and 6.3 m/s) and for 4.0 m/s.

The transition and the tree for a wave height of 2 m failed before the grass failed and the test had to be stopped before grass failure could be reached. These are the columns for "non-failure". The grass did fail, however, for the tests with 1 m and 3 m wave height, each after a different test duration. The section for 1 m wave height failed after 6 hours tests with 0.1; 1; 10; 30 l/s per m and another 2:07 hours with 50 l/s per m. The section with 3 m wave height failed after 6 hours tests with 0.1; 1; 10 l/s per m and another 1:03 hour with 30 l/s per m. The large wave height gave earlier damage and for both wave heights the damage was mainly caused by many mole holes just below the crest.

Figures 20-22 can be used to establish the correct critical velocity for this dike section. If the height of the columns in the graphs are equal, then the correct critical velocity is found. As "non-failure" is only found for one wave height of 2 m and "first damage" is not very reliable, the most interesting columns are those for "various damages" and for "failure". Both Figures 20 and 22 show that the columns have different height. The best graph is given in Figure 21, where the critical velocity used was 4 m/s. This is the critical velocity that should be used for this sandy dike.

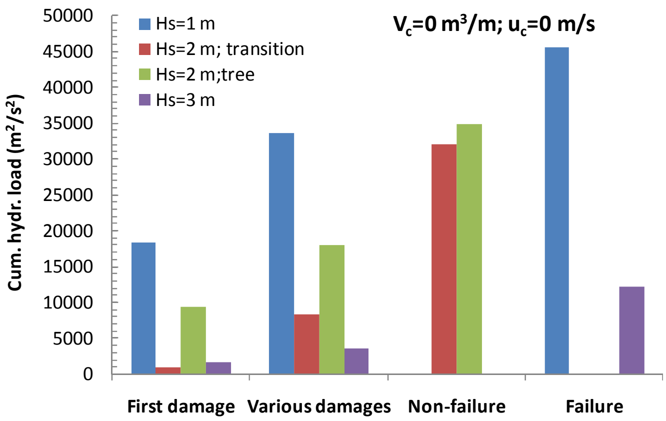

Figure 20. Comparison of cumulative hydraulic loads for various damage criteria; u_c = 0 m/s.

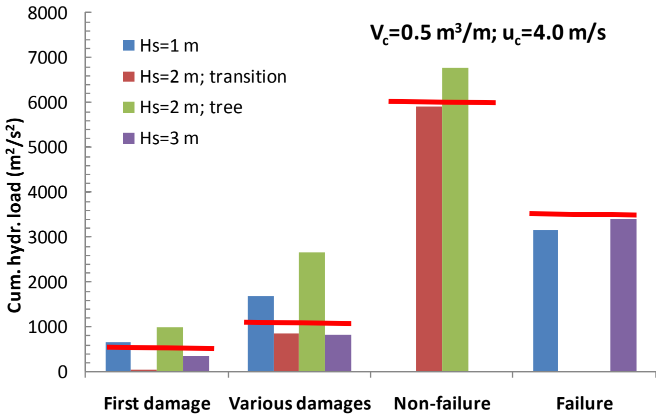

Figure 21. Comparison of cumulative hydraulic loads for various damage criteria; u_c = 4 m/s.

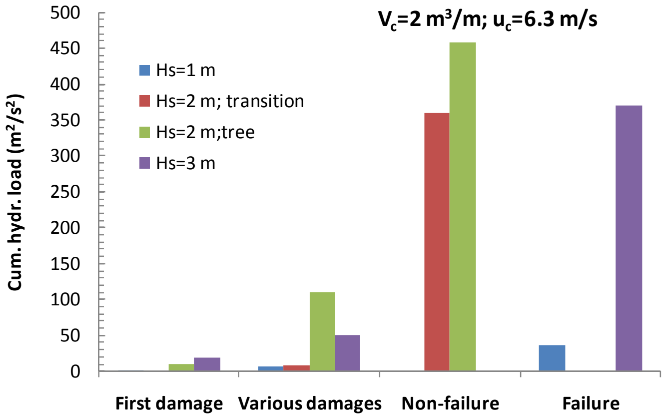

Figure 22. Comparison of cumulative hydraulic loads for various damage criteria; u_c = 6.3 m/s.

Based on Figure 21 the following conclusions can be made for the Vechtdijk and the limits are given in the graph:

- A critical velocity should be used of $u_c = 4$ m/s ($V_c = 0.5$ m³/m)
- Start of damage: $\Sigma(u^2 - u_c^2) = 500$ m²/s²
- Various damaged locations: $\Sigma(u^2 - u_c^2) = 1000$ m²/s²
- Failure (by mole holes): $\Sigma(u^2 - u_c^2) = 3500$ m²/s²
- Non-failure for normal slope: $\Sigma(u^2 - u_c^2) < 6000$ m²/s²

A confirmation of above analysis and conclusions could be established by looking at the damage on the slope after the hydraulic measurements. Here only about 40 overtopping waves rushed down the slope instead of many hours like for normal testing, but many large volumes were present. The hypothesis of cumulative hydraulic load should work for many hours of testing, but also for the "artificial" distribution of a small number, but mainly very large overtopping waves.

The observation of the slope after the hydraulic measurements could best be described as "various damaged locations". A number of small holes were observed and one location with a little larger damaged area.

The cumulative hydraulic load for these 40 waves, using u_c = 4 m/s, amounted to 946 m^2/s^2. This is very well comparable with the 1000 m^2/s^2 that was given for this damage criterion. It can be concluded that this very short session of large waves can very well be compared with many hours of testing of real wave overtopping. The analysis confirmed the hypothesis of cumulative hydraulic load.

In future also the method of "excess of work" (Equation 15), which was preferred by Dean et al. (2010), should be elaborated, maybe with ongoing work in the US with a new Wave Overtopping Simulator. The reason for Dean et al., however, to choose for excess of work instead of excess of shear stress was that excess of work fitted better to known stability curves for continuous overflow, not wave overtopping. Dean et al. (2010) did not possess the results of simulation of wave overtopping at real dikes as in the Netherlands.

Another difference between the two methods is the value of the critical velocity u_c. Based on continuous overflow critical velocities are in the range of 1-2 m/s. But the very "weak" Vechtdijk (sand with a very thin layer of soil with grass) needs a critical velocity of 4 m/s and this can be considered as a lower boundary. Other dike sections tested need probably a critical velocity in the range of 5-7 m/s. It is, therefore, still an open question which method would work best with real wave overtopping at dikes.

CONCLUSIONS AND RECOMMENDATIONS

Improved equations (Eqs. 5-7) for flow depth and flow velocity under wave overtopping at the crest of dikes or levees have been developed, using new data from the Hydralab Flowdike project. The present knowledge, however, on flow depth, flow velocity and overtopping duration are not consistent with the mass balance. More research is required to solve this discrepancy and probably the flow depth and velocity must become more dependent on wave period. Also the assumption about both flow depth and flow velocity having a Rayleigh distribution may be questioned.

Successful hydraulic measurements have been performed at the slope of a real dike under wave overtopping simulation. Analysis gives flow depth, flow velocity and overtopping duration as a function of overtopping wave volumes (Eqs. 8-10). The combination of these equations fulfill fairly well the requirements for the mass balance. These equations are only valid for the Dutch Wave Overtopping Simulator.

The measurements confirm that the boundary layer of the turbulent aerated flow during wave overtopping at a grass covered slope is very small and that the front velocity can be considered equal to the depth-averaged maximum velocity as well as to the velocity on top of the flow.

It is important to use various damage descriptions or criteria in order to describe the behaviour of a grass covered landward slope under wave overtopping. Useful criteria, based on testing at a real dike with the Wave Overtopping Simulator, were: first damage; various damaged locations; failure and non-failure after testing.

The erosional index "cumulative hydraulic load" was developed, which to a certain extent is comparable with the erosional equivalence of Dean et al. (2010). The method is based on excess of shear stress and not on excess of work. Tests at the sandy Vechtdijk with three different wave heights showed that a critical velocity of u_c = 4 m/s was needed to give similar damage for similar cumulative hydraulic loads. The method was confirmed by the damage after the hydraulic measurements, which was caused by only 40 overtopping waves instead of many hours of real overtopping simulation. As the Vechtdijk was a "weak" slope (sand covered with 0.15 m of soil and grass) it can be expected that for better grass covers the critical velocity may increase to 5 or 6 m/s or even more.

It is recommended to compare, elaborate and improve the two methods of erosional equivalence and cumulative hydraulic load for more situations, maybe with ongoing work in the US with their new Wave Overtopping Simulator.

ACKNOWLEDGMENTS

All Dutch tests with the Wave Overtopping Simulator were conducted under the SBW-project (Strength and Loads on Water Defences) of the Ministry of Transport, Public Works and Water Management, Rijkswaterstaat.

The model tests under the Flowdike project were conducted by RWTHUG, Aachen, in the Shallow Water Basin at DHI, Denmark, under Contract Number 022441 of the European Community – Structuring the European Research Area – Research Infrastructures. The financial contribution from the EC is appreciated.

REFERENCES

Bosman, G, J.W. van der Meer, G. Hoffmans, H. Schüttrumpf and H.J. Verhagen. 2008. Individual overtopping events at dikes. ASCE, *proc. ICCE 2008*, Hamburg, Germany, p. 2944-2956.

Dean, R.G., J.D. Rosati, T.L. Walton and B.L. Edge (2010). Erosional equivalences of levees: Steady and intermittent wave overtopping. *Journal of Ocean Engineering 37 (2010) 104-113.*

EurOtop Manual. 2007. Wave Overtopping of Sea Defences and Related Structures – Assessment Manual. UK: N.W.H. Allsop, T. Pullen, T. Bruce. NL: J.W. van der Meer. DE: H. Schüttrumpf, A. Kortenhaus. *www.overtopping-manual.com*.

Hoffmans, G., G.J. Akkerman, H. Verheij, A. van Hoven and J.W. van der Meer. The erodibility of grassed inner dike slopes against wave overtopping. *ASCE, Proc. ICCE 2008*, Hamburg, p. 3224-3236.

Schüttrumpf H. and H. Oumeraci (2005). Layer thicknesses and velocities of wave overtopping flow at seadikes. *Journal of Coastal Engineering, Volume 52, Issue 6, p.* 473-495.

Schüttrumpf, H. and M.R.A. van Gent, 2003. Wave overtopping at seadikes. *ASCE, proc. Coastal Structures 2003*, p. 431-443.

Schüttrumpf, H.F.R. 2001. Wellenüberlaufströmung bei See-deichen, *Ph.D.-thesis*, Technical University Braunschweig.

Steendam, G.J., J.W. van der Meer, B. Hardeman and A. van Hoven (2010). Destructive wave overtopping tests on grass covered landward slopes of dikes and transitions to berms. *ASCE, Proc. ICCE 2010*, Shanghai, China.

Van Gent, M.R.A. 2002. Low-exceedance wave overtopping events. *Delft Hydraulics project id. DC030202/H3803*.

Van der Meer, J.W., R. Schrijver, B. Hardeman, A. van Hoven, H. Verheij and G.J. Steendam. 2009. Guidance on erosion resistance of inner slopes of dikes from three years of testing with the Wave Overtopping Simulator. *Proc. ICE, Breakwaters, Marine Structures and Coastlines*; Edinburgh, UK.

Van der Meer, J.W., G.J. Steendam, G. de Raat and P. Bernardini. 2008. Further developments on the wave overtopping simulator. ASCE, *proc. ICCE 2008*, Hamburg.

Van der Meer, J.W., P. Bernardini, G.J. Akkerman and G.J.C.M. Hoffmans, 2007. The wave overtopping simulator in action. *ASCE, proc Coastal Structures*, Venice, Italy, p. 645-656.

Van der Meer, J.W., W. Snijders and E. Regeling, 2006. The wave overtopping simulator. *ASCE, proc. ICCE 2006*, San Diego, p. 4654-4666.